TUNED MASS DAMPER APPLICATIONS ON SLENDER STRUCTURES TO IMPROVE EARTHQUAKE AND WIND RESPONSE

by

Veysel Doğan

B.S, Mechanical Engineering, Middle East Technical University, 1984

Submitted to the Institute for Graduate Studies in
Science and Engineering in partial fulfillment of
the requirements for the degree of
Master of Science

Graduate Program in Mechanical Engineering
Boğaziçi University
2011

TUNED MASS DAMPER APPLICATIONS
ON SLENDER STRUCTURES
TO IMPROVE
EARTHQUAKE AND WIND RESPONSE

APPROVED BY:

Assist. Prof. Çetin Yılmaz . . . . . .
(Thesis Supervisor)

Prof. Emre Köse . . . . . .

Assist. Prof. Serdar Soyöz . . . . . .

DATE OF APPROVAL: 27.01.2011

ACKNOWLEDGEMENTS

The author would like to express sincere gratitude to his advisor, Assist. Prof. Çetin Yılmaz, for the immense amount of support, patience and guidance provided for this thesis.

The author specifically, thanks to all engineers who contributed on this study by suggesting and advising their experiences.

This thesis was prepared during the times which were stolen from the author's family. The author wishes to thanks his family and dedicates this thesis to his lovely daughter Gülce and lovely wife Meral.

ABSTRACT

TUNED MASS DAMPER APPLICATIONS ON SLENDER STRUCTURES TO IMPROVE EARTHQUAKE AND WIND RESPONSE

The subject of the study is to improve earthquake and wind response of slender structures by using Tuned Mass Damper (TMD) applications. TMD application on main structure reduces the structural response amplitude by creating additional damping. A vibration analysis employing transfer matrices was applied for a slender structure with varying cross sections. The analysis is applied to an existing reinforced concrete minaret structure as a case study due to its poor dynamic response and lack of sufficient studies. Best applicable and efficient TMD type was investigated to improve the dynamic response of selected minaret structure. Structure response was analyzed with and without TMD installation by using MATLAB for discrete mass model. Harmonic excitation was considered to simulate the ground motion and improvements in the response were discussed. SAP2000 software was also used to analyze the same structure through Finite Element Method technique. 1999 Kocaeli and 1999 Düzce earthquakes ground motion records were used to verify the effectiveness of the developed TMD. Wind response is also considered. Detailed fabrication drawings were prepared by considering the challenging installation constraints. Feasibility study of the developed TMD was discussed for applications either in new structures or retrofits.

ÖZET

NARİN YAPILARDAKİ DEPREM VE RÜZGAR TEPKİLERİNİN İYİLEŞTİRİLMESİ İÇİN AYARLI KÜTLE SÖNÜMLEYİCİSİ UYGULAMALARI

Bu tez çalışmasının amacı, narin yapıların deprem ve rüzgâr etkileri karşısındaki dinamik davranışlarının 'Ayarlı Kütle Sönümleyicisi (AKS)' sistemi kullanılarak iyileştirilmesidir. Ana yapı üzerine monte edilen AKS ilave bir sönümleme oluşturarak ana yapının titreşim genliğini azaltır. Bu çalışmada transfer matrisleri kullanılarak değişken kesitli narin yapıların titreşim analizi yapıldı. Söz konusu analiz betonarme bir minare için örnek çalışma olarak uygulandı. Dinamik davranışlarının iyi olmaması ve üzerinde yeterince çalışma olmaması sebebi ile tipik bir minare örnek çalışmaya konu edildi. Seçilen minare yapısının dinamik davranışını iyileştirmek için en ekonomik, en verimli ve uygulanabilir AKS tipi araştırıldı. Yapının davranışı, AKS'siz ve AKS'li olarak MATLAB programı aracılığı ile müstakil kütle modeli kullanılarak analiz edildi. Deprem hareketini simule etmek amacı ile harmonik bir yer etkisi uygulandı ve yapının davranışındaki iyileştirmeler tartışıldı. Aynı yapı üzerinde SAP2000 yazılımı kullanılarak Sonlu Elemanlar Yöntemi metodu ile analiz yapıldı. AKS uygulamasının etkinliğini görmek amacı ile minare modeline 1999 Kocaeli Depremi ve 1999 Düzce Depremi uygulanarak titreşim analizi yapıldı. Minarenin rüzgâr etkisi altındaki davranışı çalışıldı. Zor montaj şartları göz önünde bulundurularak, detaylı imalat projeleri hazırlandı. Geliştirilen AKS'nin fizibilite hesabı yapılarak gerek yeni projelerde gerekse eski yapılarda güçlendirme amaçlı kullanılması araştırıldı.

TABLE OF CONTENTS

ACKNOWLEDGEMENTS iii
ABSTRACT iv
ÖZET v
LIST OF FIGURES ix
LIST OF TABLES xvii
LIST OF SYMBOLS / ABBREVIATIONS xix
1. INTRODUCTION 1
2. SLENDER STRUCTURES & DAMPING 3
2.1. Introduction 3
2.2. Damping Sources 4
2.3. Auxiliary Damping Sources 5
2.3.1. Passive Dampers (With Indirect Energy Dissipation) 6
2.3.1.1. Tuned Mass Dampers (TMDs) 6
2.3.1.2. Tuned Liquid Dampers (TLDs) 7
2.3.1.3. Impact Dampers (TlDs) 8
2.3.2. Passive Dampers (With Direct Energy Dissipation) 9
2.3.3. Active Dampers 9
2.3.4. Hybrid Dampers 10
2.3.5. Semi-Active Dampers 11
3. TUNED MASS DAMPER SYSTEMS 12
3.1. Introduction 12
3.2. Tuned Mass Damper Theory for SDOF Systems 12
3.2.1. Undamped Structure: Dynamic Vibration Absorber 13
3.2.2. Undamped Structure: Tuned Mass Damper 16
3.3. Examples of Existing Tuned Mass Damper Systems 29
3.3.1. Translational Tuned Mass Dampers 29
3.3.2. Pendulum Tuned Mass Dampers 33
4. TRANSFER MATRICES 39
4.1. Transfer Matrix of Spring-Mass System 39
4.2. Plane Flexural Vibration of a Straight Beam 41

4.3. Elimination of Intermediate State Vectors 46
4.4. Determination of Natural Frequencies 48
4.5. Determination of Mode Shapes 51
4.6. Forced Vibrations of a Straight Beam 52
4.7. Transfer Matrices Applied to Forced Damped Vibrations 53
5. CASE STUDY 61
5.1. Structure Selection for the Case Study 61
5.2. Minaret Structures 61
5.3. TMD Type Selection 64
5.4. Vibration Analysis of the Minaret with Transfer Matrix Method 67
5.4.1. Natural Frequencies of the Minaret 72
5.4.2. Natural Modes of the Minaret 75
5.4.3. TMD Model 83
5.4.4. TMD Optimization 88
5.4.5. Dynamic Analysis against Harmonic Base Excitation 94
5.4.5.1. Dynamic Analysis of Minaret without TMD 94
5.4.5.2. Dynamic Analysis of Minaret with TMD 101
5.5. Vibration Analysis of the Minaret with Finite Element Method 108
5.5.1. Natural Frequencies of the Minaret 110
5.5.2. Natural Modes of the Minaret 110
5.5.3. Dynamic Analysis Against Earthquake Ground Motion 111
5.5.4. Dynamic Analysis Against Harmonic Base Excitation 121
5.6. Wind response 125
5.6.1. Vibration Due To Vortex Shedding 126
5.6.2. Prediction of Vortex-Induced Oscillation 127
5.6.3. Harmonic Excitation of structures by Vortex Shedding 128
5.6.4. Vortex Shedding in Case Study 129
6. TMD DESIGN FOR THE MINARET 132
6.1. TMD Design 132
6.2. TMD Cost Analysis 137
7. CONCLUSION 138
7.1. Results 138
7.2. Recommendations 139

APPENDIX A: MATLAB CODES & OUTPUTS 140
APPENDIX B: SAP 2000 OUTPUTS 171
APPENDIX C: STIFFNESS VERIFICATION FOR ORTHOGONAL SPRINGS . . 177
APPENDIX D: TECHNICAL DRAWINGS 185
REFERENCES 196

LIST OF FIGURES

Figure 2.1. Various auxiliary damping devices utilizing inertial effects 5

Figure 2.2. Schematic of the TLD Family 7

Figure 2.3. Schematic of an impact damper 8

Figure 3.1. SDOF system coupled with a TMD 13

Figure 3.2. Undamped SDOF system coupled with a damped TMD system 16

Figure 3.3. Plot of H_2 versus ρ 20

Figure 3.4. Plot of H_2 versus ρ for f_{opt} 21

Figure 3.5. Optimum tuning frequency ratio, f_{opt} 23

Figure 3.6. Input frequency ratios at which the response is independent of damping 23

Figure 3.7. Optimal damping ratio for TMD 24

Figure 3.8. Maximum dynamic amplification factor for SDOF system 24

Figure 3.9. Maximum dynamic amplification factor for TMD 25

Figure 3.10. Ratio of maximum TMD amplitude to maximum system amplitude . 25

Figure 3.11. Response curves for amplitude of system with optimally tuned TMD 26

Figure 3.12. Response curves for amplitude of optimally tuned TMD 26

Figure 3.13. Equivalent damping ratio for optimally tuned TMD 28

Figure 3.14. Schematic diagram of a translational tuned mass damper 29

Figure 3.15. Tuned mass damper for Chiba-Port Tower 32

Figure 3.16. Tuned mass damper with spring and damper assemblage 32

Figure 3.17. Deformed position-tuned mass damper 33

Figure 3.18. Tuned mass damper-Huis Ten Bosch Tower, Nagasaki 33

Figure 3.19. A simple pendulum tuned mass damper 34

Figure 3.20. Compound pendulum 35

Figure 3.21. Ice storage tank-Crystal Tower 37

Figure 3.22. Rocker pendulum 38

Figure 4.1. Spring mass system 39

Figure 4.2. Free-body diagram of spring *i* 40

Figure 4.3. Free-body diagram of mass m_i 41

Figure 4.4. Beam with concentrated masses 42

Figure 4.5. Sign convention for beam 42

Figure 4.6. End forces and deflections for massless beam 42

Figure 4.7. Cantilever subjected to force *V* and moment *M* 43

Figure 4.8. Free-body diagram of mass m_i 45

Figure 4.9. Beam on elastic support 45

Figure 4.10. Free-body diagram of the elastic support 46

Figure 4.11. Beam with discrete masses 47

Figure 4.12. Two cases of boundary conditions 49

Figure 4.13. Beam of three sections 50

Figure 4.14. Beam subjected to uniformly distributed load $q \cos \Omega t$ 52

Figure 4.15. Simple damped system in steady state oscillation 54

Figure 4.16. (a) Spring of stiffness k and (b) damper of complex stiffness $jc\Omega$ . . 55

Figure 4.17. Spring and damper in parallel 56

Figure 4.18. Spring and damper in series 58

Figure 4.19. Point mass with harmonic exciting force 59

Figure 5.1. Typical reinforced concrete minarets in Turkey 62

Figure 5.2. Collapse of a minaret onto a nearby building 63

Figure 5.3. Collapse of minaret on its main building 63

Figure 5.4. Minaret structure for the case study 64

Figure 5.5. Springs and Dampers in two orthogonal directions 66

Figure 5.6. TMD layout developed for minarets 66

Figure 5.7. TMD used in La Prade Heavy Water Plant 67

Figure 5.8. Discrete mass model of minaret 69

Figure 5.9. Simplified minaret model 70

Figure 5.10. Cross section of minaret boot 71

Figure 5.11. Cross section of cylindrical minaret body 72

Figure 5.12. 1st Normal Mode Shape 77

Figure 5.13. 2nd Normal Mode Shape 77

Figure 5.14. 3rd Normal Mode Shape 78

.

Figure 5.15. 4th Normal Mode Shape 78

Figure 5.16. 5th Normal Mode Shape 79

Figure 5.17. 6th Normal Mode Shape 79

Figure 5.18. 7th Normal Mode Shape 80

Figure 5.19. 8th Normal Mode Shape 80

Figure 5.20. 9th Normal Mode Shape 81

Figure 5.21. 10th Normal Mode Shape 81

Figure 5.22. 11th Normal Mode Shape 82

Figure 5.23. 12^{th} Normal Mode Shape 82

Figure 5.24. 13^{th} Normal Mode Shape 83

Figure 5.25. Minaret model with a DVA 84

Figure 5.26. DVA model 84

Figure 5.27. Free body diagram mass m_{12} 85

Figure 5.28. TMD model without damping 86

Figure 5.29. SDOF model of minaret 89

Figure 5.30. Equivalent mass for SDOF model 90

Figure 5.31. SDOF model of minaret with TMD 90

Figure 5.32. Normalized frequency response of m_{12} without TMD 92

Figure 5.33. Normalized frequency response of m_{12} with TMD 93

Figure 5.34. Normalized frequency response of m_{12} with optimized TMD around 1^{st} natural frequency 93

Figure 5.35. Normalized frequency response of m_{12} with optimized TMD around 1^{st} and 2^{nd} natural frequency 94

Figure 5.36. Flexural vibration model of minaret without TMD 95

Figure 5.37. Displacement curve / case 1 no TMD 97

Figure 5.38. Rotation diagram / case 1 no TMD 97

Figure 5.39. Moment diagram / case 1 no TMD 98

Figure 5.40. Shear diagram / case 1 no TMD 98

Figure 5.41. Absolute Displacement curve / case 2 no TMD 99

Figure 5.42. Absolute Rotation diagram / case 2 no TMD 99

Figure 5.43. Absolute Moment diagram / case 2 no TMD 100

Figure 5.44. Absolute Shear diagram / case 2 no TMD 100

Figure 5.45. Displacement curve / case 1 with TMD 103

Figure 5.46. Rotation diagram / case 1 with TMD 103

Figure 5.47. Moment diagram / case 1 with TMD 104

Figure 5.48. Shear diagram / case 1 with TMD 104

Figure 5.49. Absolute Displacement curve / case 2 with TMD 105

Figure 5.50. Absolute Rotation diagram / case 2 with TMD 105

Figure 5.51. Absolute Moment diagram / case 2 with TMD 106

Figure 5.52. Absolute Shear diagram / case 2 with TMD 106

Figure 5.53. Minaret model used in SAP2000 program 109

Figure 5.54. First 5 modal shapes in one direction of FEM model obtained from SAP2000 111

Figure 5.55. Acceleration graph of Kocaeli earthquake recorded at Izmit Meteroloji station 112

Figure 5.56. Acceleration graph of Düzce earthquake recorded at Düzce Meteroloji station 112

Figure 5.57. Displacement plot of joint 1026 without TMD against Kocaeli Earthquake by SAP2000 112

Figure 5.58. Displacement plot of joint 1026 without TMD against Düzce Earthquake by SAP2000 113

Figure 5.59. Uncoupled spring and damper from Link elements to model TMD in SAP2000 114

Figure 5.60. Displacement plot of joint 1026 with TMD against Kocaeli Earthquake by SAP2000 115

Figure 5.61. Displacement plot of joint 1026 with TMD against Düzce Earthquake by SAP2000 115

Figure 5.62. Displacement plot of TMD mass (Joint 1562) against Kocaeli Earthquake by SAP2000 116

Figure 5.63. Displacement plot of TMD mass (Joint 1562) against Düzce Earthquake by SAP2000 116

Figure 5.64. Düzce earthquake ground acceleration records in time domain . . 118

Figure 5.65. Düzce earthquake ground acceleration records in frequency domain . 118

Figure 5.66. Enlarged view of Düzce earthquake ground acceleration records in frequency domain 119

Figure 5.67. Kocaeli earthquake ground acceleration records in time domain . . 119

Figure 5.68. Kocaeli earthquake ground acceleration records in frequency domain 120

Figure 5.69. Enlarged view of Kocaeli earthquake ground acceleration records in frequency domain 120

Figure 5.70. Displacement plot of joint 1026 without TMD against harmonic base excitation with $\omega = 7.0$ 122

Figure 5.71. Displacement plot of joint 1026 without TMD against harmonic base excitation with $\omega = 32.8$ 122

Figure 5.72. Displacement plot of joint 1026 with TMD against harmonic base excitation with $\omega = 7.0$ 123

Figure 5.73. Displacement plot of joint 1026 with TMD against harmonic base excitation with $\omega = 32.8$ 123

Figure 5.74. Displacement plot of joint 1562 with TMD against harmonic base excitation with $\omega = 7.0$ 124

Figure 5.75. Displacement plot of joint 1562 with TMD against harmonic base excitation with $\omega = 32.8$ 125

Figure 5.76. Normal airflow around a Cylindrical object 126

Figure 5.77. Disturbed airflow around a Cylindrical object 126

Figure 6.1. Equivalent model a translational TMD 132

Figure 6.2. Equivalent model of the selected hybrid TMD 133

LIST OF TABLES

Table 5.1. Mass, Length and Inertia values of the minaret model 70

Table 5.2. Natural frequencies and periods of discrete mass model obtained from Matlab 75

Table 5.3. Response outputs of minaret without TMD against harmonic base excitation 101

Table 5.4. Response outputs of minaret with TMD against harmonic base excitation 107

Table 5.5. Response improvement of minaret via TMD installation against harmonic base excitation 107

Table 5.6. First 5 natural frequencies and periods of FEM model obtained from SAP2000 110

Table 5.7. Response outputs of minaret without TMD against earthquake ground motion 112

Table 5.8. Response outputs of minaret with TMD against earthquake ground motion 115

Table 5.9. Response improvement of minaret via TMD installation against Kocaeli and Düzce earthquakes 117

Table 5.10. Response outputs of minaret without TMD against harmonic base excitation 121

Table 5.11. Response outputs of minaret with TMD against harmonic base excitation 123

Table 5.12. Response improvement of minaret via TMD installation against harmonic base excitation 124

Table 5.13. Response outputs of minaret without TMD against vortex shedding . 130

Table 5.14. Response outputs of minaret with TMD against vortex shedding . . 131

Table 5.15. Response improvement of minaret via TMD installation against vortex shedding 131

LIST OF SYMBOLS / ABBREVIATIONS

a_g	Absolute ground acceleration
c	Damping value main structure
c_d	Damping value of damper
C_L	Amplitude of lift coefficient
D	Width of the object
E	Modulus of elasticity
f	Ratio of damper natural frequency to system natural frequency
f_i	Natural frequencies of the structure
f_s	Dominant frequency of vortex shedding
F_L	Lift force per unit length
F	Field transfer matrix
H	Amplification factor
I	Inertia
k	Stiffness of main structure
k_d	Stiffness of damper
k_{eq}	Equivalent spring stiffness
L	Length
m	Mass
m_d	Damper mass
m_{eq}	Equivalent mass
$\bar{m}$	Mass ratio
M	Bending moment
N	Spring force
N_i^L	Spring force at left
N_i^R	Spring force at right
p	External force applied to the primary mass
P	Point transfer matrix
Re	Reynolds number
S	Strouhal number

T	Natural period
T_d	Natural period of pendulum
u	Relative displacement between primary mass and ground
u_d	Relative displacement between damper and primary mass
u_g	Absolute ground motion
v	Kinematic viscosity
V	Shear force
V_c	Resonant amplitude of mode *i* at the critical wind velocity
$\overline{V}$	Mean wind velocity
w	Displacement
x_i	Coordinate of i^{th} node
$\mathbf{z}_i^R$	State vector at right
$\mathbf{z}_i^L$	State vector at left
ξ	System damping ratio
ξ_d	Damper damping ratio
ξ_e	Equivalent damping ratio
ρ	Ratio of excitating frequency to system natural frequency
ρ_d	Ratio of excitating frequency to damper natural frequency
Ψ	Slope
Ω	Excitation frequency
δ	Phase angles between the response and the excitation
ω	Natural frequency of primary mass
ω_d	Natural frequency of damper

1. INTRODUCTION

This thesis concerns the dynamic response improvement of slender structures by using Tuned Mass Dampers (TMD). A TMD consists of a relatively small mass which is attached to the main structure via springs and dampers. Mass, spring and damping parameters are tuned in regard to the natural frequency of the system to reduce the amplification factor at resonance during any earthquake or wind effect. TMD installation mainly improves the structural response by increasing the damping characteristic of the structure.

The particular problem chosen for the case study is that a typical reinforced concrete minaret structure which are built as one of the major structures in a Mosque project. Turkish style minarets are very sensitive and fragile against low frequency excitations. The reason for this selection is mainly their poor performance during the major earthquakes in Turkey and lack of sufficient studies about the subject. Majority of the minarets either collapsed or severely damaged during these earthquakes. They created significant impact on the casualties and property losses directly or indirectly. Any improvement of dynamic response through TMD installation will solve the problem of structural engineers who are trying to find a solution for earthquake strengthening of exiting minarets. This study will also allow them to built better performing new minarets for the mosque construction projects in the future.

Discrete mass model was used to perform the vibration analysis on the structure. It was not so easy to obtain stiffness matrix of such non-uniform cantilever beam model. Therefore, traditional equation of motion originated by Newton's 2^{nd} law and dynamic equilibrium was not preferred. Instead of this well known equation of motion, Transfer Matrix method was selected to perform the vibration analysis of the slender structure. This method allows the successive determination of the deflection, slope, moment, and shear diagrams for any chosen frequency. Boundary conditions can be applied to the analysis by relatively straightforward means, and structural damping can be included by introducing complex impedance. The transfer matrix method is particularly well adapted to numerical calculations and avoids the complexity of obtaining stiffness matrix of non-uniform

cantilever beams. Structure's response was analyzed with and without TMD installation by using MATLAB. Harmonic base excitation was considered in the analysis and the TMD is optimized for the first natural frequency. Results show significant decrease in lateral displacements.

SAP2000 software was also used to analyze the same structure through Finite Element Method technique in a more sophisticated manner. Ground motions recorded during 1999 Kocaeli and 1999 Düzce earthquakes were used to perform time history analysis. SAP2000 analysis results confirm the improvement on response. By this way, benefits of TMD installation on slender structures like minarets were demonstrated.

Wind response of slender structures is also studied. Vortex shedding frequency which might trigger the resonance and its related critical wind velocity is estimated for the sample structure. The most cost-effective way to improve the structure's response to vortex shedding is studied and improvements by TMD application are discussed.

Another issue was the feasibility of the developed TMD application. To have a better cost estimation, detailed fabrication drawings were prepared. Feasibility study shows that developed TMD for minarets is a feasible tool to improve their dynamic behavior. However a shake table test should be performed on a model structure before a real application. Results of the shake table test should be encouraging to initiate the real applications at site. This can be a target of future studies.

2. SLENDER STRUCTURES & DAMPING

2.1. Introduction

Slender structures are widely available in the world and they are built due to technical, architectural, cultural, social and economical reasons. They are named as slender structures due to their geometry which can be described as relatively high structures with low widths. A structure can also be characterized as slender, when its structural analysis and design are mainly governed by lateral loads (earthquake and wind) versus gravity loads. Typical slender structures are; skyscrapers, high-rise buildings, telecommunication towers, industrial chimneys, towers, minarets, poles, masts, bridges etc. Most of the construction projects nowadays have many constraints regarding very different aspects. Economical restrictions as well as architectural preferences do not always satisfy engineering requirements even for structures like bridges and high-rise buildings. Sometimes it becomes also necessary to find compromises regarding the serviceability and even the structural integrity of a structure. High and slender structures as well as the need for light-weight materials increase the danger of unintended disturbing and even dangerous vibration. Hence, the check of dynamic performance should always be taken into consideration when wind, pedestrians, traffic, machinery or earthquakes have to be considered. Natural structural frequencies as well as possible excitation frequencies are always very important first indicators for the judgment of structural behavior. Resonance effects may occur when the excitation frequency is close to structural ones. Sometimes this does not play a very important role or it can be accepted. In other cases, the serviceability level of the structure is reduced significantly; people do not feel comfortable. There are even cases in which fatigue problems may occur. By increased amplitudes the stress levels are also increasing in a dangerous manner and thus, fatigue has always to be investigated for bridges and similar structures. [1]

2.2 Damping Sources

Slender structures generally have little damping characteristic which is coming from the nature of their construction materials. Therefore they are easily excited by dynamic loads like wind and earthquakes. Ground motions generated by earthquakes and vortex shedding due to wind create flexural vibrations on slender structures. When the frequency of the excitation approaches to the natural frequency of the structure, resonance phenomenon occurs and response of the structure becomes out of control due to light damping. Displacement response increases under resonance condition and most of the structures are not capable of handling such high displacements due to structural constraints. Eventually total energy of the structure will reach a limit where the structure can't resist and failure occurs. Failure of the slender structure can severely damage the neighboring buildings as well as itself. Therefore, any excitation with a frequency closer to the natural frequency of the structure should be prevented somehow.

An increase in the effective damping of a structure, accomplished by any of the four major sources of damping: structural, aerodynamic, soil, and auxiliary, will also lead to decreased structural motion. Structural damping is limited to the damping already available inherently in the materials: steel, concrete, or their composite. At times, aerodynamic damping may also contribute in the along wind direction, depending on the wind velocity, structural shape, and building dynamic characteristics. However, the contribution in the across wind direction is negligible and may even become adverse at higher wind speeds, though the presence of adjacent structures may introduce different effects. Although not marked for high rise buildings, damping contributions may also be obtained from the soil-foundation interaction, i.e. soil damping. Unfortunately, these three forms of damping make only limited contributions. In addition, the damping in the structure cannot be engineered like the mass and stiffness properties of the structure, nor can it be accurately estimated until the structure is completed, resulting a certain level of uncertainty. In cases where the inherent damping is not sufficient, auxiliary damping devices may be introduced, offering a somewhat more predictable, adaptable, and reliable method of imparting additional damping to a system. [2]

2.3. Auxiliary Damping Sources

Unlike the mass and stiffness characteristics of the structural system, damping does not relate to a unique physical phenomenon and is often difficult to engineer without the addition of external damping systems. Furthermore, the amount of inherent damping cannot be estimated with certainty; however, a known level of damping may be introduced through an auxiliary source. Such sources come in the form of both active and passive systems, illustrated schematically in Figure 2.1, which may be further subcategorized based on their mechanism of energy dissipation and system requirements. [2]

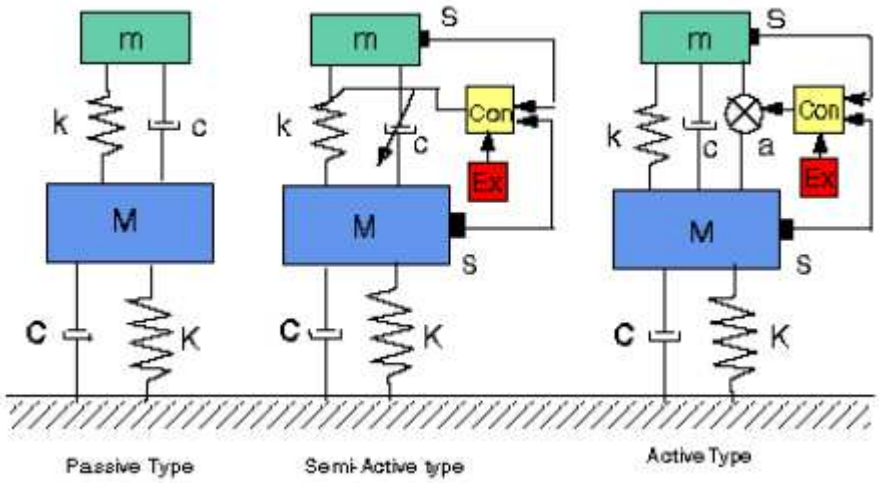

Figure 2.1. Various auxiliary damping devices utilizing inertial effects.[2]
(Con: controller, a: actuator, Ex: excitation, S: sensor)

Such systems have become increasingly popular, especially in Japan, for the mitigation of motions as a result of wind, and in some cases, for wind and seismic considerations. Accordingly, each of these auxiliary damping systems will be discussed herein, with specific attention to notable applications of these devices to actual structures in Australia, China, Canada, Japan, and the United States to control wind induced vibrations. [2]

2.3.1. Passive Dampers (With Indirect Energy Dissipation)

Commonly, auxiliary damping may be supplied through the incorporation of some secondary system capable of passive energy dissipation, for example, the addition of a secondary mass attached to the structure by a spring and damping element in order to counteract the building motion. Such passive systems were embraced for their simplicity and ability to reduce the structural response. Among the passive devices that impart indirect damping through modification of the system characteristic, the most popular concept is the damped secondary inertial system, which will be discussed below. These systems impart indirect damping to the structure by modifying its frequency response. [2]

2.3.1.1. Tuned Mass Dampers (TMDs). Typically a TMD consists of an inertial mass attached to the building location with maximum motion, generally near the top, through a spring and damping mechanism, typically viscous and viscoelastic dampers, shown previously in Figure 2.1. TMDs transmit inertial force to the building's frame to reduce its motion, with their effectiveness determined by their dynamic characteristics, stroke and the amount of added mass they employ. Additional damping introduced by the system is also dependent on the ratio of the damper mass to the effective mass of the building in the mode of interest, typically resulting in TMDs which weigh 0.25 % - 1.0 % of the building's weight in the fundamental mode (typically around one third). Often, space restrictions will not permit traditional TMD configurations, requiring the installation of alternative configurations including multi-stage pendulums, inverted pendulums, and systems with mechanically-guided slide tables, hydrostatic bearings, and laminated rubber bearings. Coil springs or variable stiffness pneumatic springs typically provide the stiffness for the tuning of TMDs. Although TMDs are often effective, even better responses have been noted through the use of multiple-damper configurations (MDCs) which consist of several dampers placed in parallel with distributed natural frequencies around the control tuning frequency. For the same total mass, a multiple mass damper can significantly increase the equivalent damping introduced to the system. Presently, there are several types of TMDs in use in Japan, typically employing oil dampers, though a few viscous and viscoelastic dampers being used. In addition, several other structures in the United States, Australia, and Canada employ TMDs. [2]

2.3.1.2. Tuned Liquid Dampers (TLDs). Tuned Liquid Dampers, encompassing both Tuned Sloshing Dampers (TSDs) and Tuned Liquid Column Dampers (TLCDs) delineated in Figure 2.2, have become a popular form of inertial damping device since their first applications to ground structures in the 1980's. In particular, the TSDs are extremely practical, currently being proposed for existing water tanks on the building by configuring internal partitions into multiple dampers without adversely affecting the functional use of the water supply tanks. Considering only a small additional mass, if any, is added to the building, these systems and their counterpart TMDs can reduce acceleration responses to 1/2 to 1/3 of the original response, depending on the amount of liquid mass. This, coupled with their low maintenance requirements, has been responsible for their wide use. [2]

Currently, both deep and shallow water configurations of TSDs, which exploit the amplitude of fluid motion and wave-breaking patterns to provide additional damping, are in application worldwide. The shallow water configurations dissipate energy through the viscous action and wave breaking, though recently, Yalla and Kareem (1999) have noted and modeled the high amplitude liquid impacts or slamming phenomena. The addition of PVC floater beads may also add to the dissipation of sloshing energy. Deep water TSDs, on the other hand, requires baffles or screens to increase the energy dissipation of the sloshing fluid. However, the entire water mass often does not participate in providing the secondary mass in these configurations. [2]

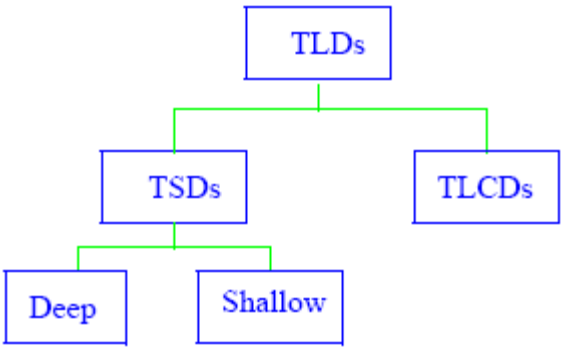

Figure 2.2. Schematic of the TLD Family. [2]

While the natural frequency of a TLD may be simply adjusted by the depth of water, h_w, and the dimension of the container D_D, there are practical limitations on the water depth and thus the frequency which may be obtained by a given container design. One

possible solution is a special device, which adjusts the sloshing frequency of the damper using a spring mechanism so that the same device can be effective and the building experience a change in the dynamic characteristics. With this device, the TLD can be made into one large tank instead of using multiple containers. The extension of the TLCD concept to active control strategies is currently being investigated using a nine story steel building. At the structure's top floor, a pressurized u-shaped oscillator is installed with a natural frequency which may be adjusted through the modulation of the pressure in the air chamber. In addition, other configurations such as LCVA, adaptive TLCDs and inertia pump dampers, amplitude-dependent orifice and multiple orifice systems have been explored as effective sources of secondary damping for structures. [2]

2.3.1.3. Impact Dampers (TIDs). Impact Dampers serve as a practical and unique form of inertial system. The devices are typically in the form of small rigid masses suspended from the top of a container mounted at its side to the structure, as shown schematically in Figure 2.3. The container is designed to a specified dimension so that an optimal spacing is left between the suspended mass and the container, allowing collisions to occur between the two as the structure vibrates. While gap distance serves as a major parameter in the design of such systems, the suspension length and mass size are also of extreme importance, dictating the frequency of the system. This type of damper is particularly effective for masts and tower-like structures with oscillations in one plane and is being used widely, particularly for roof-top masts. [2]

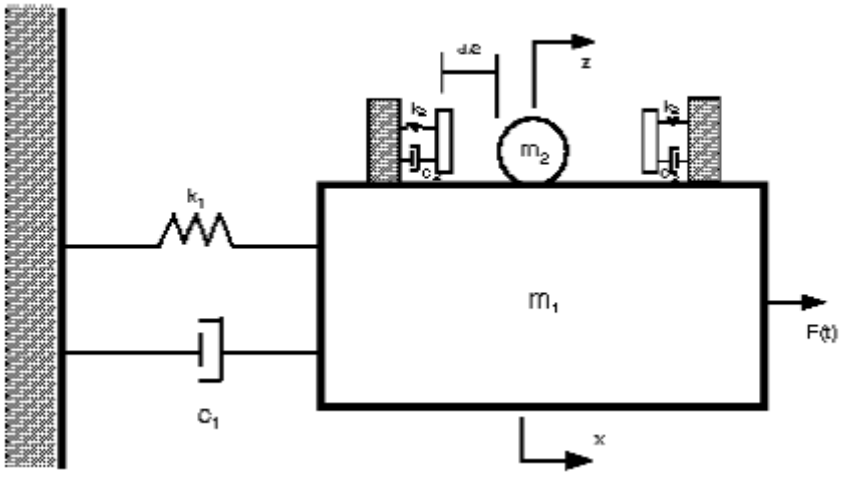

Figure 2.3. Schematic of an impact damper. [2]

While impact dampers have been used extensively to control the vibrations of turbine blades, printed circuit boards, and machine tools, their application for the vibration of large structures is still relatively limited. Early applications of impact dampers in the form of chains encased in plastic were utilized by the Navy in their communications antennas. These pioneering applications proved that displacements could be significantly reduced via the impact of the coated chains. This form of impact damper, termed Hanging Chain Damper (HCD), with rubber coated chains housed in cylinders combines the benefits of the inelastic impacts with the added internal friction of the chain links rubbing against each other. These technologies have been repeatedly used in towers, masts, and light poles in Australia and Japan to control vibrations due to wind. [2]

2.3.2. Passive Dampers (With Direct Energy Dissipation)

Passive systems may also raise the level of damping in a structure through a direct energy dissipation mechanism, such as the flow of a highly viscous fluid through an orifice or by the shearing action of a polymeric/rubber-like (viscoelastic) material. Other classes of passive systems with direct energy dissipation include Viscous Damping Devices (VDDs), Friction Systems, and Metallic Dissipaters. The application of such mechanisms to structures, particularly for seismic events, has grown in popularity both in the United States and in Japan, as they require very little space and can be easily retrofitted into existing frames. Their efficiency under large amplitude events such as earthquakes has made them a popular choice in seismic areas. [2]

2.3.3. Active Dampers

In the quest to control the vibration of structures, passive control had originally been favored for its simplicity and reliability - the devices remained functional without an external power source and posed no significant risk of generating an unstable situation. Still, without the use of control mechanisms, the devices were incapable of adjusting to a variation in any parameters of the system. Clearly, more efficient and swifter control could be obtained from a system with the ability to respond to changes - hence, active control emerged, producing smaller devices that were capable of controlling the vibration of structural systems. This aim is accomplished through the use of hydraulic or electro-mechanical actuator systems driven by an appropriate control algorithm, such as: closed

loop or feedback, in which the control forces are determined by the feedback response of the structure, open loop or feed forward, in which the control forces are determined by measured external excitations, or closed-open loop or feed forward-feedback, in which the control forces are determined by both measured response of the structure and measured external excitation. Active systems include active mass drivers, active variable stiffness systems (AVS), active tendon control systems, active gyro stabilizers (AGS), active aerodynamic appendages, and active pulse control systems. [2]

2.3.4. Hybrid Dampers

Another genre of control systems, hybrid systems, were also devised to overcome the shortcomings of a passive system, e.g. its inability to respond to suddenly applied loads like earthquakes and weather fronts. In the case of a TMD, the building may be equipped with a passive auxiliary mass damper system and a tertiary small mass connected to the secondary mass with a spring, damper, and an actuator. The secondary system is set in motion by the active tertiary mass, and it is driven in the direction opposite to the TMD, magnifying its motion, and hence, making it more effective. [2]

Hybrid Mass Dampers (HMDs), behave as either a TMD, utilizing the concept of moving mass supported mechanisms of the same natural period as the building, or an AMD according to the wind conditions, building and damper mass vibration characteristics. As a result of this unique feature, the devices are often termed tuned active dampers (TAD). The active portion of the system is only used when there is high building excitation, otherwise, it behaves passively. In such systems, the device will typically maintain active control, and in the event of a power failure or extreme excitations which exceed the actuator capabilities, will automatically switch into passive mode until the system can safely resume normal operations. This combination of passive and active systems in Japan has been found to reduce structural responses by more than 50 %. While these systems are expensive to install, the reduced operation of the AMD implies low maintenance and operation costs. Japanese researchers have devoted numerous studies toward the application of hybrid devices in structures. In fact, most applications of active control technologies are of the hybrid type. [2]

2.3.5. Semi-Active Dampers

Following extensive work in both active and passive control, researchers have developed a new generation of control devices, semi-active control, which combine the best features of its parent devices. Possessing the adaptability of active control without the potential for instability, semiactive systems can respond quickly to a sudden gust front or earthquake and provide damping which is excitation-level independent, unlike passive systems which operate at non-optimal values of damping most of the time. Preliminary work indicates that such devices can approach performance levels obtained by active systems without the risk of destabilization or high power requirements. This latter feature is particularly attractive. Since the devices do not introduce mechanical energy into the system, power requirements are relatively low, insuring that the system can remain operational even on battery power during extreme events such as earthquakes. [2]

Since the implementation of TMDs is often restricted by budget and technical constraints, it is important to design a low cost TMD solution that is simple, robust, easy to install and maintenance free. Slender structures like towers, chimneys or minarets are not controlled online by qualified technicians during daily performance. Any solutions to improve dynamic response of such structures should be maintenance free and operate without any power requirement. That is the reason why passive TMDs have such wide application field. Motivated by that, a feasible passive TMD whose design is intended to overcome the aforementioned constraints is presented in this study, in spite of the summarized functional advantageous of active or semi-active TMDs.

3. TUNED MASS DAMPER SYSTEMS

3.1. Introduction

A tuned mass damper (TMD) is a device consisting of a mass, a spring, and a damper that is attached to a structure in order to reduce the dynamic response of the structure. The frequency of the damper is tuned to a particular structural frequency so that when that frequency is excited, the damper will resonate out of phase with the structural motion. Energy is dissipated by the damper force acting on the structure. The TMD concept was first applied by Frahm in 1909 to reduce the rolling motion of ships as well as ship hull vibrations. A theory for the TMD was presented later in the paper by Ormondroyd and Den Hartog in 1928, followed by a detailed discussion of optimal tuning and damping parameters in Den Hartog.[3] The initial theory was applicable for an undamped SDOF system subjected to a sinusoidal force excitation. Extension of the theory to damped SDOF systems has been investigated by numerous researchers. Significant contributions were made by Randall et al.[21], Warburton [22], Warburton and Ayorinde [23], and Tsai and Lin [24].

A rigorous theory of tuned mass dampers for SDOF systems subjected to harmonic force excitation and harmonic ground motion is discussed next. Various cases, including an undamped DVA attached to an undamped SDOF system and a damped TMD attached to an undamped SDOF system.[4]

3.2. Tuned Mass Damper Theory for SDOF Systems

In what follows, various cases ranging from fully undamped to fully damped conditions are analyzed and design procedures are presented.

3.2.1. Undamped Structure: Dynamic Vibration Absorber

When there is not any damping on TMD, the system is called as Dynamic Vibration Absorber (DVA) or Tuned Vibration Absorber (TVA). Figure 3.1 shows a SDOF system having mass m and stiffness k , subjected to both external forcing and ground motion. A DVA with mass m_d and stiffness k_d is attached to the primary mass. The various displacement measures are, the absolute ground motion u_g, the relative motion between the primary mass and the ground u , and the relative displacement between the damper and the primary mass u_d . With this notation, the governing equations take the form

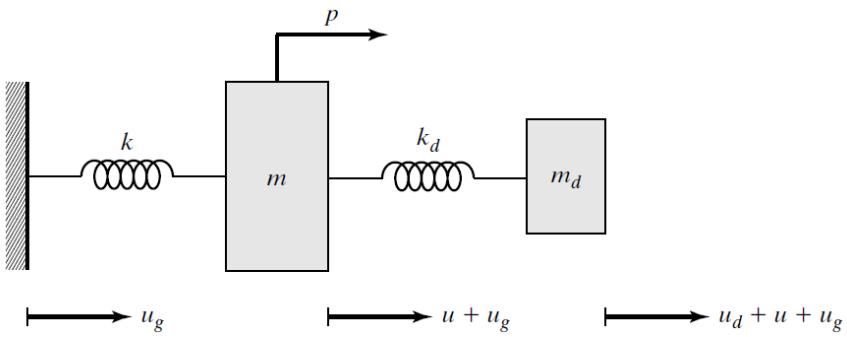

Figure 3.1. SDOF system coupled with a TMD. [4]

$$a_g = \ddot{u}_g$$

$$m_d(\ddot{u}_d + \ddot{u}) + k_d u_d = -m_d a_g \tag{3.1}$$

$$m\ddot{u} + ku - k_d u_d = -ma_g + p \tag{3.2}$$

Where a_g is the absolute ground acceleration and p is the external force applied to the primary mass. The excitation is considered to be periodic of frequency Ω,

$$a_g = \hat{a}_g \sin\Omega t \tag{3.3}$$

$$p = \hat{p} \sin\Omega t \tag{3.4}$$

Expressing the response as

$$u = \hat{u}\, sin\,\Omega t \tag{3.5}$$

$$u_d = \hat{u}_d\, sin\,\Omega t \tag{3.6}$$

and substituting for these variables, the equilibrium equations are transformed to

$$[-m_d\Omega^2 + k_d]\,\hat{u}_d - m_d\Omega^2\hat{u} = -m_d\hat{a}_g \tag{3.7}$$

$$-k_d\hat{u}_d + [-m\Omega^2 + k]\hat{u} = -m\hat{a}_g + \hat{p} \tag{3.8}$$

The solutions for $\hat{u}$ and $\hat{u}_d$ are given by

$$\hat{u} = \frac{\hat{p}}{k}\left(\frac{1-\rho_d^2}{D_1}\right) - \frac{m\hat{a}_g}{k}\left(\frac{1+\overline{m}-\rho_d^2}{D_1}\right) \tag{3.9}$$

$$\hat{u}_d = \frac{\hat{p}}{k_d}\left(\frac{\overline{m}\rho_d^2}{D_1}\right) - \frac{m\hat{a}_g}{k_d}\left(\frac{\overline{m}}{D_1}\right) \tag{3.10}$$

$$\overline{m} = \frac{m_d}{m}$$

where

$$D_1 = [1-\rho^2][1-\rho_d^2] - \overline{m}\rho^2 \tag{3.11}$$

and the ρ terms are dimensionless frequency ratios,

$$\rho = \frac{\Omega}{\omega} = \frac{\Omega}{\sqrt{k/m}} \tag{3.12}$$

$$\rho_d = \frac{\Omega}{\omega_d} = \frac{\Omega}{\sqrt{k_d/m_d}} \tag{3.13}$$

Selecting the mass ratio and damper frequency ratio such that

$$1-\rho_d^2+\bar{m}=0 \tag{3.14}$$

reduces the solution to

$$\hat{u}=\frac{\hat{p}}{k} \tag{3.15}$$

$$\hat{u}_d=-\frac{\hat{p}}{k_d}\rho^2+\frac{m\hat{a}_g}{k_d} \tag{3.16}$$

This choice isolates the primary mass from ground motion and reduces the response due to external force to the pseudo static value $\hat{p}/k$. A typical range for $\bar{m}$ is 0.01 to 0.1. Then the optimal damper frequency is very close to the forcing frequency. The exact relationship follows from Eq. 3.14;

$$\omega_{\mathrm{d}}\,|_{\mathrm{opt}}=\frac{\Omega}{\sqrt{1+\bar{m}}} \tag{3.17}$$

We determine the corresponding damper stiffness with

$$k_d\,|_{opt}=[\omega_d\,|_{opt}]^2 m_d=\frac{\Omega^2 m\bar{m}}{1+\bar{m}} \tag{3.18}$$

Finally, using Eq. 3.18 in Eq. 3.16 gives;

$$\hat{u}_d=\frac{1+\bar{m}}{\bar{m}}\left[\left|\frac{\hat{p}}{k}\right|+\left|\frac{\hat{a}_g}{\Omega^2}\right|\right] \tag{3.19}$$

We specify the amount of relative displacement for the damper and determine $\bar{m}$ with Eq. 3.19. Given $\bar{m}$ and Ω, the stiffness is found using Eq. 3.18. It should be noted that this stiffness applies for a particular forcing frequency. Once the mass damper properties are defined, Eq. 3.9 and 3.10 can be used to determine the response for a

different forcing frequency. The primary mass will move under ground motion excitation in this case.

3.2.2. Undamped Structure: Tuned Mass Damper

When damping is included in a Dynamic Vibration Absorber, then it is called as Tuned Mass Damper. Typical TMD configuration is shown in Figure 3.2. The equations of motion for this case are

$$m_d\ddot{u}_d + c_d\dot{u}_d + k_d u_d + m_d\ddot{u} = -m_d a_g \tag{3.20}$$

$$m\ddot{u} + ku - c_d\dot{u}_d - k_d u_d = -ma_g + p \tag{3.21}$$

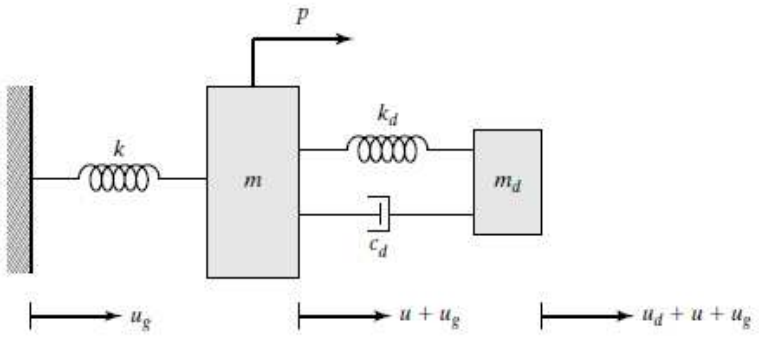

Figure 3.2. Undamped SDOF system coupled with a damped TMD system. [4]

The inclusion of the damping terms in Eq. 3.20 and 3.21 produces a phase shift between the periodic excitation and the response. It is convenient to work initially with the solution expressed in terms of complex quantities. We express the excitation as

$$a_g = \hat{a}_g e^{i\Omega t} \tag{3.22}$$

$$p = \hat{p}\, e^{i\Omega t} \tag{3.23}$$

Where $\hat{a}_g$ and $\hat{p}$ are real quantities. The response is taken as

$$u = \overline{u}e^{i\Omega t} \tag{3.24}$$

$$u_d = \overline{u}_d e^{i\Omega t} \tag{3.25}$$

Where the response amplitudes, $\overline{u}$ and $\overline{u}_d$, are considered to be complex quantities. The real and imaginary parts of a_g correspond to cosine and sine input. Then the corresponding solution is given by either the real (for cosine) or imaginary (for sine) parts of u and u_d. Substituting Eq. 3.24 and 3.25 in the set of governing equations and cancelling $e^{i\Omega t}$ from both sides results in

$$[m_d\Omega^2 + ic_d\Omega + k_d]\overline{u}_d - m_d\Omega^2\overline{u} = -m_d\hat{a}_g \tag{3.26}$$

$$-[ic_d\Omega + k_d]\overline{u}_d + [-m\Omega^2 + k]\overline{u} = -m\hat{a}_g + \hat{p} \tag{3.27}$$

The solution of the governing equations is

$$\overline{u} = \frac{\hat{p}}{kD_2}[f^2 - \rho^2 + i2\xi_d f\rho] - \frac{\hat{a}_g m}{kD_2}[(1+\overline{m})f^2 - \rho^2 + i2\xi_d f\rho(1+\overline{m})] \tag{3.28}$$

where $$\xi_d = \frac{c_d}{2\omega_d m_d}$$

$$\overline{u}_d = \frac{\hat{p}\rho^2}{kD_2} - \frac{\hat{a}_g m}{kD_2} \tag{3.29}$$

Where

$$D_2 = [1-\rho^2][f^2 - \rho^2] - \overline{m}f^2\rho^2 + i2\xi_d f\rho[1-\rho^2(1+\overline{m})] \tag{3.30}$$

$$f = \frac{\omega_d}{\omega} \tag{3.31}$$

and ρ was defined earlier as the ratio of Ω to ω [see Eq. 3.12].

Converting the complex solutions to polar form leads to the following expressions:

$$\overline{u} = \frac{\hat{p}}{k} H_1 e^{i\delta_1} - \frac{\hat{a}_g m}{k} H_2 e^{i\delta_2} \tag{3.32}$$

$$\overline{u}_d = \frac{\hat{p}}{k} H_3 e^{-i\delta_3} - \frac{\hat{a}_g m}{k} H_4 e^{-i\delta_3} \tag{3.33}$$

Where the H factors define the amplification of the pseudo-static responses, and the δ's are the phase angles between the response and the excitation. The various H and δ terms are as follows:

$$H_1 = \frac{\sqrt{[f^2 - \rho^2]^2 + [2\xi_d f \rho]^2}}{|D_2|} \tag{3.34}$$

$$H_2 = \frac{\sqrt{[(1+\overline{m}) f^2 - \rho^2]^2 + [2\xi_d f \rho (1+\overline{m})]^2}}{|D_2|} \tag{3.35}$$

$$H_3 = \frac{\rho^2}{|D_2|} \tag{3.36}$$

$$H_4 = \frac{1}{|D_2|} \tag{3.37}$$

$$|D_2| = \sqrt{([1-\rho^2][f^2 - \rho^2] - \overline{m} f^2 \rho^2)^2 + (2\xi_d f \rho [1 - \rho^2 (1+\overline{m})])^2} \tag{3.38}$$

Also

$$\delta_1 = \alpha_1 - \delta_3 \tag{3.39}$$

$$\delta_2 = \alpha_2 - \delta_3 \tag{3.40}$$

$$\tan\delta_3 = \frac{2\xi_d f\rho[1-\rho^2(1+\bar{m})]}{[1-\rho^2][f^2-\rho^2]-\bar{m}f^2\rho^2} \tag{3.41}$$

$$\tan\alpha_1 = \frac{2\xi_d f\rho}{f^2-\rho^2} \tag{3.42}$$

$$\tan\alpha_2 = \frac{2\xi_d f\rho(1+\bar{m})}{(1+\bar{m})f^2-\rho^2} \tag{3.43}$$

For most applications, the mass ratio is less than about 0.05. Then the amplification factors for external loading (H_1) and ground motion (H_2) are essentially equal. A similar conclusion applies for the phase shift. In what follows, the solution corresponding to ground motion is examined and the optimal values of the damper properties for this loading condition are established. An in-depth treatment of the external forcing case is contained in Den Hartog's text. [3]

Figure 3.3 shows the variation of (H_2) with forcing frequency for specific values of damper mass $\bar{m}$ and frequency ratio , and various values of the damper damping ratio, ξ_d. When $\xi_d = 0$, there are two peaks with infinite amplitude located on each side of $\rho = 1$. As ξ_d is increased, the peaks approach each other and then merge into a single peak located at $\rho \approx 1$. The behavior of the amplitudes suggests that there is an optimal value of ξ_d for a given damper configuration (m_d and k_d or, equivalently, $\bar{m}$ and f). Another key observation is that all the curves pass through two common points, *P* and *Q*. Since these curves correspond to different values of ξ_d, the location of *P* and *Q* must depend only on $\bar{m}$ and f. Proceeding with this line of reasoning, the expression for H_2 can be written as

$$H_2 = \sqrt{\frac{a_1^2+\xi_d^2 a_2^2}{a_3^2+\xi_d^2 a_4^2}} = \frac{a_2}{a_4}\sqrt{\frac{a_1^2/a_2^2+\xi_d^2}{a_3^2/a_4^2+\xi_d^2}} \tag{3.44}$$

$$a_1 = (1+\bar{m})f^2-\rho^2 \qquad a_2 = 2f\rho(1+\bar{m})$$

$$a_3 = [1-\rho^2][f^2-\rho^2]-\bar{m}f^2\rho^2 \qquad a_4 = 2f\rho[1-\rho^2(1+\bar{m})]$$

As seen above, the a_i terms are functions of $\bar{m}$, ρ, and f. Then for H_2 to be independent of ξ_d, the following condition must be satisfied:

$$\left|\frac{a_1}{a_2}\right| = \left|\frac{a_3}{a_4}\right| \tag{3.45}$$

The corresponding values for H_2 are

$$H_2|_{P,Q} = \left|\frac{a_2}{a_4}\right| \tag{3.46}$$

Substituting for the a_i terms in Eq. 3.45, we obtain a quadratic equation for ρ^2:

$$\rho^4 - [(1+\bar{m})f^2 + \frac{(1+0.5\bar{m})}{(1+\bar{m})}]\rho^2 + f^2 = 0 \tag{3.47}$$

The two positive roots ρ_1 and ρ_2 are the frequency ratios corresponding to points P and Q. Similarly, Eq. 3.46 expands to

$$H_2|_{P,Q} = \frac{1+\bar{m}}{\left|1-\rho_{1,2}^2(1+\bar{m})\right|} \tag{3.48}$$

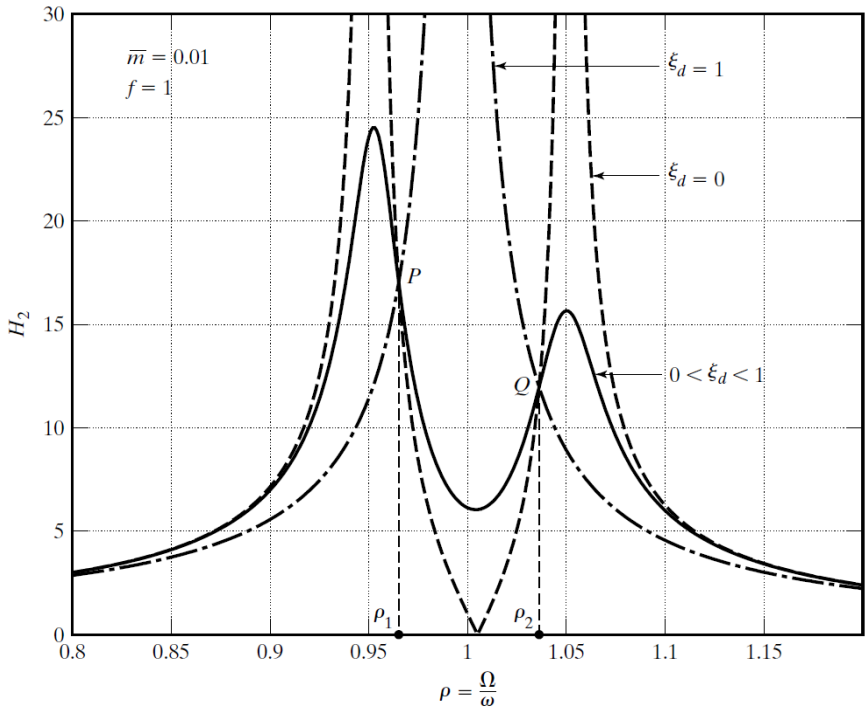

Figure 3.3. Plot of H_2 versus ρ [4]

Figure 3.3 shows different values for H_2 at points P and Q. For optimal behavior, we want to minimize the maximum amplitude. As a first step, we require the values of H_2 for ρ_1 and ρ_2 to be equal. This produces a distribution that is symmetrical about $\rho^2 = 1/(1+\bar{m})$, as illustrated in Figure 3.4. Then, by increasing the damping ratio ξ_d, we can lower the peak amplitudes until the peaks coincide with points P and Q. This state represents the optimal performance of the TMD system. A further increase in ξ_d causes the peaks to merge and the amplitude to increase beyond the optimal value.

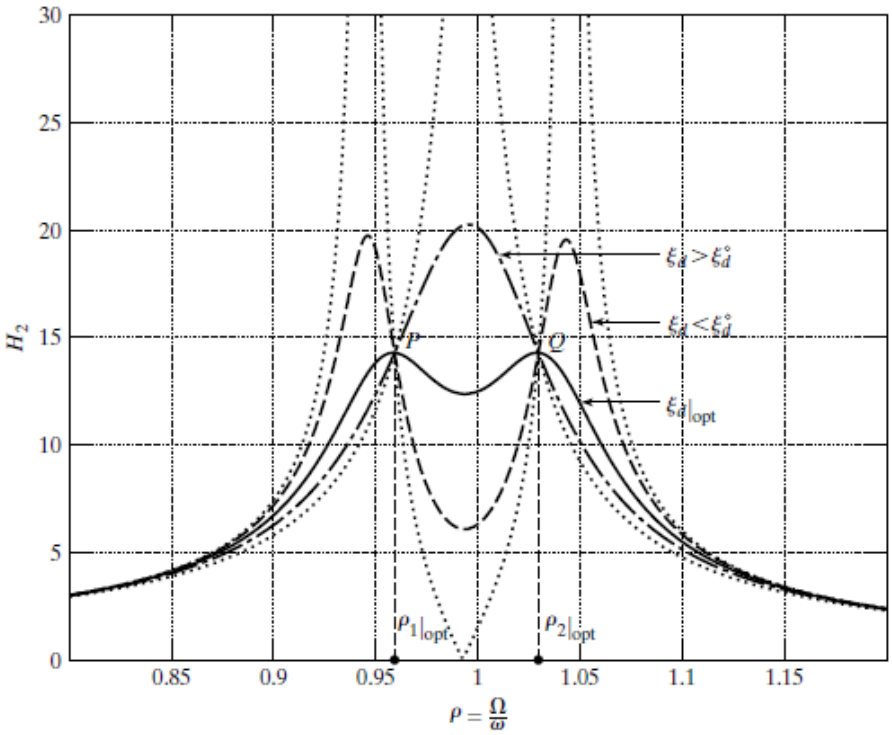

Figure 3.4. Plot of H_2 versus ρ for f_{opt}. [4]

Requiring the amplitudes to be equal at P and Q is equivalent to the following condition on the roots:

$$\left|1-\rho_1^2(1+\bar{m})\right| = \left|1-\rho_2^2(1+\bar{m})\right| \tag{3.49}$$

Then, substituting for ρ_1 and ρ_2 using Eq. 3.47, we obtain a relation between the optimal tuning frequency and the mass ratio:

$$f_{opt} = \frac{\sqrt{1-0.5\bar{m}}}{1+\bar{m}} \tag{3.50}$$

$$\omega_{\mathrm{d}}|_{opt} = f_{opt}\omega \tag{3.51}$$

The corresponding roots and optimal amplification factors are

$$\rho_{1,2}|_{opt} = \sqrt{\frac{\sqrt{1 \pm 0.5\bar{m}}}{1+\bar{m}}} \tag{3.52}$$

$$H_2|_{opt} = \frac{1+\bar{m}}{\sqrt{0.5\bar{m}}} \tag{3.53}$$

The expression for the optimal damping at the optimal tuning frequency is

$$\xi_d|_{opt} = \sqrt{\frac{\bar{m}(3-\sqrt{0.5\bar{m}})}{8(1+\bar{m})(1-0.5\bar{m})}} \tag{3.54}$$

Figure 3.5 through Figure 3.8 show the variation of the optimal parameters with the mass ratio $\bar{m}$. The response of the damper is defined by Eq. 3.33. Specializing this equation for the optimal conditions leads to the plot of amplification versus mass ratio contained in Figure 3.9. A comparison of the damper motion with respect to the motion of the primary mass for optimal conditions is shown in Figure 3.10.

Lastly, response curves for a typical mass ratio, $\bar{m} = 0.01$, and optimal tuning are plotted in Figure 3.11 and Figure 3.12. The response for no damper is also plotted in Figure 3.11. We observe that the effect of the damper is to limit the motion in a frequency range centered on the natural frequency of the primary mass and extending about 0.15ω. Outside of this range, the motion is not significantly influenced by the damper.

The maximum amplification for a damped SDOF system without a TMD, undergoing harmonic excitation, is given as:

$$H = \frac{1}{2\xi\sqrt{1-\xi^2}} \tag{3.55}$$

Where: $$\xi = \frac{c}{2\omega\, m}$$

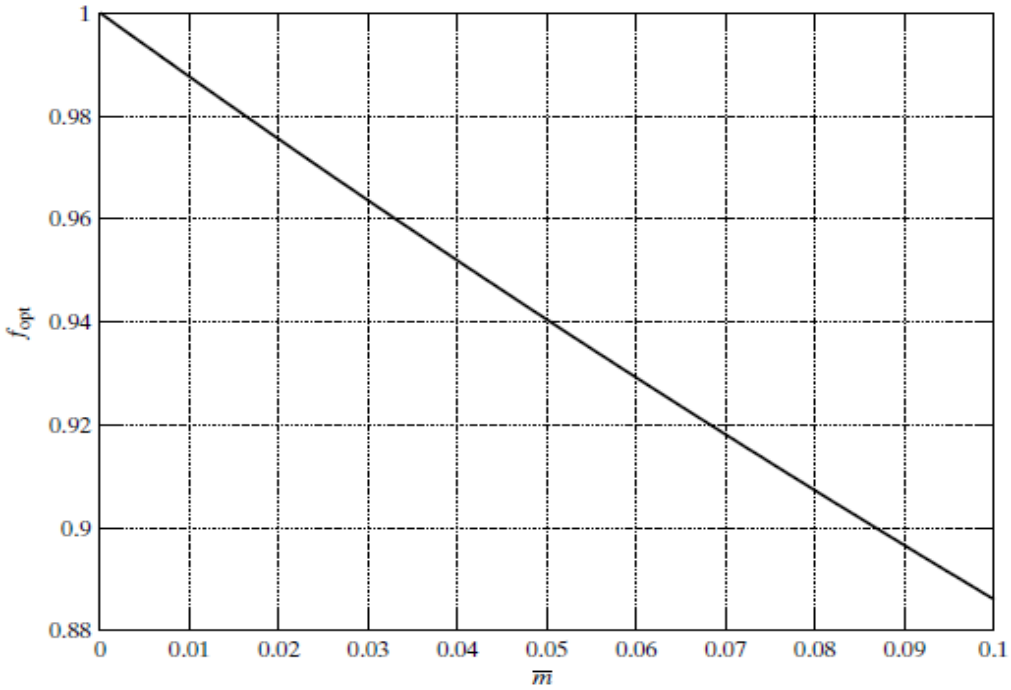

Figure 3.5. Optimum tuning frequency ratio, f_{opt}[4]

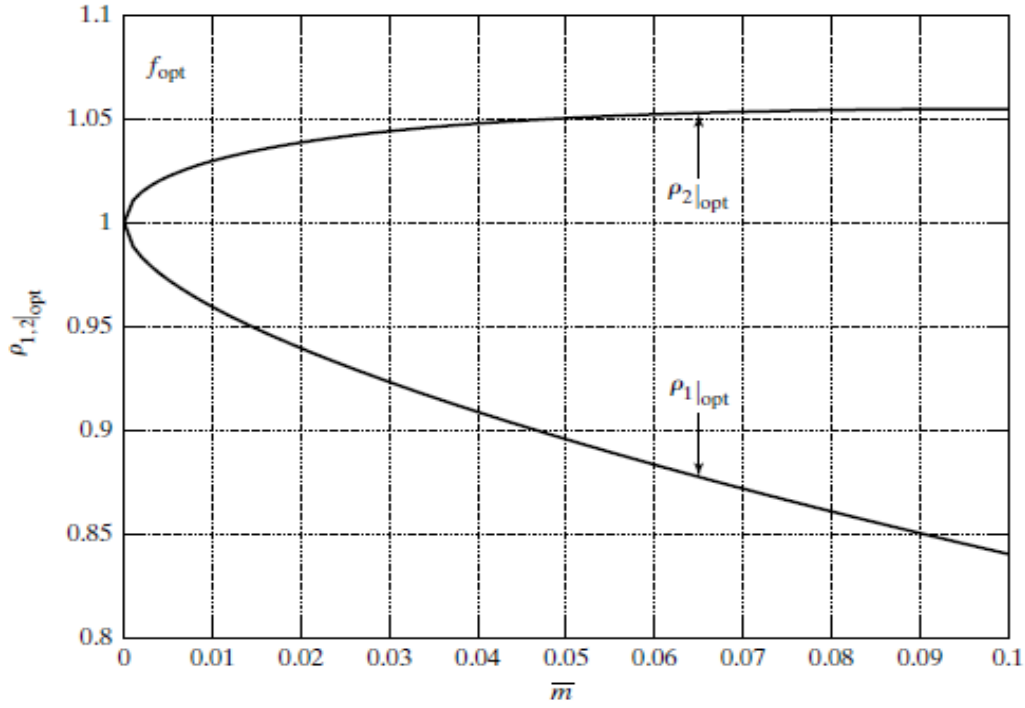

Figure 3.6. Input frequency ratios at which the response is independent of damping. [4]

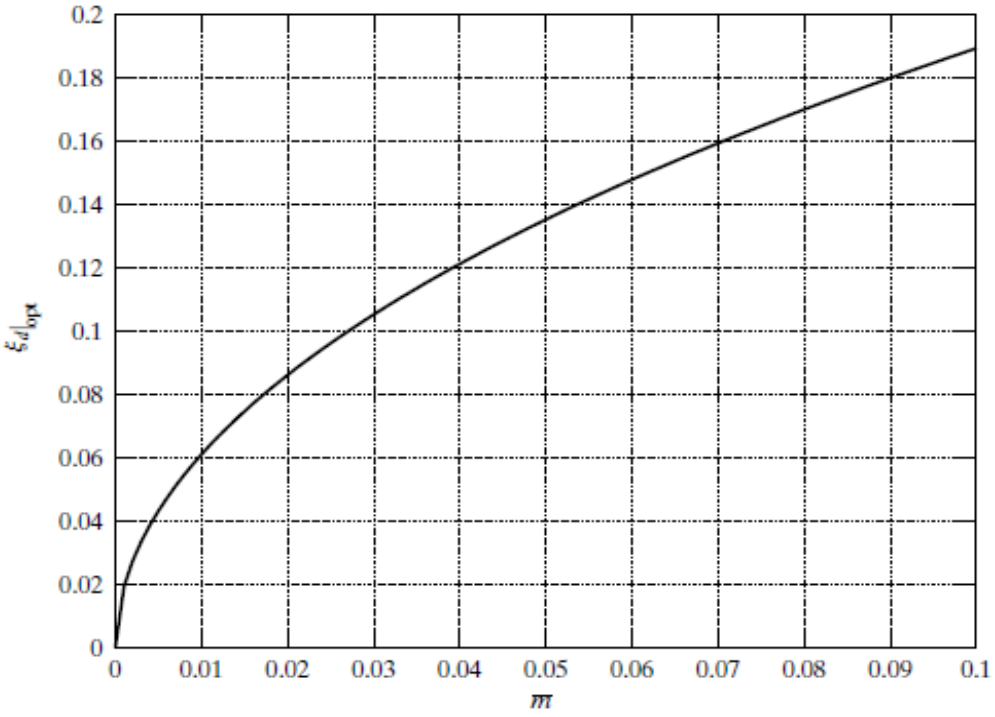

Figure 3.7. Optimal damping ratio for TMD. [4]

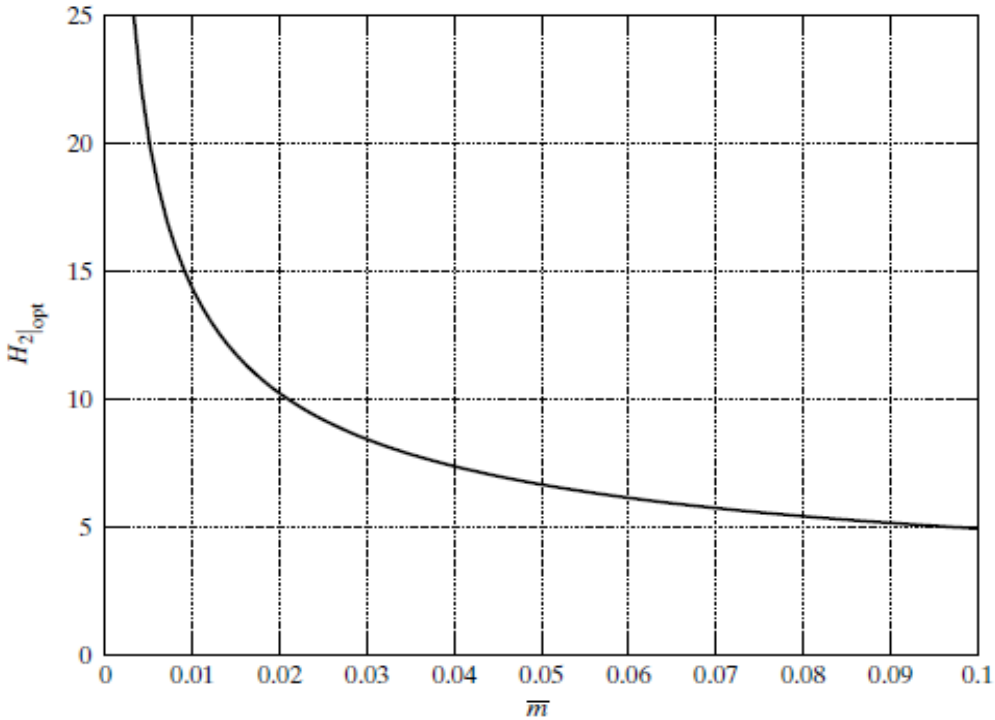

Figure 3.8. Maximum dynamic amplification factor for SDOF system (optimal tuning and damping). [4]

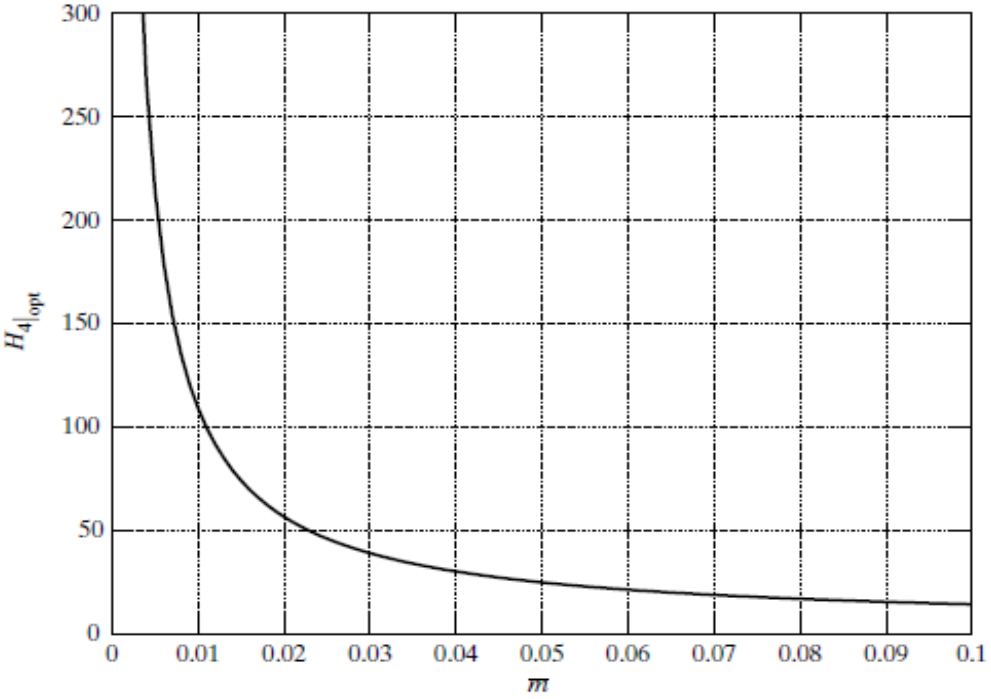

Figure 3.9. Maximum dynamic amplification factor for TMD. [4]

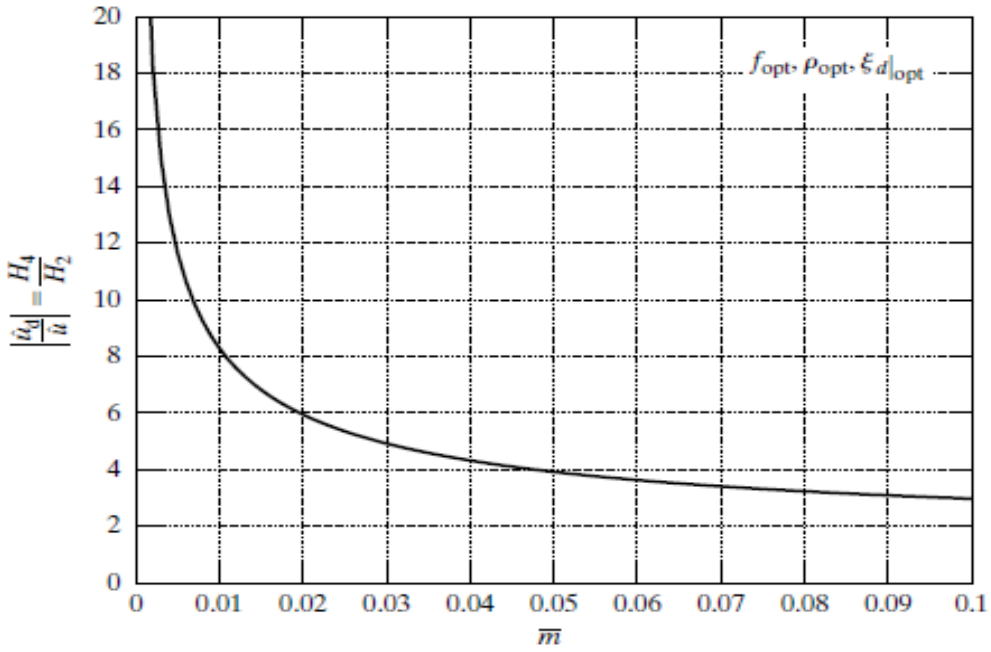

Figure 3.10. Ratio of maximum TMD amplitude to maximum system amplitude. [4]

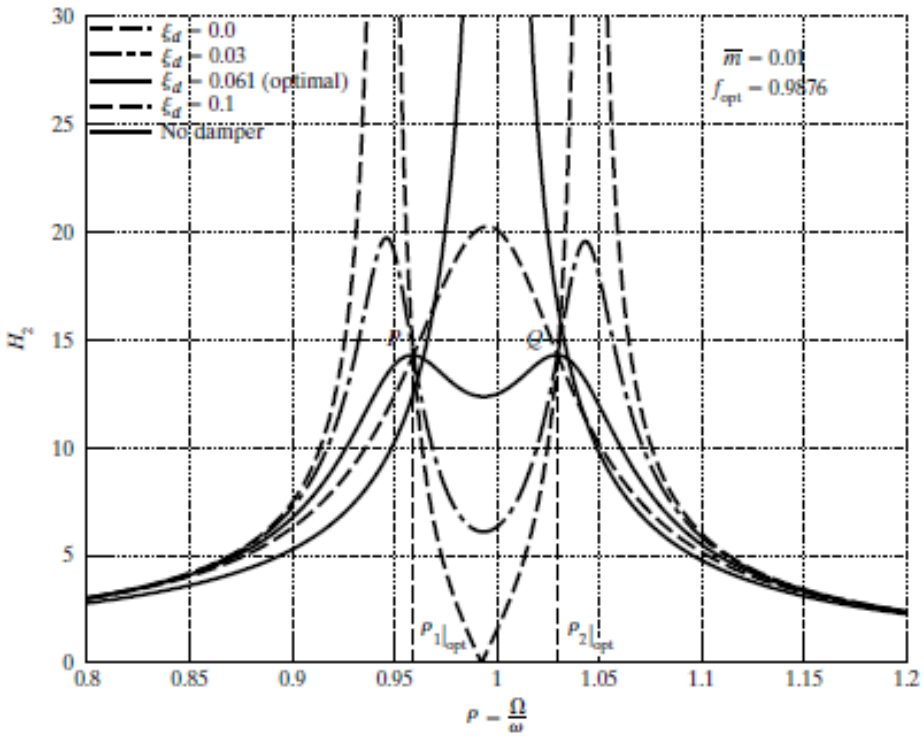

Figure 3.11. Response curves for amplitude of system with optimally tuned TMD. [4]

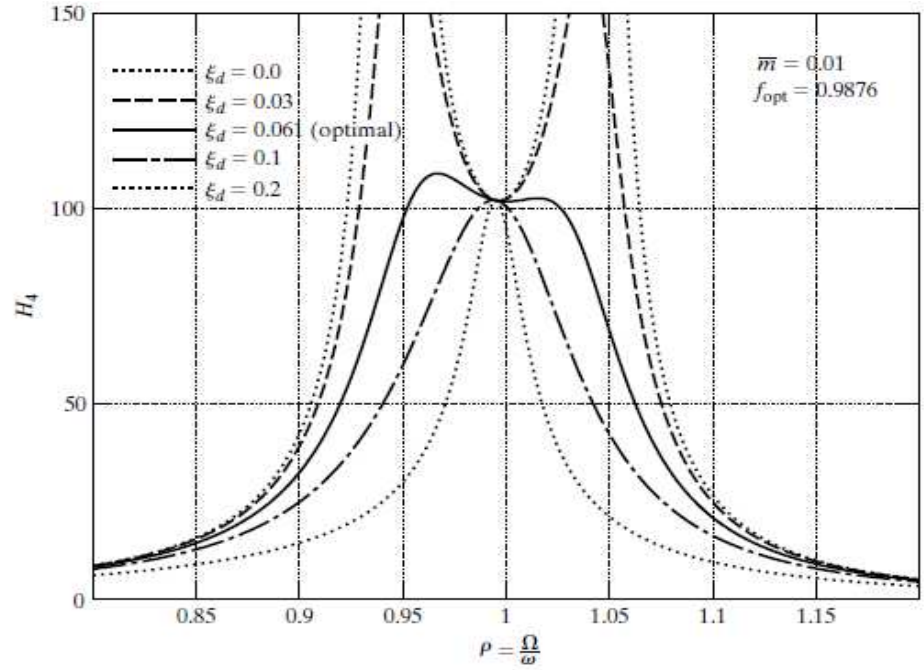

Figure 3.12. Response curves for amplitude of optimally tuned TMD. [4]

Since ξ is small, a reasonable approximation is

$$H \approx \frac{1}{2\xi} \tag{3.56}$$

Expressing the optimal H_2 in a similar form provides a measure of the equivalent damping ratio ξ_e for the primary mass:

$$\xi_e = \frac{1}{2H_2|_{\text{opt}}} \tag{3.57}$$

Figure 3.13 shows the variation of ξ_e with the mass ratio. A mass ratio of 0.02 is equivalent to about 5% damping in the primary system.

The design of a TMD involves the following steps:

- Establish the allowable values of displacement of the primary mass and the TMD for the design loading. This data provides the design values for $H_2|_{\text{opt}}$ and $H_4|_{\text{opt}}$.

- Determine the mass ratios required to satisfy these motion constraints from Figure 3.8 and Figure 3.9 Select the largest value of $\bar{m}$.

- Determine f_{opt} form Figure 3.5.

- Compute ω_d :

$$\omega_d = f_{opt}\ \omega \tag{3.58}$$

- Compute k_d :

$$k_d = m_d\ \omega_d^2 = \bar{m}\ k\ f_{opt}^2 \tag{3.59}$$

- Determine $\xi_d|_{\text{opt}}$ from Figure 3.7.

- Compute c_d :

$$c_d = 2\xi_d|_{\text{opt}}\ m_d\ \omega_d = \bar{m}\ f_{opt}\ [2\xi_{\text{d}}|_{\text{opt}}\ m\ \omega] \tag{3.60}$$

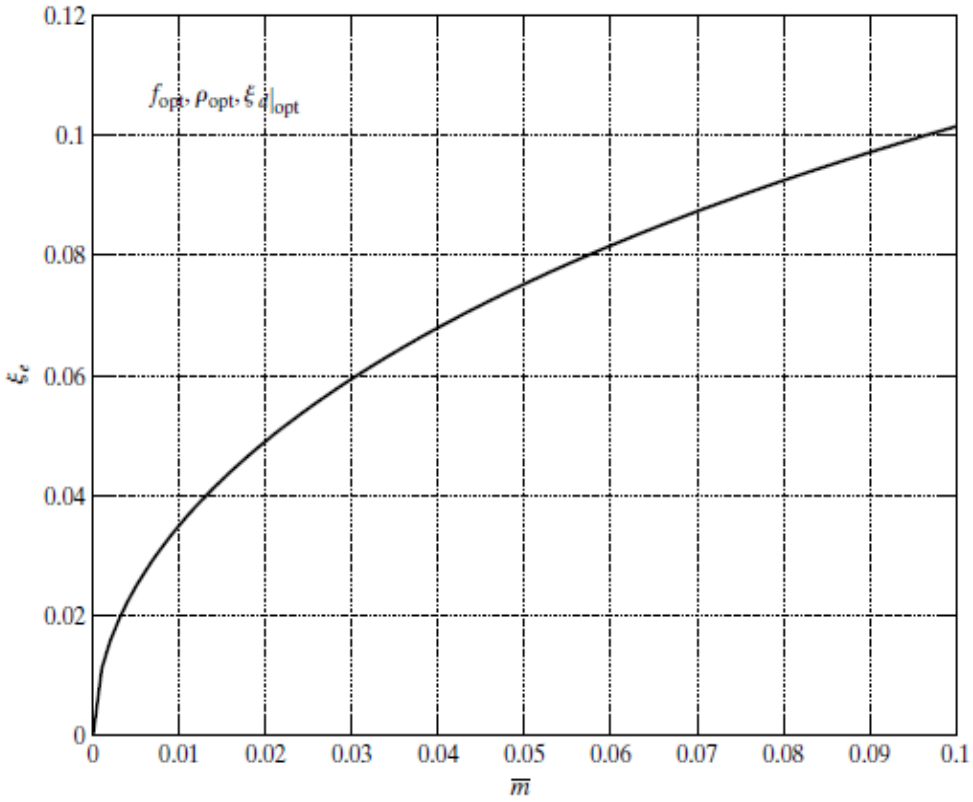

Figure 3.13. Equivalent damping ratio for optimally tuned TMD. [4]

3.3. Examples of Existing Tuned Mass Damper Systems

Although the majority of applications have been for mechanical systems, tuned mass dampers have been used to improve the response of building structures under wind and earthquake excitation. A short description of the various types of dampers and several building structures that contain tuned mass dampers follows.

3.3.1. Translational Tuned Mass Dampers

Figure 3.14 illustrates the typical configuration of a unidirectional translational tuned mass damper. The mass rests on bearings that function as rollers and allow the mass to translate laterally relative to the floor. Springs and dampers are inserted between the mass and the adjacent vertical support members, which transmit the lateral "out-of-phase" force to the floor level and then into the structural frame. Bidirectional translational dampers are configured with springs/dampers in two orthogonal directions and provide the capability for controlling structural motion in two orthogonal planes. Some examples of early versions of this type of damper are described next.[4]

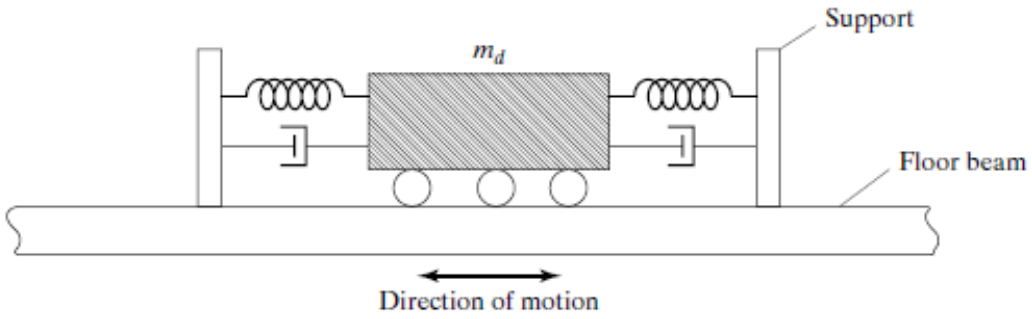

Figure 3.14. Schematic diagram of a translational tuned mass damper. [4]

John Hancock Tower: Two dampers were added to the 60-story John Hancock Tower in Chicago to reduce the response to wind gust loading. The dampers are placed at opposite ends of the fifty-eighth story, 67 m apart, and move to counteract sway as well as twisting due to the shape of the building. Each damper weighs 2700 kN and consists of a lead-filled steel box about 5.2 m square and 1 m deep that rides on a 9 m long steel plate. The lead-filled weight, laterally restrained by stiff springs anchored to the interior columns

of the building and controlled by servo-hydraulic cylinders, slides back and forth on a hydrostatic bearing consisting of a thin layer of oil forced through holes in the steel plate. Whenever the horizontal acceleration exceeds 0.003g for two consecutive cycles, the system is automatically activated. This system was designed and manufactured by LeMessurier Associates/SCI in association with MTS System Corp., at a cost of around 3 million dollars, and is expected to reduce the sway of the building by 40 to 50 %. [4]

Citicorp Center: The Citicorp (Manhattan) TMD was also designed and manufactured by LeMessurier Associates/SCI in association with MTS System Corp. This building is 279 m high and has a fundamental period of around 6.5 s with an inherent damping ratio of 1% along each axis. The Citicorp TMD, located on the sixty-third floor in the crown of the structure, has a mass of 366 Mg, about 2 % of the effective modal mass of the first mode, and was 250 times larger than any existing tuned mass damper at the time of installation. Designed to be biaxially resonant on the building structure with a variable operating period of 6.25s ± 20 %, adjustable linear damping from 8 to 14 %, and a peak relative displacement of ±1.4m, the damper is expected to reduce the building sway amplitude by about 50 %. This reduction corresponds to increasing the basic structural damping by 4 %. The concrete mass block is about 2.6 m high with a plan cross section of 9.1 m by 9.1 m and is supported on a series of twelve 60 cm diameter hydraulic pressure-balanced bearings. During operation, the bearings are supplied oil from a separate hydraulic pump, which is capable of raising the mass block about 2 cm to its operating position in about 3 minutes. The damper system is activated automatically whenever the horizontal acceleration exceeds 0.003g for two consecutive cycles and will automatically shut itself down when the building acceleration does not exceed 0.00075g in either axis over a 30-minute interval. LeMessurier estimates Citicorp's TMD, which cost about 1.5 million dollars, saved 3.5 to 4 million dollars. This sum represents the cost of some 2800 tons of structural steel that would have been required to satisfy the deflection constraints. [4]

Canadian National Tower: The 102 m steel antenna mast on top of the Canadian National Tower in Toronto (553 m high including the antenna) required two lead dampers to prevent the antenna from deflecting excessively when subjected to wind excitation. The damper system consists of two doughnut-shaped steel rings, 35 cm wide, 30 cm deep, and

2.4 m and 3 m in diameter, located at elevations 488 m and 503 m. Each ring holds about 9 metrictons of lead and is supported by three steel beams attached to the sides of the antenna mast. Four bearing universal joints that pivot in all directions connect the rings to the beams. In addition, four separate hydraulically activated fluid dampers mounted on the side of the mast and attached to the center of each universal joint dissipate energy. As the lead weighted rings move back and forth, the hydraulic damper system dissipates the input energy and reduces the tower's response. The damper system was designed by Nicolet, Carrier, Dressel, and Associates, Ltd., in collaboration with Vibron Acoustics, Ltd. The dampers are tuned to the second and fourth modes of vibration in order to minimize antenna bending loads; the first and third modes have the same characteristics as the prestressed concrete structure supporting the antenna and did not require additional damping. [4]

Chiba Port Tower: Chiba Port Tower (completed in 1986) was the first tower in Japan to be equipped with a TMD. Chiba Port Tower is a steel structure 125 m high weighing 1950 metric tons and having a rhombus-shaped plan with a side length of 15 m. The first and second mode periods are 2.25 s and 0.51 s, respectively for the *x* direction and 2.7 s and 0.57 s for the *y* direction. Damping for the fundamental mode is estimated at 0.5 %. Damping ratios proportional to frequencies were assumed for the higher modes in the analysis. The purpose of the TMD is to increase damping of the first mode for both the *x* and *y* directions. Figure 3.15 shows the damper system. Manufactured by Mitsubishi Steel Manufacturing Co., Ltd., the damper has mass ratios with respect to the modal mass of the first mode of about 1/120 in the *x* direction and 1/80 in the *y* direction; periods in the *x* and *y* directions of 2.24 s and 2.72 s, respectively; and a damper damping ratio of 15 %. The maximum relative displacement of the damper with respect to the tower is about ±1 m in each direction. Reductions of around 30 to 40% in the displacement of the top floor and 30 % in the peak bending moments are expected. The early versions of TMDs employ complex mechanisms for the bearing and damping elements, have relatively large masses, occupy considerable space, and are quite expensive. Recent versions, such as the scheme shown in Figure 3.16. have been designed to minimize these limitations. This scheme employs a multi assembly of elastomeric rubber bearings, which function as shear springs, and bitumen rubber compound (BRC) elements, which provide viscoelastic damping capability. The device is compact in size, requires unsophisticated controls, is

multidirectional, and is easily assembled and modified. Figure 3.17 shows a full-scale damper being subjected to dynamic excitation by a shaking table. An actual installation is contained in Figure 3.18. [4]

Figure 3.15. Tuned mass damper for Chiba-Port Tower. [4]

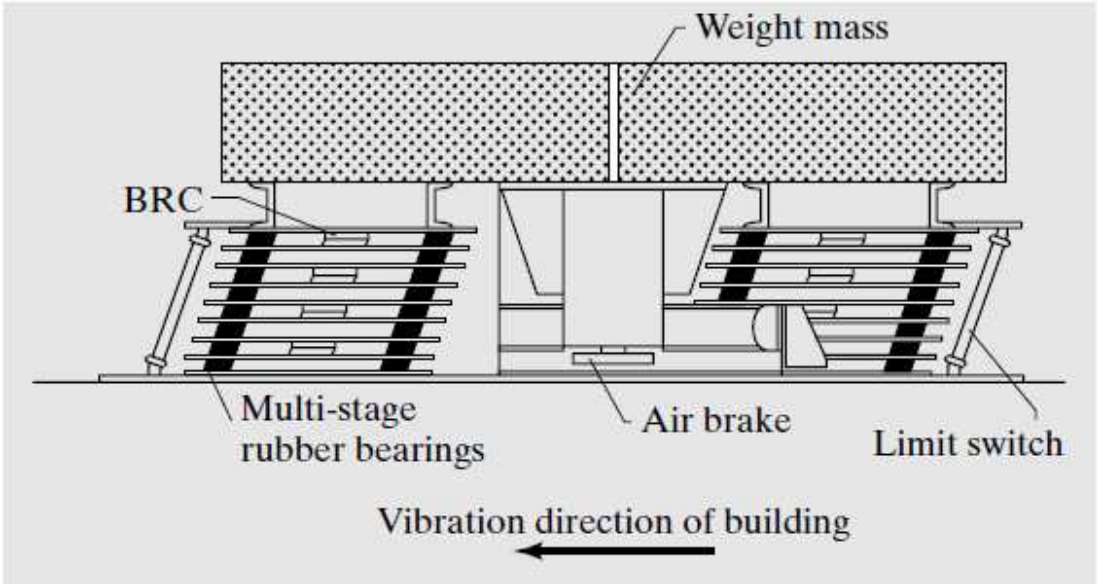

Figure 3.16. Tuned mass damper with spring and damper assemblage. [4]

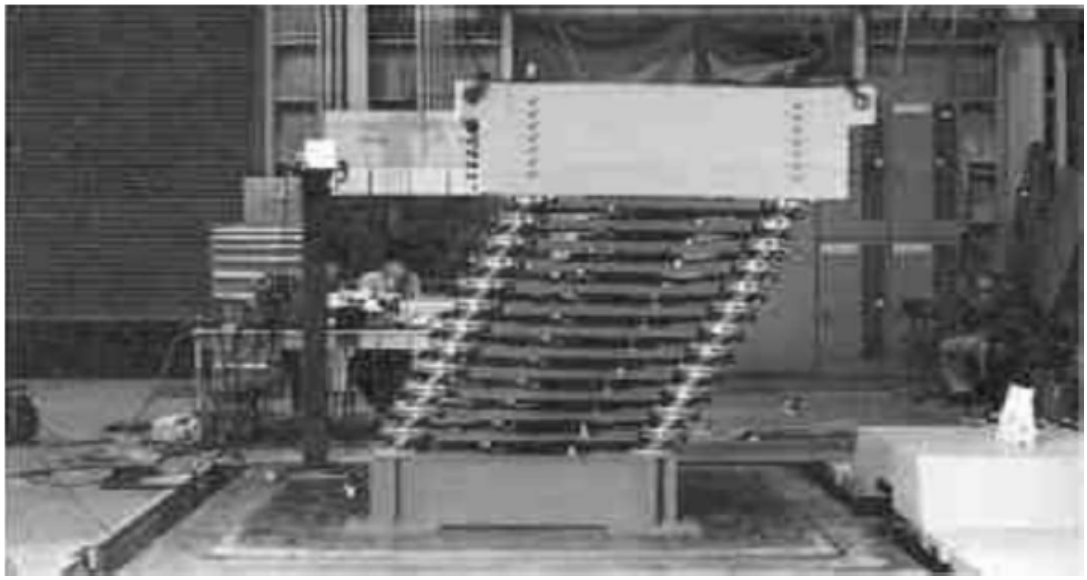

Figure 3.17. Deformed position—tuned mass damper. [4]

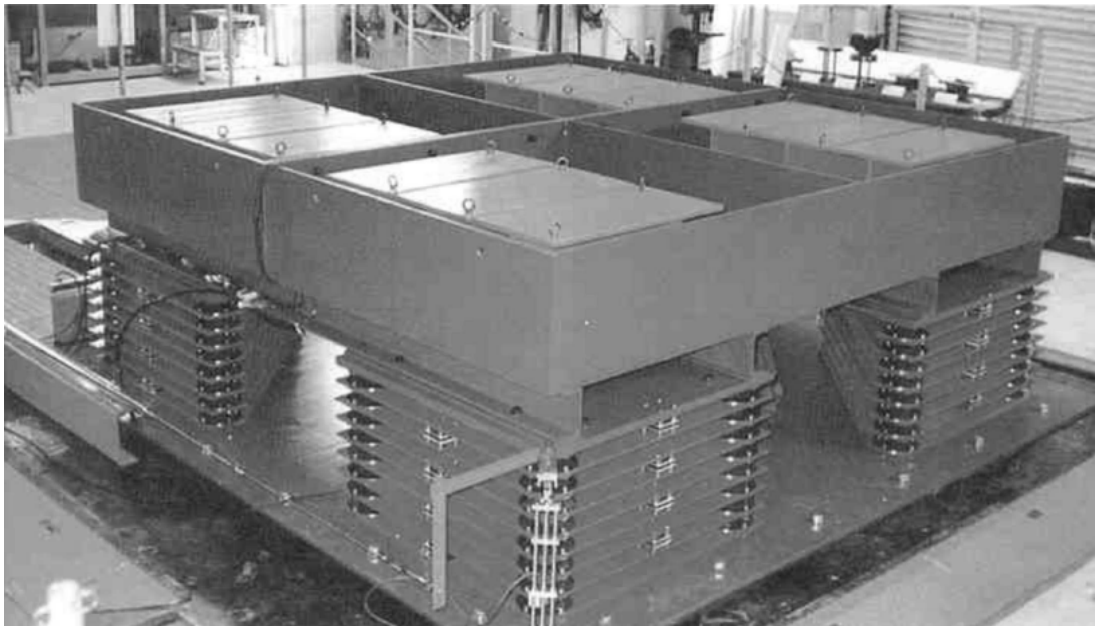

Figure 3.18. Tuned mass damper - Huis Ten Bosch Tower, Nagasaki. [4]

3.3.2. Pendulum Tuned Mass Dampers

The problems associated with the bearings can be eliminated by supporting the mass with cables which allow the system to behave as a pendulum. Figure 3.19a shows a simple

pendulum attached to a floor. Movement of the floor excites the pendulum. The relative motion of the pendulum produces a horizontal force that opposes the floor motion. This action can be represented by an equivalent SDOF system that is attached to the floor, as indicated in Figure 3.19b. The equation of motion for the horizontal direction is

$$T\,sin\theta + m_d(\ddot{u} + \ddot{u}_d) = 0 \tag{3.61}$$

where T is the tension in the cable. When θ is small, the following approximations apply:

$$u_d = L\,sin\theta \approx L\,\theta \tag{3.62}$$

$$T \approx m_d\,g \tag{3.63}$$

Introducing these approximations transforms Eq. 3.61 to

$$m_d\ddot{u}_d + \frac{m_d\,g}{L}u_d = -m_d\ddot{u} \tag{3.64}$$

and it follows that the equivalent shear spring stiffness is

$$k_{eq} = \frac{m_d\,g}{L} \tag{3.65}$$

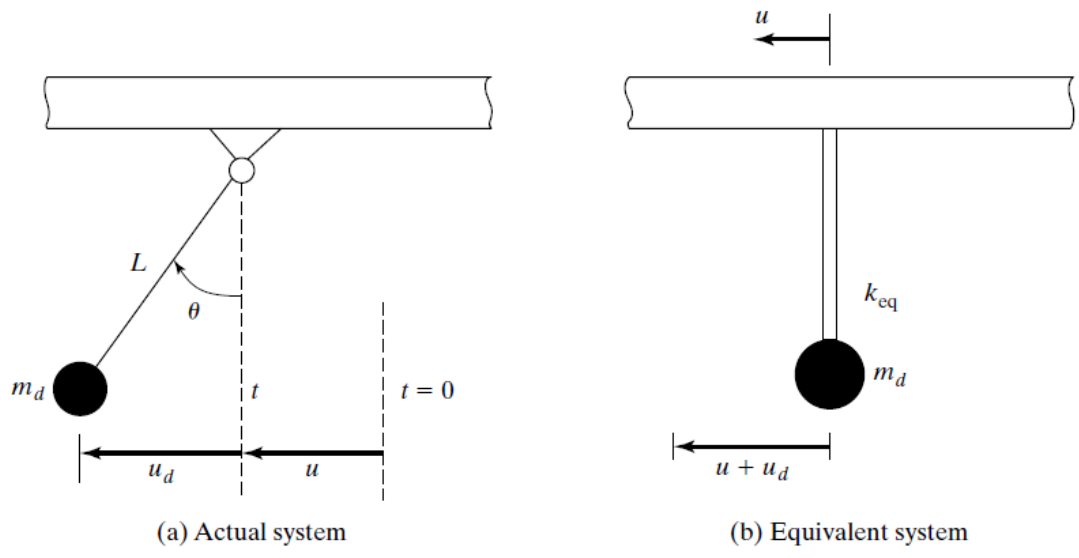

Figure 3.19. A simple pendulum tuned mass damper. [4]

The natural frequency of the pendulum is related to k_{eq} by

$$\omega_d^2 = \frac{k_{eq}}{m_d} = \frac{g}{L} \tag{3.66}$$

Then, the natural period of the pendulum is

$$T_d = 2\pi\sqrt{\frac{L}{g}} \tag{3.67}$$

The simple pendulum tuned mass damper concept has a serious limitation. Since the period depends on L, the required length for large T_d may be greater than the typical story height. For instance, the length for T_d = 5 s is 6.2 meters whereas the story height is between 4 and 5 meters. This problem can be eliminated by resorting to the scheme illustrated in Figure 3.20. The interior rigid link magnifies the support motion for the pendulum and results in the following equilibrium equation:

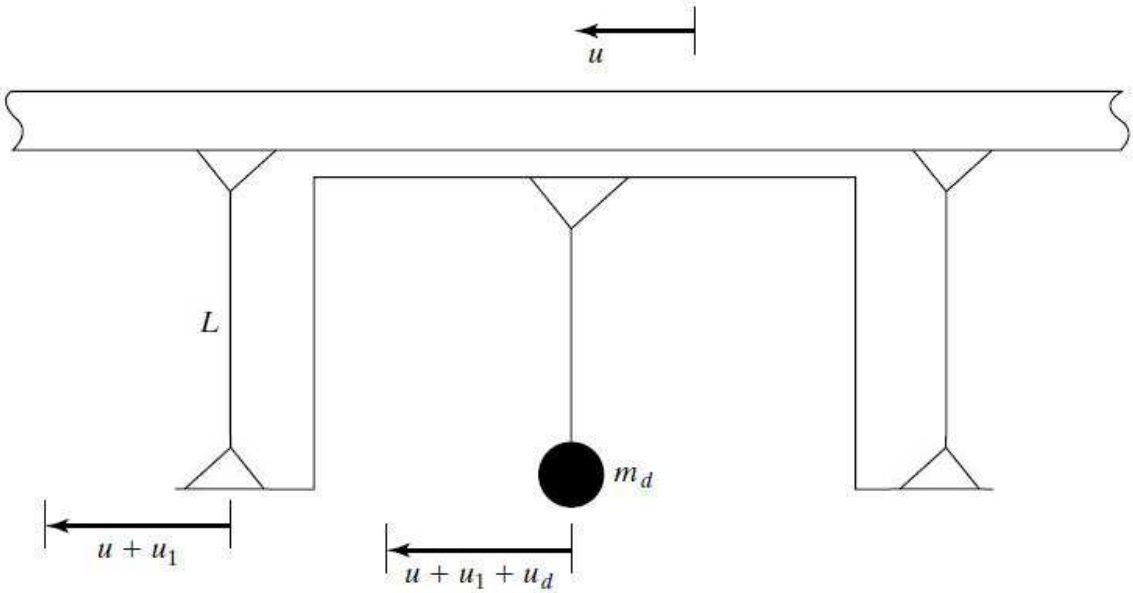

Figure 3.20. Compound pendulum. [4]

$$m_d(\ddot{u}+\ddot{u}_1+\ddot{u}_d)+\frac{m_d\ g}{L}u_d=0 \tag{3.68}$$

The rigid link moves in phase with the damper and has the same displacement amplitude. Then, taking $u_1 = u_d$ in Eq. 3.68 results in

$$m_d\ddot{u}_d+\frac{m_d\ g}{2L}u_d=-\frac{m_d}{2}\ddot{u} \tag{3.69}$$

The equivalent stiffness is $m_d\ g\ /\ 2L$, and it follows that the effective length is equal to $2L$. Each additional link increases the effective length by L. An example of a pendulum-type damper is described next.

Crystal Tower : The tower, located in Osaka, Japan, is 157 m high and 28 m by 67 m in plan, weighs 44000 metric tons, and has a fundamental period of approximately 4 s in the north south direction and 3 s in the east-west direction. A tuned pendulum mass damper was included in the early phase of the design to decrease the wind-induced motion of the building by about 50 %. Six of the nine air cooling and heating ice thermal storage tanks (each weighing 90 tons) are hung from the top roof girders and used as a pendulum mass. Four tanks have a pendulum length of 4 m and slide in the north-south direction; the other two tanks have a pendulum length of about 3 m and slide in the east-west direction. Oil dampers connected to the pendulums dissipate the pendulum energy. Views of the actual building and one of the tanks are presented in Figure 3.21. The cost of this tuned mass damper system was around $350000, less than 0.2 % of the construction cost.

A modified version of the pendulum damper is shown in Figure 3.22. The restoring force provided by the cables is generated by introducing curvature in the support surface and allowing the mass to roll on this surface. The vertical motion of the weight requires an energy input. Assuming θ is small, the equations for the case where the surface is circular are the same as for the conventional pendulum with the cable length L, replaced with the surface radius R. [4]

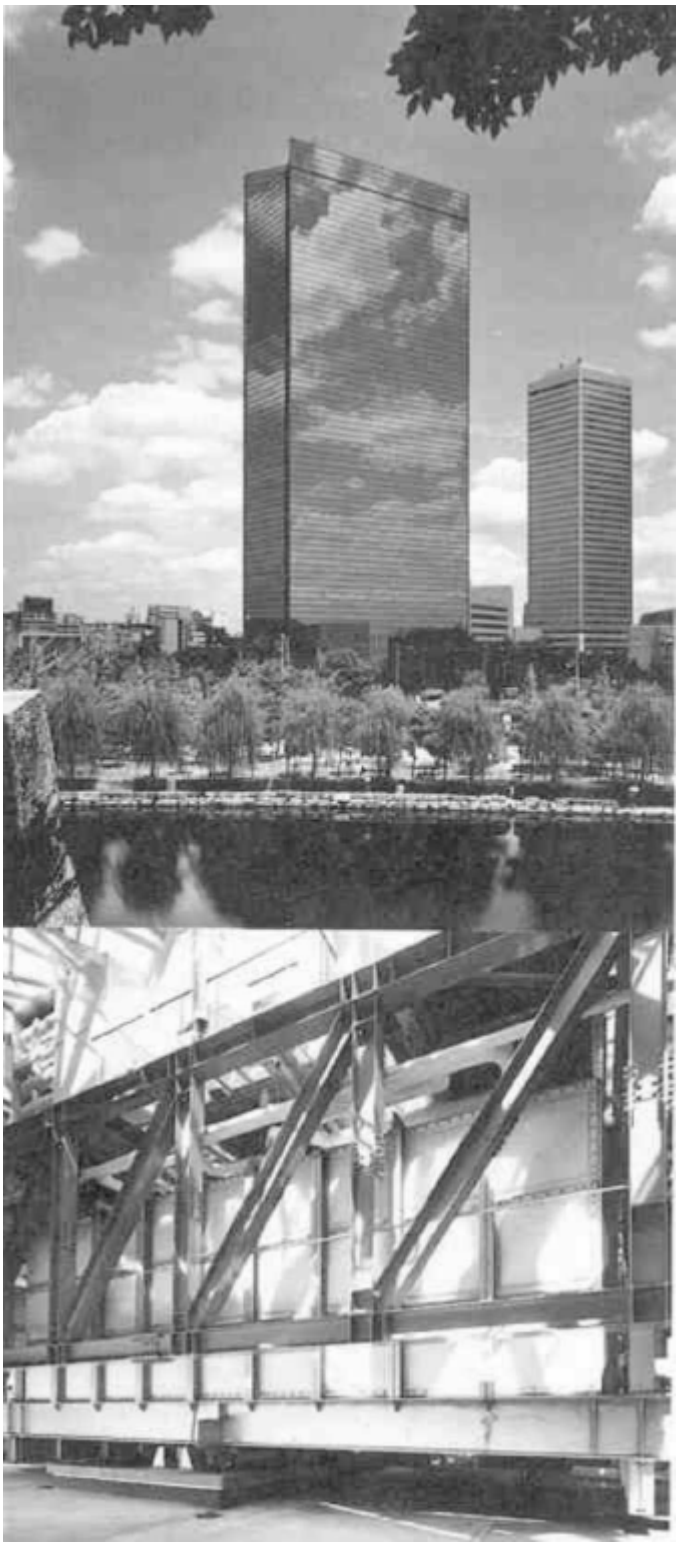

Figure 3.21. Ice storage tank—Crystal Tower. [4]

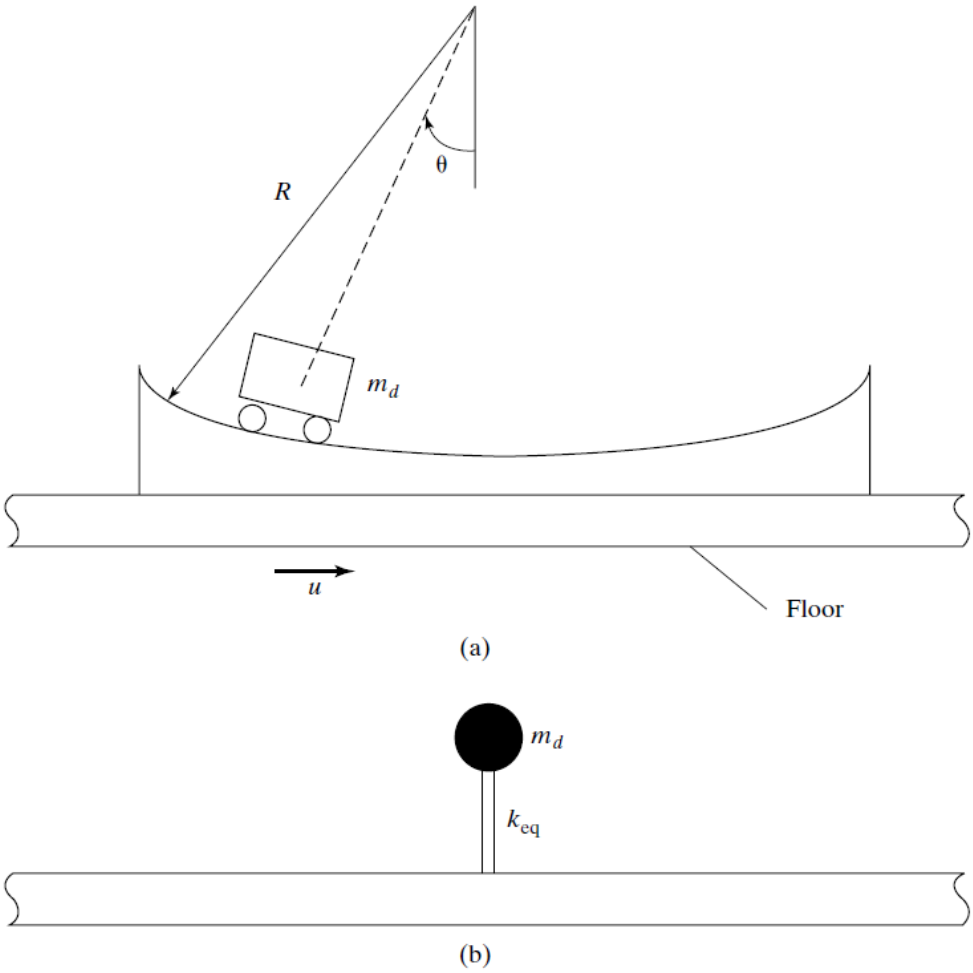

Figure 3.22. Rocker pendulum. [4]

4. TRANSFER MATRICES

In this study, variable cross section beam structures will be analyzed. Transfer matrices will be used to in the analyses due to these simplicity on beam applications. Firstly, transfer matrices of spring-mass systems and beams in free vibration mode will be introduced. Then, transfer matrices of damped and forced vibrations of spring-mass systems and beams will be studied.

4.1. Transfer Matrix of Spring-Mass System

Let us consider a spring-mass system of the type shown in Figure 4.1 which is vibrating with circular frequency ω. The masses m_{i-1} and m_i , are connected by a massless spring of stiffness k_i. The state vector just to the right of mass m_i is denoted by $\mathbf{z}_i^R$, and the state vector to the left is denoted by $\mathbf{z}_i^L$.

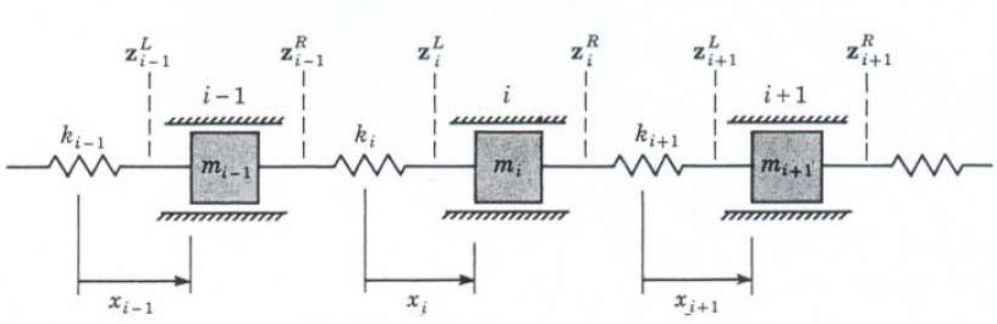

Figure 4.1. Spring mass system.[11]

If we isolate the spring k_i and use the convention explained above, the positive forces and deflections are as shown in Figure 4.2. From the equilibrium of the spring we immediately obtain;

$$N_{i-1}^R = N_i^L \tag{4.1}$$

and from the stiffness property of the spring we have the further relation

$$N_i^L = N_{i-1}^R = k_i(x_i - x_{i-1}) \tag{4.2}$$

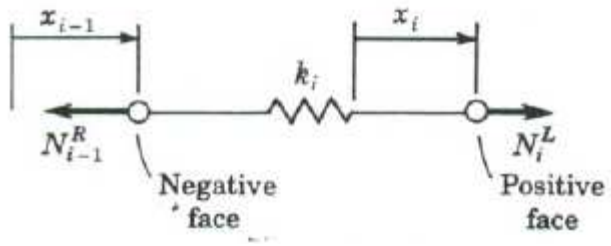

Figure 4.2. Free-body diagram of spring i. [11]

Rewriting these equations in the form

$$x_i = x_{i-1} + \frac{N_{i-1}^R}{k_i} \tag{4.3}$$

$$N_i^L = (0)x_{i-1} + N_{i-1}^R \tag{4.4}$$

We can then take one more step to express the equations in matrix notation,

$$\begin{bmatrix} x \\ N \end{bmatrix}_i^L = \begin{bmatrix} 1 & \frac{1}{k_i} \\ 0 & 1 \end{bmatrix} \begin{bmatrix} x \\ N \end{bmatrix}_{i-1}^R \tag{4.5}$$

or

$$\mathbf{z}_i^L = \mathbf{F}_i \mathbf{z}_{i-1}^R \tag{4.6}$$

Hence by means of the matrix $\mathbf{F}_i$, we have been able to express the state vector $\mathbf{z}_i^L$ in terms of the state vector $\mathbf{z}_{i-1}^R$. The matrix $\mathbf{F}_i$ is known as the field transfer matrix or more simply as the field matrix.

The matrix relation that exists between the state vectors to the left and right of mass *i* can be found by considering the forces acting on the mass as in Figure 4.3. The two spring forces are N_i^R and N_i^L, and in addition there is the inertia force $m_i\omega^2 x_i$ acting in the positive direction . Since the mass is rigid, the deflections to the left and right of mass m_i are the same, so that

$$x_i^R = x_i^L \tag{4.7}$$

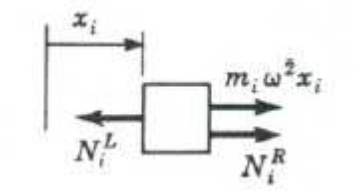

Figure 4.3. Free-body diagram of mass m_i [11]

and from the equilibrium of the forces we have

$$N_i^R = N_i^L - m_i\omega^2 x_i \tag{4.8}$$

Rewritten in matrix notation, the above equations become

$$\begin{bmatrix} x \\ N \end{bmatrix}_i^R = \begin{bmatrix} 1 & 0 \\ -m_i\omega^2 & 1 \end{bmatrix} \begin{bmatrix} x \\ N \end{bmatrix}_i^L \tag{4.9}$$

or

$$\mathbf{z}_i^R = \mathbf{P}_i \mathbf{z}_i^L \tag{4.10}$$

Again we have found a matrix relation between two adjacent state vectors. This time, since we are simply transferring over a point, the matrix is known as the point transfer matrix, or the point matrix.

4.2. Plane Flexural Vibration of a Straight Beam

When computing the flexural vibrations of beams with distributed mass, it is often advisable to follow the technique of replacing the actual beam by a beam of the same flexural stiffness which is mass-less between discrete points where the mass is concentrated. Such a system as in Figure 4.4 is easily analyzed by transfer matrices. The first step is to isolate the beam element between the points *(i-1)* and *i*. The sign convention explained at the beginning of this section is applied to the straight beam, as illustrated in Figure 4.5.

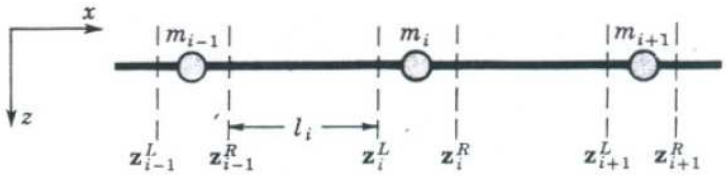

Figure 4.4. Beam with concentrated masses. [11]

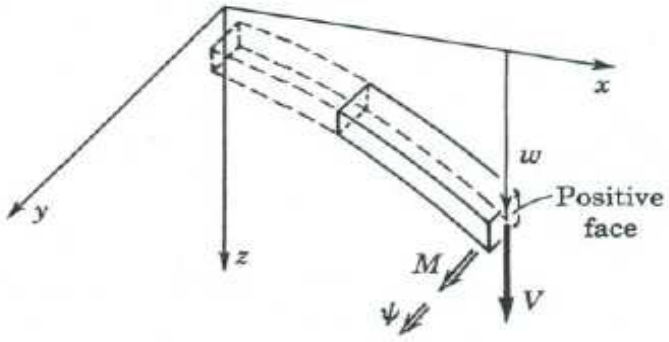

Figure 4.5. Sign convention for beam. [11]

The two displacements are the deflection w and the slope Ψ, the corresponding forces being the shear force V and the bending moment M. The forces and deflections at the extremities of the beam element are shown in Figure 4.6. The equilibrium of the element requires that the sum of the vertical forces be zero and that the sum of the moments about, let us say, point i-1 be zero. The two equilibrium equations are then

$$V_i^L - V_{i-1}^R = 0 \tag{4.11}$$

$$M_i^L - M_{i-1}^R - V_i^L l_i = 0 \tag{4.12}$$

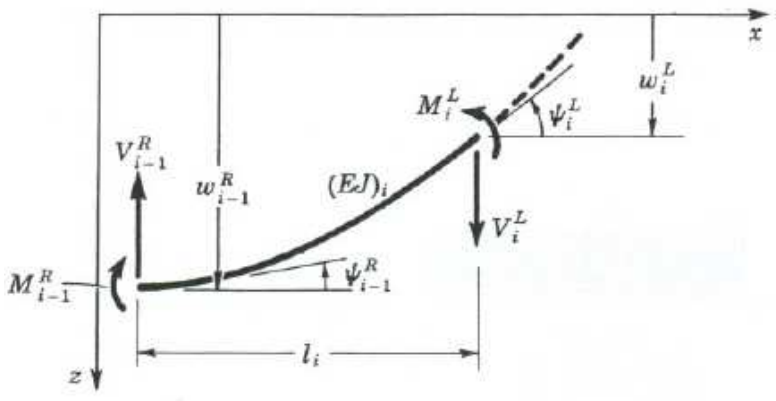

Figure 4.6. End forces and deflections for massless beam. [11]

We obtain two further equations for the end deflection and slope of a cantilever of flexural stiffness *EJ* subjected to moment *M* and shear *V* at its free end (Figure 4.7) from elementary beam theory:

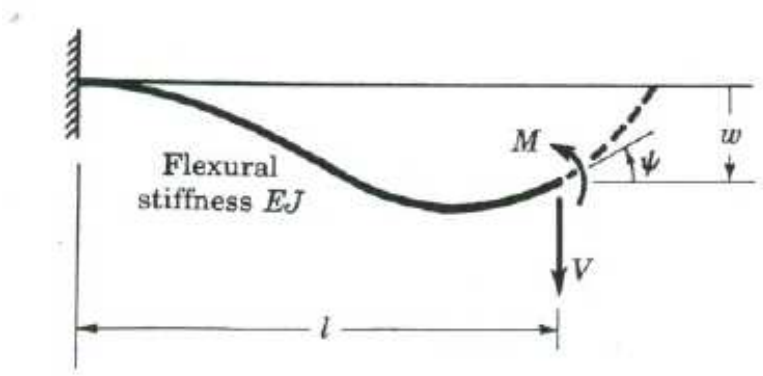

Figure 4.7. Cantilever subjected to force *V* and moment *M*. [11]

$$w = \frac{Ml^2}{2EJ} + \frac{Vl^3}{EJ} \tag{4.13}$$

$$\Psi = \frac{Ml}{EJ} - \frac{Vl^2}{2EJ} \tag{4.14}$$

Applying these results to the problem at hand and noting that the point *i*-1 has a deflection w_{i-1} and a slope Ψ_{i-1}, we obtain the equations

$$w_i^L = w_{i-1}^R - \Psi_{i-1}^R l_i - M_i^L \frac{l_i^2}{2(EJ)_i} + V_i^L \frac{l_i^3}{3(EJ)_i} \tag{4.15}$$

$$\Psi_i^L = \Psi_{i-1}^R + M_i^L \frac{l_i}{(EJ)_i} - V_i^L \frac{l_i^2}{2(EJ)_i} \tag{4.16}$$

We note from Eq. 4.11 and 4.12 that

$$V_i^L = V_{i-1}^R \tag{4.17}$$

$$M_i^L = M_{i-1}^R + V_{i-1}^R l_i \tag{4.18}$$

Eq. 3.11 and 3.12 and Eq. 3.15 and 3.16 can be rewritten such that all the state-vector elements at point i^L can be expressed in terms of those at point $i\text{-}1^R$:

$$-w_i^L = -w_{i-1}^R - \Psi_{i-1}^R l_i + M_{i-1}^R \frac{l_i^2}{2(EJ)_i} + V_{i-1}^R \frac{l_i^3}{6(EJ)_i} \tag{4.19}$$

$$\Psi_i^L = \Psi_{i-1}^R + M_{i-1}^R \frac{l_i}{(EJ)_i} + V_{i-1}^R \frac{l_i^2}{2(EJ)_i} \tag{4.20}$$

$$M_i^L = M_{i-1}^R + V_{i-1}^R l_i \tag{4.21}$$

$$V_i^L = V_{i-1}^R \tag{4.22}$$

or in matrix notation,

$$\begin{bmatrix} -w \\ \Psi \\ M \\ V \end{bmatrix}_i^L = \begin{bmatrix} 1 & l & \frac{l^2}{2EJ} & \frac{l^3}{6EJ} \\ 0 & 1 & \frac{1}{EJ} & \frac{l^2}{2EJ} \\ 0 & 0 & 1 & l \\ 0 & 0 & 0 & 1 \end{bmatrix}_i \begin{bmatrix} -w \\ \Psi \\ M \\ V \end{bmatrix}_{i-1}^R \tag{4.23}$$

or

$$\mathbf{z}_i^L = \mathbf{F}_i \mathbf{z}_{i-1}^R \tag{4.24}$$

The point matrix connecting $\mathbf{z}_i^R$ with $\mathbf{z}_i^L$ is found by noting that the deflection, slope and moment are continuous across the concentrated mass m_i, so that

$$w_i^R = w_i^L \tag{4.25}$$

$$\psi_i^R = \psi_i^L \tag{4.26}$$

$$M_i^R = M_i^L \tag{4.27}$$

The vibrating mass, however, introducing an inertia force causes a discontinuity in the shear. The free-body diagram shown in Figure 4.8 yields from simple equilibrium considerations the relation

$$V_i^R = V_i^L - m_i\omega^2 w_i \tag{4.28}$$

In matrix notation Eq. 4.25, 4.26 , 4.27 and 4.28 become

$$\begin{bmatrix} -w \\ \Psi \\ M \\ V \end{bmatrix}_i^R = \begin{bmatrix} 1 & 0 & 0 & 0 \\ 0 & 1 & 0 & 0 \\ 0 & 0 & 1 & 0 \\ m\omega^2 & 0 & 0 & 1 \end{bmatrix} \begin{bmatrix} -w \\ \Psi \\ M \\ V \end{bmatrix}_i^L \tag{4.29}$$

or

$$\mathbf{z}_i^R = \mathbf{P}_i \mathbf{z}_i^L \tag{4.30}$$

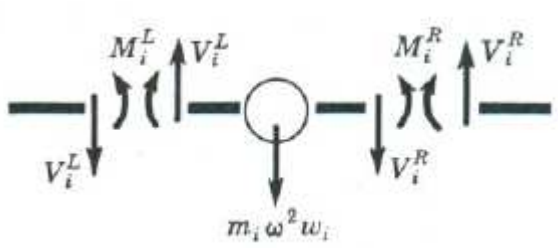

Figure 4.8: Free-body diagram of mass m_i [11]

Another point matrix that can be easily obtained covers the case when the beam has a spring support as shown in Figure 4.9. We can again relate the state vectors $\mathbf{z}_i^R$ and $\mathbf{z}_i^L$ by means of a point matrix. The deflection, slope, and moment are continuous over the point *i,* but on account of the spring restoring force a discontinuity occurs in the shear force. If the spring is deflected by an amount w_i then the restoring force is $k_i w_i$ where k_i is the stiffness of the spring as shown in Figure 4.10. The relations of the state-vector elements to the left and right of the spring are then

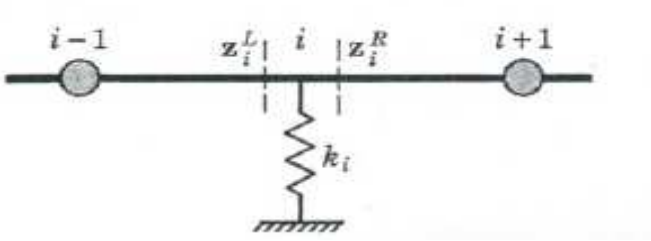

Figure 4.9. Beam on elastic support[11]

$$-w_i^R = -w_i^L \tag{4.31}$$

$$\psi_i^R = \psi_i^L \tag{4.32}$$

$$M_i^R = M_i^L \tag{4.33}$$

$$V_i^R = k_i w_i + V_i^L \tag{4.34}$$

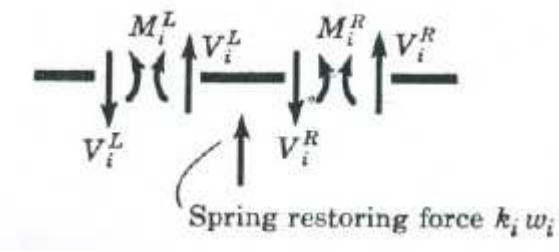

Figure 4.10. Free-body diagram of the elastic support. [11]

Which in matrix notation become

$$\begin{bmatrix} -w \\ \Psi \\ M \\ V \end{bmatrix}_i^R = \begin{bmatrix} 1 & 0 & 0 & 0 \\ 0 & 1 & 0 & 0 \\ 0 & 0 & 1 & 0 \\ -k & 0 & 0 & 1 \end{bmatrix}_i \begin{bmatrix} -w \\ \Psi \\ M \\ V \end{bmatrix}_i^L \tag{4.35}$$

or

$$\mathbf{z}_i^R = \mathbf{P}_i \mathbf{z}_i^L \tag{4.36}$$

4.3. Elimination of Intermediate State Vectors

The application of transfer matrices to more complicated problems will now be discussed. Let us consider the beam as shown in Figure 4.11 that is made up of piecewise uniform massless elements, with masses concentrated at discrete points. The transfer matrices for a uniform massless beam, Eq. 4.23, and for a concentrated mass, Eq. 4.29,

have already been derived, so that with the dimensions of the beams and the magnitude of the masses given, the following matrix relations exist between adjacent state vectors:

$$\mathbf{z}_1^{L} = \mathbf{F}_1 \mathbf{z}_0 \tag{4.37}$$

$$\mathbf{z}_1^{R} = \mathbf{P}_1 \mathbf{z}_1^{L} \tag{4.38}$$

$$\mathbf{z}_2^{L} = \mathbf{F}_2 \mathbf{z}_1^{R} \tag{4.39}$$

$$\mathbf{z}_2^{R} = \mathbf{P}_2 \mathbf{z}_2^{L} \tag{4.40}$$

$$\mathbf{z}_3^{L} = \mathbf{F}_3 \mathbf{z}_2^{R} \tag{4.41}$$

$$\mathbf{z}_3^{R} = \mathbf{P}_3 \mathbf{z}_3^{L} \tag{4.42}$$

$$\mathbf{z}_4^{L} = \mathbf{F}_4 \mathbf{z}_3^{R} \tag{4.43}$$

$$\mathbf{z}_4^{R} = \mathbf{P}_4 \mathbf{z}_4^{L} \tag{4.44}$$

$$\mathbf{z}_5^{L} = \mathbf{F}_5 \mathbf{z}_4^{R} \tag{4.45}$$

$$\mathbf{z}_5^{R} = \mathbf{P}_5 \mathbf{z}_5^{L} \tag{4.46}$$

$$\mathbf{z}_6^{L} = \mathbf{F}_6 \mathbf{z}_5^{R} \tag{4.47}$$

$$\mathbf{z}_6^{R} = \mathbf{P}_6 \mathbf{z}_6^{L} \tag{4.48}$$

$$\mathbf{z}_7 = \mathbf{F}_7 \mathbf{z}_6^{R} \tag{4.49}$$

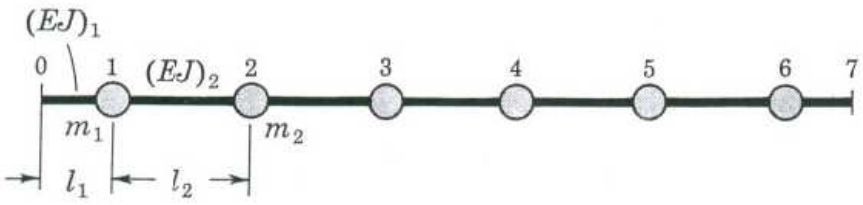

Figure 4.11. Beam with discrete masses. [11]

From the last two equations $\mathbf{z}_7 = \mathbf{F}_7 \mathbf{z}_6^{R}$ and $\mathbf{z}_6^{R} = \mathbf{P}_6 \mathbf{z}_6^{L}$ it follows that $\mathbf{z}_7 = \mathbf{F}_7 \mathbf{P}_6 \mathbf{z}_6^{L}$. Now using the relation $\mathbf{z}_6^{L} = \mathbf{F}_6 \mathbf{z}_5^{R}$, we obtain

$$\mathbf{z}_7 = \mathbf{F}_7 \mathbf{P}_6 \mathbf{F}_6 \mathbf{z}_5^{R} \tag{4.50}$$

This procedure is continued until we finally obtain the relation between the state vectors at the two ends of the beam:

$$\mathbf{z}_7 = \mathbf{F}_7 \mathbf{P}_6 \mathbf{F}_6 \mathbf{P}_5 \mathbf{F}_5 \mathbf{P}_4 \mathbf{F}_4 \mathbf{P}_3 \mathbf{F}_3 \mathbf{P}_2 \mathbf{F}_2 \mathbf{P}_1 \mathbf{F}_1 \mathbf{z}_0 \tag{4.51}$$

$$\mathbf{z}_7 = \mathbf{U}\,\mathbf{z}_0 \tag{4.52}$$

In this manner all the intermediate state vectors have been eliminated. Rewriting Eq. 4.52 in full we have

$$\begin{bmatrix} -w \\ \Psi \\ M \\ V \end{bmatrix}_7 = \begin{bmatrix} u_{11} & u_{12} & u_{13} & u_{14} \\ u_{21} & u_{22} & u_{23} & u_{24} \\ u_{31} & u_{32} & u_{33} & u_{34} \\ u_{41} & u_{42} & u_{43} & u_{44} \end{bmatrix} \begin{bmatrix} -w \\ \Psi \\ M \\ V \end{bmatrix}_0 \tag{4.53}$$

The coefficients u_{11} to u_{44} all being known functions of the circular frequency ω. Expanding the matrix product gives the four equations

$$-w_7 = -u_{11}w_0 + u_{12}\Psi_0 + u_{13}M_0 + u_{14}V_0 \tag{4.54}$$

$$\Psi_7 = -u_{21}w_0 + u_{22}\Psi_0 + u_{23}M_0 + u_{24}V_0 \tag{4.55}$$

$$M_7 = -u_{31}w_0 + u_{32}\Psi_0 + u_{33}M_0 + u_{34}V_0 \tag{4.56}$$

$$V_7 = -u_{41}w_0 + u_{42}\Psi_0 + u_{43}M_0 + u_{44}V_0 \tag{4.57}$$

4.4. Determination of Natural Frequencies

Natural frequencies of a beam can be calculated by applying the boundary conditions to the Eq. 4.54 to 4.57. Due to the characteristic of beams, four of the end conditions should have zero value and eventually two equations remain. Determinant equation of this 2 x 2 matrix gives the natural frequencies of the system. Consider the following two cases:

Case 1: Beam Simply Supported at Both Ends as shown in Figure 4.12*a*. The boundary conditions are;

$$w_7 = 0$$
$$M_7 = 0$$
$$w_0 = 0$$
$$M_0 = 0$$

Substituting these in Eq. 4.54 and 4.55, we obtain

$$0 = u_{12}\Psi_0 + u_{14}V_0 \tag{4.58}$$

$$0 = u_{32}\Psi_0 + u_{34}V_0 \tag{4.59}$$

For a nontrivial solution of these equations the determinant of the coefficients must be zero, that is,

$$\begin{bmatrix} u_{12} & u_{14} \\ u_{32} & u_{34} \end{bmatrix} = 0 \tag{4.60}$$

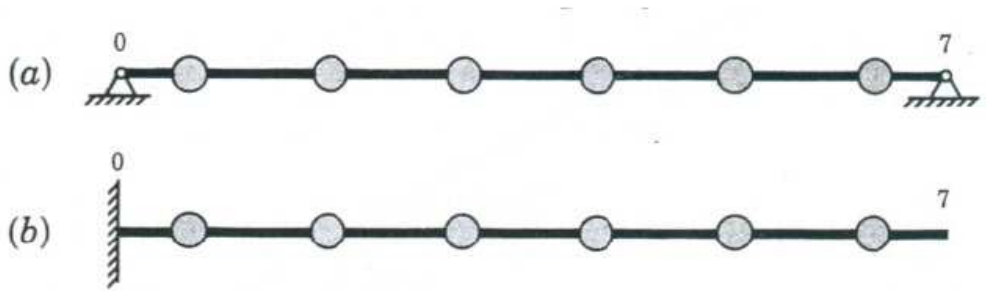

Figure 4.12. Two cases of boundary conditions. [11]

Since the elements u_{ik} are known functions of the circular frequency ω, this determinant serves to compute the natural circular frequencies. In view of the fact that the beam possesses six discrete masses, the expansion of the frequency determinant leads to an equation of sixth degree in ω^2.

Case 2: Left Side Built-in, Right Side Free (Figure 3.12*b*). The boundary conditions

$$V_7 = 0$$
$$M_7 = 0$$
$$w_0 = 0$$
$$\psi_0 = 0$$

yield, after substitution in Eq. 4.56 and 4.57, and the frequency determinant is;

$$\begin{bmatrix} u_{33} & u_{34} \\ u_{43} & u_{44} \end{bmatrix} = 0 \tag{4.61}$$

In practice we are usually interested in the natural frequencies of a particular system subjected to only one set of boundary conditions. When this is so, it is not necessary to carry through the complete matrix multiplication. Consider, for example, the beam illustrated in Figure 4.13, which is, let us say, divided into three parts whose transfer matrices **A**,**B** and **C** are known. The beam is simply supported on the left and fully built-in on the right. From our discussion above we have the relations,

$$\mathbf{z}_1 = \mathbf{A}\mathbf{z}_0 \tag{4.62}$$

$$\mathbf{z}_2 = \mathbf{B}\mathbf{A}\mathbf{z}_0 \tag{4.63}$$

$$\mathbf{z}_3 = \mathbf{C}\mathbf{B}\mathbf{A}\mathbf{z}_0 \tag{4.64}$$

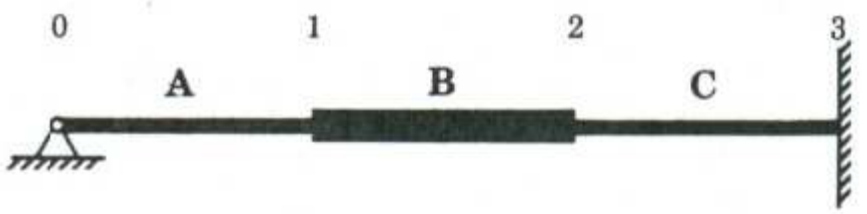

Figure 4.13. Beam of three sections. [11]

That is, the state vectors at the points 1, 2, and 3 are found by multiplying the state vector $\mathbf{z}_0$ by the matrices **A**, **BA**, and **CBA**, respectively. When the matrix multiplication has been completed, we can see that, since the deflection and moment at point 0 are zero, the first and third columns are multiplied by zero, and thus play no part in the calculation. Elements that appear in the first and third columns of the matrices **A**, **BA**, and **CBA** may therefore be dropped. This has been indicated by drawing vertical lines between the unnecessary elements. With the boundary conditions at point 3 being $w_3 = \Psi_3 = 0$, we obtain the relations;

$$e_{12}\Psi_0 + e_{14}V_0 = 0 \tag{4.65}$$

$$e_{22}\Psi_0 + e_{24}V_0 = 0 \tag{4.66}$$

from which the frequency determinant is

$$\begin{bmatrix} e_{12} & e_{14} \\ e_{22} & e_{24} \end{bmatrix} = 0 \tag{4.67}$$

In this problem it is unnecessary to compute e_{32}, e_{34}, e_{42}, and e_{44}.

4.5. Determination of Mode Shapes

With the natural frequencies of an elastic system having been found by means of transfer matrices, it is an easy matter to compute the normal modes using the calculations already carried out. Let us reconsider the example discussed in Sec. 3.2 which is illustrated in Figure 3-13. In the abridged version of the matrix layout we saw that the state vectors $\mathbf{z}_1$, $\mathbf{z}_2$ and $\mathbf{z}_3$ could be expressed in terms of the unknowns at point 0, namely, the slope ψ_0 and the shear V_0. When the boundary conditions at the right end are applied, we have the Eq. 4.65 between ψ_0 and V_0, giving $V_0 = -(e_{12}/e_{14})\psi_0$, so that the column vector $\{V_0 \;\; \psi_0\}$ can be rewritten in terms of ψ_0 alone as $\{1 \;\; -e_{12}/e_{14}\}\psi_0$. All the state vectors may then be expressed in terms of ψ_0 only, and remains undetermined but which can be arbitrarily chosen as unity. When this is done, the expressions for the state vectors are then given by;

$$\mathbf{z}_1 = \begin{bmatrix} a_{12} & a_{14} \\ a_{22} & a_{24} \\ a_{32} & a_{34} \\ a_{42} & a_{44} \end{bmatrix} \begin{bmatrix} 1 \\ -(e_{12}/e_{14}) \end{bmatrix} \tag{4.68}$$

$$\mathbf{z}_2 = \begin{bmatrix} d_{12} & d_{14} \\ d_{22} & d_{24} \\ d_{32} & d_{34} \\ d_{42} & d_{44} \end{bmatrix} \begin{bmatrix} 1 \\ -(e_{12}/e_{14}) \end{bmatrix} \tag{4.69}$$

$$\mathbf{z}_3 = \begin{bmatrix} e_{12} & e_{14} \\ e_{22} & e_{24} \\ e_{32} & e_{34} \\ e_{42} & e_{44} \end{bmatrix} \begin{bmatrix} 1 \\ -(e_{12}/e_{14}) \end{bmatrix} \tag{4.70}$$

4.6. Forced Vibrations of a Straight Beam

The transfer matrix relating the state vectors between adjacent points has already been derived in Section 4.1. Let us now find the corresponding relations when a length of beam is subjected to a uniformly distributed harmonic load $q\cos\Omega t$ (Figure 4.14).

From equilibrium conditions we have for the massless beam

$$V_i^L = V_{i-1}^R - q_i l_i \tag{4.71}$$

$$M_i^L = M_{i-1}^R + V_{i-1}^R l_i - \frac{q_i l_i^2}{2} \tag{4.72}$$

Also, from strength of materials [Eq. 4.15 and 4.16], we obtain the relations

$$w_i^L = w_{i-1}^R - \Psi_{i-1}^R l_i - M_i^L \frac{l_i^2}{2EJ_i} + V_i^L \frac{l_i^3}{3EJ_i} + \frac{q_i l_i^4}{8EJ_i} \tag{4.73}$$

$$\Psi_i^L = \Psi_{i-1}^R + M_i^L \frac{l_i}{EJ_i} - V_i^L \frac{l_i^2}{2EJ_i} - \frac{q_i l_i^3}{6EJ_i} \tag{4.74}$$

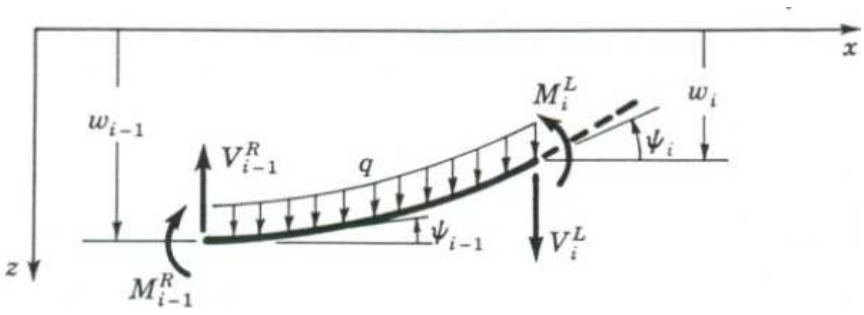

Figure 4.14. Beam subjected to uniformly distributed load $q\cos\Omega t$. [11]

The elimination of M_i^L and V_i^L from the right-hand side of these equations gives

$$-w_i^L = -w_{i-1}^R + \Psi_{i-1}^R l_i + M_{i-1}^R \frac{l_i^2}{2EJ_i} + V_{i-1}^R \frac{l_i^3}{6EJ_i} - \frac{q_i l_i^4}{24EJ_i} \tag{4.75}$$

$$\Psi_i^L = \Psi_{i-1}^R + M_{i-1}^R \frac{l_i}{EJ_i} + V_{i-1}^R \frac{l_i^2}{2EJ_i} - \frac{q_i l_i^3}{6EJ_i} \tag{4.76}$$

Repeating the equilibrium equations

$$V_i^L = V_{i-1}^R - q_i l_i \tag{4.77}$$

$$M_i^L = M_{i-1}^R + V_{i-1}^R l_i - \frac{q_i l_i^2}{2} \tag{4.78}$$

and again introducing the identity $1 \equiv 1$, the above equations in matrix form become

$$\begin{bmatrix} -w \\ \Psi \\ M \\ V \\ \hline 1 \end{bmatrix}_i^L = \left[\begin{array}{cccc:c} 1 & l & \frac{l^2}{2EJ} & \frac{l^3}{6EJ} & \frac{-ql^4}{24EJ} \\ 0 & 1 & \frac{l}{EJ} & \frac{l^2}{2EJ} & \frac{-ql^3}{6EJ} \\ 0 & 0 & 1 & l & \frac{-ql^2}{2} \\ 0 & 0 & 0 & 1 & -ql \\ \hdashline 0 & 0 & 0 & 0 & 1 \end{array}\right] \begin{bmatrix} -w \\ \Psi \\ M \\ V \\ \hline 1 \end{bmatrix}_{i-1}^R \tag{4.79}$$

$$\tilde{\mathbf{z}}_i^L = \tilde{\mathbf{F}}_i . \tilde{\mathbf{z}}_{i-1}^R \tag{4.80}$$

Where $\tilde{\mathbf{z}}$ is the extended state vector and $\tilde{\mathbf{F}}$ is the extended field transfer matrix.

4.7. Transfer Matrices Applied to Forced Damped Vibrations

We shall now compute the steady-state vibrations of the system of Figure 4.15 with the help of transfer matrices. The field transfer matrix was found for the case of free vibrations by Eq. 4.5. In case of damping, complex impedance or complex stiffness $\bar{z}(\Omega)$ should be introduced.

$$\bar{z}(\Omega) = jc\Omega \tag{4.81}$$

If we consider steady-state forced vibrations, we should add an extra column to the Eq. 4.5 with the addition of complex impedance where the stiffness values are involved. The extended transfer matrix relating $\tilde{\mathbf{z}}_1^L$ and $\tilde{\mathbf{z}}_0^L$ becomes

$$\begin{bmatrix} \bar{x} \\ \bar{N} \\ \hline 1 \end{bmatrix}_1^L = \left[\begin{array}{cc:c} 1 & \dfrac{1}{k+jc\Omega} & 0 \\ 0 & 1 & 0 \\ \hdashline 0 & 0 & 1 \end{array}\right] \begin{bmatrix} \bar{x} \\ \bar{N} \\ \hline 1 \end{bmatrix}_0 \tag{4.82}$$

The extended point matrix for the concentrated mass is given by the relation

$$\begin{bmatrix} \bar{x} \\ \bar{N} \\ \hline 1 \end{bmatrix}_1^R = \left[\begin{array}{cc:c} 1 & 0 & 0 \\ -m\Omega^2 & 1 & -\bar{P} \\ \hdashline 0 & 0 & 1 \end{array}\right] \begin{bmatrix} \bar{x} \\ \bar{N} \\ \hline 1 \end{bmatrix}_1^L \tag{4.83}$$

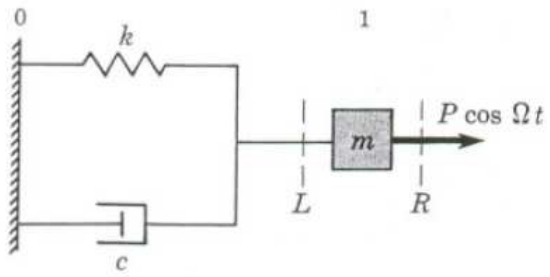

Figure 4.15. Simple damped system in steady state oscillation. [11]

Since in this case x_0=0 , we may drop the first column of Eq. 4.82 and the transfer matrix product has the form

$$\left[\begin{array}{c:c} \dfrac{1}{k + jc\Omega} & 0 \\ \dfrac{-m\Omega^2}{k + jc\Omega} + 1 & -\bar{P} \\ \hdashline 0 & 1 \end{array}\right] \begin{bmatrix} \bar{N} \\ \hline 1 \end{bmatrix}_0 = \begin{bmatrix} x \\ \bar{N} \\ \hline 1 \end{bmatrix}_1^R \tag{4.84}$$

Applying the boundary condition $\bar{N}_i^R = 0$, we obtain the relation

$$(1-\frac{m\Omega^2}{k+jc\Omega})\bar{N}_0 - \bar{P} = 0 \tag{4.85}$$

So that
$$\bar{N}_0 = \frac{\bar{P}}{1 - m\Omega^2 / (k + jc\Omega)} \tag{4.86}$$

Thus
$$\bar{x}_1 = \frac{\bar{N}_0}{k + jc\Omega} = \frac{\bar{P}}{k + jc\Omega - m\Omega^2} = \frac{\bar{P}}{k - m\Omega^2 + jc\Omega} \tag{4.87}$$

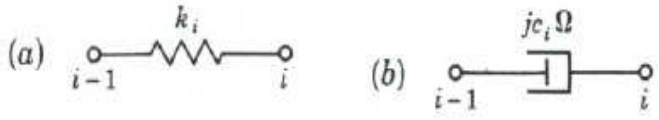

Figure 4.16. (a) Spring of stiffness k and (b) damper of complex stiffness $jc\Omega$. [11]

Two further simple examples of extended transfer matrices are given by Eq. 4.89 and 4.91 for the spring shown in Figure 3.16a and the damper in Figure 3.16b:

$$\tilde{\tilde{\mathbf{U}}}_i = \begin{array}{c} \begin{matrix} \bar{x} & \bar{N} & 1 \end{matrix} \\ \left[\begin{array}{c|c|c} 1 & \frac{1}{k} & 0 \\ \hline 0 & 1 & 0 \\ \hline 0 & 0 & 1 \end{array}\right]_i \end{array} \tag{4.88}$$

Which when written in real form is ;

$$\tilde{\mathbf{U}}_i = \begin{array}{c} \begin{matrix} x^r & N^r & x^i & N^i & 1 \end{matrix} \\ \left[\begin{array}{cc|cc|c} 1 & \frac{1}{k} & 0 & 0 & 0 \\ 0 & 1 & 0 & 0 & 0 \\ \hline 0 & 0 & 1 & \frac{1}{k} & 0 \\ 0 & 0 & 0 & 1 & 0 \\ \hline 0 & 0 & 0 & 0 & 1 \end{array}\right]_i \end{array} \tag{4.89}$$

and for the viscous damper

$$\tilde{\tilde{\mathbf{U}}}_i = \begin{array}{c} \begin{matrix} \bar{x} & \bar{N} & 1 \end{matrix} \\ \left[\begin{array}{c|c|c} 1 & \dfrac{1}{jc\Omega} & 0 \\ \hline 0 & 1 & 0 \\ \hline 0 & 0 & 1 \end{array}\right] \end{array} \tag{4.90}$$

or in real form

$$\tilde{\mathbf{U}}_i = \begin{array}{c} \begin{matrix} x^r & N^r & x^i & N^i & 1 \end{matrix} \\ \left[\begin{array}{cc|cc|c} 1 & 0 & 0 & \dfrac{1}{c\Omega} & 0 \\ 0 & 1 & 0 & 0 & 0 \\ \hline 0 & \dfrac{-1}{c\Omega} & 1 & 0 & 0 \\ 0 & 0 & 0 & 1 & 0 \\ \hline 0 & 0 & 0 & 0 & 1 \end{array}\right]_i \end{array} \tag{4.91}$$

For easier coordination the elements of the state vector have been written above the associated columns.

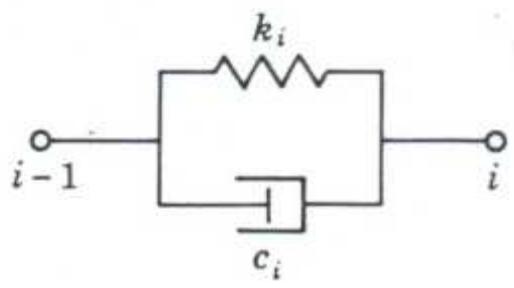

Figure 4.17. Spring and damper in parallel. [11]

We stated that a damper has a complex impedance or complex stiffness given by Eq. 4.81 at the beginning of this section. The stiffness of two springs in parallel is the sum of the two individual springs, so that the combination shown in Figure 4.17 has a complex stiffness $k + jc\Omega$. The mechanical admittance or receptance, which is defined as the reciprocal of the complex stiffness, is $1/(k + jc\Omega)$.The extended transfer matrix for the structural unit of Figure 4.17 is given below in complex as well as in real form:

$$\tilde{\tilde{\mathbf{U}}}_{\mathbf{i}} = \begin{array}{c} \begin{matrix} \bar{x} & \bar{N} & 1 \end{matrix} \\ \left[\begin{array}{c|c|c} 1 & \dfrac{1}{k + jc\Omega} & 0 \\ \hline 0 & 1 & 0 \\ \hline 0 & 0 & 1 \end{array}\right]_i \end{array} \tag{4.92}$$

or

$$\tilde{\mathbf{U}}_{\mathbf{i}} = \begin{array}{c} \begin{matrix} x^r & N^r & x^i & N^i & 1 \end{matrix} \\ \left[\begin{array}{cc|cc|c} 1 & \dfrac{k}{k^2 + c^2\Omega^2} & 0 & \dfrac{c\Omega}{k^2 + c^2\Omega^2} & 0 \\ 0 & 1 & 0 & 0 & 0 \\ \hline 0 & \dfrac{-c\Omega}{k^2 + c^2\Omega^2} & 1 & \dfrac{k}{k^2 + c^2\Omega^2} & 0 \\ 0 & 0 & 0 & 1 & 0 \\ \hline 0 & 0 & 0 & 0 & 1 \end{array}\right]_i \end{array} \tag{4.93}$$

When springs and dampers are connected in series as shown in Figure 3.18, the total admittance is found by adding the admittances of the individual elements so that the extended transfer matrix becomes

$$\tilde{\tilde{\mathbf{U}}}_i = \begin{array}{c} \begin{matrix} \bar{x} & \bar{N} & 1 \end{matrix} \\ \left[\begin{array}{c|c|c} 1 & \frac{1}{k}+\frac{1}{jc\Omega} & 0 \\ \hline 0 & 1 & 0 \\ \hline 0 & 0 & 1 \end{array}\right]_i \end{array} \tag{4.94}$$

or

$$\tilde{\mathbf{U}}_i = \begin{array}{c} \begin{matrix} x^r & N^r & x^i & N^i & 1 \end{matrix} \\ \left[\begin{array}{cc|cc|c} 1 & \frac{1}{k} & 0 & \frac{1}{c\Omega} & 0 \\ 0 & 1 & 0 & 0 & 0 \\ \hline 0 & \frac{-1}{c\Omega} & 1 & \frac{1}{k} & 0 \\ 0 & 0 & 0 & 1 & 0 \\ \hline 0 & 0 & 0 & 0 & 1 \end{array}\right]_i \end{array} \tag{4.95}$$

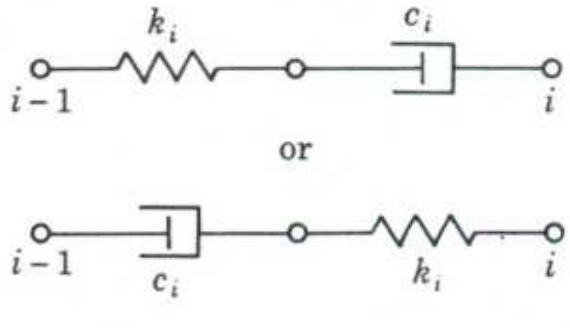

Figure 4.18: Spring and damper in series. [11]

Another important "building block" is represented in Figure 4.19, where a point mass is subjected to a harmonic force of complex amplitude and is restrained by an absolute spring and an absolute damper. The extended point matrix is then,

$$\bar{\bar{\mathbf{U}}}_i = \begin{array}{c} \begin{matrix} \bar{x} & \bar{N} & 1 \end{matrix} \\ \left[\begin{array}{c|c|c} 1 & 0 & 0 \\ \hline -m\Omega^2 + k + jr\Omega & 1 & -\bar{\bar{P}} \\ \hline 0 & 0 & 1 \end{array}\right]_i \end{array} \tag{4.96}$$

or

$$\tilde{\mathbf{U}}_i = \begin{array}{c} \begin{matrix} x^r & N^r & x^i & N^i & 1 \end{matrix} \\ \left[\begin{array}{cc|cc|c} 1 & 0 & 0 & 0 & 0 \\ -m\Omega^2 + k & 1 & -r\Omega & 0 & -P^r \\ \hline 0 & 0 & 1 & 0 & 0 \\ r\Omega & 0 & -m\Omega^2 + k & 1 & -P^i \\ \hline 0 & 0 & 0 & 0 & 1 \end{array}\right]_i \end{array} \tag{4.97}$$

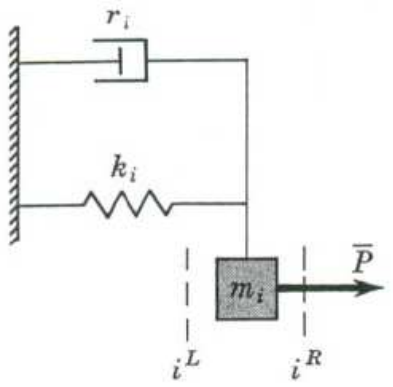

Figure 4.19: Point mass with harmonic exciting force. [11]

For the case of structural damping it is easy to establish the transfer matrix for a massless beam. According to Eq. 4.23 the transfer matrix for an undamped massless beam is

$$\mathbf{U}_i = \begin{array}{c} \begin{matrix} -w & \Psi & M & V \end{matrix} \\ \left[\begin{array}{cccc} 1 & l & \dfrac{l^2}{2EJ} & \dfrac{l^3}{6EJ} \\ 0 & 1 & \dfrac{l}{EJ} & \dfrac{l^2}{2EJ} \\ 0 & 0 & 1 & l \\ 0 & 0 & 0 & 1 \end{array}\right]_i \end{array} \tag{4.98}$$

Replacing EJ by $EJ(1+jg)$, we obtain the complex extended transfer matrix of the massless beam with structural damping in steady-state vibration, as follows:

$$\tilde{\tilde{\mathbf{U}}}_i = \begin{array}{c} \begin{matrix} -\bar{w} & \bar{\Psi} & \bar{M} & \bar{V} & 1 \end{matrix} \\ \left[\begin{array}{cccc:c} 1 & l & \dfrac{l^2}{2EJ(1+jg)} & \dfrac{l^3}{6EJ(1+jg)} & 0 \\ 0 & 1 & \dfrac{l}{EJ(1+jg)} & \dfrac{l^2}{2EJ(1+jg)} & 0 \\ 0 & 0 & 1 & l & 0 \\ 0 & 0 & 0 & 1 & 0 \\ \hdashline 0 & 0 & 0 & 0 & 1 \end{array}\right]_i \end{array} \tag{4.99}$$

We can write Eq. 4.99 in its real form, we find ;

$$\tilde{\mathbf{U}}_i = \begin{array}{c} \begin{matrix} -w^r & \Psi^r & M^r & V^r & -w^j & \Psi^i & M^i & V^i & 1 \end{matrix} \\ \left[\begin{array}{cccc:cccc:c} 1 & l & \dfrac{l^2}{2EJ\left(1+g^2\right)} & \dfrac{l^3}{6EJ\left(1+g^2\right)} & 0 & 0 & \dfrac{gl^2}{2EJ\left(1+g^2\right)} & \dfrac{gl^3}{6EJ\left(1+g^2\right)} & 0 \\ 0 & 1 & \dfrac{l}{EJ\left(1+g^2\right)} & \dfrac{l^2}{2EJ\left(1+g^2\right)} & 0 & 0 & \dfrac{gl}{EJ\left(1+g^2\right)} & \dfrac{gl^2}{2EJ\left(1+g^2\right)} & 0 \\ 0 & 0 & 1 & l & 0 & 0 & 0 & 0 & 0 \\ 0 & 0 & 0 & 1 & 0 & 0 & 0 & 0 & 0 \\ \hdashline 0 & 0 & \dfrac{-gl^2}{2EJ\left(1+g^2\right)} & \dfrac{-gl^3}{6EJ\left(1+g^2\right)} & 1 & l & \dfrac{l^2}{2EJ\left(1+g^2\right)} & \dfrac{l^3}{6EJ\left(1+g^2\right)} & 0 \\ 0 & 0 & \dfrac{-gl}{EJ\left(1+g^2\right)} & \dfrac{-gl^2}{2EJ\left(1+g^2\right)} & 0 & 1 & \dfrac{l}{EJ\left(1+g^2\right)} & \dfrac{l^2}{2EJ\left(1+g^2\right)} & 0 \\ 0 & 0 & 0 & 0 & 0 & 0 & 1 & l & 0 \\ 0 & 0 & 0 & 0 & 0 & 0 & 0 & 1 & 0 \\ \hdashline 0 & 0 & 0 & 0 & 0 & 0 & 0 & 0 & 1 \end{array}\right]_i \end{array} \tag{4.100}$$

5. CASE STUDY

5.1. Structure Selection for the Case Study

Many studies investigating the seismic and wind response of slender structures like buildings, bridges and towers are available. Also a large number of TMD applications were available on slender structures worldwide to improve their dynamic response and they were reviewed as a summary in the second chapter. However, there are only a few studies investigating the lateral response of reinforced concrete minarets. Majority of them are about modal analysis and dynamic stress analysis of these slender structures. Sezen et al. [5] attempts to identify the structural vulnerabilities of minarets based on their past seismic performance. Surprisingly no study was available that investigates TMD applications to improve their dynamic response against earthquake and wind. Architectural characteristic of Turkish style minarets are limiting the structural engineers while designing better performing minarets. They can perform perfect static design but they have no choice other than TMD application to minimize the resonance impact on dynamic response. Minarets are indispensible towers in any mosque building. Size of the mosque specifies the number of the minarets. Therefore, the number of the minarets and their vulnerability is much bigger than the expected. Because of these reasons, it will be very good to investigate the TMD applications and their effectiveness on Turkish style minaret structures.

5.2. Minaret Structures

A minaret is a slender tower built next to a mosque. While most historical minarets were constructed using reinforced or unreinforced stone or brick masonry, the majority of minarets recently constructed in Turkey are reinforced concrete (RC) structures. As shown in Figure 5.1, a typical minaret structure comprises a base or boot on top of its foundation, a tapered transition segment, a circular body or shaft with one or more balconies, and a spire at the top. The base or boot is usually square or polygonal, and is sometimes called the pulpit by architects. The minaret can be free standing or the boot may be attached to the mosque structure. The minaret contains interior spiral stairs running all the way up to the

highest balcony level which are not externally visible. Historically the balconies are built so that someone could climb up the stairs and call for prayer. With the advent of loudspeakers, these balconies are not needed; however, one or more balconies are built in each minaret mainly for architectural reasons. Balconies create mass concentrations along the minaret's height and affect its dynamic structural response. [5]

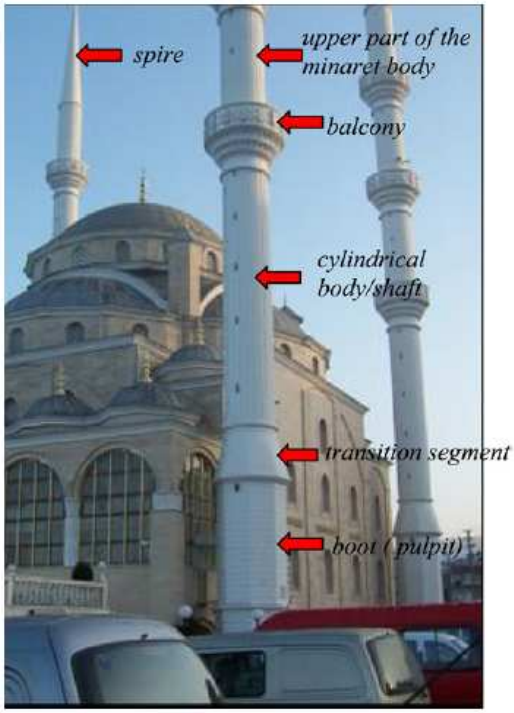

Figure 5.1. Typical reinforced concrete minarets in Turkey. [5]

Currently, there are no structural code requirements or guidelines for the design of reinforced concrete minarets, or minarets in general, in Turkey. As a result, these slender structures have been built, for the most part, by experienced contractors and construction workers with no engineering knowledge. In most cases, each contractor constructs a typical minaret with the same structural and architectural features regardless of the local soil conditions or seismicity of the region. [5]

Turkey is located in one of the most seismically active regions of the world. Fifty-seven destructive earthquakes have struck Turkey in the twentieth century, resulting in the destruction of infrastructure and more than 90 000 deaths. During these earthquakes, many minarets were damaged or have collapsed as shown in Figure 5.3. Sezen et al. [10] documents and discusses vulnerabilities and damages to 64 masonry and RC minarets after

the 1999 Kocaeli (Mw7.4) and Düzce (Mw7.2) earthquakes. As a result of these two earthquakes, the collapse of 115 minarets in the city of Düzce alone was reported [26]. Sezen et al. reports that approximately 70% of the RC and masonry minarets surveyed in Düzce sustained severe damage or collapsed. Even though the minarets are hardly ever occupied, they are located mostly in residential areas or shopping districts, and their collapse sometimes causes loss of life as shown in Figure 5.2. It is extremely important to regulate the construction and design of these slender structures for safety reasons in anticipation of future earthquakes. In addition to widespread earthquake damage and collapses, some reported failures of minarets due to wind loading indicate that most of these tower structures are vulnerable to lateral loads.

Figure 5.2. Collapse of a minaret onto a nearby building. [5]

Figure 5.3. Collapse of minaret on its main building. [5]

5.3. TMD Type Selection

The architectural, geometrical, and material properties of minarets vary widely. For example, the height of a typical minaret can be between 10 m and 55 m. The minaret may have one or more balconies. The representative RC minaret investigated in this study is assumed to be 50 m high, including a 11.5 m boot, 5.0 m transition segment, 27.7 m cylindrical body, and 6 m spire. The assumed outer diameter and thickness of the cylinder are 2.2 m and 0.25 m, respectively. The view of the representative minaret is shown in Figure 5.4. Larger technical drawings of the minaret can be found in Appendix D.

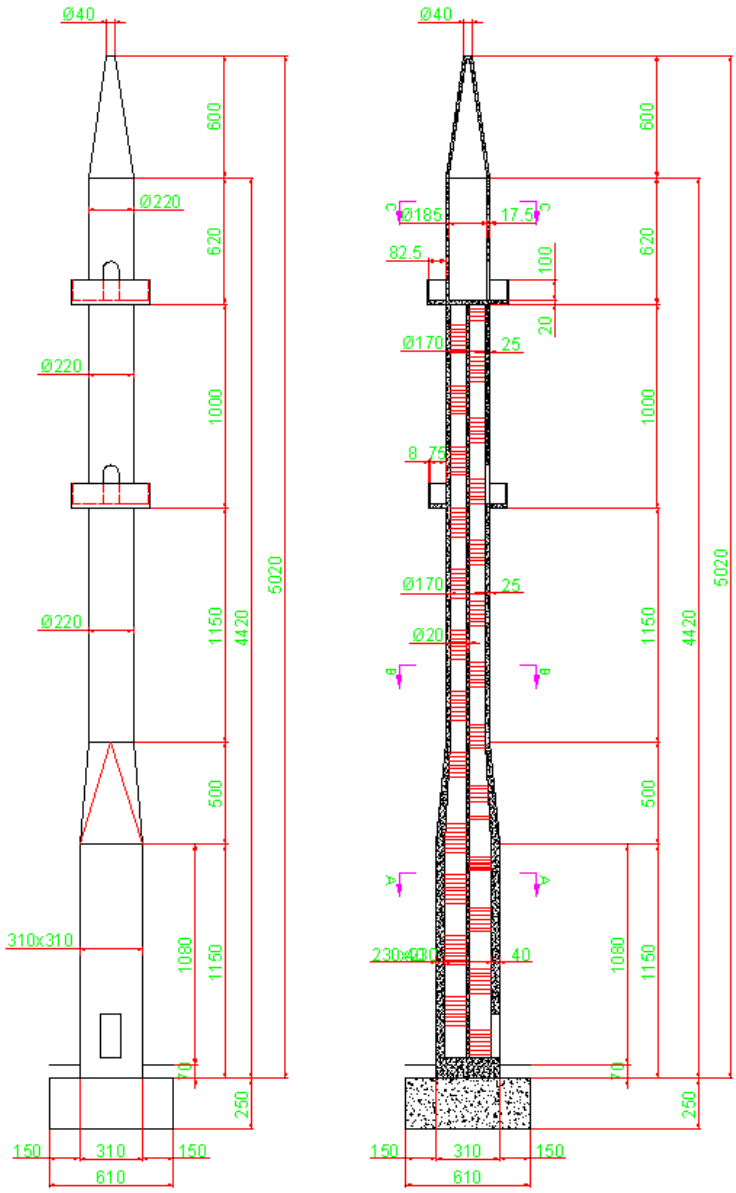

Figure 5.4. Minaret structure for the case study.

It will be a challenging job to find an appropriate place on minaret structure to install the TMD setup. Its outer view looks very slender and elegant. Any additional mass, spring, pendulum or damping unit will affect its architectural image. It might be a good idea to replace the balcony rail with rolled steel sheet and hang this sheet as additional mass with steel wires to the upper section. By this way we will not increase the total weight of the minaret by adding an additional mass on it and we might use the self weight of the balcony rails as damper mass. Hanging wires which work as pendulum length will affect the outlook of the minaret and will not be accepted by the architects. At the same time TSD or TLCD options could not be considered as a feasible option for our case due to water density. We need to store 1-2 % of the structure weight as water on top of the minaret. Unfortunately, there is not such a space there.

We should find a suitable location in the structure which does not to create any impact on outer view. Also TMD could be protected from atmospheric conditions and maintenance issue should be simplified. It was noted that inner staircase is terminated at upper balcony level. Therefore, inner room of the upper cylindrical body, from balcony level to the spire section will be a convenient place to install the TMD. Inner diameter is about 1.85 m and effective height is 4.0 m by allowing 2.0 m clearance for balcony door in case of any call for prayers.

Bidirectional translational damper can be configured with springs and dampers in two orthogonal directions and provide the capability for controlling structural motion in both directions. The layout of this configuration is shown in Figure 5.5. The problems associated with the bearings and sliding surface can be eliminated by supporting the mass with a steel rod which allow the system to behave as a pendulum. It should be a hybrid TMD between translational and pendulum type. Since the pendulum operates as a soft spring, TMD stiffness should be maintained primarily by orthogonal springs. This is a custom made pendulum type TMD with additional springs and viscous dampers. The layout of applicable TMD to the minaret is shown in Figure 5.6.

In this configuration radial displacement of TMD is less compared to the pendulum length. Therefore TMD mass makes small oscillations with an angle less than $\pi/6$ radians from vertical axis. In case of small oscillations, it is known that any system with an

orthogonal configuration of springs with $k/2$ stiffness will have an equivalent stiffness value k in any principal direction. The verification of this statement is shown in Appendix C.

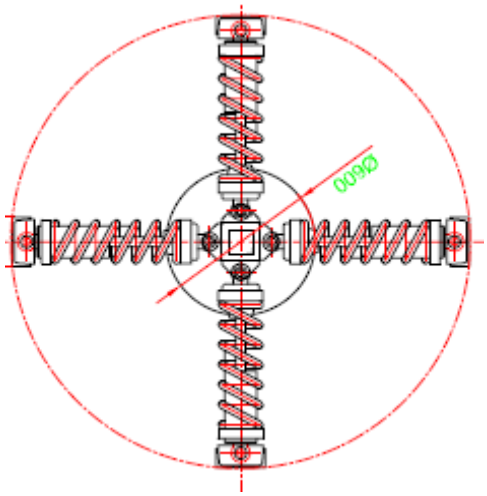

Figure 5.5. Springs and Dampers in two orthogonal directions.

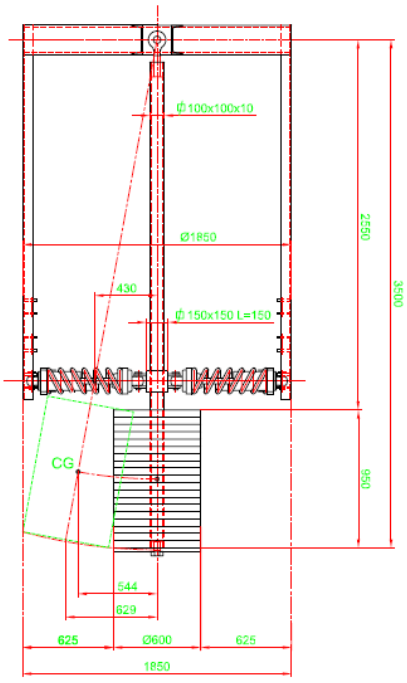

Figure 5.6. TMD layout developed for minarets

This type of TMD was used in La Prade Heavy Water Plant to improve wind response of an elevator tower.[6] Picture of this TMD is shown on Figure 5.7. Inverted pendulum was used in that project.

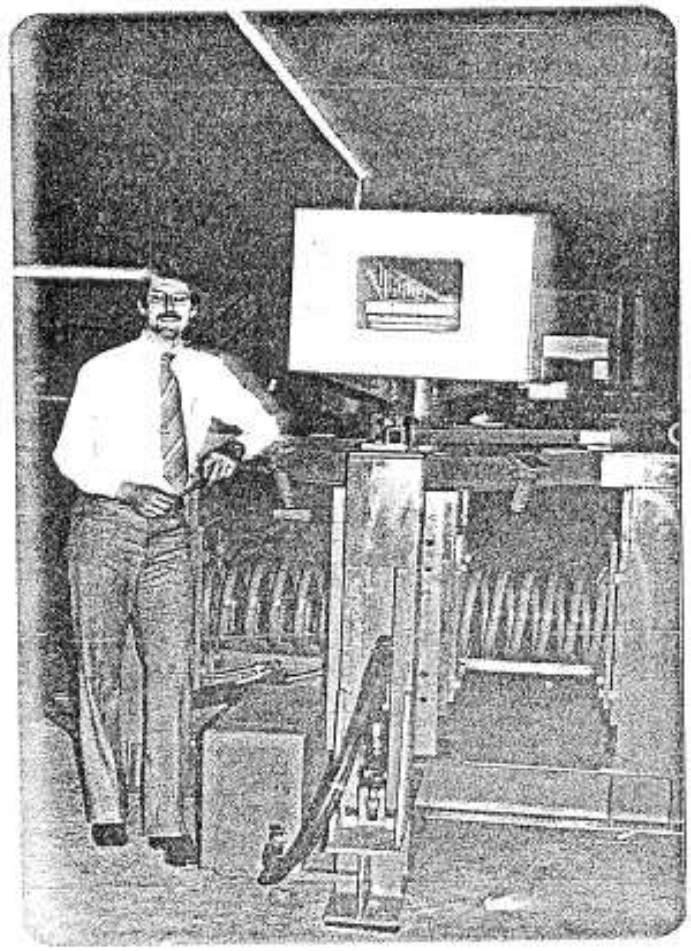

Figure 5.7. TMD used in La Prade Heavy Water Plant [6]

5.4. Vibration Analysis of the Minaret with Transfer Matrix Method

Conventional method for dynamic analysis of structures requires the well known equation of motion derived from Newton's 2nd law and dynamic equilibrium. This equation requires stiffness matrix for the system. Stiffness matrix can be obtained easily for framed structures moving on a plane or any system loaded axially. However flexural vibration creates bending and rotation effect on the system and is not so easy to obtain stiffness matrix.

Transfer Matrix Method explained in Chapter 3 was used to avoid the complexity of obtaining stiffness matrix of non-uniform cantilever beams. This method allows the successive determination of the deflection, slope, moment, and shear diagrams for any chosen frequency. Boundary conditions can be applied to the analysis by relatively

straightforward means, and structural damping can be included by introducing complex impedance.

Discrete mass model was used to perform the vibration analysis on the structure. This method of analysis considers the minaret to consist of a series of concentrated masses connected by massless beam sections. The relations which will link adjacent masses are formulated using the assumptions made for linear elastic materials. Each mass corresponds to the weight of one particular section of the minaret. The beam section which connects it to adjacent masses has a cross-section corresponding to the minaret model as shown in Figure 5.8. Average dimensions of the minaret were used at the tapered section. The relations can be mathematically combined with similar expressions for adjoining sections so that the beam equations can be represented as a series of matrices. The boundary conditions developed for the cantilever beam model are applied to the matrices corresponding to the sections at which these conditions occur. After computing the matrix resulting from the series of matrices, the determinant of the coefficients is set equal to zero to determine the eigenvalues or natural frequencies of the model. With these frequencies, deflection, slope, moment, and shear distributions against any excitation load can be plotted as a result of analysis.

Elastic material properties are used in all dynamic analyses presented below. This is mainly because the vast majority of RC minarets failed to develop plastic hinges during recent earthquakes. They either failed without any indication of ductile response as shown in Figure 5.3, or remained elastic with virtually no visible damage. [5]

It is usually burdensome to include all components in a structural model and consider their effect on the total behavior. Therefore inner stair cases can be ignored while modeling the structure.

Model of the minaret is consisting of 13 discrete masses and massless elastic sections as shown in Figure 5.8. Spire mass was modeled as concentrated mass m_{13}. Balcony and related platform masses are also considered in the value of m_{11} and m_8.

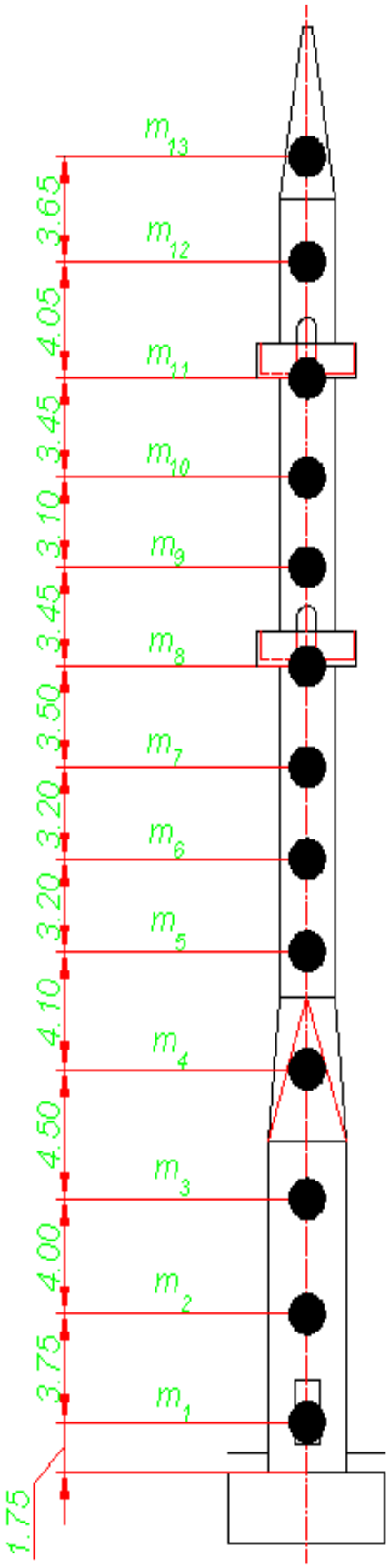

Figure 5.8. Discrete mass model of minaret

Mass, length and Inertia of the model sections are listed on Table 5.1.

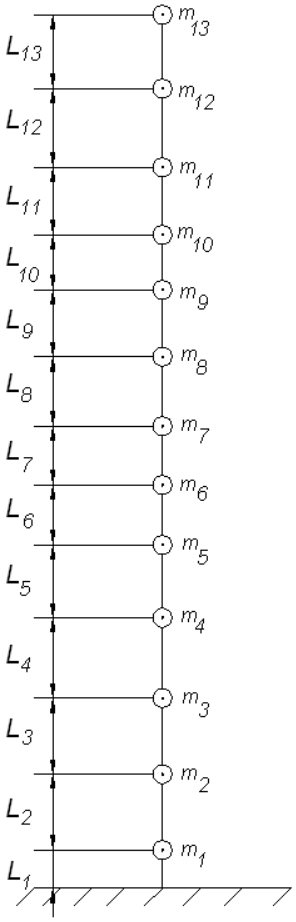

Figure 5.9. Simplified minaret model

Table 5.1. Mass, Length and Inertia values of the minaret model

m_i	Mass (kg)		L_i	Length (m)		I_i	Inertia (m^4)
m_1	36,3 10^3		L_1	1,75		I_1	5,364
m_2	41,5 10^3		L_2	3,75		I_2	5,364
m_3	41,5 10^3		L_3	4,00		I_3	5,364
m_4	35,2 10^3		L_4	4,50		I_4	5,364
m_5	11,8 10^3		L_5	4,10		I_5	0,74
m_6	11,8 10^3		L_6	3,20		I_6	0,74
m_7	11,8 10^3		L_7	3,20		I_7	0,74
m_8	20,1 10^3		L_8	3,50		I_8	0,74
m_9	11,4 10^3		L_9	3,45		I_9	0,74
m_{10}	11,4 10^3		L_{10}	3,10		I_{10}	0,74
m_{11}	18,2 10^3		L_{11}	3.45		I_{11}	0,74
m_{12}	11,5 10^3		L_{12}	4.05		I_{12}	0,575
m_{13}	7,8 10^3		L_{13}	3,65		I_{13}	0,575

Modulus of elasticity of concrete is taken as 27 GPa

E_i = 27 GPa valid for all sections.

Moment of inertia for the sections are estimated as follows;

h = 3.10 m ; b = 0.40 m

$$I_1 = I_2 = I_3 = I_4 = \frac{1}{12}\left[h^4 - (h-2b)^4\right]$$

D = 2.20 m ; d = 1.70 m

$$I_5 = I_6 = I_7 = I_8 = I_9 = I_{10} = I_{11} = \frac{\pi}{64}[D^4 - d^4] = 0,74\ m^4$$

D = 2.20 m ; d = 1.85 m

$$I_{12} = I_{13} = \frac{\pi}{64}[D^4 - d^4] = 0,575\ m^4$$

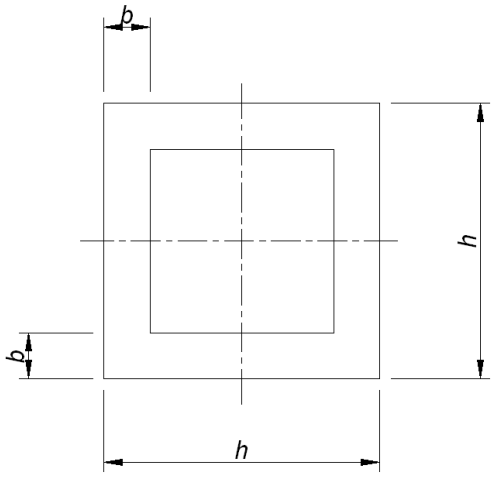

Figure 5.10: Cross section of minaret boot

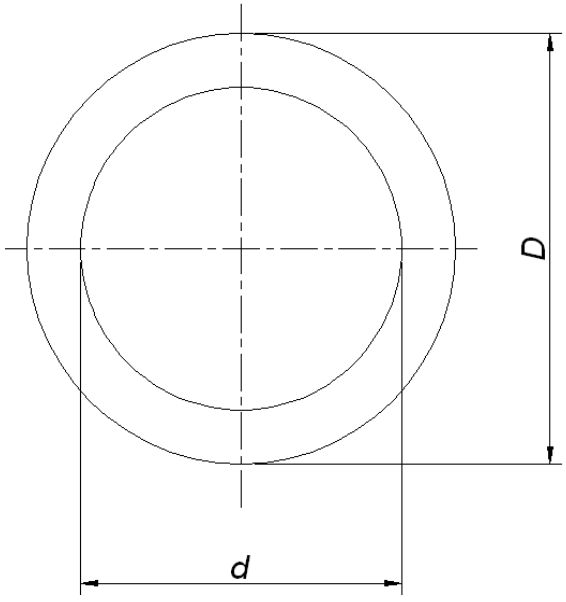

Figure 5.11. Cross section of cylindrical minaret body

5.4.1. Natural Frequencies of the Minaret

Free vibration of the model will be studied first. Since the structure has light structural damping, no damping will be assumed during free vibration. We know the relationship between state vector and field transfer matrix for free vibration as per Eq. 3.24;

$$\mathbf{z}_i^L = \mathbf{F}_i \mathbf{z}_{i-1}^R .$$

We also know the relationship between state vector and point transfer matrix for free vibration as per Eq. 3.30 is;

$$\mathbf{z}_i^R = \mathbf{P}_i \mathbf{z}_i^L$$

State vectors for each node on model will be as following;

$$\begin{aligned}
\mathbf{z}_1^L &= \mathbf{F}_1 \mathbf{z}_0 & \mathbf{z}_1^R &= \mathbf{P}_1 \mathbf{z}_1^L \\
\mathbf{z}_2^L &= \mathbf{F}_2 \mathbf{z}_1^R & \mathbf{z}_2^R &= \mathbf{P}_2 \mathbf{z}_2^L \\
\mathbf{z}_3^L &= \mathbf{F}_3 \mathbf{z}_2^R & \mathbf{z}_3^R &= \mathbf{P}_3 \mathbf{z}_3^L \\
\mathbf{z}_4^L &= \mathbf{F}_4 \mathbf{z}_3^R & \mathbf{z}_4^R &= \mathbf{P}_4 \mathbf{z}_4^L \\
\mathbf{z}_5^L &= \mathbf{F}_5 \mathbf{z}_4^R & \mathbf{z}_5^R &= \mathbf{P}_5 \mathbf{z}_5^L \\
\mathbf{z}_6^L &= \mathbf{F}_6 \mathbf{z}_5^R & \mathbf{z}_6^R &= \mathbf{P}_6 \mathbf{z}_6^L \\
\mathbf{z}_7^L &= \mathbf{F}_7 \mathbf{z}_6^R & \mathbf{z}_7^R &= \mathbf{P}_7 \mathbf{z}_7^L \\
\mathbf{z}_8^L &= \mathbf{F}_8 \mathbf{z}_7^R & \mathbf{z}_8^R &= \mathbf{P}_8 \mathbf{z}_8^L \\
\mathbf{z}_9^L &= \mathbf{F}_9 \mathbf{z}_8^R & \mathbf{z}_9^R &= \mathbf{P}_9 \mathbf{z}_9^L \\
\mathbf{z}_{10}^L &= \mathbf{F}_{10} \mathbf{z}_9^R & \mathbf{z}_{10}^R &= \mathbf{P}_{10} \mathbf{z}_{10}^L \\
\mathbf{z}_{11}^L &= \mathbf{F}_{11} \mathbf{z}_{10}^R & \mathbf{z}_{11}^R &= \mathbf{P}_{11} \mathbf{z}_{11}^L \\
\mathbf{z}_{12}^L &= \mathbf{F}_{12} \mathbf{z}_{11}^R & \mathbf{z}_{12}^R &= \mathbf{P}_{12} \mathbf{z}_{12}^L \\
\mathbf{z}_{13}^L &= \mathbf{F}_{13} \mathbf{z}_{12}^R & \mathbf{z}_{13}^R &= \mathbf{P}_{13} \mathbf{z}_{13}^L
\end{aligned}$$

State vectors are also defined in a shorter form;

$$\mathbf{z}_1^R = \mathbf{P}_1\,\mathbf{F}_1\,\mathbf{z}_0 \qquad \mathbf{z}_2^R = \mathbf{P}_2\,\mathbf{F}_2\,\mathbf{z}_1^R$$
$$\mathbf{z}_3^R = \mathbf{P}_3\,\mathbf{F}_3\,\mathbf{z}_2^R \qquad \mathbf{z}_4^R = \mathbf{P}_4\,\mathbf{F}_4\,\mathbf{z}_3^R$$
$$\mathbf{z}_5^R = \mathbf{P}_5\,\mathbf{F}_5\,\mathbf{z}_4^R \qquad \mathbf{z}_6^R = \mathbf{P}_6\,\mathbf{F}_6\,\mathbf{z}_5^R$$
$$\mathbf{z}_7^R = \mathbf{P}_7\,\mathbf{F}_7\,\mathbf{z}_6^R \qquad \mathbf{z}_8^R = \mathbf{P}_8\,\mathbf{F}_8\,\mathbf{z}_7^R$$
$$\mathbf{z}_9^R = \mathbf{P}_9\,\mathbf{F}_9\,\mathbf{z}_8^R \qquad \mathbf{z}_{10}^R = \mathbf{P}_{10}\,\mathbf{F}_{10}\,\mathbf{z}_9^R$$
$$\mathbf{z}_{11}^R = \mathbf{P}_{11}\,\mathbf{F}_{11}\,\mathbf{z}_{10}^R \qquad \mathbf{z}_{12}^R = \mathbf{P}_{12}\,\mathbf{F}_{12}\,\mathbf{z}_{11}^R$$
$$\mathbf{z}_{13} = \mathbf{P}_{13}\,\mathbf{F}_{13}\,\mathbf{z}_{12}^R$$

Eq. 3.52 allows to make in a more compact way;

$$\mathbf{z}_{13} = \mathbf{P}_{13}\,\mathbf{F}_{13}\,\mathbf{P}_{12}\,\mathbf{F}_{12}\,\mathbf{P}_{11}\,\mathbf{F}_{11}\,\mathbf{P}_{10}\,\mathbf{F}_{10}\,\mathbf{P}_9\,\mathbf{F}_9\,\mathbf{P}_8\,\mathbf{F}_8\,\mathbf{P}_7\,\mathbf{F}_7\,\mathbf{P}_6\,\mathbf{F}_6\,\mathbf{P}_5\,\mathbf{F}_5\,\mathbf{P}_4\,\mathbf{F}_4\,\mathbf{P}_3\,\mathbf{F}_3\,\mathbf{P}_2\,\mathbf{F}_2\,\mathbf{P}_1\,\mathbf{F}_1\,\mathbf{z}_0 \tag{5.1}$$

$$\mathbf{z}_{13} = \mathbf{U}\mathbf{z}_0 \tag{5.2}$$

$$\mathbf{U} = \mathbf{P}_{13}\,\mathbf{F}_{13}\,\mathbf{P}_{12}\,\mathbf{F}_{12}\,\mathbf{P}_{11}\,\mathbf{F}_{11}\,\mathbf{P}_{10}\,\mathbf{F}_{10}\,\mathbf{P}_9\,\mathbf{F}_9\,\mathbf{P}_8\,\mathbf{F}_8\,\mathbf{P}_7\,\mathbf{F}_7\,\mathbf{P}_6\,\mathbf{F}_6\,\mathbf{P}_5\,\mathbf{F}_5\,\mathbf{P}_4\,\mathbf{F}_4\,\mathbf{P}_3\,\mathbf{F}_3\,\mathbf{P}_2\,\mathbf{F}_2\,\mathbf{P}_1\,\mathbf{F}_1 \tag{5.3}$$

All field matrices are constructed by using the Eq. 4.23

$$\mathbf{F}_i = \begin{bmatrix} 1 & L_i & \dfrac{L_i^2}{2EI_i} & \dfrac{L_i^3}{6EI_i} \\ 0 & 1 & \dfrac{L_i}{EI_i} & \dfrac{L_i^2}{2EI_i} \\ 0 & 0 & 1 & L_i \\ 0 & 0 & 0 & 1 \end{bmatrix} \tag{5.4}$$

All point matrices are constructed by using the Eq. 4.29

$$\mathbf{P}_i = \begin{bmatrix} 1 & 0 & 0 & 0 \\ 0 & 1 & 0 & 0 \\ 0 & 0 & 1 & 0 \\ m_i\omega^2 & 0 & 0 & 1 \end{bmatrix} \tag{5.5}$$

Then, general transfer matrix **U** will be a 4x4 ;

$$\begin{bmatrix} u_{11} & u_{12} & u_{13} & u_{14} \\ u_{21} & u_{22} & u_{23} & u_{24} \\ u_{31} & u_{32} & u_{33} & u_{34} \\ u_{41} & u_{42} & u_{43} & u_{44} \end{bmatrix} \tag{5.6}$$

Boundary Conditions due to clamped at the base (node 0) and free at the tip (node 13) requires;

$$M_{13}= 0 \quad , \quad V_{13} = 0 \quad , \quad w_0 = 0 \quad , \quad \Psi_0 = 0$$

Governing equation between base and tip will be ;

$$\begin{bmatrix} -w \\ \Psi \\ 0 \\ 0 \end{bmatrix}_{13} = \begin{bmatrix} u_{11} & u_{12} & u_{13} & u_{14} \\ u_{21} & u_{22} & u_{23} & u_{24} \\ u_{31} & u_{32} & u_{33} & u_{34} \\ u_{41} & u_{42} & u_{43} & u_{44} \end{bmatrix} \begin{bmatrix} 0 \\ 0 \\ M \\ V \end{bmatrix}_0 \tag{5.7}$$

Eventually frequency determinant will be obtained by Eq. 4.61;

$$\begin{bmatrix} u_{33} & u_{34} \\ u_{43} & u_{44} \end{bmatrix} = 0 \tag{5.8}$$

Roots of the frequency determinant will give the square of natural frequencies. Matlab codes are submitted in Appendix A.1. for our case study. The natural frequencies of minaret structure obtained through Matlab are listed on Table 5.2.

Table 5.2. Natural frequencies and periods of discrete mass model obtained from Matlab

ω_i	Natural Frequencies (rad/sec)		f_i	Natural Frequencies (Hz)
ω_1	6,6		f_1	1,1
ω_2	32,2		f_2	5,1
ω_3	72,6		f_3	11,6
ω_4	137,2		f_4	21,8
ω_5	239,6		f_5	38,1
ω_6	355,5		f_6	56,6
ω_7	453,5		f_7	72,2
ω_8	630,2		f_8	100,3
ω_9	779,4		f_9	124,0
ω_{10}	1.010,0		f_{10}	160,8
ω_{11}	1.165,3		f_{11}	185.5
ω_{12}	1.336,9		f_{12}	212,8
ω_{13}	2.550,4		f_{13}	405,9

5.4.2. Natural Modes of the Minaret

Boundary conditions of fixed base structure requires w_0 (displacement at fixed end) and Ψ_0 (slope at fixed end) should be 0. Then the governing equation becomes;

$$u_{33} M_o + u_{34} V_0 = 0 \tag{5.9}$$

$$u_{34} M_o + u_{44} V_0 = 0 \tag{5.10}$$

Let's consider the Eq. 5.9 and get V_0 in terms of M_o

$$V_0 = -\frac{u_{33}}{u_{34}} M_0 \tag{5.11}$$

$$\begin{bmatrix} M \\ V \end{bmatrix}_0 = \begin{bmatrix} 1 \\ -\dfrac{u_{33}}{u_{34}} \end{bmatrix} M_0 \tag{5.12}$$

To determine the normal modes M_0 can be taken as unity;

$$\mathbf{z}_1 = \left(\mathbf{P}_1 \mathbf{F}_1\right)^* \begin{bmatrix} 1 \\ -\dfrac{u_{33}}{u_{34}} \end{bmatrix} \tag{5.13}$$

$(\mathbf{P}_i\ \mathbf{F}_i)^*$ means that 1st and 2nd column of matrix multiplication are multiplied by 0. Therefore they should be dropped.

$$\mathbf{z}_2 = (\mathbf{P}_2\ \mathbf{F}_2)^*\ \mathbf{z}_1 \tag{5.14}$$
$$\mathbf{z}_3 = (\mathbf{P}_3\ \mathbf{F}_3)^*\ \mathbf{z}_2 \tag{5.15}$$
$$\mathbf{z}_4 = (\mathbf{P}_4\ \mathbf{F}_4)^*\ \mathbf{z}_3 \tag{5.16}$$
$$\mathbf{z}_5 = (\mathbf{P}_5\ \mathbf{F}_5)^*\ \mathbf{z}_4 \tag{5.17}$$
$$\mathbf{z}_6 = (\mathbf{P}_6\ \mathbf{F}_6)^*\ \mathbf{z}_5 \tag{5.18}$$
$$\mathbf{z}_7 = (\mathbf{P}_7\ \mathbf{F}_7)^*\ \mathbf{z}_6 \tag{5.19}$$
$$\mathbf{z}_8 = (\mathbf{P}_8\ \mathbf{F}_8)^*\ \mathbf{z}_7 \tag{5.20}$$
$$\mathbf{z}_9 = (\mathbf{P}_9\ \mathbf{F}_9)^*\ \mathbf{z}_8 \tag{5.21}$$
$$\mathbf{z}_{10} = (\mathbf{P}_{10}\ \mathbf{F}_{10})^*\ \mathbf{z}_9 \tag{5.22}$$
$$\mathbf{z}_{11} = (\mathbf{P}_{11}\ \mathbf{F}_{11})^*\ \mathbf{z}_{10} \tag{5.23}$$
$$\mathbf{z}_{12} = (\mathbf{P}_{12}\ \mathbf{F}_{12})^*\ \mathbf{z}_{11} \tag{5.24}$$
$$\mathbf{z}_{13} = (\mathbf{P}_{13}\ \mathbf{F}_{13})^*\ \mathbf{z}_{12} \tag{5.25}$$

Any mode shape will be obtained by using the related natural frequency in the above mentioned calculations. Lateral displacement values (w) will be extracted from each state vector and their values are plotted after normalization against height of each node. Matlab codes are submitted in the Appendix A.2 for our case study. Mode shapes of minaret structure for flexural vibrations obtained through Matlab are shown in figures from 5.12 to 5.24.

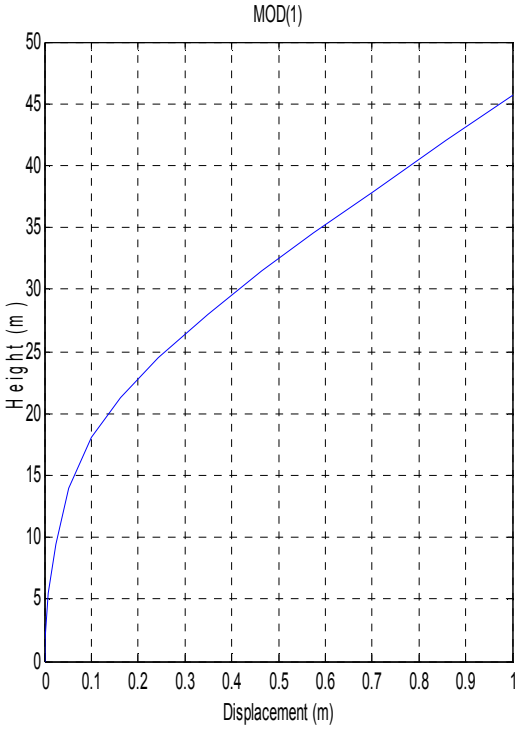

Figure 5.12. 1st Normal Mode Shape

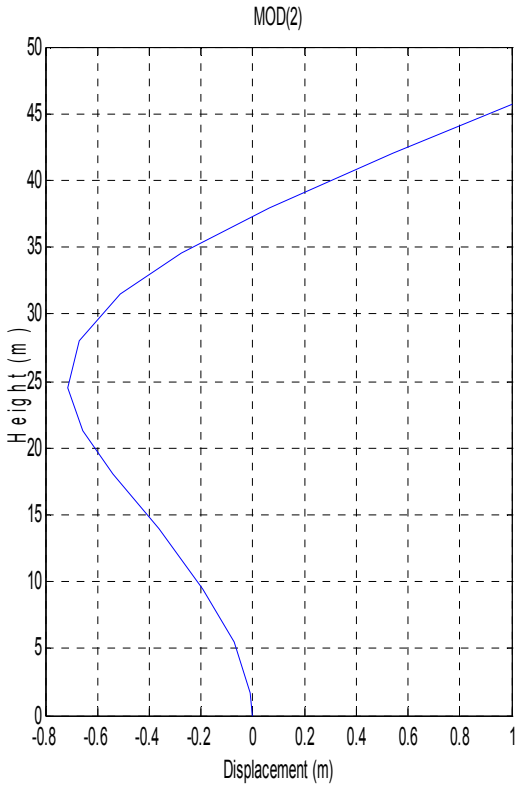

Figure 5.13. 2nd Normal Mode Shape

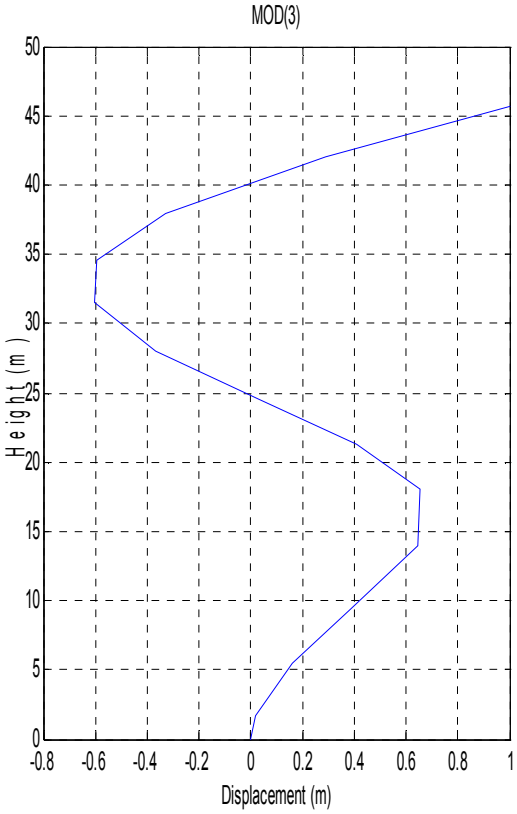

Figure 5.14. 3rd Normal Mode Shape

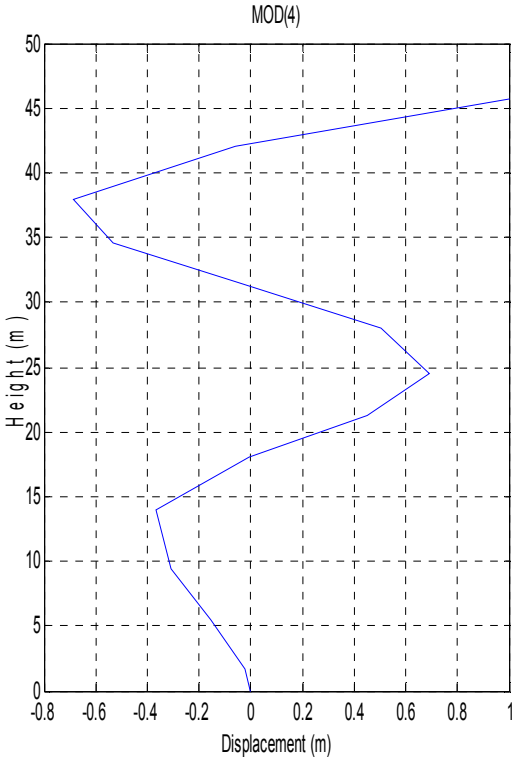

Figure 5.15. 4th Normal Mode Shape

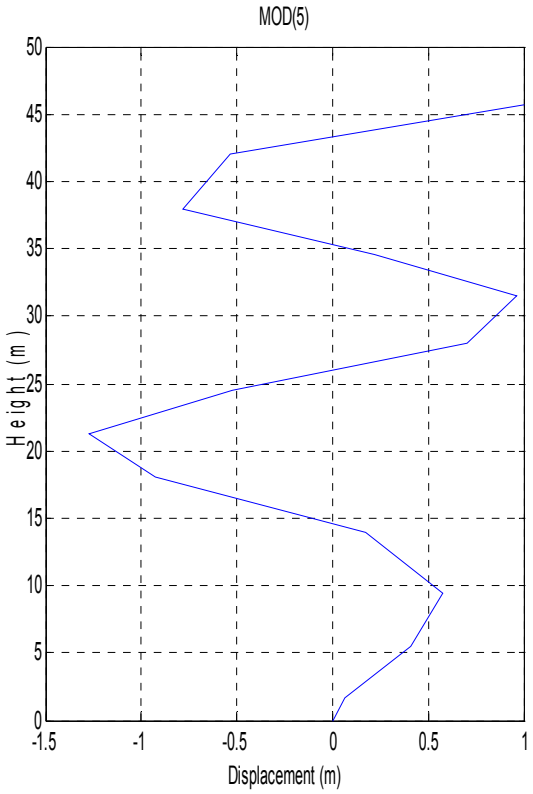

Figure 5.16. 5th Normal Mode Shape

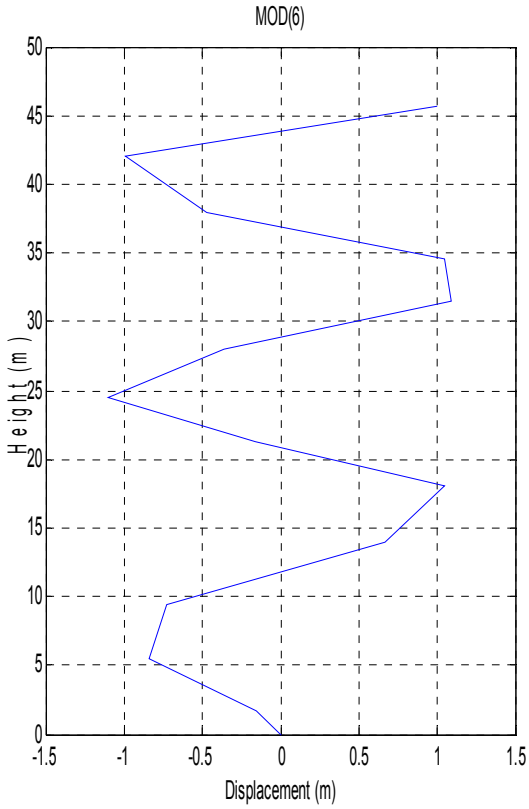

Figure 5.17. 6th Normal Mode Shape

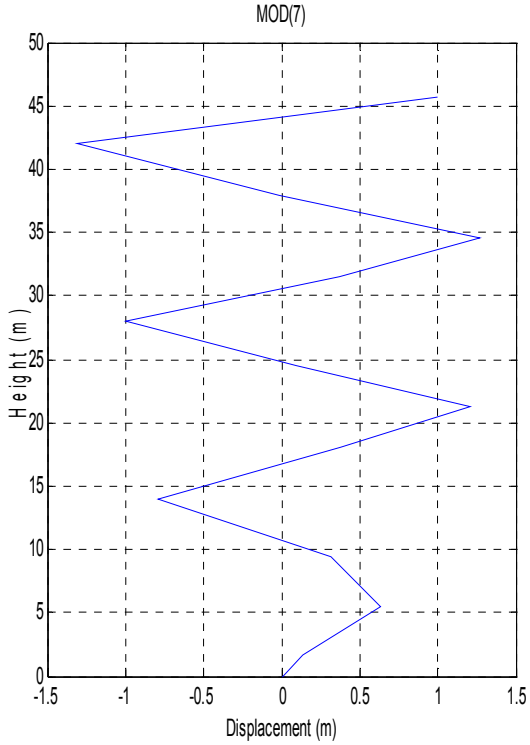

Figure 5.18. 7th Normal Mode Shape

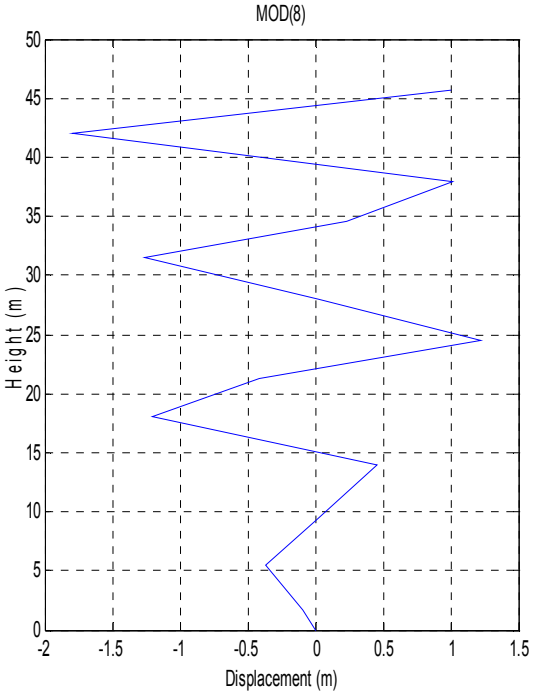

Figure 5.19. 8th Normal Mode Shape

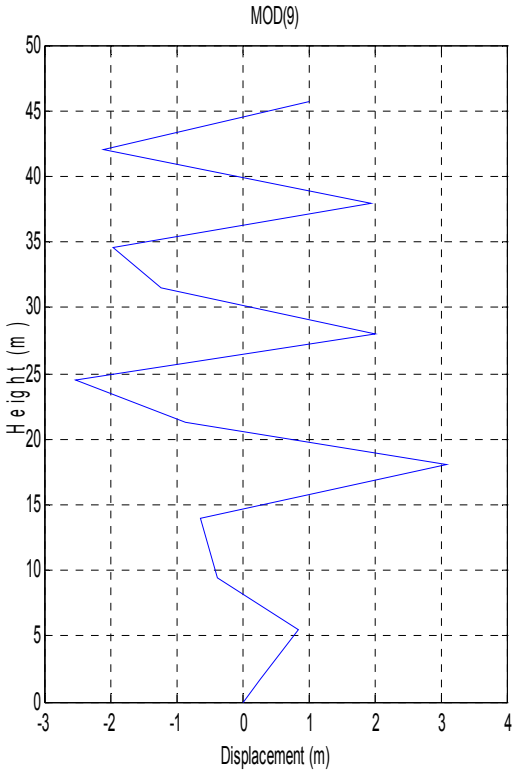

Figure 5.20. 9th Normal Mode Shape

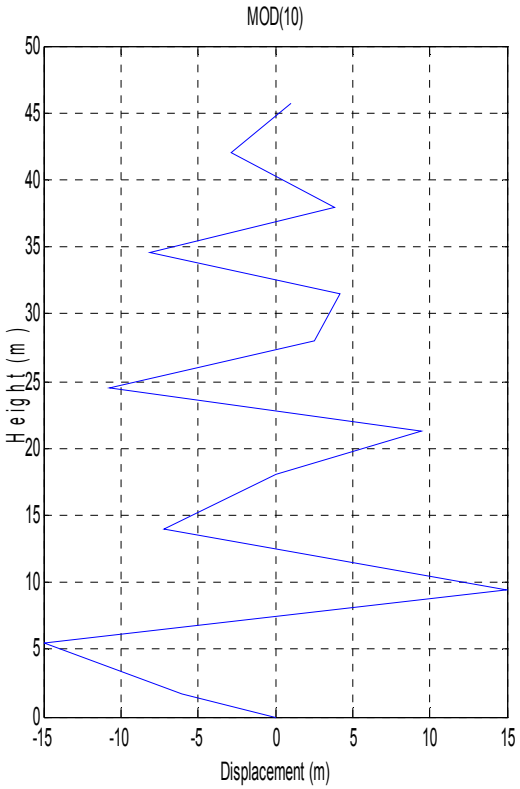

Figure 5.21. 10th Normal Mode Shape

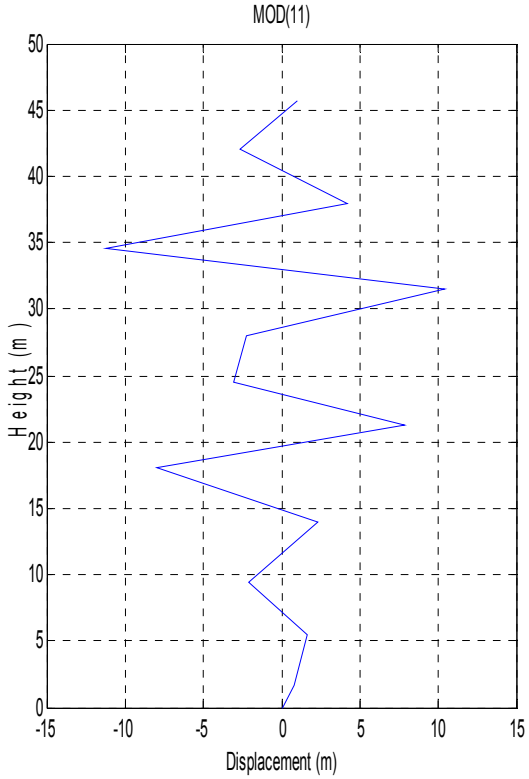

Figure 5.22. 11th Normal Mode Shape

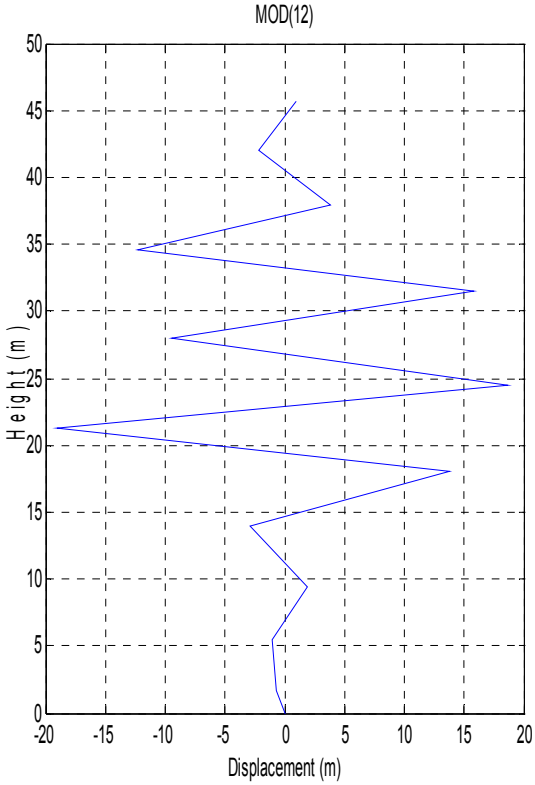

Figure 5.23. 12th Normal Mode Shape

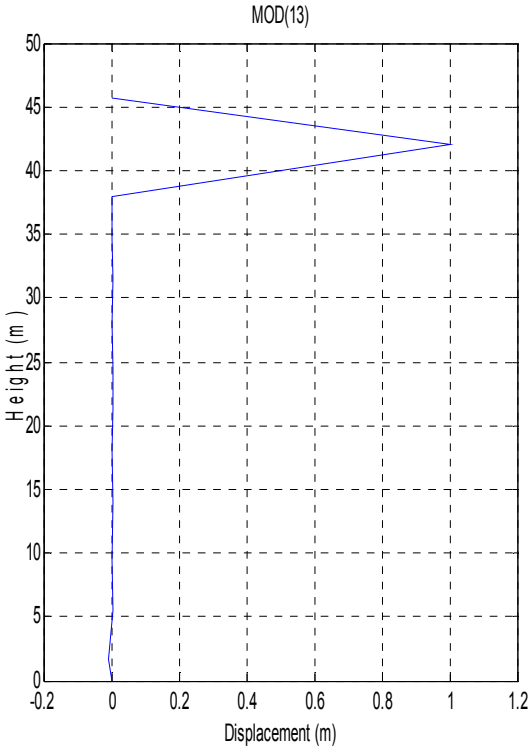

Figure 5.24. 13th Normal Mode Shape

5.4.3. TMD Model

Linear Elastic vibration analysis of a beam by using transfer matrix method was studied in Chapter 4. In case of a TMD application on main beam, branch formulation should be derived to account for TMD effect in the system. Due to geometrical constraints mentioned in section 5.3, upper part of the minaret body just below the spire was selected as best location for TMD installation. In fact, the best efficiency will be obtained when TMD is located in the spire. However there is not such a possibility. Therefore the selected location is considered almost the top level of the structure where TMD could be installed. We first consider no damping. A branch formulation for DVA which is connected to the node 12 is derived hereafter;

$$\begin{bmatrix} x \\ N \end{bmatrix}_2^L = \begin{bmatrix} 1 & \frac{1}{k_d} \\ 0 & 1 \end{bmatrix} \begin{bmatrix} x \\ N \end{bmatrix}_1^R \tag{5.26}$$

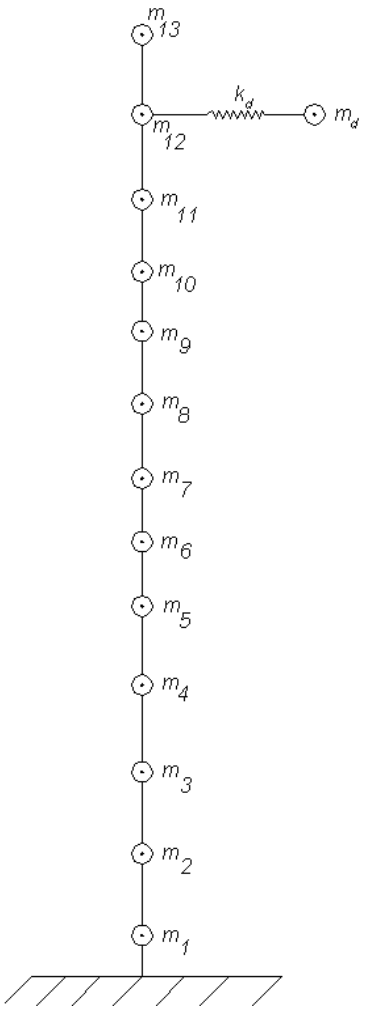

Figure 5.25. Minaret model with a DVA

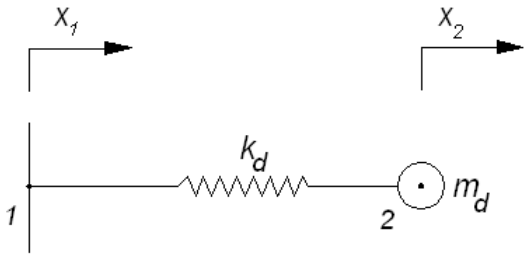

Figure 5.26. DVA model

$$N_1 = N_2 = k_d\,(x_2 - x_1) \tag{5.27}$$

$$x_2 = \frac{N_1}{k_d} + x_1 \tag{5.28}$$

$$\begin{bmatrix} x \\ N \end{bmatrix}_2^R = \begin{bmatrix} 1 & 0 \\ -m_d\omega^2 & 1 \end{bmatrix} \begin{bmatrix} x \\ N \end{bmatrix}_2^L \tag{5.29}$$

$$\begin{bmatrix} x \\ N \end{bmatrix}_2^R = \begin{bmatrix} 1 & 0 \\ -m_d\omega^2 & 1 \end{bmatrix} \begin{bmatrix} 1 & \frac{1}{k_d} \\ 0 & 1 \end{bmatrix} \begin{bmatrix} x \\ N \end{bmatrix}_1^R \tag{5.30}$$

$$\begin{bmatrix} x \\ 0 \end{bmatrix}_2^R = \begin{bmatrix} 1 & \frac{1}{k_d} \\ -m_d\omega^2 & \frac{-m_d\omega^2}{k_d}+1 \end{bmatrix}_1^R \begin{bmatrix} x \\ N \end{bmatrix}_1^R = \begin{bmatrix} A & B \\ C & D \end{bmatrix} \begin{bmatrix} x \\ N \end{bmatrix}_1^R \tag{5.31}$$

$$x_2 = A x_1 + B\, N \tag{5.32}$$

$$0 = C\, x_1 + D\, N \tag{5.33}$$

$$N = -\frac{C}{D} x_1 \tag{5.34}$$

$$N = k_{eq}\ x_1 \tag{5.35}$$

$$k_{eq} = \frac{k_d\ m_d\ \omega^2}{(k_d - m_d\ \omega^2)} \tag{5.36}$$

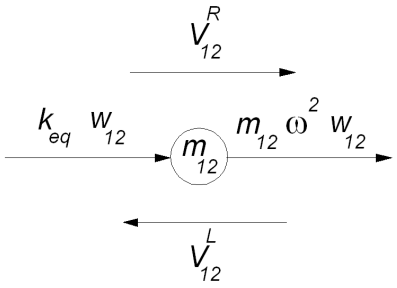

Figure 5.27. Free body diagram mass m_{12}

Free body diagram of m_{12} shown on Figure 5.27 yields simple equilibrium condition;

$$V_{12}^{R} = V_{12}^{L} - (m_{12}\ \omega^2 + k_{eq})\ w_{12} \tag{5.37}$$

Point transfer matrix for mass m_{12} will be as following;

$$\mathbf{P}_{12} = \begin{bmatrix} 1 & 0 & 0 & 0 \\ 0 & 1 & 0 & 0 \\ 0 & 0 & 1 & 0 \\ m_{12}\ \omega^2 + k_{eq} & 0 & 0 & 1 \end{bmatrix} \tag{5.38}$$

All other transfer matrices $\mathbf{F}_i$ and $\mathbf{P}_i$ are the same as in the case of without DVA except $\mathbf{P}_{12}$. $\mathbf{P}_{12}$ should be a special one due to DVA effect. When damping is included in a DVA, then it is called TMD configuration as shown in Figure 5.28. Damping effect should be inserted in the stiffness value of the spring by considering the damper's complex impedance or complex stiffness $jc\omega$.

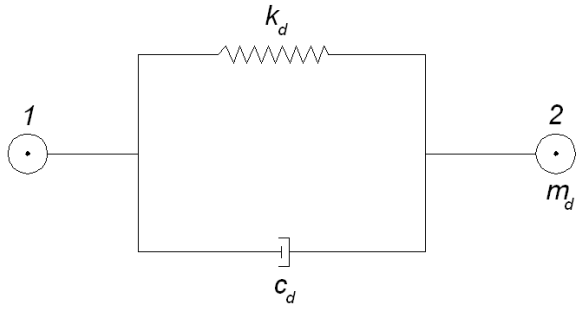

Figure 5.28: TMD model without mass

k_{dc} = Total stiffness of the damped system.

$$k_{dc} = k_d + jc_d\omega \tag{5.39}$$

$$j = \sqrt{-1} \tag{5.40}$$

We obtain the equivalent stiffness of a TMD on mass m_{12} by inserting Eq. 5.39 in Eq. 5.36;

k_{deq} = Equivalent stiffness of TMD on mass m_{12}

$$k_{deq} = \frac{k_{dc}\ m_d\ \omega^2}{k_{dc} - m_d\ \omega^2} \tag{5.41}$$

$$k_{deq} = \frac{k_d{}^2\ m_d\ \omega^2 - k_d\ m_d^2\ \omega^4 + c_d{}^2\ m_d\ \omega^4}{(k_d - m_d\ \omega^2)^2 + c_d{}^2\ \omega^2} - j\frac{c_d\ m_d^2\ \omega^5}{(k_d - m_d\ \omega^2)^2 + c_d{}^2\ \omega^2} \tag{5.42}$$

In case of an earthquake ground motion, there will be an external force on all masses in the system with $m_i\ \ddot{u}_g$ magnitude.

where

m_i : discrete mass of each element

$\ddot{u}_g$: peak ground displacement

TMD mass will also receive this earthquake force. Eq. 5.33 should be changed due to equivalent earthquake force.

$$0 = C\,x_1 + D\,N + E \tag{5.43}$$

where $E = -\ m_d\ \ddot{u}_g$

$$N = -\frac{C}{D}\ x_1 - \frac{E}{D} \tag{5.44}$$

$$N = k_{deq}\ x_1 + F \tag{5.45}$$

$$F = -\frac{m_d\ddot{u}_g(k_d{}^2 - k_d m_d\omega^2 + c_d{}^2\omega^2)}{(k_d - m_d\omega^2)^2 + c_d{}^2\omega^2} + j\frac{m_d\ddot{u}_g(c_d m_d\omega^3)}{(k_d - m_d\omega^2)^2 + c_d{}^2\omega^2} \tag{5.46}$$

5.4.4. TMD Optimization

We need to develop a Single Degree of Freedom (SDOF) system to obtain the optimized TMD parameters as explained in section 3.2.2. Fixed base structure should be converted to a model with a single mass on top of a massless beam. This is a typical SDOF system as shown in Figure 5.29. Natural frequency of the SDOF model should be identical with the 1st natural frequency of minaret. Equivalent mass at free end where TMD located should be calculated. Therefore the height of the beam should be considered as height of the TMD in minaret. It is assumed that structure has uniform bending stiffness. Lateral deflection of such beam with *m/L* unit mass from basic strength of materials will be as follows;

$$y(x) = \frac{Px^2}{6EI}(3L - x) \tag{5.47}$$

$$y(x) = \frac{y_{max}x^2}{2L^3}(3L - x) \tag{5.48}$$

$$\dot{y}(x) = \frac{\dot{y}_{max}}{2L^3}(3x^2L - x^3) \tag{5.49}$$

$$T = \frac{1}{2}m\,[\dot{y}(x)]^2 \tag{5.50}$$

$$T_{\max} = \frac{1}{2}\frac{m}{L}\left(\frac{\dot{y}_{\max}}{2L^3}\right)^2 \int_0^L (3x\,L - x^3)^2\,dx \tag{5.51}$$

$$T_{\max} = \frac{1}{2}\frac{m}{L}\frac{(\dot{y}_{\max})^2}{4L^6}\frac{33}{35}L^7 \tag{5.52}$$

$$T_{\max} = \frac{1}{2}\frac{33}{140}m\,(\dot{y}_{\max})^2 \tag{5.53}$$

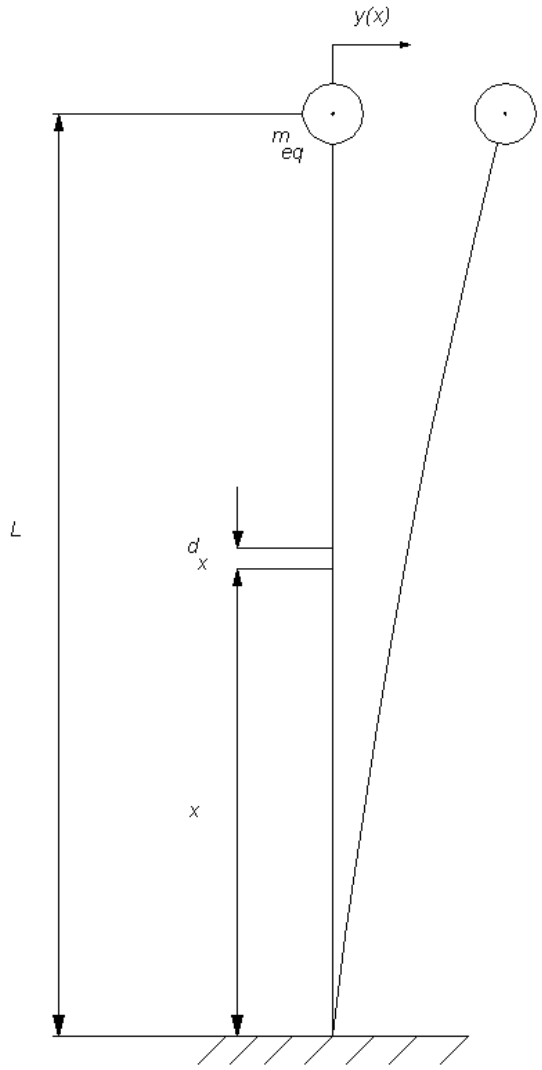

Figure 5.29. SDOF model of minaret

By Rayleigh's Energy Method

$$T_1+U_1 = T_2+U_2 \tag{5.54}$$

$$T_{\max} = \frac{1}{2} m_{eq} (\dot{y}_{\max})^2 \tag{5.55}$$

$$m_{eq} = 0.236 \text{ m} \tag{5.56}$$

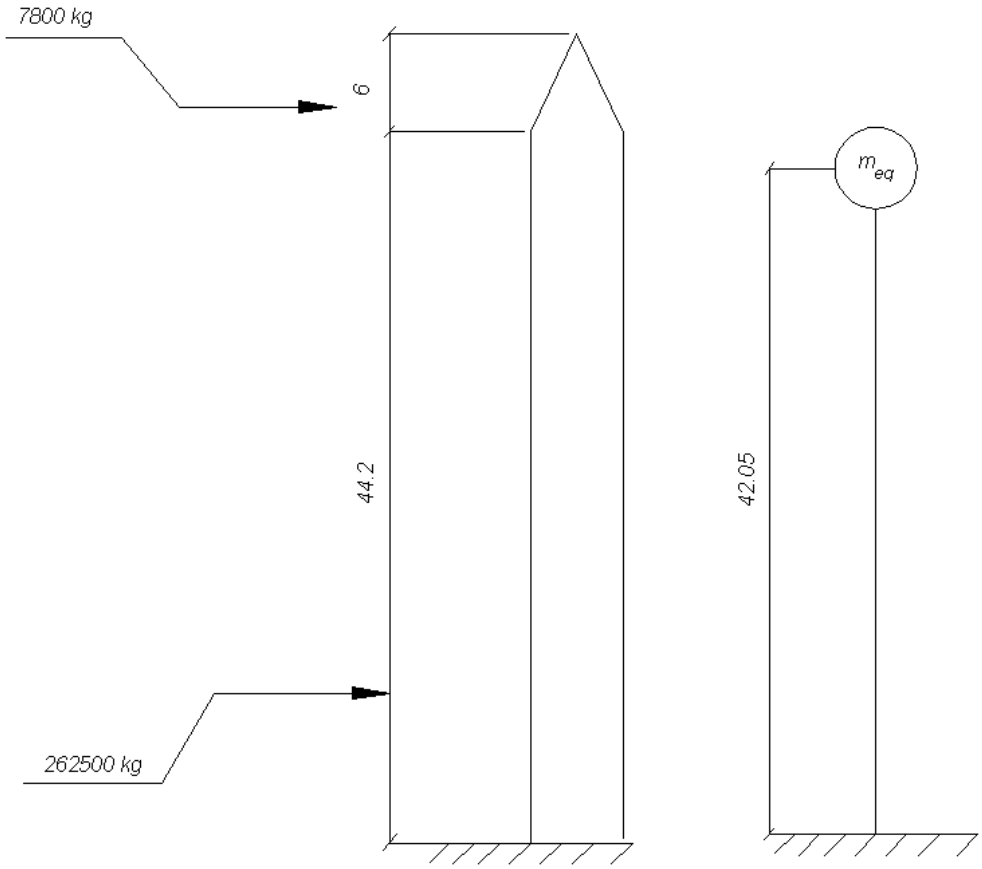

Figure 5.30: Equivalent mass for SDOF model

It is also assumed that minaret has a constant bending stiffness.

$$m_{eq} = 262500 \text{ x } 0.236 + 7800$$

$$m_{eq} = 69750 \text{ kg}$$

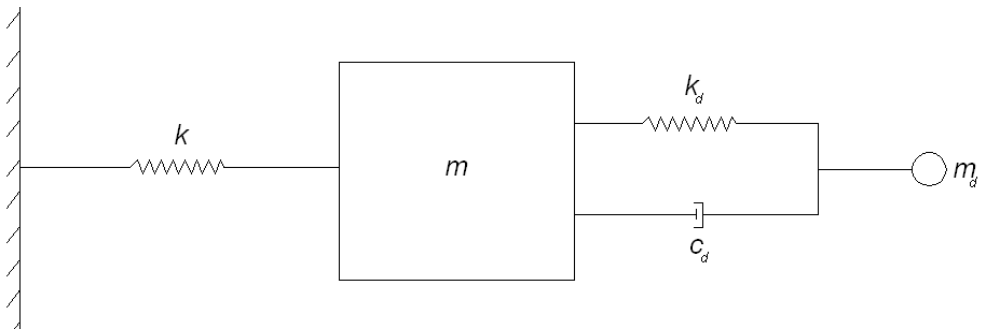

Figure 5.31. SDOF model of minaret with TMD

Due to geometrical constrains, there is a limited space inside the minaret to locate the TMD. Therefore the size of TMD mass should be minimized. We also know that when the mass ratio is smaller, the displacement of the TMD mass is increased. Section 3.2.2 states that the allowable values of primary mass displacement and TMD mass should be estimated for the design loading at first. This data provides the design values for $H_2|_{opt}$ and $H_4|_{opt}$.

- Let's assume a mass ratio as 0.05 due to space limitation at the upper part of the minaret. Figure 3.10 shows that optimum displacement ratio is 4 against 0.05 mass ratio [19]. Given displacement ratio looks acceptable.

  m = 69750 kg , m_d = 3490 kg

- Determine f_{opt} from Figure 3.5.
  f_{opt} = 0.94

- Compute ω_d, $\omega_d = f_{opt}\,\omega$
  ω_d = 6.2 rad/sec

- Compute k_d, $k_d = m_d\,\omega_d^2$
  k_d = 134.155 N/m

- Determine $\xi_d|_{opt}$ from Figure 3.7.
  $\xi_d|_{opt}$ = 0.135

- Compute c_d, $c_d = 2\xi_d|_{opt}\,m_d\,\omega_d$
  c_d = 5842 N sec/m

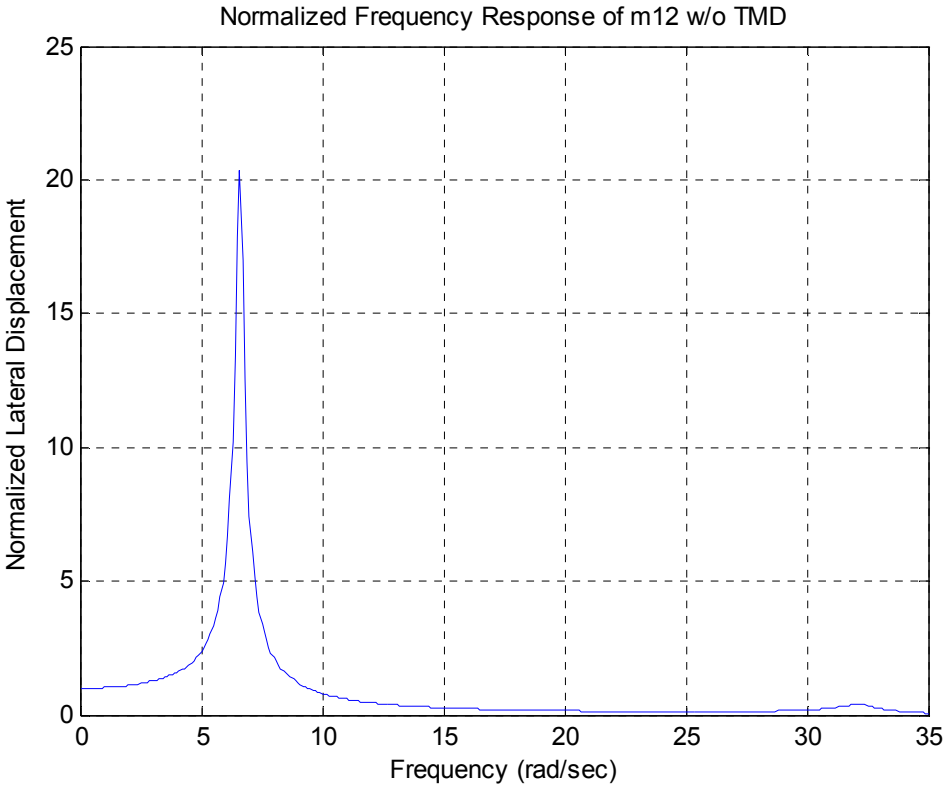

Figure 5.32. Normalized frequency response of m_{12} without TMD

Frequency response of minaret model without a TMD is shown in Figure 5.32. Frequency response of minaret model with TMD at m_{12} elevation is also shown in Figure 5.33. Optimized TMD parameters obtained through SDOF approximation were used in this response. It is easily seen that optimization is not perfect. Two peaks of the response curve are not at same level. The main reason for this deviation from the optimum state is the SDOF approximation.

A Matlab code was developed to estimate the optimized TMD parameters by applying iterations. We will use the existing parameters as an initial guess values for the new optimization program. The related Matlab codes are available in Appendix A.3. Optimized stiffness and damping values are estimated as follows;

k_d = 125.970 N/m $\qquad\qquad$ c_d = 7.020 N sec/m

Frequency response with optimized parameters are shown in Figure 5.33 and Figure 5.34. The related Matlab codes are available in Appendix A.4.

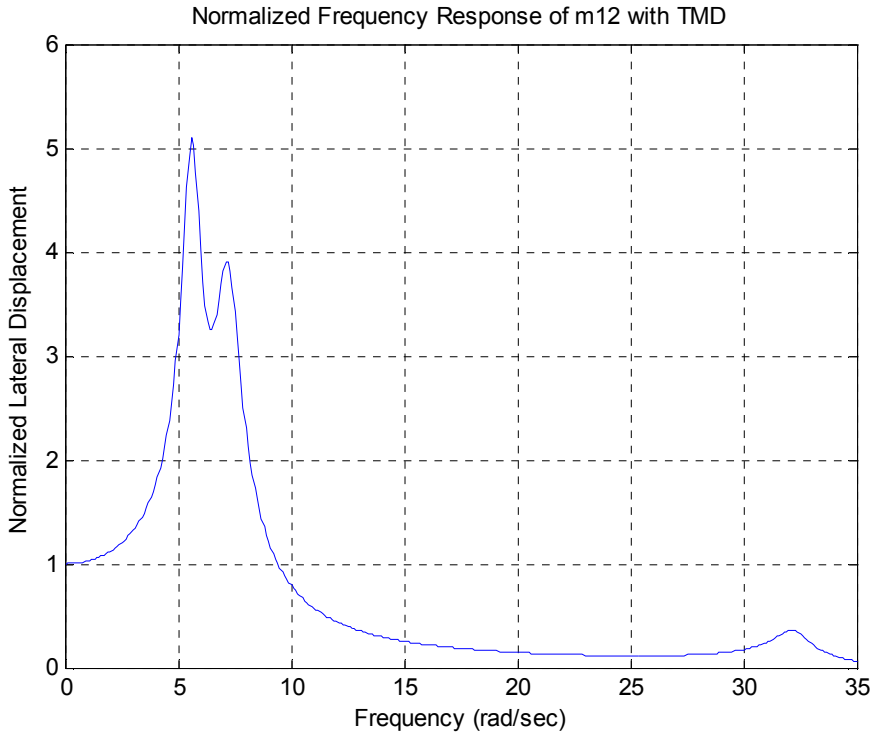

Figure 5.33. Normalized frequency response of m_{12} with TMD

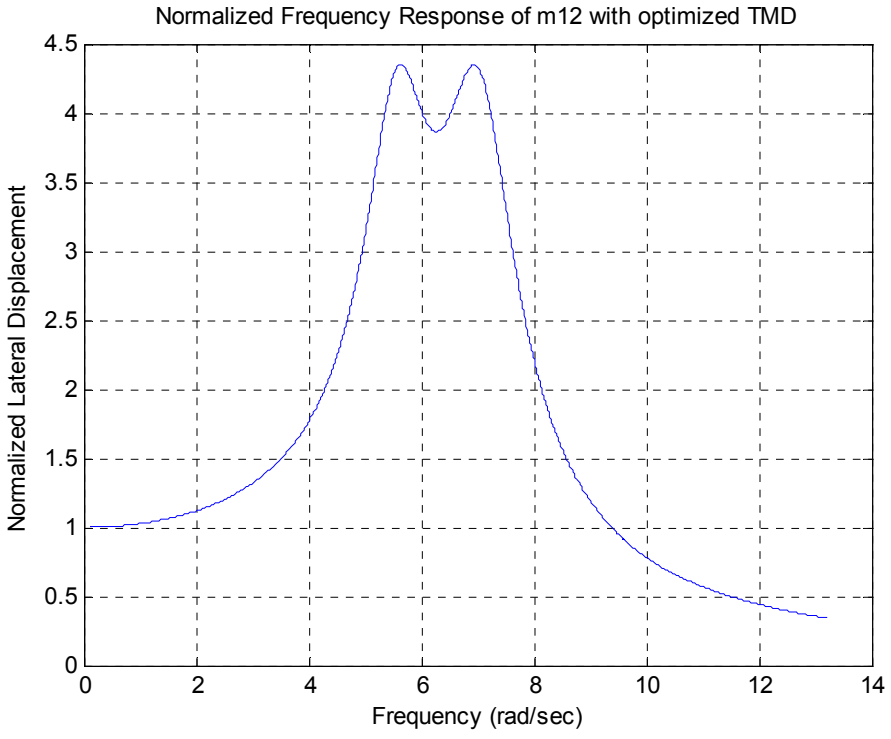

Figure 5.34. Normalized frequency response of m_{12} with optimized TMD around 1st natural frequency

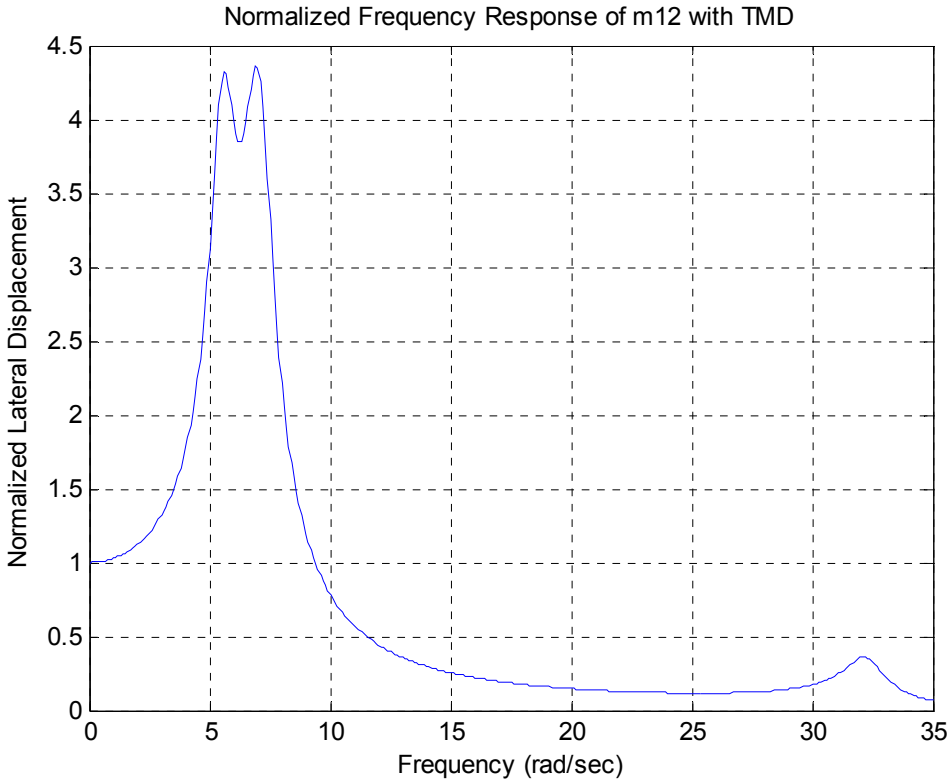

Figure 5.35. Normalized frequency response of m_{12} with optimized TMD around 1st and 2nd natural frequency

5.4.5. Dynamic Analysis of Minaret Against Harmonic Base Excitation Through MATLAB

Discrete mass model described in section 5.4 was used also here. First, the minaret without TMD is analyzed then the minaret with TMD.

5.4.5.1. Dynamic Analysis of Minaret without TMD. Structural damping values are taken as 5% for reinforced concrete structures. Transfer functions which accommodate the structural damping were mentioned in Section 4.7. Eq. 4.101 shows the field transfer function for a flexural massless beam in case of a forced vibration. Point transfer function on a flexural massless beam will be as following in case of base excitation;

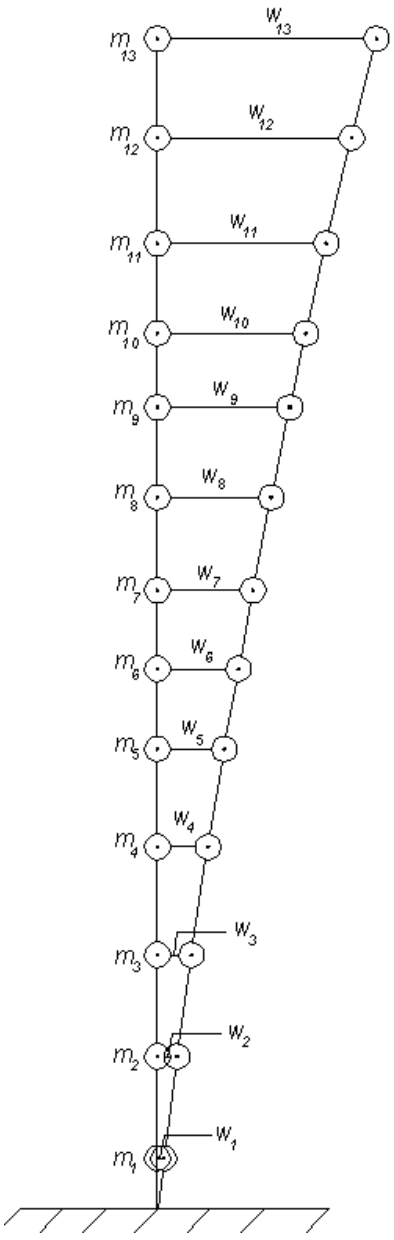

Figure 5.36. Flexural vibration model of minaret without TMD

w_i = Displacement of ith node

$\ddot{u}_g$ = Base excitation acceleration

m_i = Concentrated masses

$$\tilde{\mathbf{U}}_i = \left[\begin{array}{cccc:cccc:c} 1 & 0 & 0 & 0 & 0 & 0 & 0 & 0 & 0 \\ 0 & 1 & 0 & 0 & 0 & 0 & 0 & 0 & 0 \\ 0 & 0 & 1 & 0 & 0 & 0 & 0 & 0 & 0 \\ m_i\omega^2 & 0 & 0 & 1 & 0 & 0 & 0 & 0 & -m_i u_g \\ \hdashline 0 & 0 & 0 & 0 & 0 & 0 & 0 & 0 & 0 \\ 0 & 0 & 0 & 0 & 0 & 1 & 0 & 0 & 0 \\ 0 & 0 & 0 & 0 & 0 & 0 & 1 & 0 & 0 \\ 0 & 0 & 0 & 0 & m_i\omega^2 & 0 & 0 & 1 & 0 \\ \hdashline 0 & 0 & 0 & 0 & 0 & 0 & 0 & 0 & 1 \end{array}\right]_i \quad (5.57)$$

Similar matrix operations should be performed here as applied in Section 5.4.3. Only forcing terms and structural damping coefficients should be added in transfer functions. Related MATLAB codes are submitted in Appendix A.5.

Let's apply 2 harmonic base excitation as following;

Case 1: $\omega = 6{,}6$ rad/sec (1^{st} natural frequency)

$\ddot{u}_g = A \sin \omega t$

$A = 1.0$ m /sec^2

Case 2: $\omega = 32{,}2$ rad/sec(2^{nd} natural frequency)

$\ddot{u}_g = A \sin \omega t$

$A = 1.0$ m/ sec^2

Output response of the model for 1^{st} Case are plotted in Figure 5.37 to Figure 5.44 and 2^{nd} Case are plotted in Figure 5.45 to Figure 5.52.

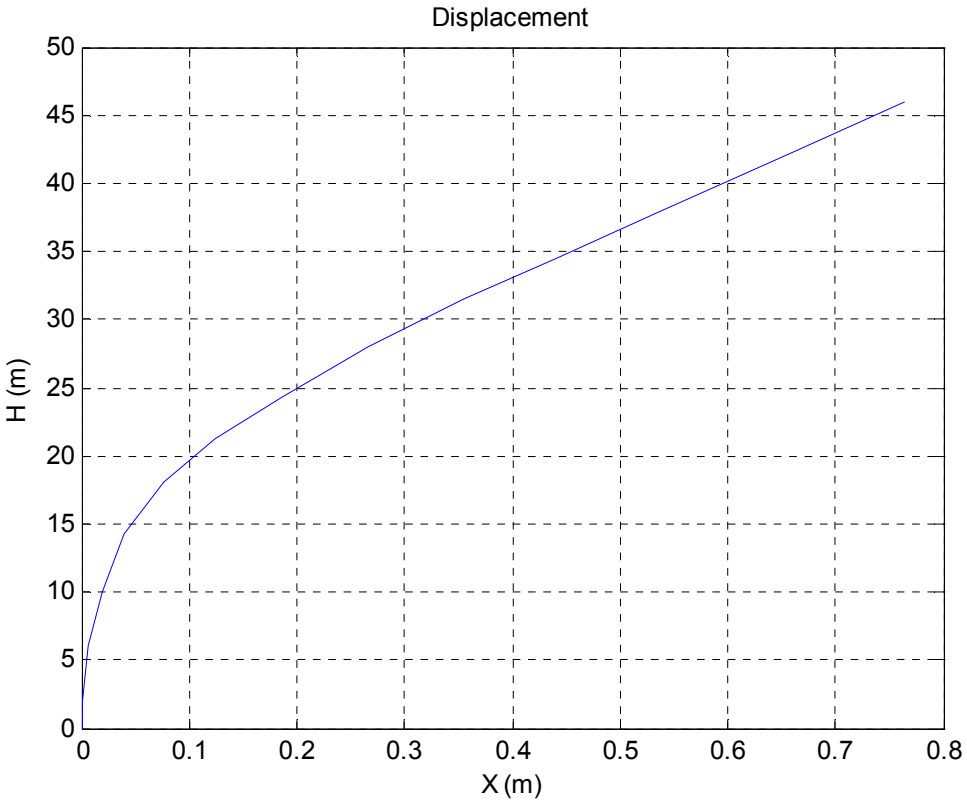

Figure 5.37. Displacement curve / case 1 no TMD

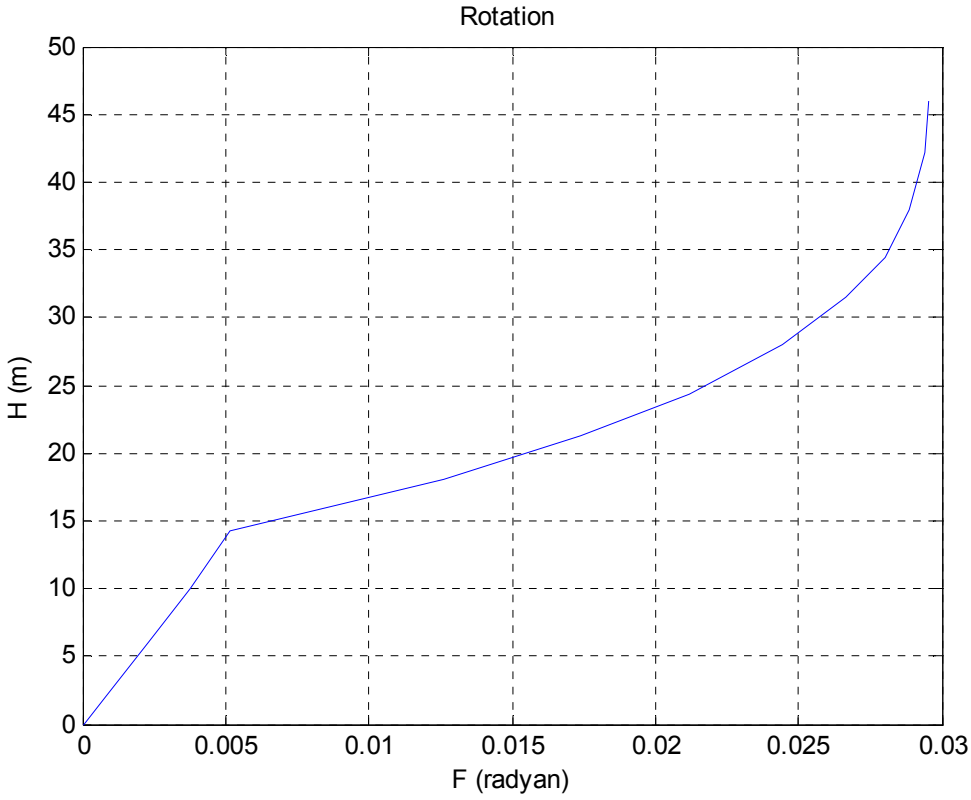

Figure 5.38. Rotation diagram / case 1 no TMD

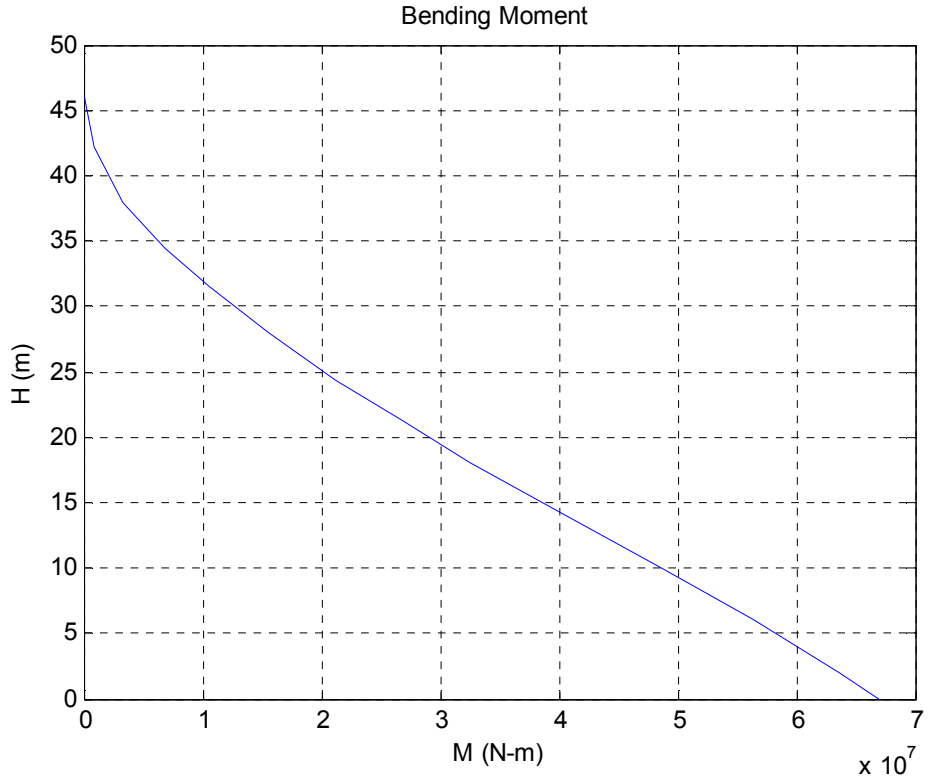

Figure 5.39. Moment diagram / case 1 no TMD

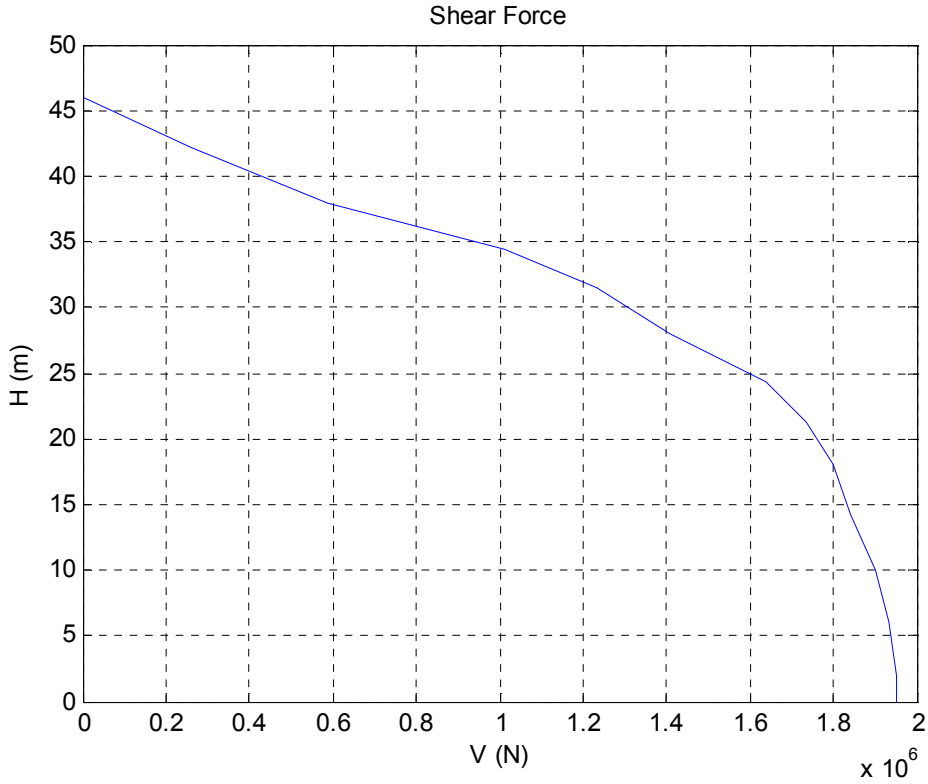

Figure 5.40. Shear diagram / case 1 no TMD

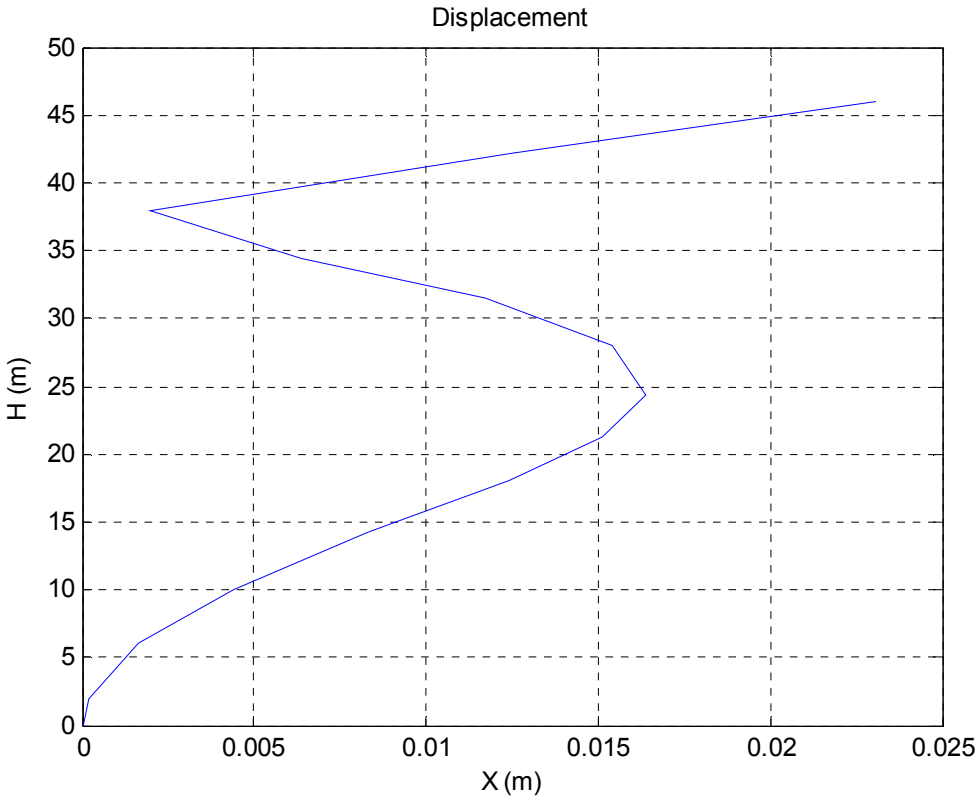

Figure 5.41. Absolute Displacement curve / case 2 no TMD

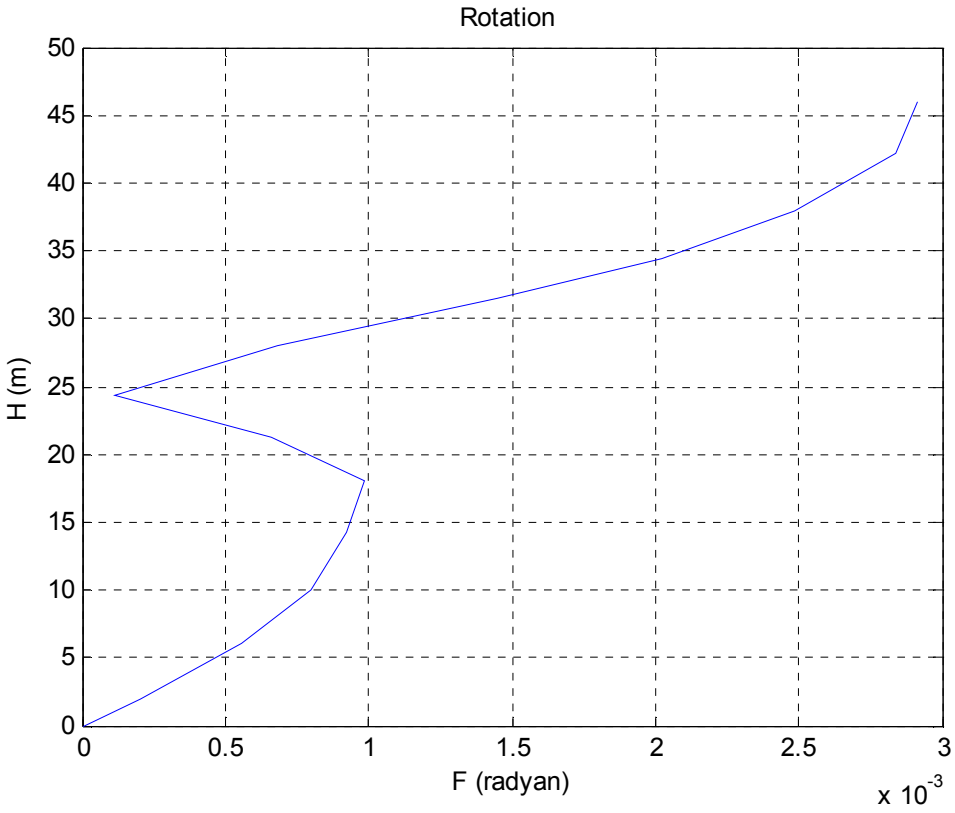

Figure 5.42. Absolute Rotation diagram / case 2 no TMD

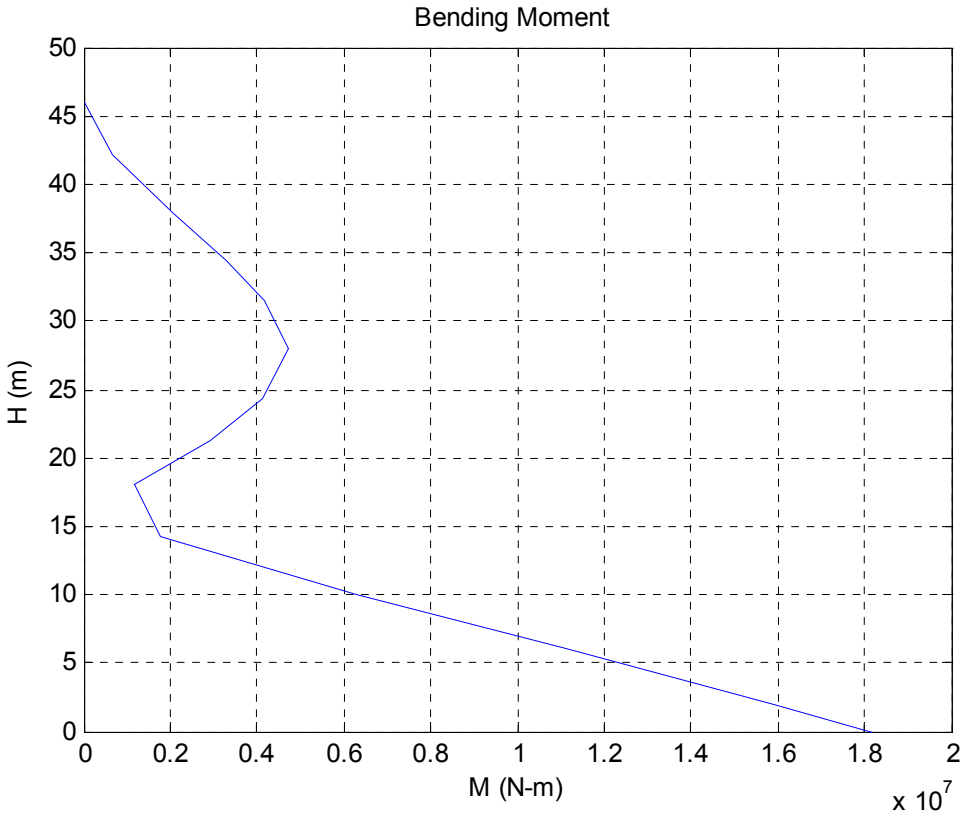

Figure 5.43. Absolute Moment diagram / case 2 no TMD

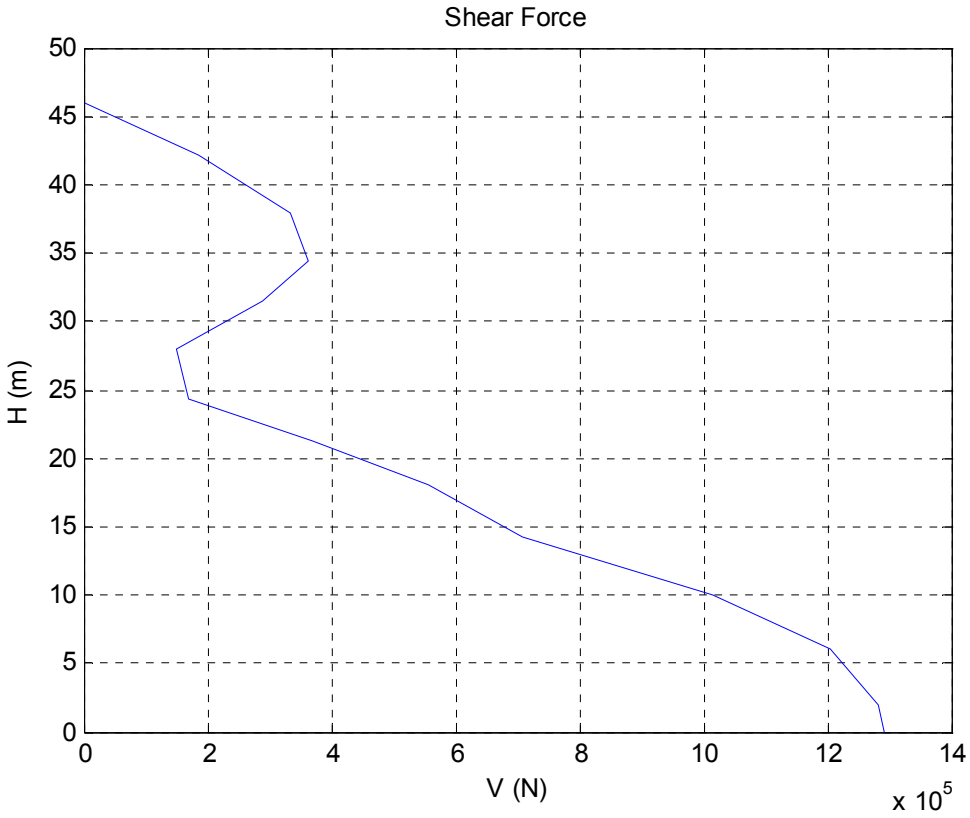

Figure 5.44. Absolute Shear diagram / case 2 no TMD

Observations from the minarets that collapsed during recent earthquakes showed that the bottom of the cylindrical minaret body immediately above the transition segment is the most vulnerable section under seismic loading [5]. Therefore, reactions and stress state at 4^{th} node will also be investigated together with base reactions and deflections at 12^{th} node where TMD installation is planned. They are listed on the Table 5.3.

Table 5.3. Response outputs of minaret without TMD against harmonic base excitation

		Case 1	Case 2
Displacement at 12^{th} node	(m)	65.6×10^{-2}	1.3×10^{-2}
Base shear	(N)	1.95×10^{6}	1.29×10^{6}
Base moment	(N m)	67.07×10^{6}	18.19×10^{6}
Shear at 4^{th} node	(N)	1.84×10^{6}	0.71×10^{6}
Moment at 4^{th} node	(N m)	40.08×10^{6}	1.76×10^{6}
Shear stress at 4^{th} node	(MPa)	1.20	0.46
Bending stress at 4^{th} node	(MPa)	59.6	2.62

It should be noted that according to the current Turkish building code [13], the minimum concrete strength is 20 MPa. It is assumed that representative minaret was constructed according to the minimum code requirements. It is easily seen that during the vibration at 1^{st} natural frequency, bending stress at 4^{th} node exceeds concrete bearing capacity and crack occurs. Structure collapse will follow the non ductile behavior. However the stresses during 2^{nd} natural frequency vibration are below the elastic limit.

5.4.5.2. Dynamic Analysis of Minaret with TMD. In case of TMD involvement, only point transfer function at 12^{th} node should be changed by the addition of Eq. 5.45 to the related transfer matrices.

$$A = \frac{k^2 m_d \omega^2 - k_d m_d^2 \omega^4 + c_d{}^2 m_d \omega^4}{(k_d - m_d \omega^2)^2 + c_d{}^2 \omega^2} \quad ; \quad B = -\frac{c_d m_d^2 \omega^5}{(k_d - m_d \omega^2)^2 + c_d{}^2 \omega^2}$$

$$C = -\frac{m_d \ddot{u}_g (k_d{}^2 - k_d m_d \omega^2 + c_d{}^2 \omega^2)}{(k_d - m_d \omega^2)^2 + c_d{}^2 \omega^2} \quad ; \quad D = \frac{m_d \ddot{u}_g (c_d m_d \omega^3)}{(k_d - m_d \omega^2)^2 + c_d{}^2 \omega^2}$$

$$\tilde{U}_{12} = \left[\begin{array}{cccc:cccc:c} 1 & 0 & 0 & 0 & 0 & 0 & 0 & 0 & 0 \\ 0 & 1 & 0 & 0 & 0 & 0 & 0 & 0 & 0 \\ 0 & 0 & 1 & 0 & 0 & 0 & 0 & 0 & 0 \\ m_{12}\omega^2 + A & 0 & 0 & 1 & -B & 0 & 0 & 0 & -m_{12}u_g + C \\ \hdashline 0 & 0 & 0 & 0 & 0 & 0 & 0 & 0 & 0 \\ 0 & 0 & 0 & 0 & 0 & 1 & 0 & 0 & 0 \\ 0 & 0 & 0 & 0 & 0 & 0 & 1 & 0 & 0 \\ B & 0 & 0 & 0 & m_{12}\omega^2 + A & 0 & 0 & 1 & D \\ \hdashline 0 & 0 & 0 & 0 & 0 & 0 & 0 & 0 & 1 \end{array}\right]_i \tag{5.58}$$

Let's use the same optimal stiffness and damping values obtained through optimization program in section 5.4.4.

Where, k_d = 125.970 N/m , c_d = 7.020 N sec/m , m_d = 3.490 kg

Matlab codes for dynamic analysis of minaret model with TMD are submitted in Appendix A.6. The same base excitation parameters are applied as in the previous section for minaret without TMD;

Case 1: ω = 6.6 rad/sec (1st natural frequency)

$\ddot{u}_g = A \sin \omega t$

A = 1.0 m/sec^2

Case 2: ω = 32.2 rad/sec(2nd natural frequency)

$\ddot{u}_g = A \sin \omega t$

A = 1.0 m/sec^2

Output response of the model for 1st Case are plotted in Figure 5.45 to Figure 5.48 and 2nd Case are plotted in Figure 5.49 to Figure 5.52.

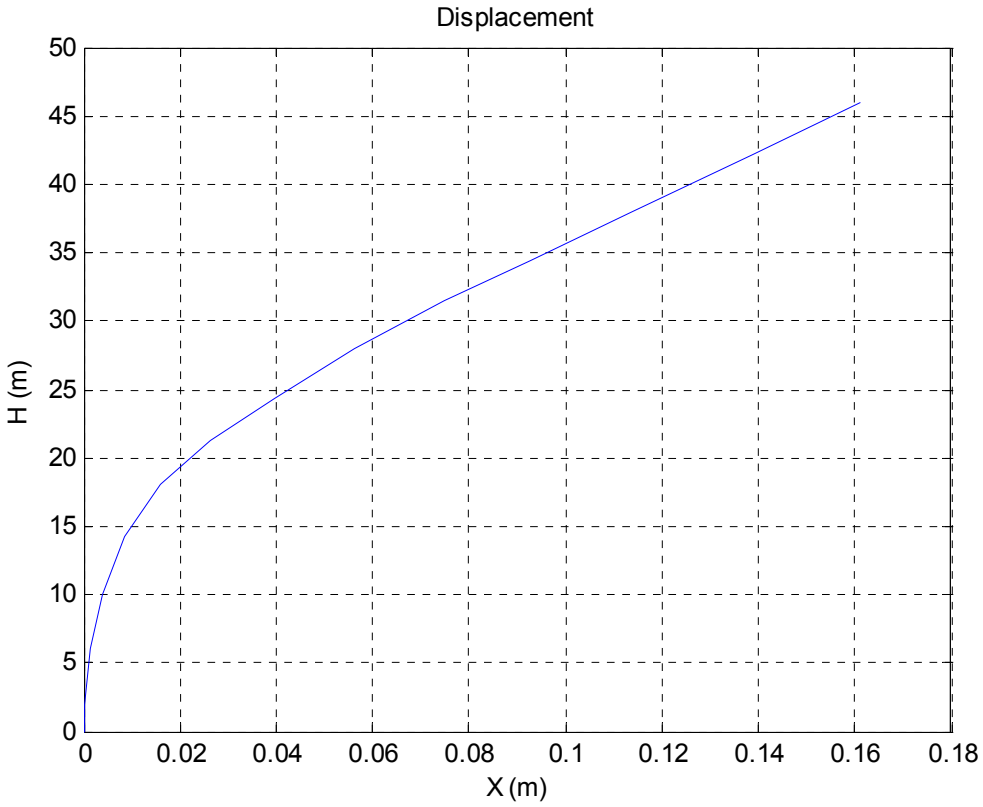

Figure 5.45. Displacement curve / case 1 with TMD

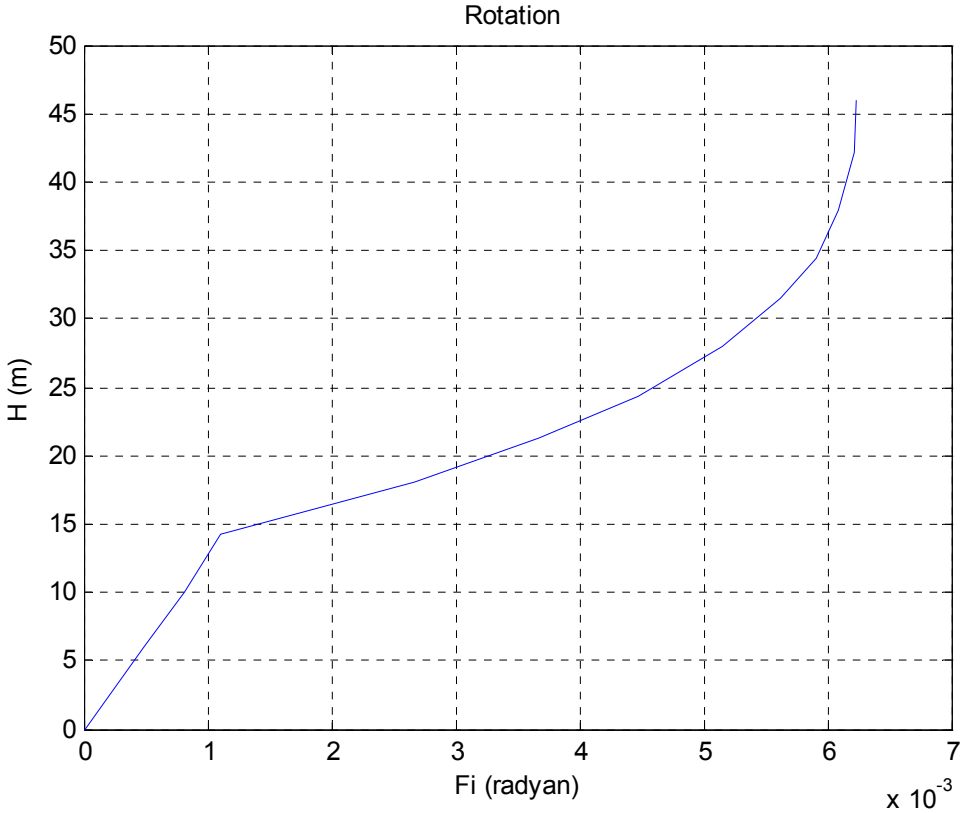

Figure 5.46. Rotation diagram / case 1 with TMD

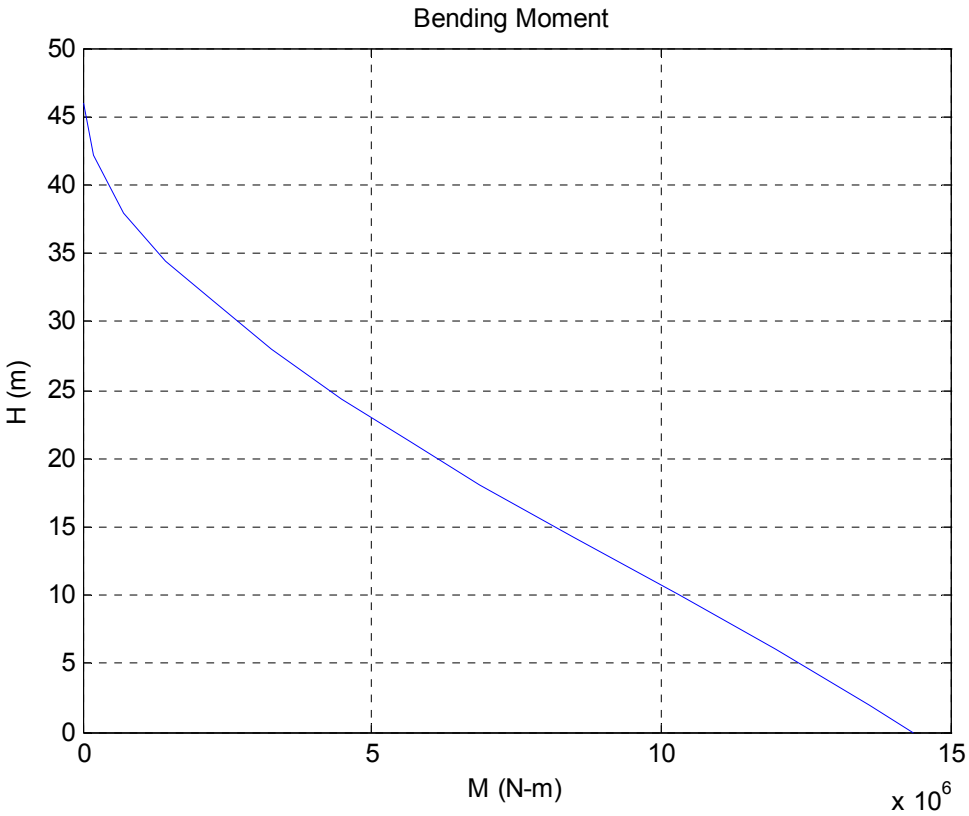

Figure 5.47. Moment diagram / case 1 with TMD

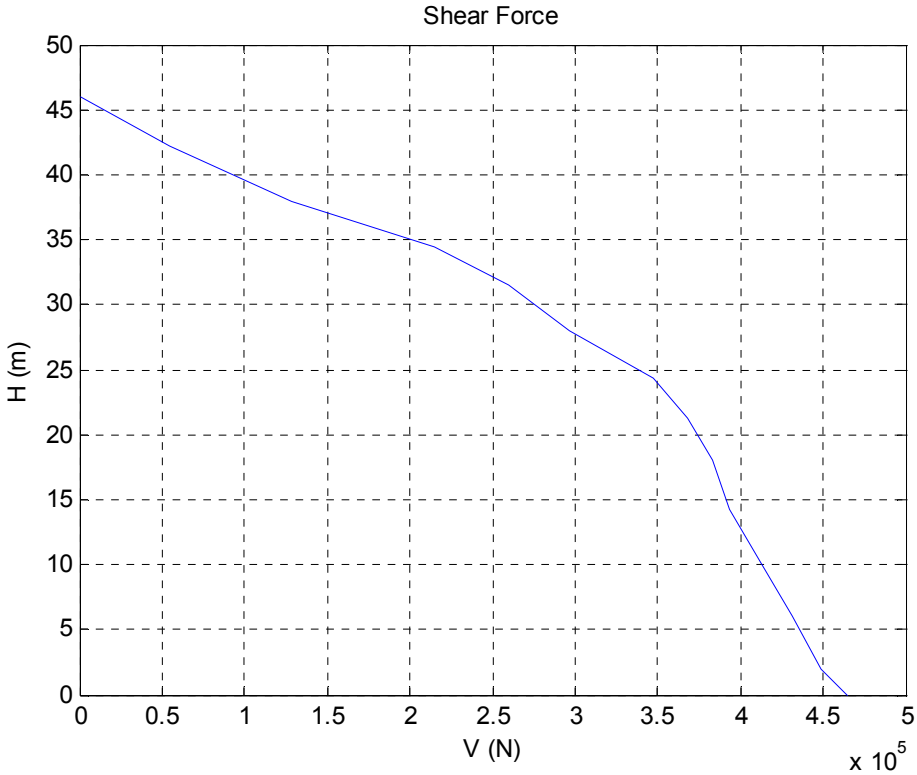

Figure 5.48. Shear diagram / case 1 with TMD

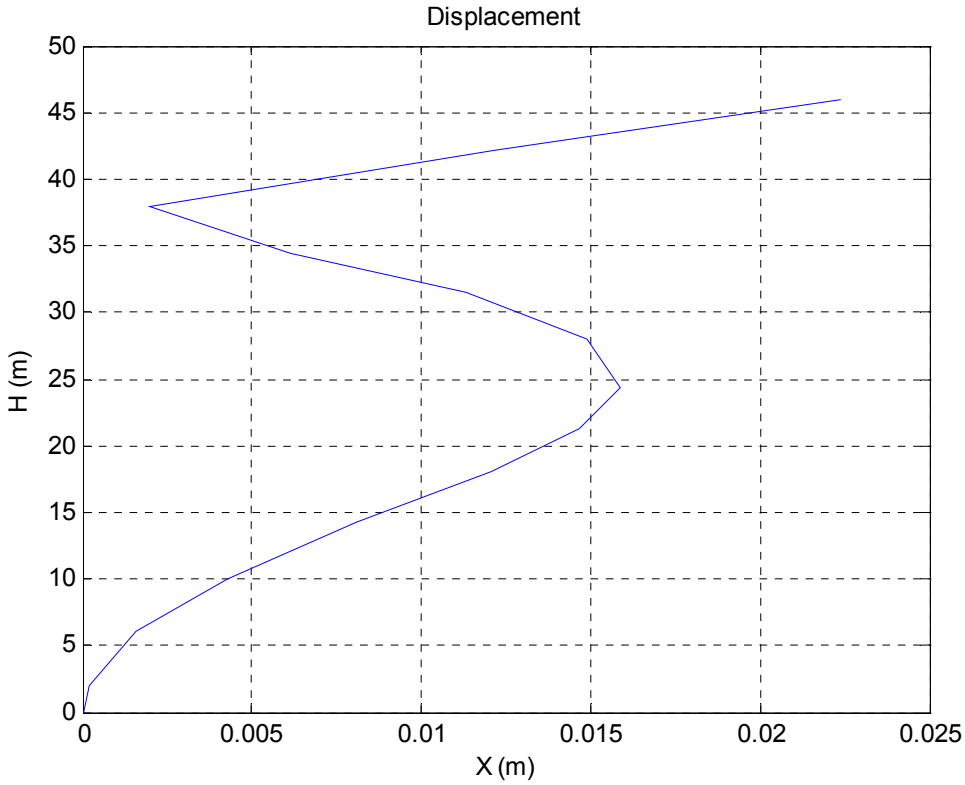

Figure 5.49. Absolute Displacement curve / case 2 with TMD

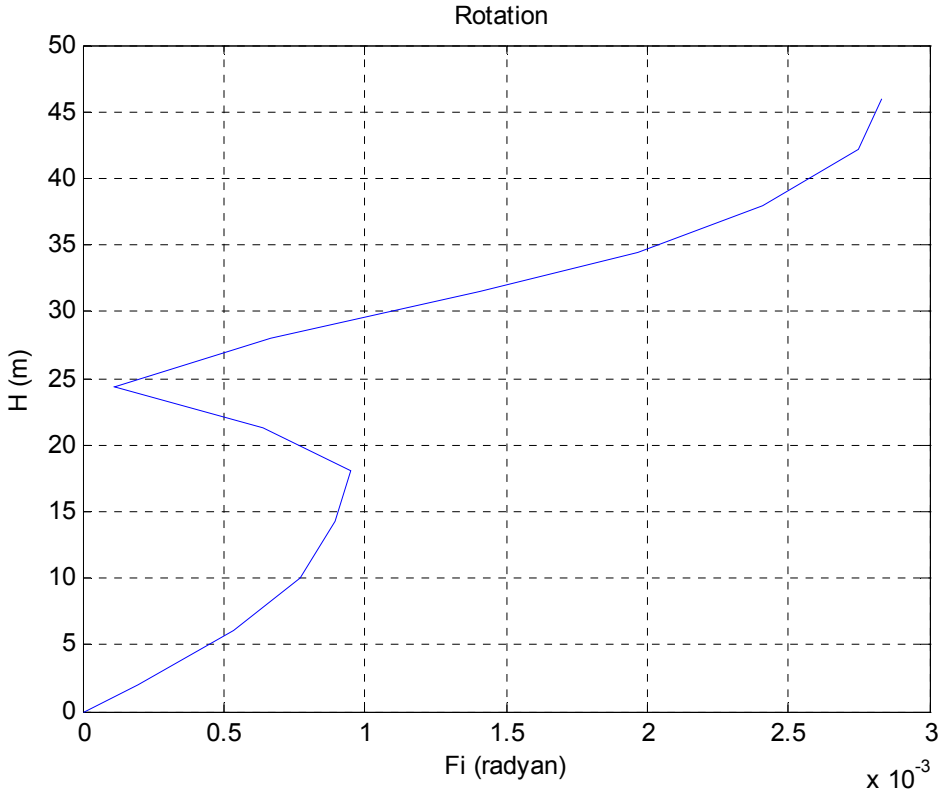

Figure.5.50. Absolute Rotation diagram / case 2 with TMD

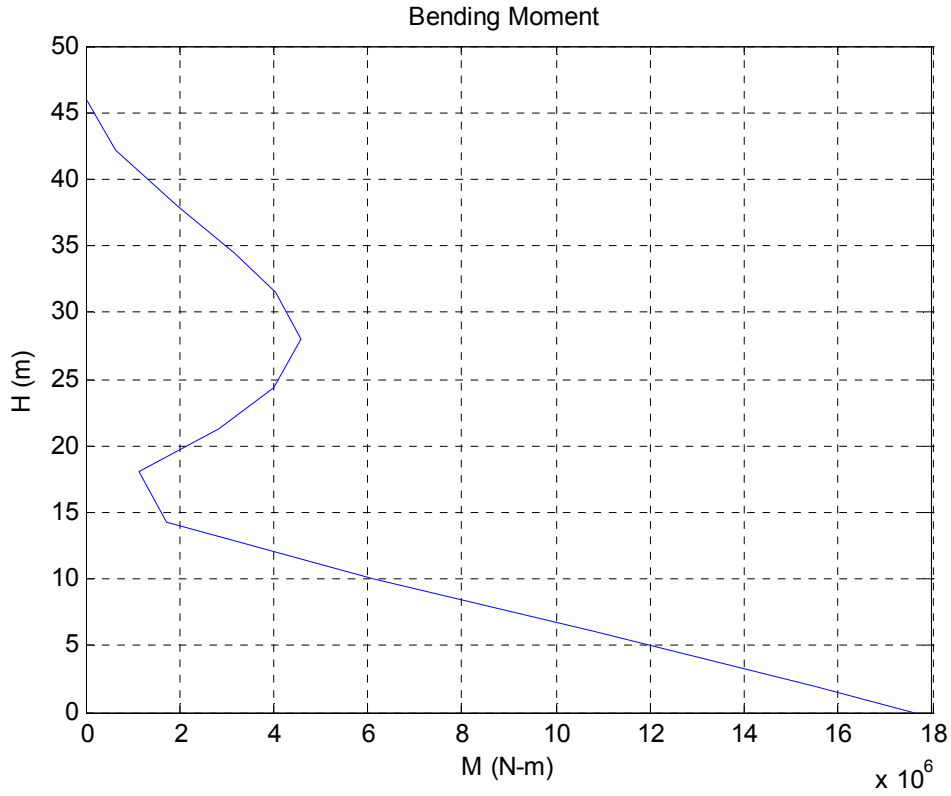

Figure 5.51. Absolute Moment diagram / case 2 with TMD

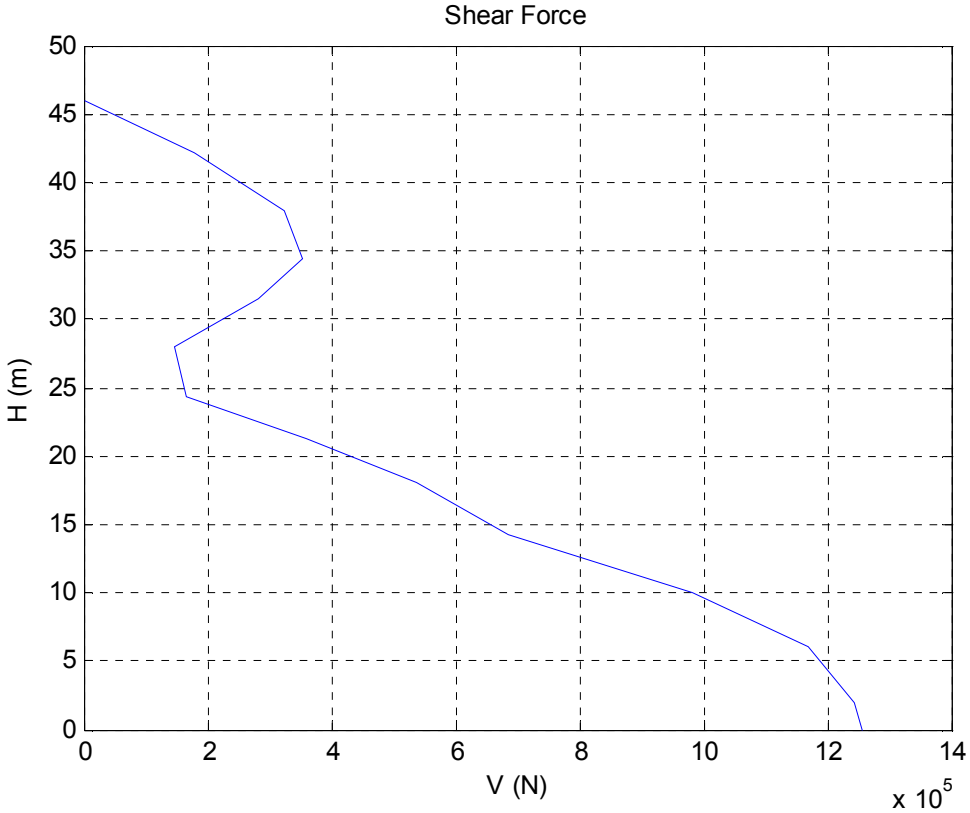

Figure 5.52. Absolute Shear diagram / case 2 with TMD

Same reactions and stress states as in the previous section are calculated and listed on Table 5.4. for minaret equipped with TMD.

Table 5.4. Response outputs of minaret with TMD against harmonic base excitation

		Case 1	Case 2
Displacement at 12th node	(m)	13.9 x 10^{-2}	1.2 x 10^{-2}
Base shear	(N)	0.47 x 10^{6}	1.26 x 10^{6}
Base moment	(N m)	14.37 x 10^{6}	17.65 x 10^{6}
Shear at 4th node	(N)	0.38 x 10^{6}	0.54 x 10^{6}
Moment at 4th node	(N m)	6.87 x 10^{6}	1.13 x 10^{6}
Shear stress at 4th node	(MPa)	0.25	0.35
Bending stress at 4th node	(MPa)	10.21	1.68

Response improvements are listed on Table 5.5. It is seen that there is significant improvement on response at 1st natural frequency. Bending stresses are below the elastic limit. It is verified that TMD installation performs excellent improvement at 1st natural vibration mode.

Table 5.5. Response improvement of minaret via TMD installation against harmonic base excitation. Case 1: 1st natural frequency. Case 2: 2nd natural frequency.

	Case 1	Case 2
Displacement at 12th node	79 %	8 %
Base shear	76 %	2 %
Base moment	79 %	3 %
Shear at 4th node	79 %	24 %
Moment at 4th node	83 %	36 %
Shear stress at 4th node	79 %	24 %
Bending stress at 4th node	83 %	36 %

TMD mass makes relative displacement against minaret wall which is modeled as m_{12}. This relative displacement is important while designing TMD and its connections. Such a free space should be allocated for TMD mass to allow free vibration. Any touch up

to the main structure will create an impact which is not desired and substantially structure can collapse. Therefore this relative displacement has significant role in a TMD design.

Eq. 5.32 gives the displacement of TMD in terms of displacement of m_{12}, other TMD parameters and circular frequency. It can be simplified as following;

$$x_2 - x_1 = \frac{N}{k_d + jc_d\omega} \tag{5.59}$$

where

$$N = k_{deq}\, x_1 + F \tag{5.60}$$

$$k_{deq} = \frac{k_d{}^2\, m_d\, \omega^2 - k_d\, m_d^2\, \omega^4 + c_d{}^2\, m_d\, \omega^4}{(k_d - m_d\, \omega^2)^2 + c_d{}^2\, \omega^2} - j\frac{c_d\, m_d^2\, \omega^5}{(k_d - m_d\, \omega^2)^2 + c_d{}^2\, \omega^2} \tag{5.61}$$

$$F = -\frac{m_d\ddot{u}_g(k_d{}^2 - k_d m_d\omega^2 + c_d{}^2\omega^2)}{(k_d - m_d\omega^2)^2 + c_d{}^2\omega^2} + j\frac{m_d\ddot{u}_g(c_d m_d\omega^3)}{(k_d - m_d\omega^2)^2 + c_d{}^2\omega^2} \tag{5.62}$$

Since maximum x_1 value was estimated during the vibration analysis and listed on Table 5.4., relative displacement can be easily estimated by using Eq. 5.59. A Matlab code is created to calculate relative displacement of TMD mass against connection point and listed in Appendix A.11. Relative displacement was estimated as 0.33 m by using above mentioned Matlab codes. It should be pointed out that relative displacement is strongly depending on the excitation amplitude.

5.5. Vibration Analysis of the Minaret with Finite Element Method

Earthquake ground motions are typical random vibrations of ground which occur during seismic movements of earth. Each earthquake has its own characteristic displacement, velocity and acceleration records. Amplitude and frequency parameters of each specific earthquake vary at different locations due to several reasons. Distance to fault line and soil conditions could be some of the major reasons. Therefore ground motion data of a specific earthquake is recorded differently at other locations. The ground acceleration is defined by numerical values at discrete time instants. These time instants should be closely spaced to describe accurately the highly irregular variation of acceleration with

time. Typically, the time interval is chosen to be 5/1000 to 1/50 of a second requiring 6000 to 1500 ordinates to describe the ground motion of 30 sec. [7]

Ground acceleration during earthquake varies irregularly to such an extent that analytical solution of the equation must be ruled out. Therefore, numerical methods are necessary to determine the structural response and any of the methods presented in chapter 5 of ref. [7] could be used.

Greatest interest in structural engineering is the deformation of the system or the displacement of the mass relative to the moving ground, to which the internal forces are linearly related. These are the bending moments and shears in the beams and columns of the structure. [7] Therefore it is sufficient to analyze and compare the displacement of structure with and without TMD application. Displacement of structure with and without TMD installation gives enough information about the response improvement due to linear relationship of force, moment and displacement parameters. Sezen et al. [5] documents that maximum displacements and maximum stresses occur at about the same time, respectively.

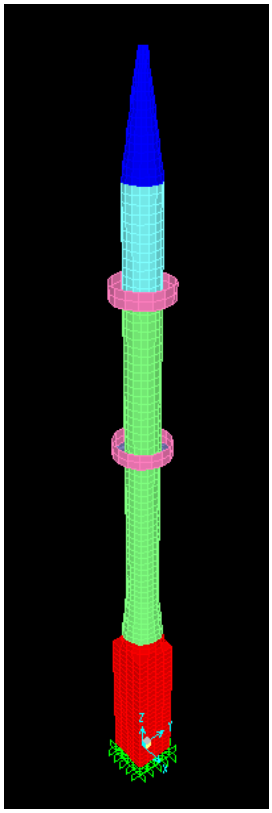

Figure 5.53. Minaret model used in SAP2000 program

It is usually burdensome to include all components in a structural model and consider their effect on the total behavior. In this study, a finite element model representing the same minaret will be used to analyze the dynamic response. Shell type model is developed. The interior spiral stairs are ignored in model as shown in Figure 4.53. SAP2000 [8] FEM software was used to analyze the model.

5.5.1. Natural Frequencies of the Minaret

Natural frequencies for the first 5 modes estimated from the modal analyses are given in Table 5.6. All natural frequencies and periods obtained from SAP2000 are listed in Appendix B.1.

Table 5.6. First 5 natural frequencies of FEM model obtained from SAP2000

ω_i	Natural Frequencies (rad/sec)		f_i	Natural Frequencies (Hz)
ω_1	7,0		f_1	1,1
ω_2	32,8		f_2	5,2
ω_3	71,2		f_3	11,3
ω_4	121,8		f_4	19,4
ω_5	193,0		f_5	30,7

When we compare Table 5.2 and Table 5.6, we see that the first three natural frequencies match pretty closely.

5.5.2. Natural Modes of the Minaret

First 5 modal shapes in one direction obtained from modal analysis through SAP2000 are shown in Figure 5.54.

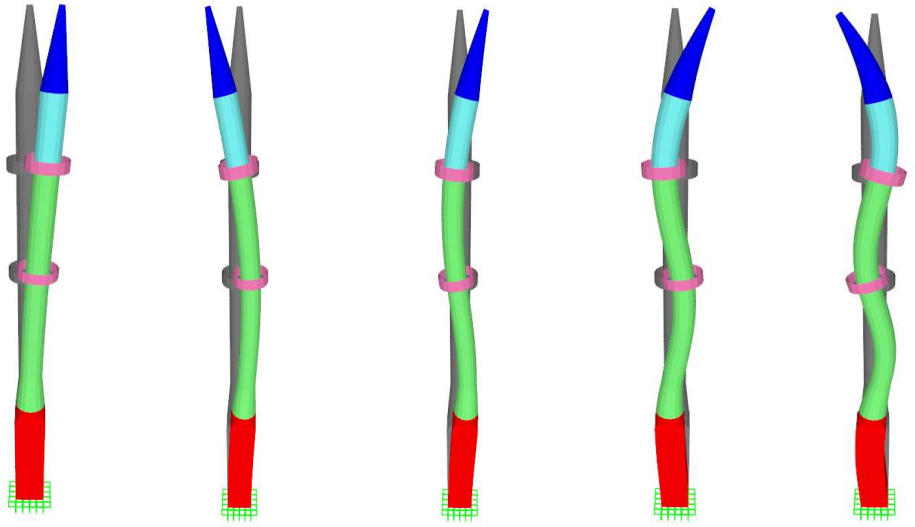

Figure 5.54. First 5 modal shapes in one direction of FEM model obtained from SAP2000

5.5.3. Dynamic Analysis Against Earthquake Ground Motion

Two ground motions are used in the dynamic time history analyses of the minaret model with and without TMD installation. 17 August 1999 Kocaeli earthquake record in East-West direction which is shown in Figure 5.55 is used for the 1st case. Then 12 November Düzce earthquake record in East-West direction which is shown in Figure 5.56 is used for the 2nd case. Optimized TMD parameters are adjusted slightly to correlate the differences in the natural frequencies of finite element method analysis against discrete mass model.

The lateral displacement graphs of joint 1026 at upper cylindrical body of minaret model without TMD are shown in Figure 5.57. Joint 1026 specifies a point on the shell model at 43.250 m elevation from the ground level which belongs to the plane of TMD installation. The maximum lateral displacements at the top of the cylindrical body (joint 1026) are 8.4 cm and 31.5 cm as calculated using the Kocaeli and Düzce ground motions, respectively.

The lateral displacements of joint 1026 and base reactions of model without TMD, as calculated from the time history analysis of model using the 1999 Düzce and Kocaeli input motions, are shown on Table 5.7. Base reactions of the model against Kocaeli and Düzce earthquakes are listed on Table B.2. and B.3. respectively.

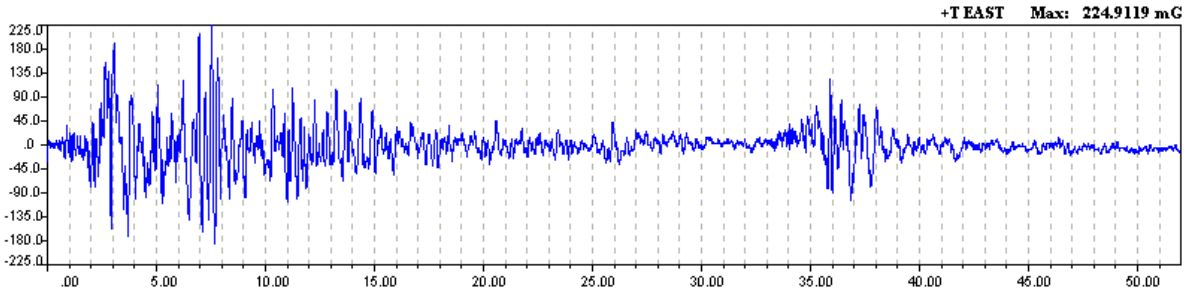

Figure 5.55. Acceleration of Kocaeli earthquake recorded at Izmit Meteroloji station. [9]

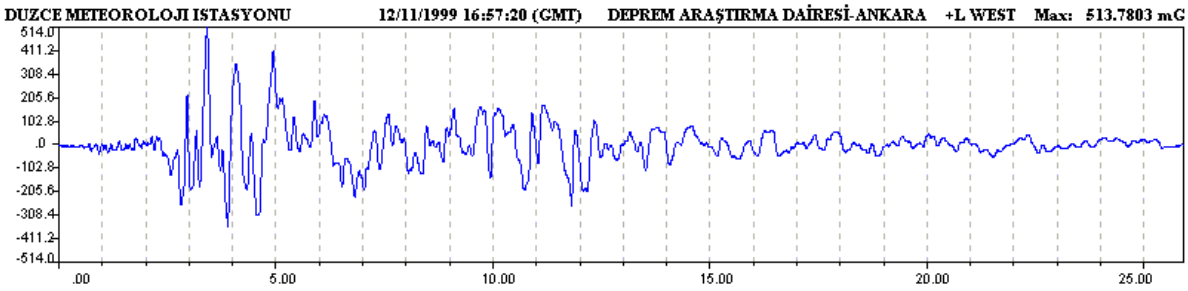

Figure 5.56. Acceleration of Düzce earthquake recorded at Düzce Meteroloji station. [9]

Table 5.7. Response outputs of minaret without TMD against earthquake ground motion.

	Kocaeli EQ	Düzce EQ
Displacement at the top of cylindrical body (joint 1026) (m)	8.4×10^{-2}	31.5×10^{-2}
Base shear (N)	0.74×10^{6}	1.47×10^{6}
Base moment (N m)	11.34×10^{6}	39.65×10^{6}

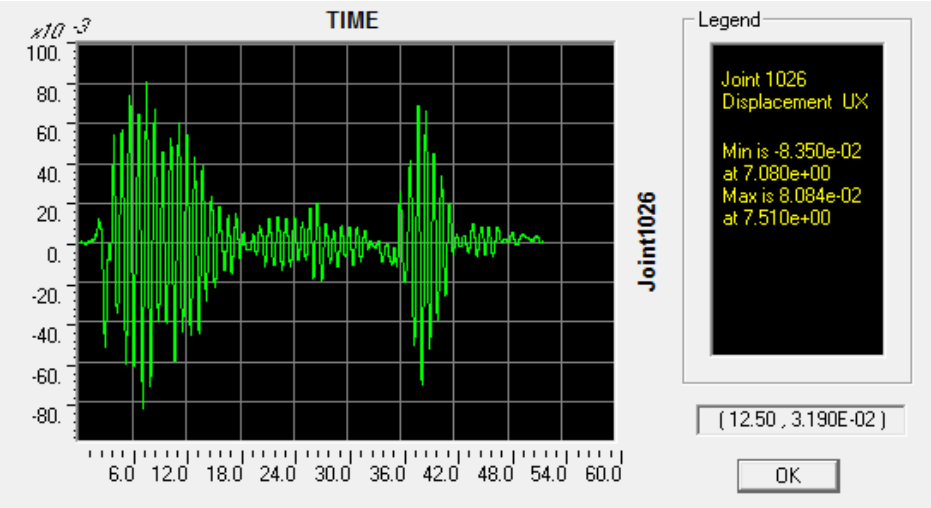

Figure 5.57. Displacement plot of joint 1026 without TMD against Kocaeli Earthquake by SAP2000

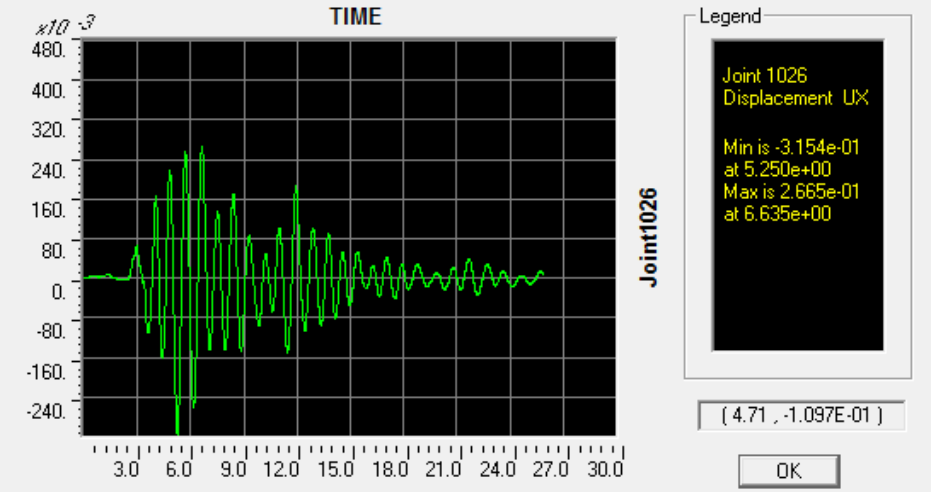

Figure 5.58. Displacement plot of joint 1026 without TMD against Düzce Earthquake by SAP2000

Now, response of the model equipped with TMD will be studied. Optimized TMD parameters obtained in section 5.4.4 should be revised due to slight differences in the natural frequencies of FEM and discrete mass models. Natural frequencies and periods of the model with TMD are listed in Appendix B.4. As shown on Table 5.7 there is only 6 % difference in the 1st natural frequency. Therefore similar procedure should be repeated here as in section 5.4.4.

- Let's assume the same 0.05 mass ratio as in section 5.4.4.
  m_d = 3490 kg

- Determine f_{opt} from Figure 3.5
  f_{opt} = 0.94

- Compute ω_d, $\omega_d = f_{opt}\ \omega$
  ω_d = 6.58 rad/sec

- Compute k_d, $k_d = m_d\ \omega_d^2$
  k_d = 151104

  Since there are 2 springs in parallel, stiffness of each spring in the model should be half value.

- Determine $\xi_d|_{opt}$ from Figure 3.7

  $\xi_d|_{opt} = 0.135$

- Compute c_d , $c_d = 2\xi_d|_{opt} m_d \omega_d$

  $c_d = 6200$

  Since there are 2 viscous dampers in parallel, coefficient of each damper in the model should be half value.

Uncoupled spring and damper from link elements are used to specify the TMD parameters like stiffness and damping. Joint mass was assigned to simulate the TMD mass. Sketch of the TMD elements and their connection to shell joints in SAP2000 model is shown in Figure 5.59. The lateral displacements of joint 1026 and base reactions of model with TMD, as calculated from the time history analysis of model using the 1999 Düzce and Kocaeli input motions, are shown on Table 5.8.

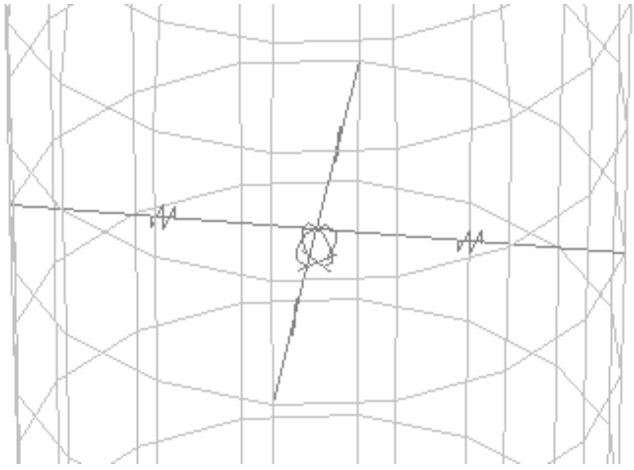

Figure 5.59. Uncoupled spring and damper from Link elements to model TMD in SAP2000

The lateral displacement graphs of joint 1026 at upper cylindrical body of minaret model with TMD are shown in Figure 5.60 and Figure 5.61. Base reactions of the model against Kocaeli and Düzce earthquakes are listed on Table B.5. and B.6. respectively.

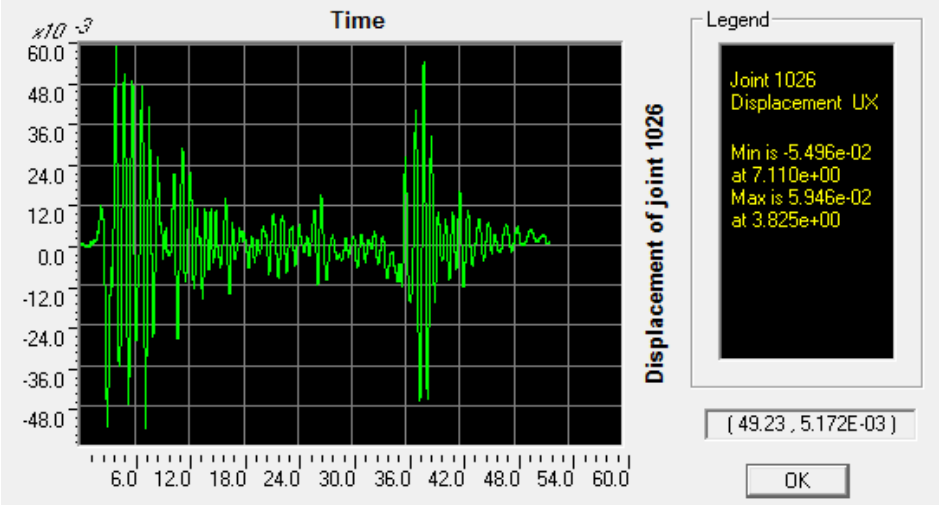

Figure 5.60. Displacement plot of joint 1026 with TMD against Kocaeli Earthquake by SAP2000

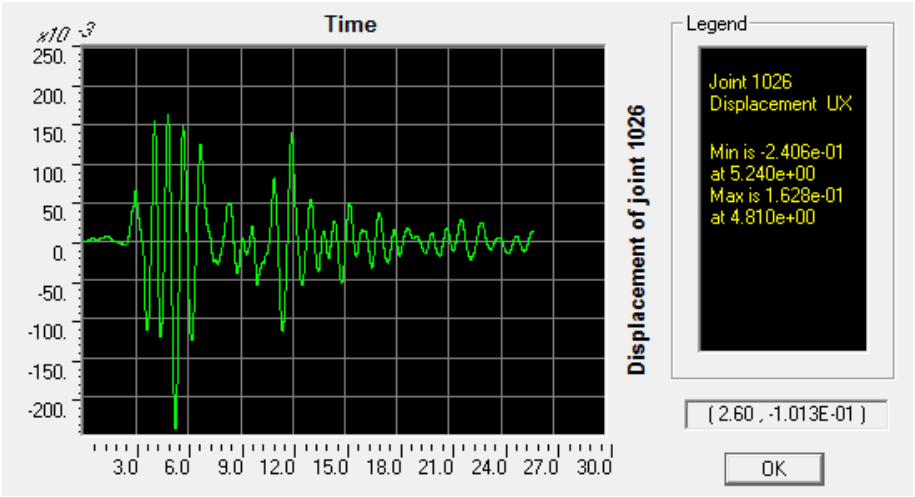

Figure 5.61. Displacement plot of joint 1026 with TMD against Düzce Earthquake by SAP2000

Table 5.8. Response outputs of minaret with TMD against earthquake ground motion.

	Kocaeli EQ	Düzce EQ
Displacement at the top of cylindrical body (joint 1026) (m)	6.0×10^{-2}	24.1×10^{-2}
Base shear (N)	0.75×10^{6}	1.4×10^{6}
Base moment (N m)	10.22×10^{6}	32.53×10^{6}

TMD mass displacement has to be checked against minaret wall to prevent any impact. Junction point of the spring and damper combination is joint 1562. Displacement plot of joint 1562 for Kocaeli Earthquake is shown in Figure 5.62 and Düzce Earthquake in

Figure 5.63. As seen in the related figures, maximum displacement occurs as 13 cm at 4.89 sec for Kocaeli case. Minaret wall at that elevation (joint 1026) makes maximum displacement as 6 cm. The worst case for the relative displacement can be approximated with π phase shift. In this case, maximum relative displacement reaches 19 cm. However the same calculation ends with 71cm for the maximum relative displacement against Düzce earthquake. There should be sufficient gap between the TMD mass and minaret wall to prevent any impact. This issue is very important and should be considered during TMD detailed design.

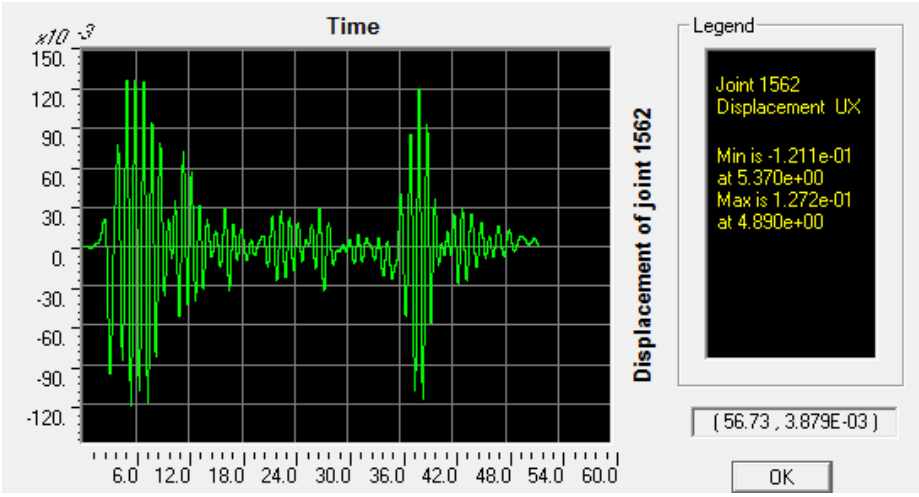

Figure 5.62. Displacement plot of TMD mass (Joint 1562) against Kocaeli Earthquake by SAP2000

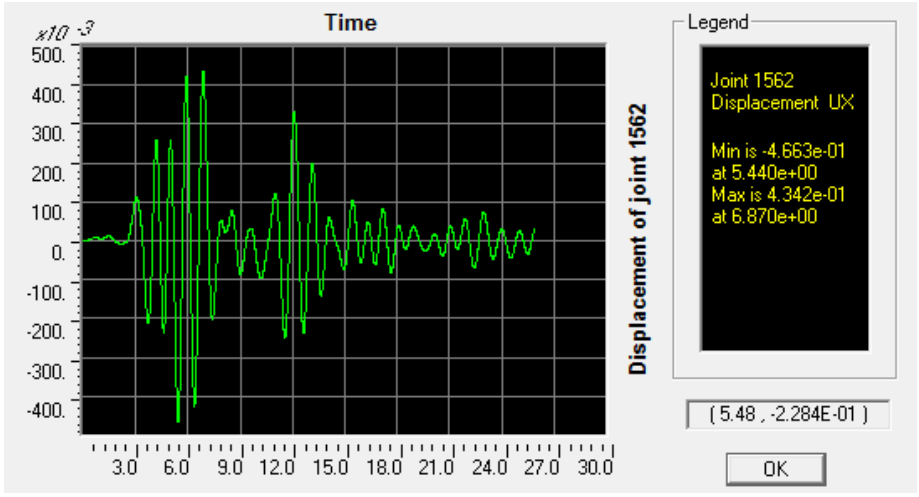

Figure 5.63. Displacement plot of TMD mass (Joint 1562) against Düzce Earthquake by SAP2000

Dynamic response improvement on displacements, base shears and base moments against Kocaeli and Düzce earthquakes are listed on Table 5.9.

Table 5.9. Response improvement of minaret via TMD installation against Kocaeli and Düzce earthquakes

	Kocaeli EQ	Düzce EQ
Improvement in Displacement of joint 1026	29 %	24 %
Improvement in Base shear	- 1 %	5 %
Improvement in Base moment	10 %	18 %

It is seen that response improvement is not as good as the case with harmonic base excitation at the 1st natural frequency. The reason can be explained with the dominating frequency of the earthquake itself. We should change the earthquake ground acceleration records from time domain to frequency domain by using Fourier transform to find out the dominating frequencies. A matlab code is prepared to make Fourier transformation and it is listed in Appendix A.8. Figure 5.64 and Figure 5.67 show the ground acceleration records of Düzce and Kocaeli earthquakes respectively in time domain. Figure 5.65 and Figure 5.68 show frequency spectrum of each earthquake respectively. Dominating frequency is not so visible in such large frequency range. Therefore, Figure 5.66 and Figure 5.69 were prepared to get dominating frequencies easily. Dominating frequencies of Düzce earthquake are recorded as 0.235 Hz, 0.811 Hz and 1.197 Hz from Figure 4.66. Dominating frequencies of Kocaeli earthquake are recorded as 1.097 Hz, 1.732 Hz and 2.598 Hz from Figure 5.66. Especially 3rd dominating frequency of Düzce and 1st dominating frequency of Kocaeli are very close to the 1st natural frequency of our structure. However other major dominating frequencies are affecting the performance of the TMD. It is a well-known fact that TMDs are very efficient in narrow band excitations. Generally earthquakes are not narrow band excitations. As a result, their efficiencies are not as high as in the case of harmonic excitations'.

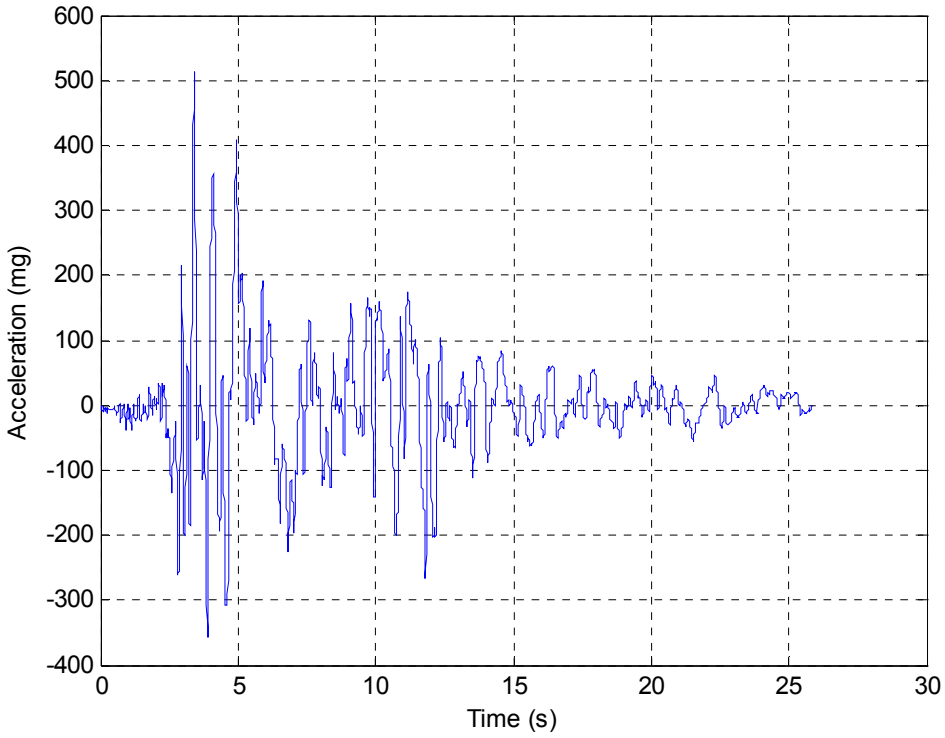

Figure 5.64. Düzce earthquake ground acceleration records in time domain

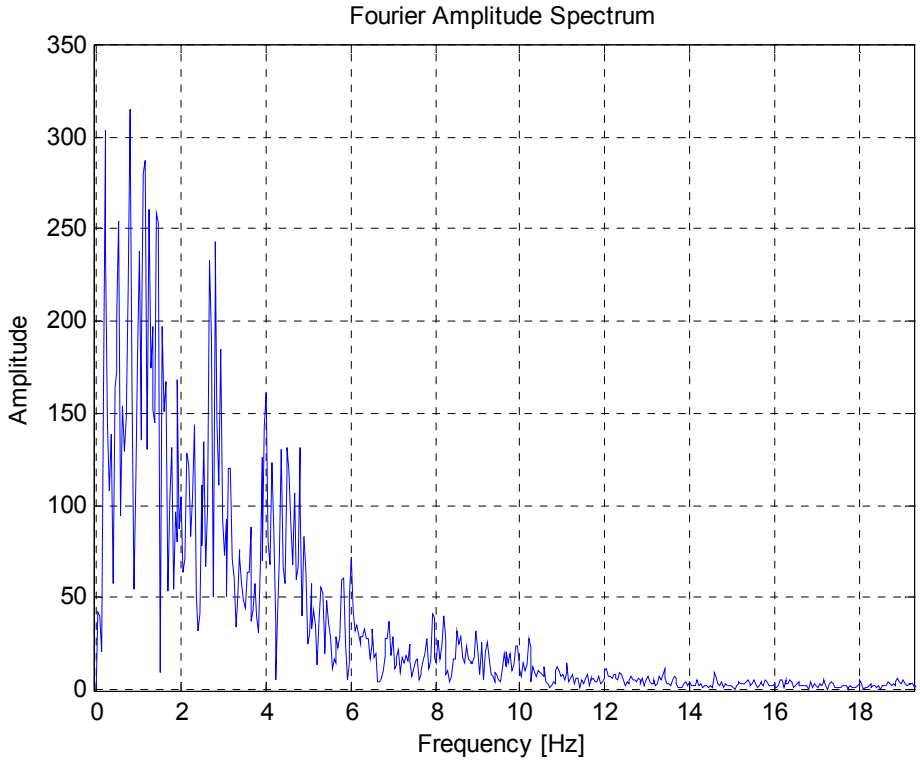

Figure 5.65. Düzce earthquake ground acceleration records in frequency domain

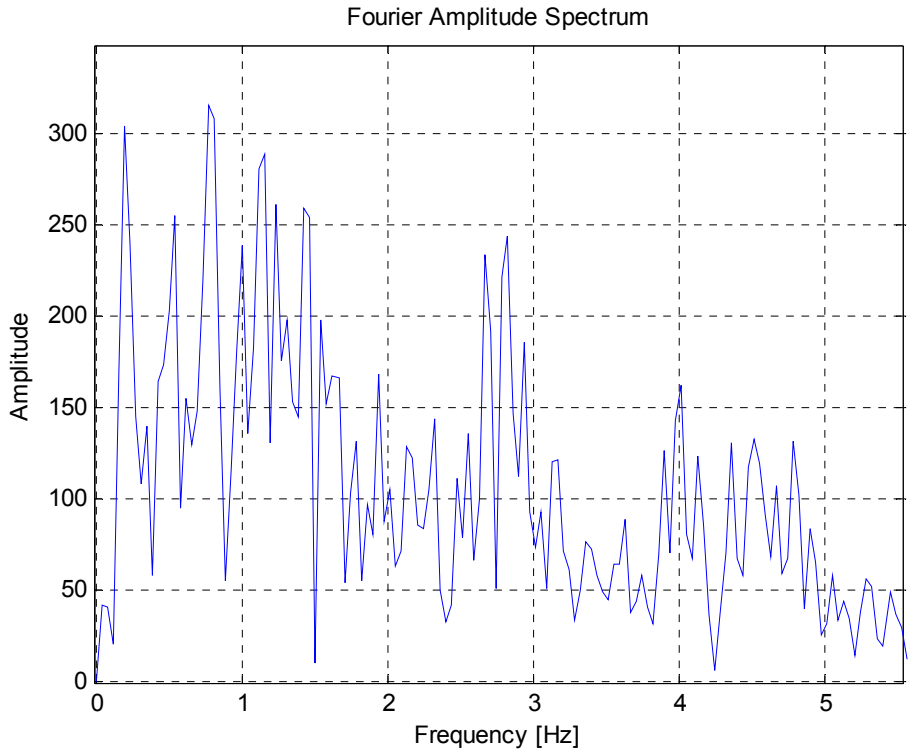

Figure 5.66. Enlarged view of Düzce earthquake ground acceleration records in frequency domain

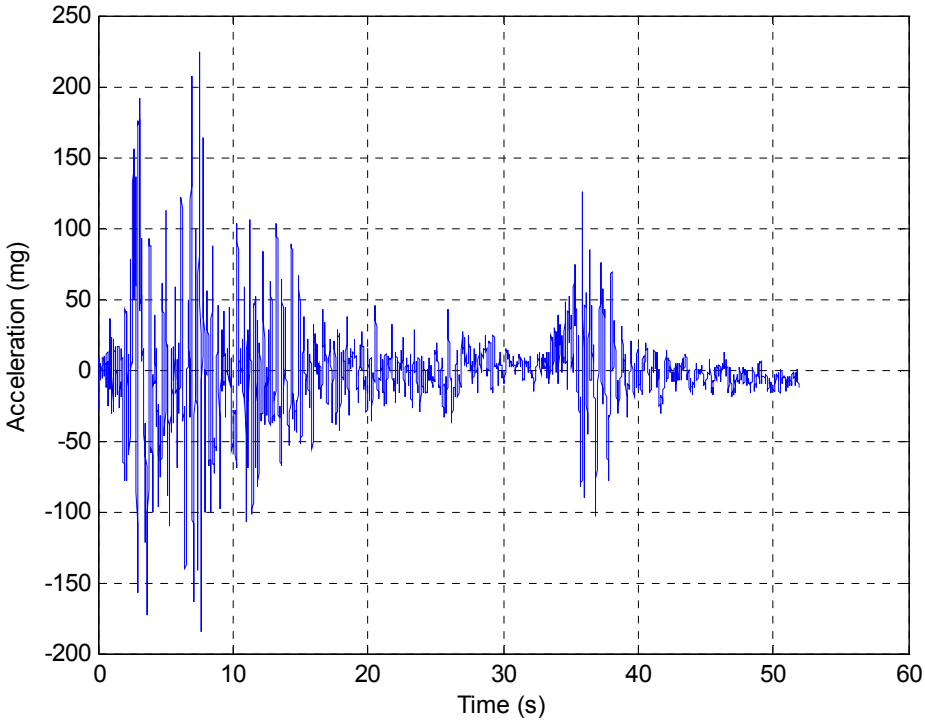

Figure 5.67. Kocaeli earthquake ground acceleration records in time domain

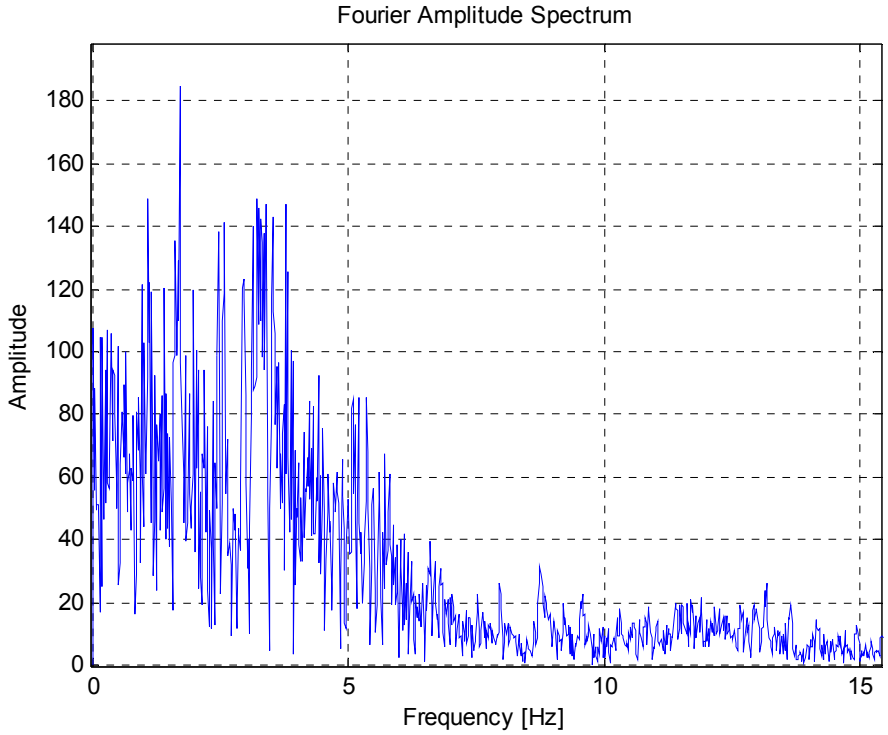

Figure 5.68. Kocaeli earthquake ground acceleration records in frequency domain

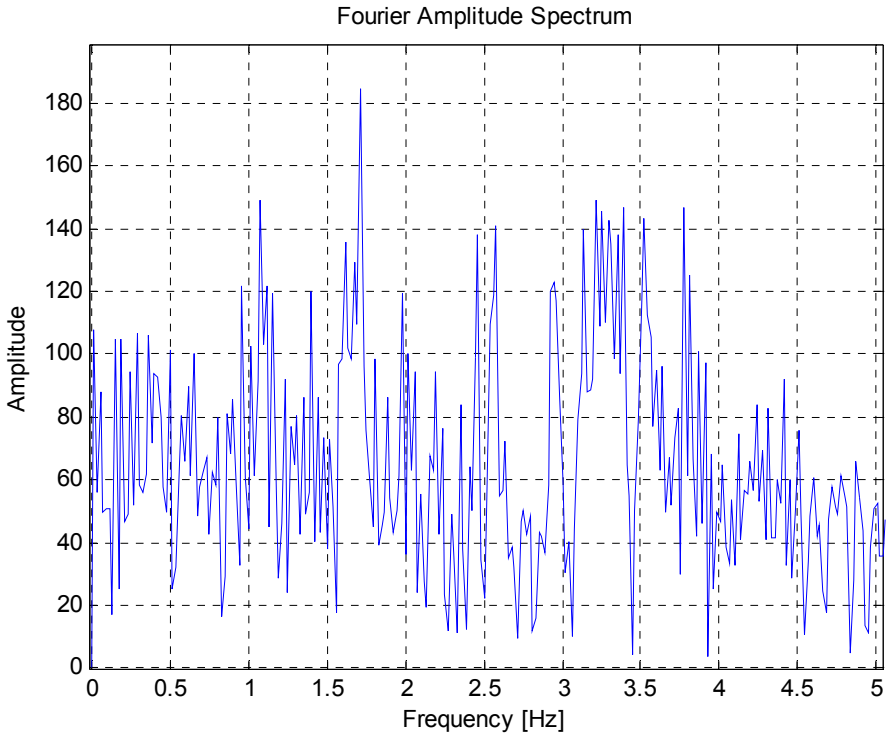

Figure 5.69. Enlarged view of Kocaeli earthquake ground acceleration records in frequency domain

5.5.4. Dynamic Analysis Against Harmonic Base Excitation

Same minaret model will be used in this section to analysis the structure against harmonic base excitation through SAP2000. Let's apply 2 harmonic base excitations as following to the model without TMD;

Case 1: $\ddot{u}_g = A \sin \omega t$

ω = 7.0 rad/sec (1st natural frequency)

T = 0.898 sec

A = 1.0 m /sec^2

Number of cycles = 10 cycles

Case 2: $\ddot{u}_g = A \sin \omega t$

ω = 32.8 rad/sec (2nd natural frequency)

T = 0.192 sec

A = 1.0 m /sec^2

Number of cycles = 40 cycles

Displacement response of joint 1026 without TMD for Case 1 is plotted in Figure 5.70 and Case 2 is plotted in Figure 5.71. Base reactions of the model against Case 1 and Case 2 excitations are listed in Appendix B.7. and B.8. respectively. Response output summary of structure without TMD is listed on Table 5.10.

Table 5.10. Response outputs of minaret without TMD against harmonic base excitation.

	Case 1	Case 2
Displacement at the top of cylindrical body (joint 1026) (m)	22.7 x 10^{-2}	0.65 x 10^{-2}
Base shear (N)	1.00 x 10^6	0.64 x 10^6
Base moment (N m)	31.08 x 10^6	8.52 x 10^6

Now, response of the model equipped with TMD will be studied. Optimized TMD parameters obtained in section 5.5.3 will also be used for this analysis. The lateral

displacement graphs of joint 1026 at upper cylindrical body of minaret model with TMD are shown in Figure 5.72 and Figure 5.73 for Case 1 and Case 2 excitations respectively. Base reactions of the model against Case 1 and Case 2 excitations are listed in Appendix B.9. and B.10. respectively. Response output summary of structure with TMD is listed on Table 5.11.

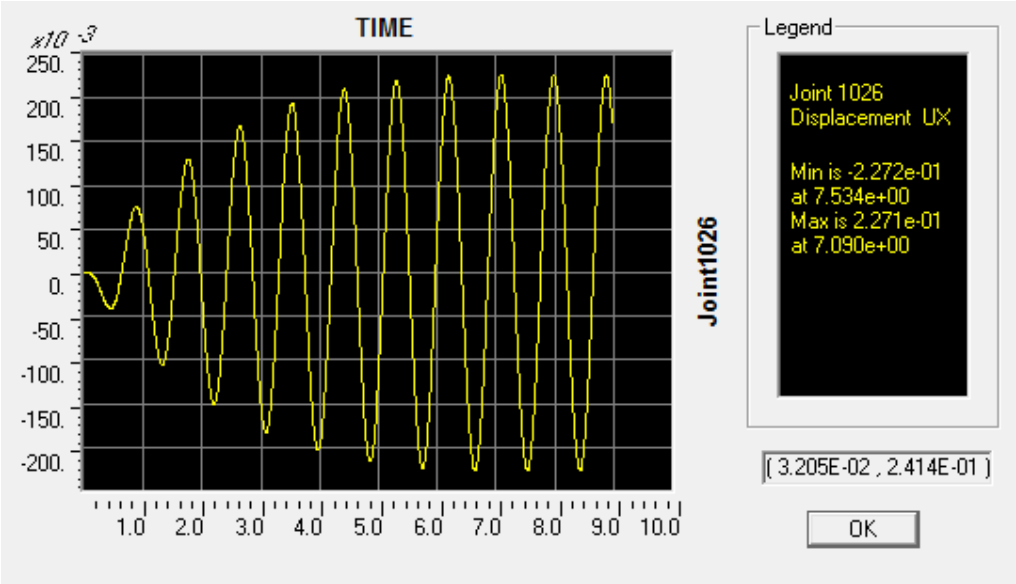

Figure 5.70. Displacement plot of joint 1026 without TMD against harmonic base excitation with $\omega = 7.0$

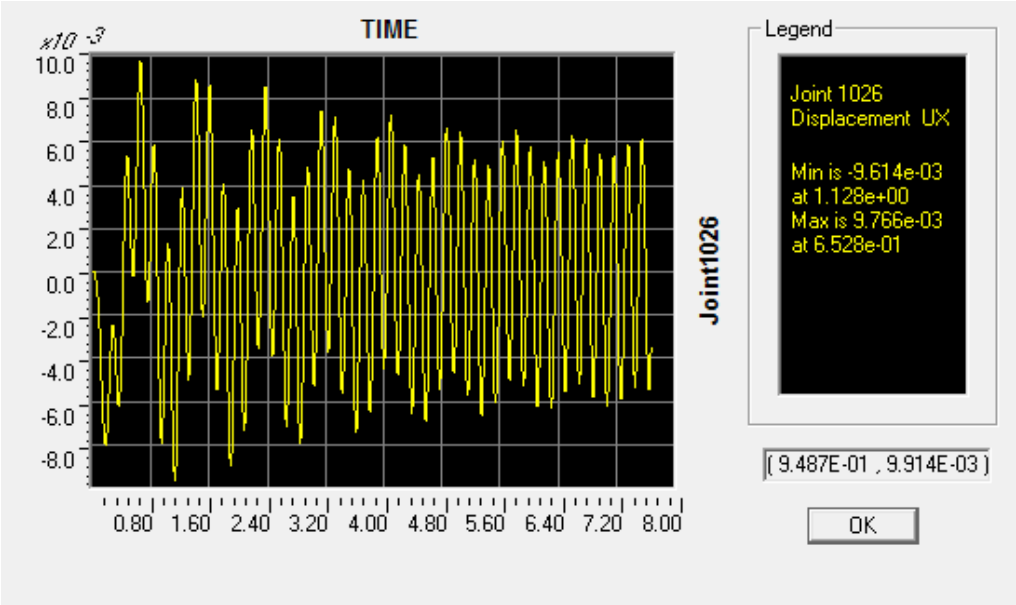

Figure 5.71. Displacement plot of joint 1026 without TMD against harmonic base excitation with $\omega = 32.8$

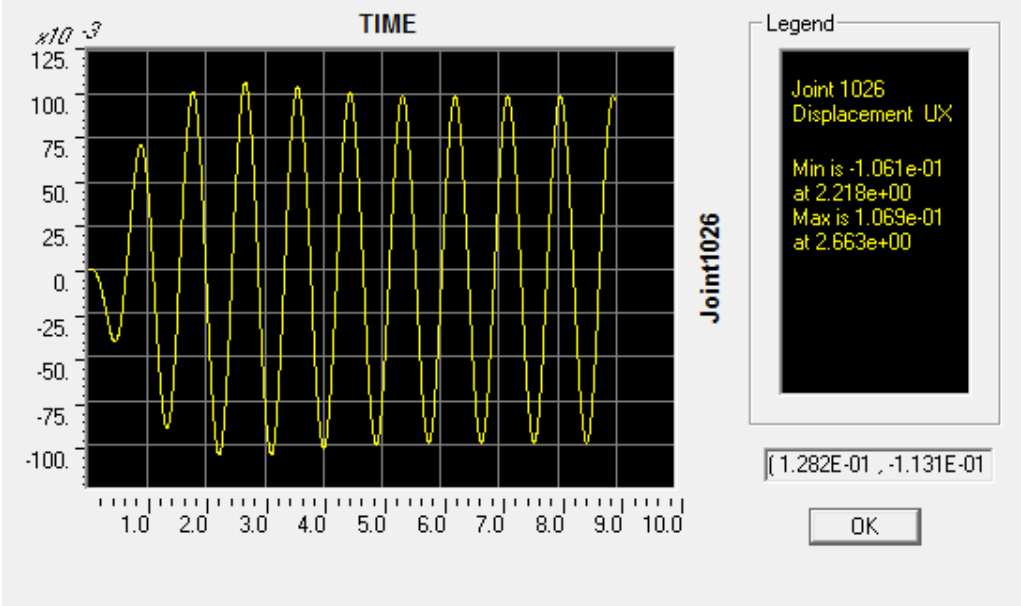

Figure 5.72. Displacement plot of joint 1026 with TMD against harmonic base excitation with $\omega = 7.0$

Table 5.11. Response outputs of minaret with TMD against harmonic base excitation.

	Case 1	Case 2
Displacement at the top of cylindrical body (joint 1026) (m)	10.6×10^{-2}	0.6×10^{-2}
Base shear (N)	0.49×10^{6}	0.62×10^{6}
Base moment (N m)	14.57×10^{6}	8.13×10^{6}

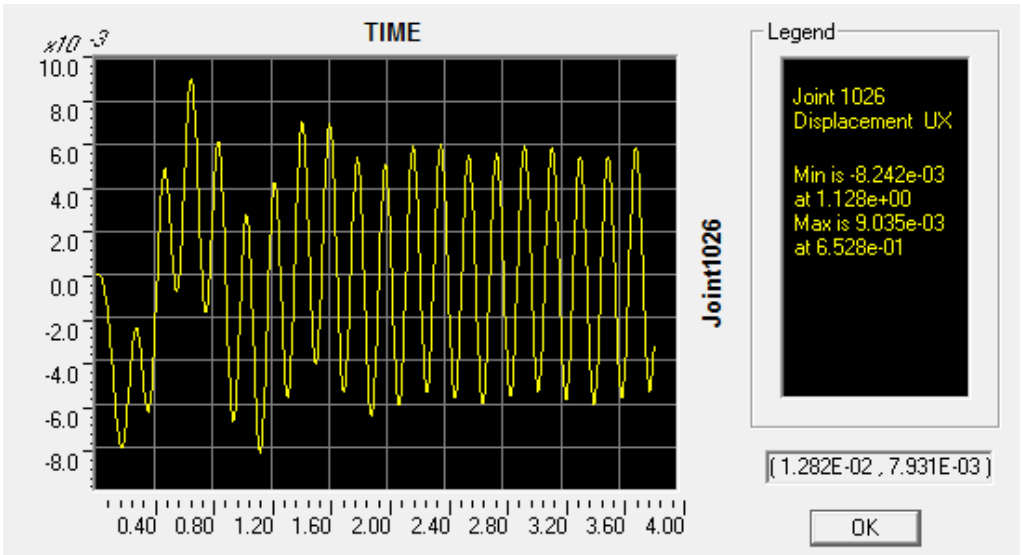

Figure 5.73. Displacement plot of joint 1026 with TMD against harmonic base excitation with $\omega = 32.8$

Table 5.12. Response improvement of minaret via TMD installation against harmonic base excitation

	Case 1	Case 2
Improvement in Displacement of joint 1026	53 %	8 %
Improvement in Base shear	51 %	3 %
Improvement in Base moment	53 %	5 %

Relative displacement between TMD mass and minaret inner wall should be also checked. TMD mass was assigned at joint 1562 as joint mass. Its displacement plot is shown in Figure 5.74 and Figure 5.75 for Case 1 and Case 2 excitations. It is noted that maximum displacement occurs at case 1 with a value of 0.29 m. At the same time minaret wall has a maximum displacement value as 0.11 m. By considering the phase shift, there should be minimum 0.40 m clear distance to allow TMD mass travel radially in all directions.

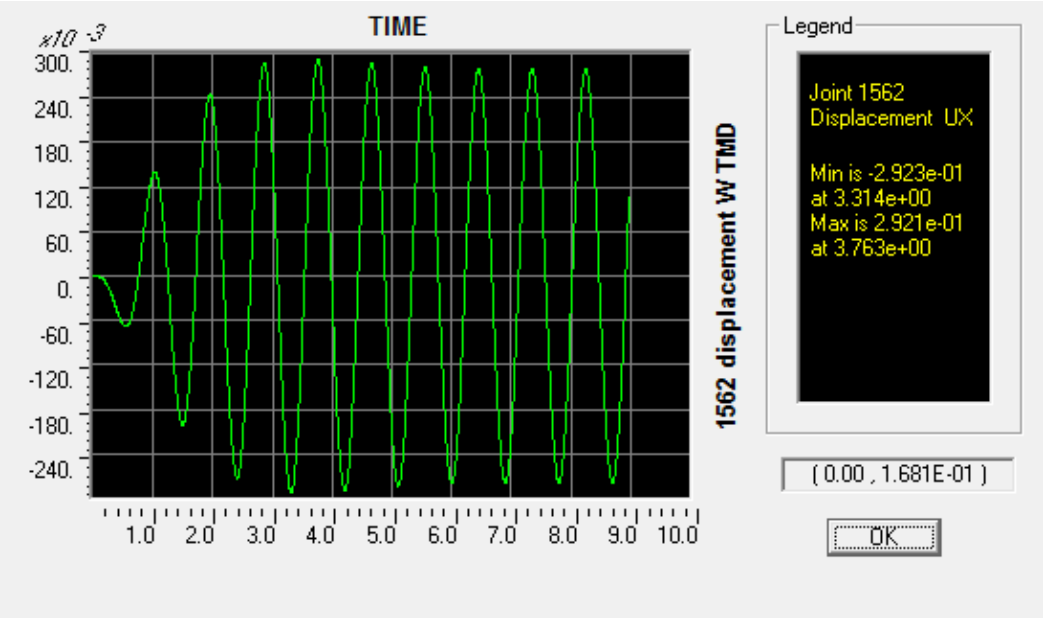

Figure 5.74. Displacement plot of joint 1562 with TMD against harmonic base excitation with $\omega = 7.0$

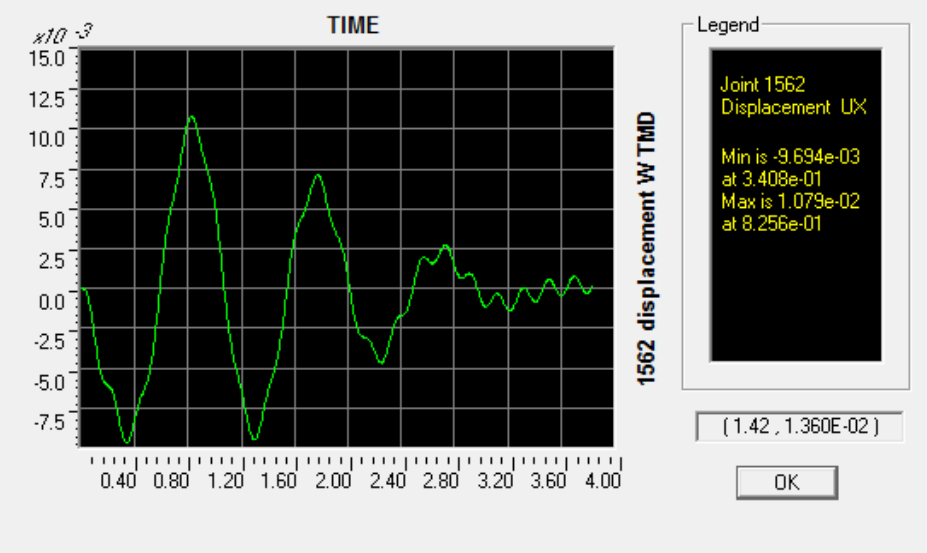

Figure 5.75. Displacement plot of joint 1562 with TMD against harmonic base excitation with $\omega = 32.8$

5.6. Wind Response

Two basic types of loads can be applied by wind, namely static pressure and harmonic excitation. These loads are normally experienced simultaneously, although static drag can exist without harmonic excitation under certain conditions. Static drag forces can cause a structure to deflect significantly, especially in strong storms. However the presence of dynamic loading on structures does not require extremely high wind velocities, only that one or more harmonic excitation sources be present. These dynamic loads, if acting at or near a structural resonance, can cause large vibration amplitudes. [14] Static pressure is out of our concern, only dynamic response of the structures against harmonic excitations will be studied in this section. There are three types of sources which create dynamic wind forces on structures: [12]

- Forces due to turbulence within the structure's wake, particularly due to vortex shedding,
- Turbulent forces in the earth's boundary layer,
- Forces induced by motion of the structure,

Only vortex shedding will be studied in the next chapter due to its easy occurrence especially on the cylindrical structures like minarets.

5.6.1. Vibration Due To Vortex Shedding

When wind flows around a circular body like minaret, it applies static pressure on the structure as shown in Figure 5.76. Since the air has a certain viscosity, air speed gets down slightly where it contacts the structure during flowing. This causes a speed change between the layers of wind due to boundary layer condition. As wind speed increases, this boundary layer can separate from the leeward side of the structure because of its excessive curvature. This causes a phenomenon called vortex shedding. As this separation occurs, vortices are formed on either side of the structure as shown in Figure 5.77. Vortex shedding produces forces which originate in the wake behind the structure, act mainly in the across-wind direction, and are, in general, rather regular. The resultant oscillation is resonant in character, is often almost periodic, and usually appears in the direction perpendicular to that of the wind. Lightly damped structures such as minarets, chimneys and towers are particularly susceptible to vortex shedding.

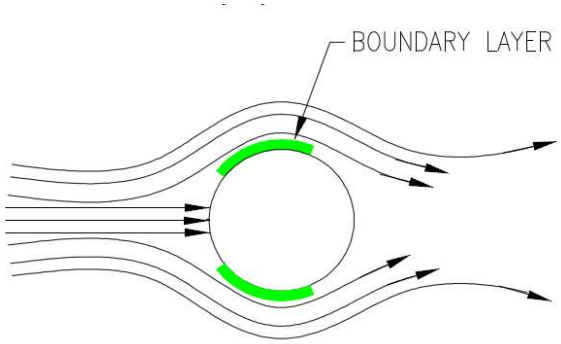

Figure 5.76. Normal airflow around a cylindrical object [17]

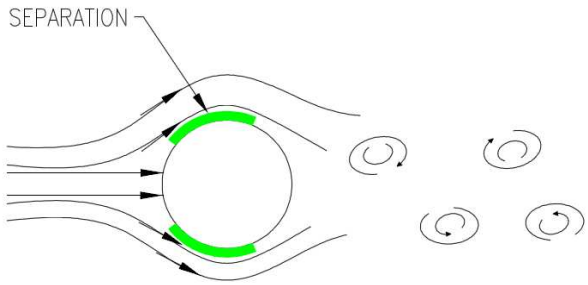

Figure 5.77. Disturbed airflow around a cylindrical object [17]

The frequency of the shedding, nearly constant in many cases, depends on the shape and size of the body, the velocity of the flow, and to a lesser degree on the surface

roughness and the turbulence of the flow. If the cross section of the body is noncircular, it also depends on the wind direction. The dominant frequency of vortex shedding, f_s is given by

$$f_s = S\frac{\bar{V}}{D} \qquad \text{cps} \tag{5.63}$$

Where $S =$ Strouhal number

$\bar{V} =$ Mean wind velocity

$D =$ Width of the object.

For a body having a rectangular or square cross section, the Strouhal number is almost independent of the Reynolds number.

$$Re = \frac{\bar{V}D}{v} \tag{5.64}$$

Where v = kinematic viscosity

v = 1.51 10^{-5} m^2/sec. (For air under normal conditions; 20 ˚C and 1 atm)

For a body having a circular cross section, the Strouhal number varies with the regime of the flow as characterized by the Reynolds number. There are three major regions: the subcritical region for $Re \le 3\ 10^5$, the supercritical region for $3\ 10^5 \le Re \le 3\ 10^6$, and the transcritical region for $Re \ge 3\ 10^6$. Approximate values of the Strouhal number for typical cross sections are given in Table 29.2 of reference [18].

5.6.2. Prediction of Vortex-Induced Oscillations

Although the mechanism of vortex shedding and the character of the lift forces have been the subject of a great number of studies, the available information does not permit an accurate prediction of these oscillations.[18] The motion is most often viewed as forced oscillation due to the lift force, which, per unit length, may be written as:

$$F_L = \frac{1}{2}\rho D \bar{V}^2 C_L(t) \tag{5.65}$$

Where $C_L(t)$ is a lift coefficient fluctuating in a harmonic or random way. Hence, the solution of the response depends on the time-history assumed for $C_L(t)$. The variation of structure diameter and wind velocity makes this lift force vary along the length of the structure. In order to apply the lift forces in the calculations, relationships suggested by the ASME standards [14] should be used to apply the across-wind lift forces. The standards exploit the near-uniform velocity profile on the upper one-third of the structure to provide a lateral force ("lift" force) per unit length that is independent of height. Moreover, the dynamic loads near the top of the stack are much more effective in exciting the first and second modes of concern in this work.

5.6.3. Harmonic Excitation of Structures by Vortex Shedding

Harmonic excitation represents a traditional model for vortex excitation, but it is really justified only for very low Reynolds numbers ($\leq$ 300) or possibly for large vibration where the motion starts controlling both the wake and the lift forces in the form of the "locking-in" phenomenon. Strongest oscillations arise at that wind velocity for which the frequency of vortex shedding f_s is equal to one of the natural frequencies of the structure f_i. This resonant wind velocity is, from Eq. 5.63,

$$V_c = \frac{1}{S} f_i D \tag{5.66}$$

With free-standing towers and stacks, resonance in the first two modes is met most often; resonance with higher modes has been observed as well with guyed towers. At the resonant wind velocity, the lift force is given by Eq. 5.65 in which

$$C_L(t) = C_L \sin 2\pi f_i t \tag{5.67}$$

and C_L = amplitude of lift coefficient. Assuming a uniform wind profile and a constant diameter D, the resonant amplitude of mode i at the critical wind velocity V_c will be as follow:

$$u_i(z) = \frac{\rho\, C_L}{16\, \pi^2\, S^2} \frac{D^3}{\zeta M_i} \phi_i(z) \int_0^H \phi_i(z)\, dz \tag{5.68}$$

Where M_i is given by Eq. 5.69 and ζ = structural damping ratio.

$$M_i = \int_0^H m(z)\, \phi_i^2(z)\, dz \tag{5.69}$$

The formula can be further simplified if it is assumed that the lift force is distributed along the structure in proportion to the mode $\phi_i(z)$. (This assumption reflects the loss of span wise correlation of the forces.) Then, with constant mass per unit length $m(z) = m$, the resonant amplitude at the height where the modal displacement is maximum:

$$u_i = \frac{\rho\, C_L}{16\, \pi^2\, \mathrm{S}^2}\, \frac{D^3}{\zeta m} \tag{5.70}$$

For the first mode of a free-standing structure, this occurs at the tip. In higher modes, this amplitude appears at the height where local resonance takes place. For circular cylinders, a design value of the lift coefficient C_L is about $\sqrt{2}\ \sigma_L$. This simple formula can be used for the first estimate of the amplitudes that are likely to represent the upper bound. It is also indicative of the role of the diameter, mass, and damping of the structure.

5.6.4. Vortex Shedding in the Case Study

When wind speed reaches to the critical wind speed for structure, resonance occurs. V_c is estimated by Eq. 5.66;

V_c = 12.1 m/sec	by considering,	S = 0.2	From table 29.2 of [18]
		f_i = 1.1 Hz	1st natural speed of the minaret
		D= 2.2 m	Outer diameter of the minaret

This critical speed is quite low, when compared with the recorded maximum wind speeds all over Turkey.[10] It means that minaret structures have the high risk of vortex shedding excitations.

Lift force per unit length at the critical wind speed is estimated by using Eq. 4.65.

F_L = 137.1 N/m by considering, ρ = 1.2041 kg/m^3 at 20 ^{0}C

σ_L = 0.5 From table 29.2 of [18]

Response against harmonic lift force which is assumed uniformly distributed over the structure can be improved in a couple of ways. First, stiffness of the structure can be increased by thicker structural walls or additional supports. This results in significant additional cost and conflicts with architectural concept. Also increased mass will affect the earthquake performance of the structure. There might be the second solution as to remove exciting vortex shedding occurrence by eliminating the wind around the structure or vortex breakers on the structure. These solutions again have the same disadvantageous as in the stiffness increasing. It seems that the developed TMD against earthquake excitations will also improve the response of the structure against vortex shedding without any additional cost.

Now the same TMD design and its performance will be checked against vortex shedding excitations here. Let's use lift force as exciting force *q* in the related field transfer matrix Eq. 3.79. Then revise the Matlab codes already prepared for the base excitations model with and without TMD installation. Matlab codes without TMD are presented in Appendix A.9. and with TMD in Appendix A.10. The response parameters of the structure without TMD are listed on Table 5.13 and for the structure equipped with TMD on Table 5.14. Response improvements are listed on Table 5.15. There are significant improvements in the response as seen on the table. It is verified that TMD application is a cost effective way of improving dynamic response against vortex shedding.

Table 5.13. Response outputs of minaret without TMD against vortex shedding

		Vortex shedding without TMD
Displacement at 12th node	(m)	2.2 x 10^{-2}
Base shear	(N)	6.57 x 10^4
Base moment	(N m)	2.62 x 10^6

Table 5.14. Response outputs of minaret with TMD against vortex shedding

		Vortex shedding with TMD
Displacement at 12^{th} node	(m)	0.3×10^{-2}
Base shear	(N)	3.19×10^{4}
Base moment	(N m)	4.49×10^{5}

Table 5.15. Response improvement of minaret via TMD installation against vortex shedding

Displacement at 12^{th} node	86 %
Base shear	51 %
Base moment	83 %

6. TMD DESIGN FOR MINARET

6.1 TMD Design

TMD type selection and the reasons for this selection were elaborated in Section 5.3. General layout was also decided by considering the severe constraints. Now, all components of TMD should be designed according to the above mentioned issues and analysis results. In section 5.4.4 optimized TMD stiffness, damping and mass values were estimated on the basis of translational TMD assumption as shown in Figure 6.1. However selected TMD type is a hybrid one, like combination of pendulum and a translational TMD as shown in Figure 6.2.

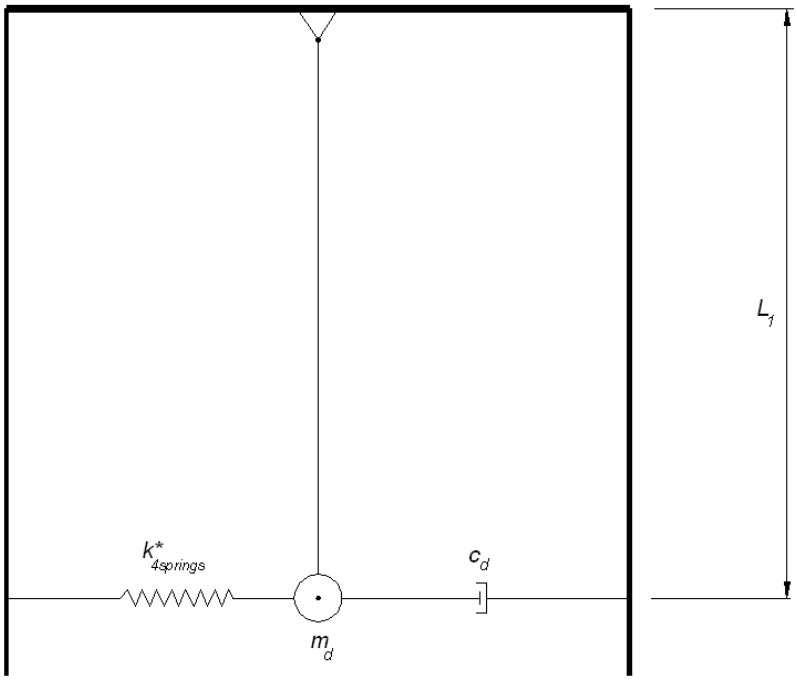

Figure 6.1. Equivalent model a translational TMD

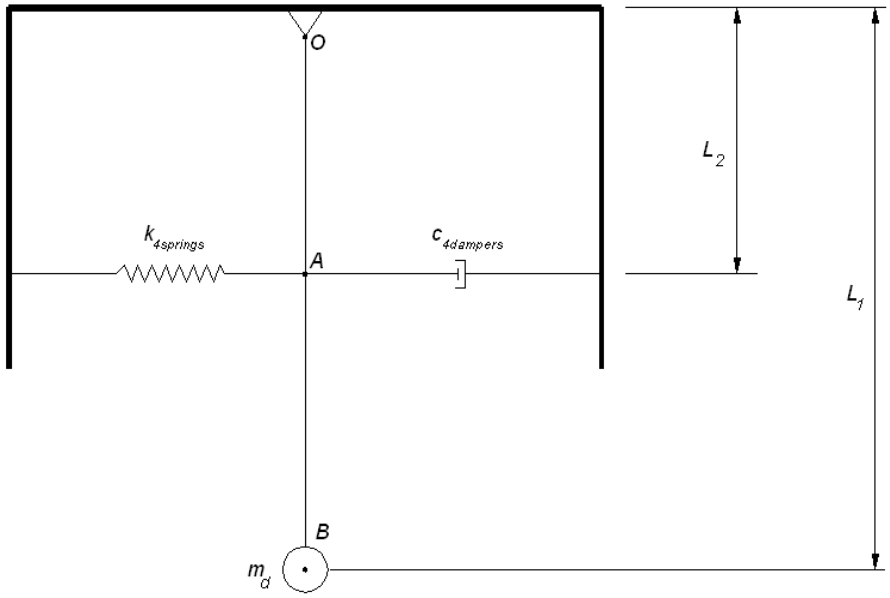

Figure 6.2. Equivalent model of the selected hybrid TMD

There are 2 components which creates real stiffness in selected hybrid TMD configuration. They are springs and pendulum. Since they are in parallel connections, their stiffness values should be added.

$$k_{pendulum} = m_d g / L_1 \tag{6.1}$$

Where; m_d=3490 kg , L_1=2.95 m , L_2=1.25 m

$k_{pendulum}$= 11606 N/m

$$k_d = k^*_{4springs} + k_{pendulum} \tag{6.2}$$

$k^*_{4springs}$ =114364 N/m

$$k_{4springs} = \left(\frac{L_1}{L_2}\right)^2 k^*_{4springs} \tag{6.3}$$

$k_{4springs}$ =636962 N/m (Total stiffness value of four orthogonal springs)

$$c_{4dampers} = (\frac{L_1}{L_2})^2 \, c_d \tag{6.4}$$

Where; c_d=7020 N s/m

$c_{4dampers}$ = 39099 N s/m (Total damping coefficient value of four orthogonal damper)

It is verified in Appendix C that general stiffness value of 4 orthogonal springs with stiffness k will be $2k$ for small displacements. Accuracy of this approximation decreases with increasing displacements. It is anticipated that displacement ratio will be less than 0.4 in our TMD design. Then maximum variation in stiffness value will be 11 %. It was noted in section 5.4.4 that such changes in stiffness and damping values do not affect the response of the structure significantly.

k_{spring} = 318481 N/m (Stiffness value of each spring)

c_{damper} = 19550 N s/m (Damping coefficient value of each damper)

Frame Structure: Main concern is the access difficulties to the top of cylindrical body of minaret just under the spire section. There are not any hoisting possibilities inside or outside of the structure. Even mobile cranes will not be good choice due to closer distances of neighboring buildings around the minaret. Therefore frame structure should be designed for bolt connection and all components should be loose. They will be carried to their final location by the workers via the ladders.

S235 quality steel was preferred for the structure due to low cost and easy availability. Chemical anchors were selected to fix the frame to the minaret wall to prevent any local stress concentration in the cylindrical body. Detailed design of frame structure is available in Appendix D

Pendulum Rod: In spite of translational TMD assumption, outlook of designed TMD looks like a pendulum type. Access difficulties to the TMD location for future maintenance and integrity of the TMD with minaret structure forced us to select such a hybrid type

TMD. We could select an inverted pendulum as in reference [6]. But instability of inverted pendulum will be disturbing the springs in case of any excitation. Normal pendulum will work better by creating additional stiffness and restoring force due to gravity. It will help to the springs to reach their neutral position just after any excitation.

S355 quality square bar is selected for the rod material due to high strength demand against bending stresses. It is connected to the frame via universal rod end bearing. Rod end bearing allows it to oscillate in any radial directions. Spring damper combination is connected to the rod via sliding joint. This joint is free to slide on the rod. A circular plate is screwed to the rod to support the lamellar pendulum mass. Rod mass was also considered while estimating the lamellar pendulum mass. Rod mass consideration was shown in Pendulum Mass section. Pendulum rod is supported by spring and damper configuration at point A as shown in Figure 6.2. Although it is not a fixed connection, let's assume as fixed. Natural frequency of this cantilever pendulum rod should not match with the natural frequency of the system.

$$k_{rod} = \frac{3\,E_{rod}\,I_{rod}}{(L_1 - L_2)^3}$$

Where; E=210 10^3 MPa I_{rod}= 8.333 10^{-6} m^4 k_{rod}=1068550 N/m

$$\omega_{rod} = \sqrt{k_{rod} / m_d}$$

ω_{rod} = 17.5 rad/sec

ω_{rod} is quite far from natural frequency of the system which was 6.6 rad/sec. Therefore rod design is acceptable.

Pendulum Mass: There is a limited space to locate the pendulum mass. Lead is preferred due to high density against steel or other ordinary materials which is 11.34 g/cm^3. It should be lamellar type to maintain the installation at site one by one. Also it will be easier for workers to carry them all the way to the upper sections of the minaret. Space between the mass and structure wall should be convenient for the relative movement

during any excitation. It is considered that 62.5 cm is sufficient for that purpose. Finally diameter of the lamellar weight is selected as 60 cm. Lamellar mass quantities can be increased or decreased to tune the TMD mass at site. Pendulum rod mass was considered while estimating the lamellar pendulum mass.

$$m_d = m_{rodeq} + m_{lamellar}$$

$$m_{rodeq} = \frac{1}{4} m_{rod}$$

Where; $m_{rod} = 263$ kg

$m_{rodeq} = 66$ kg

$m_{lamellar} = 3424$ kg

Spring and Damper Combination: Four mutually perpendicular and horizontal spring and damper combinations are attached to the pendulum rod via a sliding joint. Their vertical position can be adjusted in case of any demand at site. While the plane of orthogonal springs is being changed, stiffness of the system will be affected. Eventually natural frequency of the TMD will be affected due to changes in the equivalent mass value. This reality can be a good tool to tune the TMD under real conditions.

The maximum relative displacement of the TMD mass corresponds to an angular displacement of 10 degrees from the vertical axis. The pendulum mass contacts to the minaret wall at that point. Urethane bumper ring should be installed on to the wall to cushion any potential impacts. General assembly drawings and related fabrication drawings for each items described above are available in Appendix D.

Springs and dampers can be purchased from relevant suppliers. Stiffness value for springs, damping coefficient for dampers are the key issues while procuring from the market. Technical parameters and dimensions are given in their detailed fabrication drawings. Standard components from the market should be preferred if their dimensions and technical parameters are in close range to the design values.

6.2 TMD Cost Analysis

Cost items for the designed TMD will be as following;

Description .	Quantity	Unit Rate	Cost
Frame Structure	500 kg	4 $/kg	2.000 $
Pendulum Rod	60 kg	6 $/kg	360 $
Pendulum mass	3.490 kg	1 $/kg	3.490 $
Spring / Damper Combination	4 set	800 $/set	3.200 $
Freight charges to site	1 set	500 $/set	500 $
Installation charges	1 set	2.750 $/set	2.750 $
		Total Cost:	**12.300 $**

Cost items for a typical new minaret construction will be as following;

Description	Quantity	Unit Rate	Cost
Concrete	115 m^3	100 $/$m^3$	11.500 $
Reinforcing bar	13 ton	1.000 $/kg	13.000 $
Formwork	700 m^2	40 $/$m^2$	28.000 $
Others	1 set	5.000 $/set	5.000 $
		Total Cost:	**57.500 $**

TMD will cost approximately 20 % of a new minaret construction. This ratio will make TMD application feasible to improve their earthquake and wind response.

7. CONCLUSION

7.1. Results

In this study, the process of analyzing and improving the response of slender structures subjected to earthquake and wind loads by using TMD application was studied in detail. Dynamic response and improvements by TMD application of a minaret as an example slender structure was studied in detail against various earthquake and aerodynamic forces such as harmonic base excitation, earthquake ground acceleration and vortex shedding due to wind. First, a computer program was developed which utilizes the transfer matrix method. Then, FEM analysis was carried out. TMD's response improvements are estimated clearly.

It was noted that TMD application improves the displacement and base bending moments approximately 80-90 % in case of harmonic base excitation or vortex shedding with 1^{st} natural frequency. TMD does not improve the response at the same level with 2^{nd} natural frequency excitation, due to TMD tuning according to the 1^{st} natural mode. It was also noted that TMD application does not drastically improve the response of the slender structures against earthquake loads as in the case with harmonic excitations. The reason was discussed in the related section in detail. Earthquakes become very destructive if their dominant frequency matches with the one of the natural modes of the slender structures. TMD will improve the performance of the structure in this coincidence. Therefore TMD installation will improve the response when the structure gets into the resonance.

One of the goals of this study was to design a cost effective and applicable TMD setup. Feasibility study in section 5.2 encourages the TMD application. Structural response is improved by spending approximately 20 % of its original construction cost. This ratio will be much less when other indirect cost arises after the structure collapse.

It was verified that TMD application is a cost effective and innovative solution to improve the dynamic response of slender structures against earthquake and wind excitations.

7.2. Recommendations

For the future studies, the following recommendations are suggested:

- Only bending vibration is treated in this study. Structural designers concerns other modes of vibration, such as axial or ovalling as well. These vibration modes should also be added to the analyze in more detail.

- Linear elastic vibration analysis is carried out in this study. Nonlinear analysis should be also considered in future studies.

- This study was done according to the theory of bending vibration of beams. No testing was included. Results of this study should be verified with testing a small model on a shake table.

- Real TMD application on minarets or slender structures should be done according to a valid building code. Unfortunately Turkish Seismic Design Code [20] does not refer any TMD applications and its performance criteria. Building code should allow the TMD applications to increase the damping of structures.

- TMD applications should be designed according to a design earthquake. It can be a moderate or maximum credible earthquake (MCE). Also local soil conditions should be considered. Design earthquake will dictate the TMD mass displacement amplitude. TMD mass displacement is one of the major constraints in slender structures.

- Gravity loads were not considered in this study. Future studies may include gravity loads as well.

APPENDIX A: MATLAB CODES & OUTPUTS

A.1. CODES TO DETERMINE NATURAL FREQUENCIES

```
clear all; close all; clc;
m=zeros(13,1);  % Mass matrix
L=zeros(13,1);  % Length matrix
I=zeros(13,1);  % Inertia matrix
F=zeros(13,1);  % Field transfer matrix
P=zeros(13,1);  % Point transfer matrix
% Discrete mass values of the minaret (kg)
m(1,1)=36.3*10^3;
m(2,1)=41.5*10^3;
m(3,1)=41.5*10^3;
m(4,1)=35.2*10^3;
m(5,1)=11.8*10^3;
m(6,1)=11.8*10^3;
m(7,1)=11.8*10^3;
m(8,1)=20.1*10^3;
m(9,1)=11.4*10^3;
m(10,1)=11.4*10^3;
m(11,1)=18.2*10^3;
m(12,1)=11.5*10^3;
m(13,1)=7.8*10^3
% Distances between Discrete masses (m)
L(1,1)=1.75;
L(2,1)=3.75;
L(3,1)=4.0;
L(4,1)=4.50;
L(5,1)=4.10;
L(6,1)=3.20;
L(7,1)=3.20;
L(8,1)=3.50;
L(9,1)=3.45;
L(10,1)=3.1;
L(11,1)=3.45;
L(12,1)=4.05;
L(13,1)=3.65
% Inertia values between Discrete masses (m4)
I(1,1)=5.364;
I(2,1)=5.364;
I(3,1)=5.364;
I(4,1)=5.364;
I(5,1)=0.74;
I(6,1)=0.74;
I(7,1)=0.74;
I(8,1)=0.74;
I(9,1)=0.74;
I(10,1)=0.74;
I(11,1)=0.74;
I(12,1)=0.575;
I(13,1)=0.575
% Modulus of elasticity for reinforced concrete (Pa)
E=27*10^9
% Elements of Field Transfer Matrix
for i=1.13;
Fi=[1 L(i) ((L(i))^2)/(2*E*I(i)) ((L(i))^3)/(6*E*I(i)) ; 0 1
L(i)/(E*I(i)) ((L(i))^2)/(2*E*I(i)) ; 0 0 1 L(i) ; 0 0 0 1];
    if i==1
        F1=Fi;
    elseif i==2
        F2=Fi;
```

```
    elseif i==3
        F3=Fi;
    elseif i==4
        F4=Fi;
    elseif i==5
        F5=Fi;
    elseif i==6
        F6=Fi;
    elseif i==7
        F7=Fi;
    elseif i==8
        F8=Fi;
    elseif i==9
        F9=Fi;
    elseif i==10
        F10=Fi;
    elseif i==11
        F11=Fi;
    elseif i==12
        F12=Fi;
    elseif i==13
        F13=Fi;
end
end
a = sym('a');
% Elements of Point Transfer Matrix
for i=1.13;
    Pi=[1 0 0 0 ; 0 1 0 0 ; 0 0 1 0 ; m(i)*a 0 0 1];
    if i==1
        P1=Pi;
    elseif i==2
        P2=Pi;
    elseif i==3
        P3=Pi;
    elseif i==4
        P4=Pi;
    elseif i==5
        P5=Pi;
    elseif i==6
        P6=Pi;
    elseif i==7
        P7=Pi;
    elseif i==8
        P8=Pi;
    elseif i==9
        P9=Pi;
    elseif i==10
        P10=Pi;
    elseif i==11
        P11=Pi;
    elseif i==12
        P12=Pi;
    elseif i==13
        P13=Pi;
end
end
% Short form of F1 due to cantilever boundary condition
F1K=F1(1.4,3.4);
% Total Transfer matrixes
```

```
U=P13*F13*P12*F12*P11*F11*P10*F10*P9*F9*P8*F8*P7*F7*P6*F6*P5*F5*P4*F4*P3*
F3*P2*F2*P1*F1K;
% Frequency determinant
U1=U(3.4,1.2);
Z=det(U1);
digits (10);
syms a;
p = sym2poly(Z);
r = roots(p);
% Natural frequencies of minaret (rad/sec)
w=realsqrt(r)
% Natural frequencies of minaret (1/sec)
f=realsqrt(r)/(2*(pi))
```

A.2. CODES TO DETERMINE NORMAL MODE SHAPES

```
clear all; close all; clc;
w=[6.6 32.2 72.6 137.2 239.6 355.5 453.5 630.2 779.4 1010 1165.3 1336.9
2550.4]; % Natural frequencies of the system
E=27*10^9;   % Modulus of elasticity for reinforced concrete (Pa)
m=zeros(13,1);  % Mass matrix
L=zeros(13,1);  % Length matrix
I=zeros(13,1);  % Inertia matrix
F=zeros(13,1);  % Field transfer matrix
P=zeros(13,1);  % Point transfer matrix
dis=zeros(13,1);  % Displacement matrix
% Discrete mass values of the minaret (kg)
m(1,1)=36.3*10^3;
m(2,1)=41.5*10^3;
m(3,1)=41.5*10^3;
m(4,1)=35.2*10^3;
m(5,1)=11.8*10^3;
m(6,1)=11.8*10^3;
m(7,1)=11.8*10^3;
m(8,1)=20.1*10^3;
m(9,1)=11.4*10^3;
m(10,1)=11.4*10^3;
m(11,1)=18.2*10^3;
m(12,1)=11.5*10^3;
m(13,1)=7.8*10^3;
% Distances between Discrete masses (m)
L(1,1)=1.75;
L(2,1)=3.75;
L(3,1)=4.0;
L(4,1)=4.50;
L(5,1)=4.10;
L(6,1)=3.20;
L(7,1)=3.20;
L(8,1)=3.50;
L(9,1)=3.45;
L(10,1)=3.1;
L(11,1)=3.45;
L(12,1)=4.05;
L(13,1)=3.65;
% Inertia values between Discrete masses (m4)
I(1,1)=5.364;
I(2,1)=5.364;
I(3,1)=5.364;
```

```
I(4,1)=5.364;
I(5,1)=0.74;
I(6,1)=0.74;
I(7,1)=0.74;
I(8,1)=0.74;
I(9,1)=0.74;
I(10,1)=0.74;
I(11,1)=0.74;
I(12,1)=0.575;
I(13,1)=0.575;
% Elements of Field Transfer Matrix
for i=1.13;
Fi=[1 L(i) ((L(i))^2)/(2*E*I(i)) ((L(i))^3)/(6*E*I(i)) ; 0 1
L(i)/(E*I(i)) ((L(i))^2)/(2*E*I(i)) ; 0 0 1 L(i) ; 0 0 0 1];
    if i==1
        F1=Fi;
    elseif i==2
        F2=Fi;
    elseif i==3
        F3=Fi;
    elseif i==4
        F4=Fi;
    elseif i==5
        F5=Fi;
    elseif i==6
        F6=Fi;
    elseif i==7
        F7=Fi;
    elseif i==8
        F8=Fi;
    elseif i==9
        F9=Fi;
    elseif i==10
        F10=Fi;
    elseif i==11
        F11=Fi;
    elseif i==12
        F12=Fi;
    elseif i==13
        F13=Fi;
end
end
for ii=1.13
% Elements of Point Transfer Matrix
for i=1.13;
    Pi=[1 0 0 0 ; 0 1 0 0 ; 0 0 1 0 ; m(i)*w(ii)^2 0 0 1];
    if i==1
        P1=Pi;
    elseif i==2
        P2=Pi;
    elseif i==3
        P3=Pi;
    elseif i==4
        P4=Pi;
    elseif i==5
        P5=Pi;
    elseif i==6
        P6=Pi;
    elseif i==7
        P7=Pi;
```

```
    elseif i==8
        P8=Pi;
    elseif i==9
        P9=Pi;
    elseif i==10
        P10=Pi;
    elseif i==11
        P11=Pi;
    elseif i==12
        P12=Pi;
    elseif i==13
        P13=Pi;
end
end
% Transfer matrices
U1=P1*F1;
U2=P2*F2*U1;
U3=P3*F3*U2;
U4=P4*F4*U3;
U5=P5*F5*U4;
U6=P6*F6*U5;
U7=P7*F7*U6;
U8=P8*F8*U7;
U9=P9*F9*U8;
U10=P10*F10*U9;
U11=P11*F11*U10;
U12=P12*F12*U11;
U13=P13*F13*U12;
Z0=[0 0 1 -(U13(3,3)/U13(3,4))]'
% Estimation of state vectors for each nodes
Z1=U1*Z0;
Z2=U2*Z0;
Z3=U3*Z0;
Z4=U4*Z0;
Z5=U5*Z0;
Z6=U6*Z0;
Z7=U7*Z0;
Z8=U8*Z0;
Z9=U9*Z0;
Z10=U10*Z0;
Z11=U11*Z0;
Z12=U12*Z0;
Z13=U13*Z0;
% Lateral displacements at each node
dis=[Z0(1)/Z13(1) Z1(1)/Z13(1) Z2(1)/Z13(1) Z3(1)/Z13(1) Z4(1)/Z13(1)
Z5(1)/Z13(1) Z6(1)/Z13(1) Z7(1)/Z13(1) Z8(1)/Z13(1) Z9(1)/Z13(1)
Z10(1)/Z13(1) Z11(1)/Z13(1) Z12(1)/Z13(1) Z13(1)/Z13(1)]
y=[0 1.75 5.5 9.5 14.0 18.1 21.3 24.5 28 31.45 34.55 38.0 42.05 45.7];
figure
plot(dis,y)
grid
title('MOD(ii)')
xlabel('Displacement (m)')
ylabel('Height (m)')
end
```

A.3. CODES FOR TMD OPTIMIZATION

```
clear all
close all
global  md  eval
md = 3490;      % TMD mass (kg)
eval=[6.6 32.2 72.6 137.2 239.6 355.5 453.5 630.2 779.4 1010 1165.3
1336.9 2550.4]; % Natural frequencies of the system
x0 = [125970; 7020];    % Starting guess of the solution [kd ; cd]
options = optimset('TolX',1e-10,'TolFun',1e-
10,'MaxFunEvals',100000,'MaxIter',100000);
[x,fval] = fminimax(@trans,x0,[],[],[],[],[0; 0],[],[],options);
tmax=max(fval)
x

% The aim is to minimize the peak of the nth natural frequency
% in the transmissibility plot
function f = trans(x)
global md eval
kd=x(1);
cd=x(2);
g=0.05 ;     % Structural Damping for R/C structure
ug=5 ;        % Max harmonic ground acceleration  (m/sec2)
E=27*10^9; % Modulus of elasticity for Reinforced concrete (N/m2)
m=zeros(13,1);  % Mass matrix
L=zeros(13,1);  % Length matrix
I=zeros(13,1);  % Inertia matrix
F=zeros(13,1);  % Field transfer matrix
P=zeros(13,1);  % Point transfer matrix
% Discrete mass values of the minaret (kg)
m(1,1)=36.3*10^3;
m(2,1)=41.5*10^3;
m(3,1)=41.5*10^3;
m(4,1)=35.2*10^3;
m(5,1)=11.8*10^3;
m(6,1)=11.8*10^3;
m(7,1)=11.8*10^3;
m(8,1)=20.1*10^3;
m(9,1)=11.4*10^3;
m(10,1)=11.4*10^3;
m(11,1)=18.2*10^3;
m(12,1)=11.5*10^3;
m(13,1)=7.8*10^3;
% Distances between Discrete masses (m)
L(1,1)=1.75;
L(2,1)=3.75;
L(3,1)=4.0;
L(4,1)=4.50;
L(5,1)=4.10;
L(6,1)=3.20;
L(7,1)=3.20;
L(8,1)=3.50;
L(9,1)=3.45;
L(10,1)=3.1;
L(11,1)=3.45;
L(12,1)=4.05;
L(13,1)=3.65;
% Inertia values between Discrete masses (m4)
I(1,1)=5.364;
I(2,1)=5.364;
```

```
I(3,1)=5.364;
I(4,1)=5.364;
I(5,1)=0.74;
I(6,1)=0.74;
I(7,1)=0.74;
I(8,1)=0.74;
I(9,1)=0.74;
I(10,1)=0.74;
I(11,1)=0.74;
I(12,1)=0.575;
I(13,1)=0.575;
% Elements of Field Transfer Matrix
for i=1.13;
Fi=[1 L(i) ((L(i))^2)/(2*E*I(i)*(1+g^2)) ((L(i))^3)/(6*E*I(i)*(1+g^2)) 0
0 g*((L(i))^2)/(2*E*I(i)*(1+g^2)) g*((L(i))^3)/(6*E*I(i)*(1+g^2)) 0 ; 0 1
L(i)/(E*I(i)*(1+g^2)) ((L(i))^2)/(2*E*I(i)*(1+g^2)) 0 0
g*L(i)/(E*I(i)*(1+g^2)) g*((L(i))^2)/(2*E*I(i)*(1+g^2)) 0 ; 0 0 1 L(i) 0
0 0 0 0 ; 0 0 0 1 0 0 0 0 0 ; 0 0 -g*((L(i))^2)/(2*E*I(i)*(1+g^2)) -
g*((L(i))^3)/(6*E*I(i)*(1+g^2)) 1 L(i) ((L(i))^2)/(2*E*I(i)*(1+g^2))
((L(i))^3)/(6*E*I(i)*(1+g^2)) 0 ; 0 0 -g*L(i)/(E*I(i)*(1+g^2)) -
g*((L(i))^2)/(2*E*I(i)*(1+g^2)) 0 1 L(i)/(E*I(i)*(1+g^2))
((L(i))^2)/(2*E*I(i)*(1+g^2)) 0 ; 0 0 0 0 0 0 1 L(i) 0 ; 0 0 0 0 0 0 0 1
0 ; 0 0 0 0 0 0 0 0 1 ];
    if i==1
        F1=Fi;
    elseif i==2
        F2=Fi;
    elseif i==3
        F3=Fi;
    elseif i==4
        F4=Fi;
    elseif i==5
        F5=Fi;
    elseif i==6
        F6=Fi;
    elseif i==7
        F7=Fi;
    elseif i==8
        F8=Fi;
    elseif i==9
        F9=Fi;
    elseif i==10
        F10=Fi;
    elseif i==11
        F11=Fi;
    elseif i==12
        F12=Fi;
    elseif i==13
        F13=Fi;
end
end
j=sqrt(-1);
%w=0.1.0.01.1*eval(1); % Optimization frequency range
w=0.5*eval(1):0.01.1.5*eval(1); % Optimization frequency range
X=zeros(1,length(w));
for ii=1.length(w);
% Elements of Point Transfer Matrix
for i=1.13;
     Pi=[1 0 0 0 0 0 0 0 0 ; 0 1 0 0 0 0 0 0 0 ; 0 0 1 0 0 0 0 0 0 ;
m(i)*w(ii)^2 0 0 1 0 0 0 0 -m(i)*ug ; 0 0 0 0 1 0 0 0 0 ; 0 0 0 0 0 1 0 0
```

```
0 ; 0 0 0 0 0 0 1 0 0 ; 0 0 0 0 m(i)*w(ii)^2 0 0 1 0 ; 0 0 0 0 0 0 0 0 0 1
];
    if i==1;
        P1=Pi;
    elseif i==2;
        P2=Pi;
    elseif i==3;
        P3=Pi;
    elseif i==4;
        P4=Pi;
    elseif i==5;
        P5=Pi;
    elseif i==6;
        P6=Pi;
    elseif i==7;
        P7=Pi;
    elseif i==8;
        P8=Pi;
    elseif i==9;
        P9=Pi;
    elseif i==10;
        P10=Pi;
    elseif i==11;
        P11=Pi;
    elseif i==12;
        P12=Pi;
    elseif i==13;
        P13=Pi;
end
end
A=(((kd^2)*md*(w(ii)^2))-
(kd*((md)^2)*(w(ii)^4))+((cd^2)*md*(w(ii)^4)))/(((kd-
(md*(w(ii)^2)))^2)+(((cd)^2)*(w(ii)^2)));
B=-((cd*md^2)*w(ii)^5)/(((kd-(md*(w(ii)^2)))^2)+((cd^2)*(w(ii)^2)));
C=-md*ug*(((-kd*md*(w(ii)^2))+(kd^2)+((cd^2)*(w(ii)^2)))/(((kd-
(md*(w(ii)^2)))^2)+((cd^2)*(w(ii)^2))));
D=md*ug*((md*cd*(w(ii)^3))/(((kd-(md*(w(ii)^2)))^2)+((cd^2)*(w(ii)^2))));
% Changes in P12 due to TMD impact
P12=[1 0 0 0 0 0 0 0 0 ; 0 1 0 0 0 0 0 0 0 ; 0 0 1 0 0 0 0 0 0 ;
((m(12)*w(ii)^2)+A) 0 0 1 -B 0 0 0 -m(12)*ug+C ; 0 0 0 0 1 0 0 0 0 ; 0 0
0 0 0 1 0 0 0 ; 0 0 0 0 0 0 1 0 0 ; B 0 0 0 ((m(12)*w(ii)^2)+A) 0 0 1 D ;
0 0 0 0 0 0 0 0 1];
% Transfer matrixes for nodes
U1=P1*F1;
U2=P2*F2*U1;
U3=P3*F3*U2;
U4=P4*F4*U3;
U5=P5*F5*U4;
U6=P6*F6*U5;
U7=P7*F7*U6;
U8=P8*F8*U7;
U9=P9*F9*U8;
U10=P10*F10*U9;
U11=P11*F11*U10;
U12=P12*F12*U11;
U13=P13*F13*U12;
% Estimation of state vector at ground level (Z0)by applying the boundary
conditions
```

```
A=[U13(3,3) U13(3,4) U13(3,7)  U13(3,8); U13(4,3) U13(4,4) U13(4,7)
U13(4,8) ; U13(7,3) U13(7,4) U13(7,7) U13(7,8) ; U13(8,3) U13(8,4)
U13(8,7) U13(8,8)];
B=[-U13(3,9) -U13(4,9) -U13(7,9) -U13(8,9)]';
C=inv(A)*B;
Z0=[0 0 C(1) C(2) 0 0 C(3) C(4) 1]' ;
% Estimation of state vectors for 12th node
Z12=U12*Z0;
X(ii)=Z12(1)+j*Z12(5);  % Complex lateral displacements at 12th node
end
f=abs(X(1,:));
w=0.1.0.01.2*eval(1); % Ploting frequency range
X=zeros(1,length(w));
for ii=1.length(w)
% Elements of Point Transfer Matrix
for i=1.13;
     Pi=[1 0 0 0 0 0 0 0 0 ; 0 1 0 0 0 0 0 0 0 ; 0 0 1 0 0 0 0 0 0 ;
m(i)*w(ii)^2 0 0 1 0 0 0 0 -m(i)*ug ; 0 0 0 0 1 0 0 0 0 ; 0 0 0 0 0 0 1 0 0
0 ; 0 0 0 0 0 0 0 1 0 0 ; 0 0 0 0 m(i)*w(ii)^2 0 0 1 0 ; 0 0 0 0 0 0 0 0 0 1
];
    if i==1;
        P1=Pi;
    elseif i==2;
        P2=Pi;
    elseif i==3;
        P3=Pi;
    elseif i==4;
        P4=Pi;
    elseif i==5;
        P5=Pi;
    elseif i==6;
        P6=Pi;
    elseif i==7;
        P7=Pi;
    elseif i==8;
        P8=Pi;
    elseif i==9;
        P9=Pi;
    elseif i==10;
        P10=Pi;
    elseif i==11;
        P11=Pi;
    elseif i==12;
        P12=Pi;
    elseif i==13;
        P13=Pi;
end
end
A=(((kd^2)*md*(w(ii)^2))-
(kd*((md)^2)*(w(ii)^4))+((cd^2)*md*(w(ii)^4)))/(((kd-
(md*(w(ii)^2)))^2)+(((cd)^2)*(w(ii)^2)));
B=-((cd*md^2)*w(ii)^5)/(((kd-(md*(w(ii)^2)))^2)+((cd^2)*(w(ii)^2)));
C=-md*ug*(((-kd*md*(w(ii)^2))+(kd^2)+((cd^2)*(w(ii)^2)))/(((kd-
(md*(w(ii)^2)))^2)+((cd^2)*(w(ii)^2))));
D=md*ug*((md*cd*(w(ii)^3))/(((kd-(md*(w(ii)^2)))^2)+((cd^2)*(w(ii)^2))));
% Changes in P12 due to TMD impact
P12=[1 0 0 0 0 0 0 0 0 ; 0 1 0 0 0 0 0 0 0 ; 0 0 1 0 0 0 0 0 0 ;
((m(12)*w(ii)^2)+A) 0 0 1 -B 0 0 0 -m(12)*ug+C ; 0 0 0 0 1 0 0 0 0 ; 0 0
0 0 0 1 0 0 0 ; 0 0 0 0 0 0 1 0 0 ; B 0 0 0 ((m(12)*w(ii)^2)+A) 0 0 1 D ;
0 0 0 0 0 0 0 0 1];
```

```
% Transfer matrixes for nodes
U1=P1*F1;
U2=P2*F2*U1;
U3=P3*F3*U2;
U4=P4*F4*U3;
U5=P5*F5*U4;
U6=P6*F6*U5;
U7=P7*F7*U6;
U8=P8*F8*U7;
U9=P9*F9*U8;
U10=P10*F10*U9;
U11=P11*F11*U10;
U12=P12*F12*U11;
U13=P13*F13*U12;
% Estimation of state vector at ground level (Z0)by applying the boundary
conditions
A=[U13(3,3) U13(3,4) U13(3,7)  U13(3,8); U13(4,3) U13(4,4) U13(4,7)
U13(4,8) ; U13(7,3) U13(7,4) U13(7,7) U13(7,8) ; U13(8,3) U13(8,4)
U13(8,7) U13(8,8)];
B=[-U13(3,9) -U13(4,9) -U13(7,9) -U13(8,9)]';
C=inv(A)*B;
Z0=[0 0 C(1) C(2) 0 0 C(3) C(4) 1]' ;
% Estimation of state vector for 12th node
Z12=U12*Z0;
X(ii)=Z12(1)+j*Z12(5);  % Complex lateral displacements at 12th node
end
plot(w,abs(X(1,:)))
grid
title('Frequency Response of m12 with optimized TMD')
xlabel('Frequency (rad/sec)')
ylabel('Lateral displacement (m)')
```

A.4. CODES FOR FREQUENCY PLOT

```
clear all; close all; clc;
range=35% Frequency range for plotting (rad/sec)
n=(range/0.1);
w=zeros(1,n+1);  % Exciting frequency (rad/sec)
X=zeros(1,n+1);  % Displacement of mass m12 (m)
g=0.05      % Structural Damping for R/C structure
ug=5       % Max harmonic ground acceleration  (m/sec2)
kd=125970  % Stiffnes value of TMD (N/m)
cd=7020 % Damping coeficient of TMD
md=3500     % TMD mass (kg)
E=27*10^9 % Modulus of elasticity for Reinforced concrete (N/m2)
m=zeros(13,1);  % Mass matrix
L=zeros(13,1);  % Length matrix
I=zeros(13,1);  % Inertia matrix
F=zeros(13,1);  % Field transfer matrix
P=zeros(13,1);  % Point transfer matrix
% Discrete mass values of the minaret (kg)
m(1,1)=36.3*10^3;
m(2,1)=41.5*10^3;
m(3,1)=41.5*10^3;
m(4,1)=35.2*10^3;
m(5,1)=11.8*10^3;
m(6,1)=11.8*10^3;
m(7,1)=11.8*10^3;
```

```
m(8,1)=20.1*10^3;
m(9,1)=11.4*10^3;
m(10,1)=11.4*10^3;
m(11,1)=18.2*10^3;
m(12,1)=11.5*10^3;
m(13,1)=7.8*10^3
% Distances between Discrete masses (m)
L(1,1)=1.75;
L(2,1)=3.75;
L(3,1)=4.0;
L(4,1)=4.50;
L(5,1)=4.10;
L(6,1)=3.20;
L(7,1)=3.20;
L(8,1)=3.50;
L(9,1)=3.45;
L(10,1)=3.1;
L(11,1)=3.45;
L(12,1)=4.05;
L(13,1)=3.65
% Inertia values between Discrete masses (m4)
I(1,1)=5.364;
I(2,1)=5.364;
I(3,1)=5.364;
I(4,1)=5.364;
I(5,1)=0.74;
I(6,1)=0.74;
I(7,1)=0.74;
I(8,1)=0.74;
I(9,1)=0.74;
I(10,1)=0.74;
I(11,1)=0.74;
I(12,1)=0.575;
I(13,1)=0.575
% Elements of Field Transfer Matrix
for i=1.13;
Fi=[1 L(i) ((L(i))^2)/(2*E*I(i)*(1+g^2)) ((L(i))^3)/(6*E*I(i)*(1+g^2)) 0
0 g*((L(i))^2)/(2*E*I(i)*(1+g^2)) g*((L(i))^3)/(6*E*I(i)*(1+g^2)) 0 ; 0 1
L(i)/(E*I(i)*(1+g^2)) ((L(i))^2)/(2*E*I(i)*(1+g^2)) 0 0
g*L(i)/(E*I(i)*(1+g^2)) g*((L(i))^2)/(2*E*I(i)*(1+g^2)) 0 ; 0 0 1 L(i) 0
0 0 0 0 ; 0 0 0 1 0 0 0 0 0 0 ; 0 0 -g*((L(i))^2)/(2*E*I(i)*(1+g^2)) -
g*((L(i))^3)/(6*E*I(i)*(1+g^2)) 1 L(i) ((L(i))^2)/(2*E*I(i)*(1+g^2))
((L(i))^3)/(6*E*I(i)*(1+g^2)) 0 ; 0 0 -g*L(i)/(E*I(i)*(1+g^2)) -
g*((L(i))^2)/(2*E*I(i)*(1+g^2)) 0 1 L(i)/(E*I(i)*(1+g^2))
((L(i))^2)/(2*E*I(i)*(1+g^2)) 0 ; 0 0 0 0 0 0 1 L(i) 0 ; 0 0 0 0 0 0 0 1
0 ; 0 0 0 0 0 0 0 0 1 ];
    if i==1
        F1=Fi
    elseif i==2
        F2=Fi
    elseif i==3
        F3=Fi
    elseif i==4
        F4=Fi
    elseif i==5
        F5=Fi
    elseif i==6
        F6=Fi
    elseif i==7
        F7=Fi
```

```
    elseif i==8
        F8=Fi
    elseif i==9
        F9=Fi
    elseif i==10
        F10=Fi
    elseif i==11
        F11=Fi
    elseif i==12
        F12=Fi
    elseif i==13
        F13=Fi
end
end
for ii=1.n+1
    w(ii)=(ii*0.1)-0.1;
% Elements of Point Transfer Matrix
for i=1.13;
     Pi=[1 0 0 0 0 0 0 0 0 ; 0 1 0 0 0 0 0 0 0 ; 0 0 1 0 0 0 0 0 0 ;
m(i)*w(ii)^2 0 0 1 0 0 0 0 -m(i)*ug ; 0 0 0 0 1 0 0 0 0 ; 0 0 0 0 0 0 1 0 0
0 ; 0 0 0 0 0 0 1 0 0 ; 0 0 0 0 m(i)*w(ii)^2 0 0 1 0 ; 0 0 0 0 0 0 0 0 0 1
];
    if i==1
        P1=Pi
    elseif i==2
        P2=Pi
    elseif i==3
        P3=Pi
    elseif i==4
        P4=Pi
    elseif i==5
        P5=Pi
    elseif i==6
        P6=Pi
    elseif i==7
        P7=Pi
    elseif i==8
        P8=Pi
    elseif i==9
        P9=Pi
    elseif i==10
        P10=Pi
    elseif i==11
        P11=Pi
    elseif i==12
        P12=Pi
    elseif i==13
        P13=Pi
end
end
% Equivalent stiffnes of TMD
A=(((kd^2)*md*(w(ii)^2))-
(kd*(md^2)*(w(ii)^4))+((cd^2)*md*(w(ii)^4)))/(((kd-
(md*(w(ii)^2)))^2)+((cd^2)*(w(ii)^2)))
B=-((cd*md^2)*w(ii)^5)/(((kd-(md*(w(ii)^2)))^2)+((cd^2)*(w(ii)^2)))
C=-md*ug*(((-kd*md*(w(ii)^2))+(kd^2)+((cd^2)*(w(ii)^2)))/(((kd-
(md*(w(ii)^2)))^2)+((cd^2)*(w(ii)^2))))
D=md*ug*((md*cd*(w(ii)^3))/(((kd-(md*(w(ii)^2)))^2)+((cd^2)*(w(ii)^2))))
% Changes in P12 due to TMD impact
```

```
P12=[1 0 0 0 0 0 0 0 0 ; 0 1 0 0 0 0 0 0 0 ; 0 0 1 0 0 0 0 0 0 ;
((m(12)*w(ii)^2)+A) 0 0 1 -B 0 0 0 -m(12)*ug+C ; 0 0 0 0 1 0 0 0 ; 0 0
0 0 0 1 0 0 0 ; 0 0 0 0 0 0 1 0 0 ; B 0 0 0 ((m(12)*w(ii)^2)+A) 0 0 1 D ;
0 0 0 0 0 0 0 0 1]
% Transfer matrixes for nodes
U1=P1*F1;
U2=P2*F2*U1;
U3=P3*F3*U2;
U4=P4*F4*U3;
U5=P5*F5*U4;
U6=P6*F6*U5;
U7=P7*F7*U6;
U8=P8*F8*U7;
U9=P9*F9*U8;
U10=P10*F10*U9;
U11=P11*F11*U10;
U12=P12*F12*U11;
U13=P13*F13*U12;
% Estimation of state vector at ground level (Z0)by applying the boundary
conditions
A=[U13(3,3) U13(3,4) U13(3,7)  U13(3,8); U13(4,3) U13(4,4) U13(4,7)
U13(4,8) ; U13(7,3) U13(7,4) U13(7,7) U13(7,8) ; U13(8,3) U13(8,4)
U13(8,7) U13(8,8)];
B=[-U13(3,9) -U13(4,9) -U13(7,9) -U13(8,9)]';
C=inv(A)*B;
Z0=[0 0 C(1) C(2) 0 0 C(3) C(4) 1]'
% Estimation of state vectors for each nodes
Z12=U12*Z0;
j=sqrt(-1);
XJ(ii)=Z12(1)+j*Z12(5)  % Complex lateral displacements at each node
X(ii)=abs(XJ(ii))/abs(XJ(1));
end
plot(w,X)
grid
title('Frequency Response of m12 with TMD')
xlabel('Frequency (rad/sec)')
ylabel('Lateral displacement (m)')
```

A.5. CODES FOR DYNAMIC ANALYSIS OF MODEL WITHOUT TMD

```
clear all; close all; clc;
w=6.6;      % Exciting frequency (rad/sec)
g=0.05;      % Structural Damping for R/C structure
ug=1;       % Max harmonic ground acceleration  (m/sec2)
E=27*10^9; % Modulus of elasticity for Reinforced concrete (N/m2)
m=zeros(13,1);  % Mass matrix
L=zeros(13,1);  % Length matrix
I=zeros(13,1);  % Inertia matrix
F=zeros(13,1);  % Field transfer matrix
P=zeros(13,1);  % Point transfer matrix
% Discrete mass values of the minaret (kg)
m(1,1)=36.3*10^3;
m(2,1)=41.5*10^3;
m(3,1)=41.5*10^3;
m(4,1)=35.2*10^3;
m(5,1)=11.8*10^3;
m(6,1)=11.8*10^3;
m(7,1)=11.8*10^3;
```

```
m(8,1)=20.1*10^3;
m(9,1)=11.4*10^3;
m(10,1)=11.4*10^3;
m(11,1)=18.2*10^3;
m(12,1)=11.5*10^3;
m(13,1)=7.8*10^3;
% Distances between Discrete masses (m)
L(1,1)=1.75;
L(2,1)=3.75;
L(3,1)=4.0;
L(4,1)=4.50;
L(5,1)=4.10;
L(6,1)=3.20;
L(7,1)=3.20;
L(8,1)=3.50;
L(9,1)=3.45;
L(10,1)=3.1;
L(11,1)=3.45;
L(12,1)=4.05;
L(13,1)=3.65;
% Inertia values between Discrete masses (m4)
I(1,1)=5.364;
I(2,1)=5.364;
I(3,1)=5.364;
I(4,1)=5.364;
I(5,1)=0.74;
I(6,1)=0.74;
I(7,1)=0.74;
I(8,1)=0.74;
I(9,1)=0.74;
I(10,1)=0.74;
I(11,1)=0.74;
I(12,1)=0.575;
I(13,1)=0.575;
 % Elements of Field Transfer Matrix
for i=1.13;
Fi=[1 L(i) ((L(i))^2)/(2*E*I(i)*(1+g^2)) ((L(i))^3)/(6*E*I(i)*(1+g^2)) 0
0 g*((L(i))^2)/(2*E*I(i)*(1+g^2)) g*((L(i))^3)/(6*E*I(i)*(1+g^2)) 0 ; 0 1
L(i)/(E*I(i)*(1+g^2)) ((L(i))^2)/(2*E*I(i)*(1+g^2)) 0 0
g*L(i)/(E*I(i)*(1+g^2)) g*((L(i))^2)/(2*E*I(i)*(1+g^2)) 0 ; 0 0 1 L(i) 0
0 0 0 0 ; 0 0 0 1 0 0 0 0 0 0 ; 0 0 -g*((L(i))^2)/(2*E*I(i)*(1+g^2)) -
g*((L(i))^3)/(6*E*I(i)*(1+g^2)) 1 L(i) ((L(i))^2)/(2*E*I(i)*(1+g^2))
((L(i))^3)/(6*E*I(i)*(1+g^2)) 0 ; 0 0 -g*L(i)/(E*I(i)*(1+g^2)) -
g*((L(i))^2)/(2*E*I(i)*(1+g^2)) 0 1 L(i)/(E*I(i)*(1+g^2))
((L(i))^2)/(2*E*I(i)*(1+g^2)) 0 ; 0 0 0 0 0 0 1 L(i) 0 ; 0 0 0 0 0 0 0 1
0 ; 0 0 0 0 0 0 0 0 1 ];
    if i==1
        F1=Fi;
    elseif i==2
        F2=Fi;
    elseif i==3
        F3=Fi;
    elseif i==4
        F4=Fi;
    elseif i==5
        F5=Fi;
    elseif i==6
        F6=Fi;
    elseif i==7
        F7=Fi;
```

```
    elseif i==8
        F8=Fi;
    elseif i==9
        F9=Fi;
    elseif i==10
        F10=Fi;
    elseif i==11
        F11=Fi;
    elseif i==12
        F12=Fi;
    elseif i==13
        F13=Fi;
end
end
% Elements of Point Transfer Matrix
for i=1.13;
     Pi=[1 0 0 0 0 0 0 0 0 ; 0 1 0 0 0 0 0 0 0 ; 0 0 1 0 0 0 0 0 0 ;
m(i)*w^2 0 0 1 0 0 0 0 -m(i)*ug ; 0 0 0 0 1 0 0 0 0 ; 0 0 0 0 0 1 0 0 0 ;
0 0 0 0 0 0 1 0 0 ; 0 0 0 0 m(i)*w^2 0 0 1 0 ; 0 0 0 0 0 0 0 0 0 1 ];
    if i==1
        P1=Pi;
    elseif i==2
        P2=Pi;
    elseif i==3
        P3=Pi;
    elseif i==4
        P4=Pi;
    elseif i==5
        P5=Pi;
    elseif i==6
        P6=Pi;
    elseif i==7
        P7=Pi;
    elseif i==8
        P8=Pi;
    elseif i==9
        P9=Pi;
    elseif i==10
        P10=Pi;
    elseif i==11
        P11=Pi;
    elseif i==12
        P12=Pi;
    elseif i==13
        P13=Pi;
end
end
% Total Transfer matrixes for each node
U1=P1*F1;
U2=P2*F2*U1;
U3=P3*F3*U2;
U4=P4*F4*U3;
U5=P5*F5*U4;
U6=P6*F6*U5;
U7=P7*F7*U6;
U8=P8*F8*U7;
U9=P9*F9*U8;
U10=P10*F10*U9;
U11=P11*F11*U10;
U12=P12*F12*U11;
```

```
U13=P13*F13*U12;
% Estimation of state vector at ground level (Z0)by applying the boundary
conditions
A=[U13(3,3) U13(3,4) U13(3,7)  U13(3,8) ; U13(4,3) U13(4,4) U13(4,7)
U13(4,8) ; U13(7,3) U13(7,4) U13(7,7) U13(7,8) ; U13(8,3) U13(8,4)
U13(8,7) U13(8,8)];
B=[-U13(3,9) -U13(4,9) -U13(7,9) -U13(8,9)]';
C=inv(A)*B;
Z0=[0 0 C(1) C(2) 0 0 C(3) C(4) 1]';
% Estimation of state vectors for each nodes
Z1=U1*Z0;
Z2=U2*Z0;
Z3=U3*Z0;
Z4=U4*Z0;
Z5=U5*Z0;
Z6=U6*Z0;
Z7=U7*Z0;
Z8=U8*Z0;
Z9=U9*Z0;
Z10=U10*Z0;
Z11=U11*Z0;
Z12=U12*Z0;
Z13=U13*Z0;
j=sqrt(-1);
% Lateral displacements at each node
X=[Z0(1)+j*Z0(5) Z1(1)+j*Z1(5) Z2(1)+j*Z2(5) Z3(1)+j*Z3(5) Z4(1)+j*Z4(5)
Z5(1)+j*Z5(5) Z6(1)+j*Z6(5) Z7(1)+j*Z7(5) Z8(1)+j*Z8(5) Z9(1)+j*Z9(5)
Z10(1)+j*Z10(5) Z11(1)+j*Z11(5) Z12(1)+j*Z12(5) Z13(1)+j*Z13(5)];
% Rotations at each node
F=[Z0(2)+j*Z0(6) Z1(2)+j*Z1(6) Z2(2)+j*Z2(6) Z3(2)+j*Z3(6) Z4(2)+j*Z4(6)
Z5(2)+j*Z5(6) Z6(2)+j*Z6(6) Z7(2)+j*Z7(6) Z8(2)+j*Z8(6) Z9(2)+j*Z9(6)
Z10(2)+j*Z10(6) Z11(2)+j*Z11(6) Z12(2)+j*Z12(6) Z13(2)+j*Z13(6)];
% Bending moments at each node
M=[Z0(3)+j*Z0(7) Z1(3)+j*Z1(7) Z2(3)+j*Z2(7) Z3(3)+j*Z3(7) Z4(3)+j*Z4(7)
Z5(3)+j*Z5(7) Z6(3)+j*Z6(7) Z7(3)+j*Z7(7) Z8(3)+j*Z8(7) Z9(3)+j*Z9(7)
Z10(3)+j*Z10(7) Z11(3)+j*Z11(7) Z12(3)+j*Z12(7) Z13(3)+j*Z13(7)];
% Shear Forces at each node
V=[Z0(4)+j*Z0(8) Z1(4)+j*Z1(8) Z2(4)+j*Z2(8) Z3(4)+j*Z3(8) Z4(4)+j*Z4(8)
Z5(4)+j*Z5(8) Z6(4)+j*Z6(8) Z7(4)+j*Z7(8) Z8(4)+j*Z8(8) Z9(4)+j*Z9(8)
Z10(4)+j*Z10(8) Z11(4)+j*Z11(8) Z12(4)+j*Z12(8) Z13(4)+j*Z13(8)];
% Vertical coordiantes of each node
y=[0 2.0 6.0 10.0 14.25 18.1 21.25 24.35 28 31.55 34.45 38 42.15 46.05];
plot(abs(X),y)
grid
title('Displacement')
xlabel('X (m)')
ylabel('H (m)')
figure,plot(abs(F),y)
grid
title('Rotation ')
xlabel('F (radyan)')
ylabel('H (m)')
figure,plot(abs(M),y)
grid
title('Bending Moment ')
xlabel('M (N-m)')
ylabel('H (m)')
figure,plot(abs(V),y)
grid
title('Shear Force')
```

```
xlabel('V (N)')
ylabel('H (m)')
abs(X(13))
abs(M(1))
abs(V(1))
abs(M(5))
abs(V(5))
```

A.6. CODES FOR DYNAMIC ANALYSIS OF MODEL WITH TMD

```
clear all; close all; clc;
w=32.2;      % Exciting frequency (rad/sec)
g=0.05;      % Structural Damping for R/C structure
ug=1;       % Max harmonic ground acceleration  (m/sec2)
E=27*10^9; % Modulus of elasticity for Reinforced concrete (N/m2)
kd=125970    % Stiffnes value of TMD (N/m)
cd=7020      % Damping coeficient of TMD
md=3490     % TMD mass (kg)
m=zeros(13,1);  % Mass matrix
L=zeros(13,1);  % Length matrix
I=zeros(13,1);  % Inertia matrix
F=zeros(13,1);  % Field transfer matrix
P=zeros(13,1);  % Point transfer matrix
% Discrete mass values of the minaret (kg)
m(1,1)=36.3*10^3;
m(2,1)=41.5*10^3;
m(3,1)=41.5*10^3;
m(4,1)=35.2*10^3;
m(5,1)=11.8*10^3;
m(6,1)=11.8*10^3;
m(7,1)=11.8*10^3;
m(8,1)=20.1*10^3;
m(9,1)=11.4*10^3;
m(10,1)=11.4*10^3;
m(11,1)=18.2*10^3;
m(12,1)=11.5*10^3;
m(13,1)=7.8*10^3;
% Distances between Discrete masses (m)
L(1,1)=1.75;
L(2,1)=3.75;
L(3,1)=4.0;
L(4,1)=4.50;
L(5,1)=4.10;
L(6,1)=3.20;
L(7,1)=3.20;
L(8,1)=3.50;
L(9,1)=3.45;
L(10,1)=3.1;
L(11,1)=3.45;
L(12,1)=4.05;
L(13,1)=3.65;
 % Inertia values between Discrete masses (m4)
I(1,1)=5.364;
I(2,1)=5.364;
I(3,1)=5.364;
I(4,1)=5.364;
I(5,1)=0.74;
I(6,1)=0.74;
I(7,1)=0.74;
```

```
I(8,1)=0.74;
I(9,1)=0.74;
I(10,1)=0.74;
I(11,1)=0.74;
I(12,1)=0.575;
I(13,1)=0.575;
% Elements of Field Transfer Matrix
for i=1.13;
Fi=[1 L(i) ((L(i))^2)/(2*E*I(i)*(1+g^2)) ((L(i))^3)/(6*E*I(i)*(1+g^2)) 0
0 g*((L(i))^2)/(2*E*I(i)*(1+g^2)) g*((L(i))^3)/(6*E*I(i)*(1+g^2)) 0 ; 0 1
L(i)/(E*I(i)*(1+g^2)) ((L(i))^2)/(2*E*I(i)*(1+g^2)) 0 0
g*L(i)/(E*I(i)*(1+g^2)) g*((L(i))^2)/(2*E*I(i)*(1+g^2)) 0 ; 0 0 1 L(i) 0
0 0 0 0 ; 0 0 0 1 0 0 0 0 0 0 ; 0 0 -g*((L(i))^2)/(2*E*I(i)*(1+g^2)) -
g*((L(i))^3)/(6*E*I(i)*(1+g^2)) 1 L(i) ((L(i))^2)/(2*E*I(i)*(1+g^2))
((L(i))^3)/(6*E*I(i)*(1+g^2)) 0 ; 0 0 -g*L(i)/(E*I(i)*(1+g^2)) -
g*((L(i))^2)/(2*E*I(i)*(1+g^2)) 0 1 L(i)/(E*I(i)*(1+g^2))
((L(i))^2)/(2*E*I(i)*(1+g^2)) 0 ; 0 0 0 0 0 0 1 L(i) 0 ; 0 0 0 0 0 0 0 1
0 ; 0 0 0 0 0 0 0 0 1 ];
    if i==1
        F1=Fi;
    elseif i==2
        F2=Fi;
    elseif i==3
        F3=Fi;
    elseif i==4
        F4=Fi;
    elseif i==5
        F5=Fi;
    elseif i==6
        F6=Fi;
    elseif i==7
        F7=Fi;
    elseif i==8
        F8=Fi;
    elseif i==9
        F9=Fi;
    elseif i==10
        F10=Fi;
    elseif i==11
        F11=Fi;
    elseif i==12
        F12=Fi;
    elseif i==13
        F13=Fi;
end
end
% Elements of Point Transfer Matrix
for i=1.13;
     Pi=[1 0 0 0 0 0 0 0 0 ; 0 1 0 0 0 0 0 0 0 ; 0 0 1 0 0 0 0 0 0 ;
m(i)*w^2 0 0 1 0 0 0 0 -m(i)*ug ; 0 0 0 0 1 0 0 0 0 ; 0 0 0 0 0 1 0 0 0 ;
0 0 0 0 0 0 1 0 0 ; 0 0 0 0 m(i)*w^2 0 0 1 0 ; 0 0 0 0 0 0 0 0 1 ];
    if i==1
        P1=Pi;
    elseif i==2
        P2=Pi;
    elseif i==3
        P3=Pi;
    elseif i==4
        P4=Pi;
    elseif i==5
```

```
        P5=Pi;
    elseif i==6
        P6=Pi;
    elseif i==7
        P7=Pi;
    elseif i==8
        P8=Pi;
    elseif i==9
        P9=Pi;
    elseif i==10
        P10=Pi;
    elseif i==11
        P11=Pi;
    elseif i==12
        P12=Pi;
    elseif i==13
        P13=Pi;
end
end
 % Equivalent stiffnes of TMD
A=(((kd^2)*md*(w^2))-(kd*(md^2)*(w^4))+((cd^2)*md*(w^4)))/(((kd-
(md*(w^2)))^2)+((cd^2)*(w^2)))
B=-((cd*md^2)*w^5)/(((kd-(md*(w^2)))^2)+((cd^2)*(w^2)))
C=-md*ug*(((-kd*md*(w^2))+(kd^2)+((cd^2)*(w^2)))/(((kd-
(md*(w^2)))^2)+((cd^2)*(w^2))))
D=md*ug*((md*cd*(w^3))/(((kd-(md*(w^2)))^2)+((cd^2)*(w^2))))
 % Changes in P12 due to TMD impact
P12=[1 0 0 0 0 0 0 0 0 0 ; 0 1 0 0 0 0 0 0 0 0 ; 0 0 1 0 0 0 0 0 0 0 ;
((m(12)*w^2)+A) 0 0 1 -B 0 0 0 -m(12)*ug+C ; 0 0 0 0 1 0 0 0 0 0 ; 0 0 0 0
0 1 0 0 0 0 ; 0 0 0 0 0 0 0 1 0 0 ; B 0 0 0 ((m(12)*w^2)+A) 0 0 1 D ; 0 0 0 0
0 0 0 0 0 1]
 % Total Transfer matrixes for each node
U1=P1*F1;
U2=P2*F2*U1;
U3=P3*F3*U2;
U4=P4*F4*U3;
U5=P5*F5*U4;
U6=P6*F6*U5;
U7=P7*F7*U6;
U8=P8*F8*U7;
U9=P9*F9*U8;
U10=P10*F10*U9;
U11=P11*F11*U10;
U12=P12*F12*U11;
U13=P13*F13*U12;
 % Estimation of state vector at ground level (Z0)by applying the
boundary conditions
A=[U13(3,3) U13(3,4) U13(3,7)  U13(3,8) ; U13(4,3) U13(4,4) U13(4,7)
U13(4,8) ; U13(7,3) U13(7,4) U13(7,7) U13(7,8) ; U13(8,3) U13(8,4)
U13(8,7) U13(8,8)];
B=[-U13(3,9) -U13(4,9) -U13(7,9) -U13(8,9)]';
C=inv(A)*B;
 Z0=[0 0 C(1) C(2) 0 0 C(3) C(4) 1]';
 % Estimation of state vectors for each nodes
Z1=U1*Z0;
Z2=U2*Z0;
Z3=U3*Z0;
Z4=U4*Z0;
Z5=U5*Z0;
Z6=U6*Z0;
```

```
Z7=U7*Z0;
Z8=U8*Z0;
Z9=U9*Z0;
Z10=U10*Z0;
Z11=U11*Z0;
Z12=U12*Z0;
Z13=U13*Z0;
j=sqrt(-1);
% Lateral displacements at each node
X=[Z0(1)+j*Z0(5) Z1(1)+j*Z1(5) Z2(1)+j*Z2(5) Z3(1)+j*Z3(5) Z4(1)+j*Z4(5)
Z5(1)+j*Z5(5) Z6(1)+j*Z6(5) Z7(1)+j*Z7(5) Z8(1)+j*Z8(5) Z9(1)+j*Z9(5)
Z10(1)+j*Z10(5) Z11(1)+j*Z11(5) Z12(1)+j*Z12(5) Z13(1)+j*Z13(5)];
% Rotations at each node
F=[Z0(2)+j*Z0(6) Z1(2)+j*Z1(6) Z2(2)+j*Z2(6) Z3(2)+j*Z3(6) Z4(2)+j*Z4(6)
Z5(2)+j*Z5(6) Z6(2)+j*Z6(6) Z7(2)+j*Z7(6) Z8(2)+j*Z8(6) Z9(2)+j*Z9(6)
Z10(2)+j*Z10(6) Z11(2)+j*Z11(6) Z12(2)+j*Z12(6) Z13(2)+j*Z13(6)];
 % Bending moments at each node
M=[Z0(3)+j*Z0(7) Z1(3)+j*Z1(7) Z2(3)+j*Z2(7) Z3(3)+j*Z3(7) Z4(3)+j*Z4(7)
Z5(3)+j*Z5(7) Z6(3)+j*Z6(7) Z7(3)+j*Z7(7) Z8(3)+j*Z8(7) Z9(3)+j*Z9(7)
Z10(3)+j*Z10(7) Z11(3)+j*Z11(7) Z12(3)+j*Z12(7) Z13(3)+j*Z13(7)];
 % Shear Forces at each node
V=[Z0(4)+j*Z0(8) Z1(4)+j*Z1(8) Z2(4)+j*Z2(8) Z3(4)+j*Z3(8) Z4(4)+j*Z4(8)
Z5(4)+j*Z5(8) Z6(4)+j*Z6(8) Z7(4)+j*Z7(8) Z8(4)+j*Z8(8) Z9(4)+j*Z9(8)
Z10(4)+j*Z10(8) Z11(4)+j*Z11(8) Z12(4)+j*Z12(8) Z13(4)+j*Z13(8)];
 % Vertical coordiantes of each node
y=[0 2.0 6.0 10.0 14.25 18.1 21.25 24.35 28 31.55 34.45 38 42.15 46.05];
 plot(abs(X),y)
grid
title('Displacement')
xlabel('X (m)')
ylabel('H (m)')
 figure,plot(abs(F),y)
grid
title('Rotation ')
xlabel('Fi (radyan)')
ylabel('H (m)')
 figure,plot(abs(M),y)
grid
title('Bending Moment ')
xlabel('M (N-m)')
ylabel('H (m)')
 figure,plot(abs(V),y)
grid
title('Shear Force')
xlabel('V (N)')
ylabel('H (m)')
abs(X(13))
abs(M(1))
abs(V(1))
abs(M(6))
abs(V(6))
```

A.7. CODES FOR ORTHOGONAL SPRINGS STIFFNESS VERIFICATION

```
clc;
clear all;
r=860;
k=50;
```

```
n=360
for ii=1.5
    h=ii*0.1*r;
for i=1.n+1
    A=(pi/180)*(i-1);
if i<=90
r1(i)=sqrt(((h*sin(A))^2+(r-h*cos(A))^2));
r2(i)=sqrt(((h*cos(A))^2+(r-h*sin(A))^2));
r3(i)=sqrt(((h*sin(A))^2+(r+h*cos(A))^2));
r4(i)=sqrt(((h*cos(A))^2+(r+h*sin(A))^2));
T1(i)=acos((r-h*(cos(A)))/r1(i));
T2(i)=acos((r-h*(sin(A)))/r2(i));
T3(i)=acos((r+h*(cos(A)))/r3(i));
T4(i)=acos((r+h*(sin(A)))/r4(i));
F1X(i)=-k*(r-r1(i))*cos(T1(i));
F2X(i)=k*(r-r2(i))*sin(T2(i));
F3X(i)=-k*(r3(i)-r)*cos(T3(i));
F4X(i)=-k*(r4(i)-r)*sin(T4(i));
F1Y(i)=k*(r-r1(i))*sin(T1(i));
F2Y(i)=-k*(r-r2(i))*cos(T2(i));
F3Y(i)=-k*(r3(i)-r)*sin(T3(i));
F4Y(i)=-k*(r4(i)-r)*cos(T4(i));
FX(i)=F1X(i)+F2X(i)+F3X(i)+F4X(i);
FY(i)=F1Y(i)+F2Y(i)+F3Y(i)+F4Y(i);
F(i)=sqrt((FX(i)^2+FY(i)^2));
Y(i)=F(i)/h;
elseif i<=180
r1(i)=sqrt(((h*sin(A))^2+(r-h*cos(A))^2));
r2(i)=sqrt(((h*cos(A))^2+(r-h*sin(A))^2));
r3(i)=sqrt(((h*sin(A))^2+(r+h*cos(A))^2));
r4(i)=sqrt(((h*cos(A))^2+(r+h*sin(A))^2));
T1(i)=acos((r-h*(cos(A)))/r1(i));
T2(i)=acos((r-h*(sin(A)))/r2(i));
T3(i)=acos((r+h*(cos(A)))/r3(i));
T4(i)=acos((r+h*(sin(A)))/r4(i));
F1X(i)=k*(r1(i)-r)*cos(T1(i));
F2X(i)=-k*(r-r2(i))*sin(T2(i));
F3X(i)=k*(r-r3(i))*cos(T3(i));
F4X(i)=k*(r4(i)-r)*sin(T4(i));
F1Y(i)=-k*(r1(i)-r)*sin(T1(i));
F2Y(i)=-k*(r-r2(i))*cos(T2(i));
F3Y(i)=k*(r-r3(i))*sin(T3(i));
F4Y(i)=-k*(r4(i)-r)*cos(T4(i));
FX(i)=F1X(i)+F2X(i)+F3X(i)+F4X(i);
FY(i)=F1Y(i)+F2Y(i)+F3Y(i)+F4Y(i);
F(i)=sqrt((FX(i)^2+FY(i)^2));
Y(i)=F(i)/h;
elseif i<=270
r1(i)=sqrt(((h*sin(A))^2+(r-h*cos(A))^2));
r2(i)=sqrt(((h*cos(A))^2+(r-h*sin(A))^2));
r3(i)=sqrt(((h*sin(A))^2+(r+h*cos(A))^2));
r4(i)=sqrt(((h*cos(A))^2+(r+h*sin(A))^2));
T1(i)=acos((r-h*(cos(A)))/r1(i));
T2(i)=acos((r-h*(sin(A)))/r2(i));
T3(i)=acos((r+h*(cos(A)))/r3(i));
T4(i)=acos((r+h*(sin(A)))/r4(i));
F1X(i)=k*(r1(i)-r)*cos(T1(i));
F2X(i)=k*(r2(i)-r)*sin(T2(i));
F3X(i)=k*(r-r3(i))*cos(T3(i));
F4X(i)=-k*(r-r4(i))*sin(T4(i));
```

```
F1Y(i)=k*(r1(i)-r)*sin(T1(i));
F2Y(i)=k*(r2(i)-r)*cos(T2(i));
F3Y(i)=-k*(r-r3(i))*sin(T3(i));
F4Y(i)=k*(r-r4(i))*cos(T4(i));
FX(i)=F1X(i)+F2X(i)+F3X(i)+F4X(i);
FY(i)=F1Y(i)+F2Y(i)+F3Y(i)+F4Y(i);
F(i)=sqrt((FX(i)^2+FY(i)^2));
Y(i)=F(i)/h;
else
r1(i)=sqrt(((h*sin(A))^2+(r-h*cos(A))^2));
r2(i)=sqrt(((h*cos(A))^2+(r-h*sin(A))^2));
r3(i)=sqrt(((h*sin(A))^2+(r+h*cos(A))^2));
r4(i)=sqrt(((h*cos(A))^2+(r+h*sin(A))^2));
T1(i)=acos((r-h*(cos(A)))/r1(i));
T2(i)=acos((r-h*(sin(A)))/r2(i));
T3(i)=acos((r+h*(cos(A)))/r3(i));
T4(i)=acos((r+h*(sin(A)))/r4(i));
F1X(i)=-k*(r-r1(i))*cos(T1(i));
F2X(i)=-k*(r2(i)-r)*sin(T2(i));
F3X(i)=-k*(r3(i)-r)*cos(T3(i));
F4X(i)=k*(r-r4(i))*sin(T4(i));
F1Y(i)=-k*(r-r1(i))*sin(T1(i));
F2Y(i)=k*(r2(i)-r)*cos(T2(i));
F3Y(i)=k*(r3(i)-r)*sin(T3(i));
F4Y(i)=k*(r-r4(i))*cos(T4(i));
FX(i)=F1X(i)+F2X(i)+F3X(i)+F4X(i);
FY(i)=F1Y(i)+F2Y(i)+F3Y(i)+F4Y(i);
F(i)=sqrt((FX(i)^2+FY(i)^2));
Y(i)=F(i)/h;
end
end
x=0:1.n
plot(x,Y)
grid
xlabel('ALFA - Degree')
ylabel('F/h - Stiffness')
figure
end
```

A.8. CODES FOR FOURIER TRANSFORMATION OF EARTHQUAKE GROUND ACCELERATION RECORDS

```
clc
clear
close all
% %[filename, pathname]=uigetfile('*.asc', 'Choose acc file for source 1
to process');
% file=input('data file name without extension=','s');
% ext='asc';
% filename=[file,'.',ext];
%Analysis Output File to be Processed
[filename1,pathname]=uigetfile('*.txt','Analysis Output File(.txt)');
filename=load([pathname filename1]);
acc=filename;
acc=detrend(acc);
delt=0.005;
n=length(acc);
```

```
t=delt:delt:delt*n;
figure(1);
plot(t,acc)
grid
xlabel('Time (s)')
ylabel('Acceleration (mg)')
fs=1/delt;
fn=fs/2;
famp1=fft(acc)*delt;
fa1=abs(famp1);
n1=length(famp1);
delf1=1/((n1-1)*delt);
f1=(0:delf1.delf1*(n1/2))';
figure(2);
grid on ;
plot(f1,fa1(1.n1/2+1));
grid
title(['Fourier Amplitude Spectrum']),xlabel('Frequency
[Hz]'),ylabel('Amplitude')
```

A.9. CODES FOR WIND RESPONSE OF STRUCTURE WITHOUT TMD

```
clear all; close all; clc;
w=6.6;       % Exciting frequency (rad/sec)
g=0.05;       % Structural Damping for R/C structure
q=137.1;        % Lift force due to vortex shedding  (N/m)
E=27*10^9; % Modulus of elasticity for Reinforced concrete (N/m2)
 m=zeros(13,1);  % Mass matrix
L=zeros(13,1);  % Length matrix
I=zeros(13,1);  % Inertia matrix
F=zeros(13,1);  % Field transfer matrix
P=zeros(13,1);  % Point transfer matrix
 % Discrete mass values of the minaret (kg)
m(1,1)=36.3*10^3;
m(2,1)=41.5*10^3;
m(3,1)=41.5*10^3;
m(4,1)=35.2*10^3;
m(5,1)=11.8*10^3;
m(6,1)=11.8*10^3;
m(7,1)=11.8*10^3;
m(8,1)=20.1*10^3;
m(9,1)=11.4*10^3;
m(10,1)=11.4*10^3;
m(11,1)=18.2*10^3;
m(12,1)=11.5*10^3;
m(13,1)=7.8*10^3;
% Distances between Discrete masses (m)
L(1,1)=1.75;
L(2,1)=3.75;
L(3,1)=4.0;
L(4,1)=4.50;
L(5,1)=4.10;
L(6,1)=3.20;
L(7,1)=3.20;
L(8,1)=3.50;
L(9,1)=3.45;
L(10,1)=3.1;
L(11,1)=3.45;
```

```
L(12,1)=4.05;
L(13,1)=3.65;
 % Inertia values between Discrete masses (m4)
I(1,1)=5.364;
I(2,1)=5.364;
I(3,1)=5.364;
I(4,1)=5.364;
I(5,1)=0.74;
I(6,1)=0.74;
I(7,1)=0.74;
I(8,1)=0.74;
I(9,1)=0.74;
I(10,1)=0.74;
I(11,1)=0.74;
I(12,1)=0.575;
I(13,1)=0.575;
 % Elements of Field Transfer Matrix
for i=1.13;
Fi=[1 L(i) ((L(i))^2)/(2*E*I(i)*(1+g^2)) ((L(i))^3)/(6*E*I(i)*(1+g^2)) 0
0 g*((L(i))^2)/(2*E*I(i)*(1+g^2)) g*((L(i))^3)/(6*E*I(i)*(1+g^2)) -
(q*(L(i))^4)/(24*E*I(i)*(1+g^2)) ; 0 1 L(i)/(E*I(i)*(1+g^2))
((L(i))^2)/(2*E*I(i)*(1+g^2)) 0 0 g*L(i)/(E*I(i)*(1+g^2))
g*((L(i))^2)/(2*E*I(i)*(1+g^2)) -(q*(L(i))^3)/(6*E*I(i)*(1+g^2)) ; 0 0 1
L(i) 0 0 0 0 -(q*(L(i))^2)/(2) ; 0 0 0 1 0 0 0 0 -q*L(i) ; 0 0 -
g*((L(i))^2)/(2*E*I(i)*(1+g^2)) -g*((L(i))^3)/(6*E*I(i)*(1+g^2)) 1 L(i)
((L(i))^2)/(2*E*I(i)*(1+g^2)) ((L(i))^3)/(6*E*I(i)*(1+g^2)) 0 ; 0 0 -
g*L(i)/(E*I(i)*(1+g^2)) -g*((L(i))^2)/(2*E*I(i)*(1+g^2)) 0 1
L(i)/(E*I(i)*(1+g^2)) ((L(i))^2)/(2*E*I(i)*(1+g^2)) 0 ; 0 0 0 0 0 0 1
L(i) 0 ; 0 0 0 0 0 0 0 1 0 ; 0 0 0 0 0 0 0 0 1 ];
    if i==1
        F1=Fi;
    elseif i==2
        F2=Fi;
    elseif i==3
        F3=Fi;
    elseif i==4
        F4=Fi;
    elseif i==5
        F5=Fi;
    elseif i==6
        F6=Fi;
    elseif i==7
        F7=Fi;
    elseif i==8
        F8=Fi;
    elseif i==9
        F9=Fi;
    elseif i==10
        F10=Fi;
    elseif i==11
        F11=Fi;
    elseif i==12
        F12=Fi;
    elseif i==13
        F13=Fi;
end
end
 % Elements of Point Transfer Matrix
for i=1.13;
```

```
     Pi=[1 0 0 0 0 0 0 0 0 ; 0 1 0 0 0 0 0 0 0 ; 0 0 1 0 0 0 0 0 0 ;
m(i)*w^2 0 0 1 0 0 0 0 ; 0 0 0 0 1 0 0 0 0 ; 0 0 0 0 0 1 0 0 0 ; 0 0 0
0 0 0 1 0 0 ; 0 0 0 0 m(i)*w^2 0 0 1 0 ; 0 0 0 0 0 0 0 0 1 ];
    if i==1
        P1=Pi;
    elseif i==2
        P2=Pi;
    elseif i==3
        P3=Pi;
    elseif i==4
        P4=Pi;
    elseif i==5
        P5=Pi;
    elseif i==6
        P6=Pi;
    elseif i==7
        P7=Pi;
    elseif i==8
        P8=Pi;
    elseif i==9
        P9=Pi;
    elseif i==10
        P10=Pi;
    elseif i==11
        P11=Pi;
    elseif i==12
        P12=Pi;
    elseif i==13
        P13=Pi;
end
end
 % Total Transfer matrixes for each node
U1=P1*F1;
U2=P2*F2*U1;
U3=P3*F3*U2;
U4=P4*F4*U3;
U5=P5*F5*U4;
U6=P6*F6*U5;
U7=P7*F7*U6;
U8=P8*F8*U7;
U9=P9*F9*U8;
U10=P10*F10*U9;
U11=P11*F11*U10;
U12=P12*F12*U11;
U13=P13*F13*U12;
% Estimation of state vector at ground level (Z0)by applying the boundary
conditions
A=[U13(3,3) U13(3,4) U13(3,7)  U13(3,8) ; U13(4,3) U13(4,4) U13(4,7)
U13(4,8) ; U13(7,3) U13(7,4) U13(7,7) U13(7,8) ; U13(8,3) U13(8,4)
U13(8,7) U13(8,8)];
B=[-U13(3,9) -U13(4,9) -U13(7,9) -U13(8,9)]';
C=inv(A)*B;
 Z0=[0 0 C(1) C(2) 0 0 C(3) C(4) 1]';
 % Estimation of state vectors for each nodes
Z1=U1*Z0;
Z2=U2*Z0;
Z3=U3*Z0;
Z4=U4*Z0;
Z5=U5*Z0;
Z6=U6*Z0;
```

```
Z7=U7*Z0;
Z8=U8*Z0;
Z9=U9*Z0;
Z10=U10*Z0;
Z11=U11*Z0;
Z12=U12*Z0;
Z13=U13*Z0;
 j=sqrt(-1);
% Lateral displacements at each node
X=[Z0(1)+j*Z0(5) Z1(1)+j*Z1(5) Z2(1)+j*Z2(5) Z3(1)+j*Z3(5) Z4(1)+j*Z4(5)
Z5(1)+j*Z5(5) Z6(1)+j*Z6(5) Z7(1)+j*Z7(5) Z8(1)+j*Z8(5) Z9(1)+j*Z9(5)
Z10(1)+j*Z10(5) Z11(1)+j*Z11(5) Z12(1)+j*Z12(5) Z13(1)+j*Z13(5)];
% Rotations at each node
F=[Z0(2)+j*Z0(6) Z1(2)+j*Z1(6) Z2(2)+j*Z2(6) Z3(2)+j*Z3(6) Z4(2)+j*Z4(6)
Z5(2)+j*Z5(6) Z6(2)+j*Z6(6) Z7(2)+j*Z7(6) Z8(2)+j*Z8(6) Z9(2)+j*Z9(6)
Z10(2)+j*Z10(6) Z11(2)+j*Z11(6) Z12(2)+j*Z12(6) Z13(2)+j*Z13(6)];
 % Bending moments at each node
M=[Z0(3)+j*Z0(7) Z1(3)+j*Z1(7) Z2(3)+j*Z2(7) Z3(3)+j*Z3(7) Z4(3)+j*Z4(7)
Z5(3)+j*Z5(7) Z6(3)+j*Z6(7) Z7(3)+j*Z7(7) Z8(3)+j*Z8(7) Z9(3)+j*Z9(7)
Z10(3)+j*Z10(7) Z11(3)+j*Z11(7) Z12(3)+j*Z12(7) Z13(3)+j*Z13(7)];
 % Shear Forces at each node
V=[Z0(4)+j*Z0(8) Z1(4)+j*Z1(8) Z2(4)+j*Z2(8) Z3(4)+j*Z3(8) Z4(4)+j*Z4(8)
Z5(4)+j*Z5(8) Z6(4)+j*Z6(8) Z7(4)+j*Z7(8) Z8(4)+j*Z8(8) Z9(4)+j*Z9(8)
Z10(4)+j*Z10(8) Z11(4)+j*Z11(8) Z12(4)+j*Z12(8) Z13(4)+j*Z13(8)];
 % Vertical coordiantes of each node
y=[0 2.0 6.0 10.0 14.25 18.1 21.25 24.35 28 31.55 34.45 38 42.15 46.05];
 plot(abs(X),y)
grid
title('Displacement')
xlabel('X (m)')
ylabel('H (m)')
 figure,plot(abs(F),y)
grid
title('Rotation ')
xlabel('F (radyan)')
ylabel('H (m)')
 figure,plot(abs(M),y)
grid
title('Bending Moment ')
xlabel('M (N-m)')
ylabel('H (m)')
 figure,plot(abs(V),y)
grid
title('Shear Force')
xlabel('V (N)')
ylabel('H (m)')
 abs(X(13))
abs(M(1))
abs(V(1))
```

A.10. CODES FOR WIND RESPONSE OF STRUCTURE EQUIPED WITH TMD

```
clear all; close all; clc;
 w=32.2;      % Exciting frequency (rad/sec)
g=0.05;      % Structural Damping for R/C structure
ug=0;        % Max harmonic ground acceleration  (m/sec2)
q=137.1      % Lift force due to vortex shedding
E=27*10^9; % Modulus of elasticity for Reinforced concrete (N/m2)
```

```
kd=125970    % Stiffnes value of TMD (N/m)
cd=7020      % Damping coeficient of TMD
md=3490     % TMD mass (kg)
m=zeros(13,1);  % Mass matrix
L=zeros(13,1);  % Length matrix
I=zeros(13,1);  % Inertia matrix
F=zeros(13,1);  % Field transfer matrix
P=zeros(13,1);  % Point transfer matrix
% Discrete mass values of the minaret (kg)
m(1,1)=36.3*10^3;
m(2,1)=41.5*10^3;
m(3,1)=41.5*10^3;
m(4,1)=35.2*10^3;
m(5,1)=11.8*10^3;
m(6,1)=11.8*10^3;
m(7,1)=11.8*10^3;
m(8,1)=20.1*10^3;
m(9,1)=11.4*10^3;
m(10,1)=11.4*10^3;
m(11,1)=18.2*10^3;
m(12,1)=11.5*10^3;
m(13,1)=7.8*10^3;
% Distances between Discrete masses (m)
L(1,1)=1.75;
L(2,1)=3.75;
L(3,1)=4.0;
L(4,1)=4.50;
L(5,1)=4.10;
L(6,1)=3.20;
L(7,1)=3.20;
L(8,1)=3.50;
L(9,1)=3.45;
L(10,1)=3.1;
L(11,1)=3.45;
L(12,1)=4.05;
L(13,1)=3.65;
% Inertia values between Discrete masses (m4)
I(1,1)=5.364;
I(2,1)=5.364;
I(3,1)=5.364;
I(4,1)=5.364;
I(5,1)=0.74;
I(6,1)=0.74;
I(7,1)=0.74;
I(8,1)=0.74;
I(9,1)=0.74;
I(10,1)=0.74;
I(11,1)=0.74;
I(12,1)=0.575;
I(13,1)=0.575;
% Elements of Field Transfer Matrix
for i=1.13;
Fi=[1 L(i) ((L(i))^2)/(2*E*I(i)*(1+g^2)) ((L(i))^3)/(6*E*I(i)*(1+g^2)) 0
0 g*((L(i))^2)/(2*E*I(i)*(1+g^2)) g*((L(i))^3)/(6*E*I(i)*(1+g^2)) -
(q*(L(i))^4)/(24*E*I(i)*(1+g^2)) ; 0 1 L(i)/(E*I(i)*(1+g^2))
((L(i))^2)/(2*E*I(i)*(1+g^2)) 0 0 g*L(i)/(E*I(i)*(1+g^2))
g*((L(i))^2)/(2*E*I(i)*(1+g^2)) -(q*(L(i))^3)/(6*E*I(i)*(1+g^2)) ; 0 0 1
L(i) 0 0 0 0 -(q*(L(i))^2)/(2) ; 0 0 0 1 0 0 0 0 -q*L(i) ; 0 0 -
g*((L(i))^2)/(2*E*I(i)*(1+g^2)) -g*((L(i))^3)/(6*E*I(i)*(1+g^2)) 1 L(i)
((L(i))^2)/(2*E*I(i)*(1+g^2)) ((L(i))^3)/(6*E*I(i)*(1+g^2)) 0 ; 0 0 -
```

```
g*L(i)/(E*I(i)*(1+g^2)) -g*((L(i))^2)/(2*E*I(i)*(1+g^2)) 0 1
L(i)/(E*I(i)*(1+g^2)) ((L(i))^2)/(2*E*I(i)*(1+g^2)) 0 ; 0 0 0 0 0 0 1
L(i) 0 ; 0 0 0 0 0 0 0 1 0 ; 0 0 0 0 0 0 0 0 1 ];
    if i==1
        F1=Fi;
    elseif i==2
        F2=Fi;
    elseif i==3
        F3=Fi;
    elseif i==4
        F4=Fi;
    elseif i==5
        F5=Fi;
    elseif i==6
        F6=Fi;
    elseif i==7
        F7=Fi;
    elseif i==8
        F8=Fi;
    elseif i==9
        F9=Fi;
    elseif i==10
        F10=Fi;
    elseif i==11
        F11=Fi;
    elseif i==12
        F12=Fi;
    elseif i==13
        F13=Fi;
end
end
% Elements of Point Transfer Matrix
for i=1.13;
     Pi=[1 0 0 0 0 0 0 0 0 ; 0 1 0 0 0 0 0 0 0 ; 0 0 1 0 0 0 0 0 0 ;
m(i)*w^2 0 0 1 0 0 0 0 0 ; 0 0 0 0 1 0 0 0 0 ; 0 0 0 0 0 1 0 0 0 ; 0 0 0
0 0 0 1 0 0 ; 0 0 0 0 m(i)*w^2 0 0 1 0 ; 0 0 0 0 0 0 0 0 1 ];
    if i==1
        P1=Pi;
    elseif i==2
        P2=Pi;
    elseif i==3
        P3=Pi;
    elseif i==4
        P4=Pi;
    elseif i==5
        P5=Pi;
    elseif i==6
        P6=Pi;
    elseif i==7
        P7=Pi;
    elseif i==8
        P8=Pi;
    elseif i==9
        P9=Pi;
    elseif i==10
        P10=Pi;
    elseif i==11
        P11=Pi;
    elseif i==12
        P12=Pi;
```

```
    elseif i==13
        P13=Pi;
end
end
% Equivalent stiffnes of TMD
A=(((kd^2)*md*(w^2))-(kd*(md^2)*(w^4))+((cd^2)*md*(w^4)))/(((kd-
(md*(w^2)))^2)+((cd^2)*(w^2)))
B=-((cd*md^2)*w^5)/(((kd-(md*(w^2)))^2)+((cd^2)*(w^2)))
C=-md*ug*(((-kd*md*(w^2))+(kd^2)+((cd^2)*(w^2)))/(((kd-
(md*(w^2)))^2)+((cd^2)*(w^2))))
D=md*ug*((md*cd*(w^3))/(((kd-(md*(w^2)))^2)+((cd^2)*(w^2))))
% Changes in P12 due to TMD impact
P12=[1 0 0 0 0 0 0 0 0 0 ; 0 1 0 0 0 0 0 0 0 0 ; 0 0 1 0 0 0 0 0 0 0 ;
((m(12)*w^2)+A) 0 0 1 -B 0 0 0 0 ; 0 0 0 0 1 0 0 0 0 ; 0 0 0 0 0 1 0 0 0
; 0 0 0 0 0 0 1 0 0 ; B 0 0 0 ((m(12)*w^2)+A) 0 0 1 D ; 0 0 0 0 0 0 0 0 0
1]
% Total Transfer matrixes for each node
U1=P1*F1;
U2=P2*F2*U1;
U3=P3*F3*U2;
U4=P4*F4*U3;
U5=P5*F5*U4;
U6=P6*F6*U5;
U7=P7*F7*U6;
U8=P8*F8*U7;
U9=P9*F9*U8;
U10=P10*F10*U9;
U11=P11*F11*U10;
U12=P12*F12*U11;
U13=P13*F13*U12;
% Estimation of state vector at ground level (Z0)by applying the boundary
conditions
A=[U13(3,3) U13(3,4) U13(3,7)  U13(3,8) ; U13(4,3) U13(4,4) U13(4,7)
U13(4,8) ; U13(7,3) U13(7,4) U13(7,7) U13(7,8) ; U13(8,3) U13(8,4)
U13(8,7) U13(8,8)];
B=[-U13(3,9) -U13(4,9) -U13(7,9) -U13(8,9)]';
C=inv(A)*B;
Z0=[0 0 C(1) C(2) 0 0 C(3) C(4) 1]';
% Estimation of state vectors for each nodes
Z1=U1*Z0;
Z2=U2*Z0;
Z3=U3*Z0;
Z4=U4*Z0;
Z5=U5*Z0;
Z6=U6*Z0;
Z7=U7*Z0;
Z8=U8*Z0;
Z9=U9*Z0;
Z10=U10*Z0;
Z11=U11*Z0;
Z12=U12*Z0;
Z13=U13*Z0;
j=sqrt(-1);
% Lateral displacements at each node
X=[Z0(1)+j*Z0(5) Z1(1)+j*Z1(5) Z2(1)+j*Z2(5) Z3(1)+j*Z3(5) Z4(1)+j*Z4(5)
Z5(1)+j*Z5(5) Z6(1)+j*Z6(5) Z7(1)+j*Z7(5) Z8(1)+j*Z8(5) Z9(1)+j*Z9(5)
Z10(1)+j*Z10(5) Z11(1)+j*Z11(5) Z12(1)+j*Z12(5) Z13(1)+j*Z13(5)];
% Rotations at each node
```

```
F=[Z0(2)+j*Z0(6) Z1(2)+j*Z1(6) Z2(2)+j*Z2(6) Z3(2)+j*Z3(6) Z4(2)+j*Z4(6)
Z5(2)+j*Z5(6) Z6(2)+j*Z6(6) Z7(2)+j*Z7(6) Z8(2)+j*Z8(6) Z9(2)+j*Z9(6)
Z10(2)+j*Z10(6) Z11(2)+j*Z11(6) Z12(2)+j*Z12(6) Z13(2)+j*Z13(6)];
% Bending moments at each node
M=[Z0(3)+j*Z0(7) Z1(3)+j*Z1(7) Z2(3)+j*Z2(7) Z3(3)+j*Z3(7) Z4(3)+j*Z4(7)
Z5(3)+j*Z5(7) Z6(3)+j*Z6(7) Z7(3)+j*Z7(7) Z8(3)+j*Z8(7) Z9(3)+j*Z9(7)
Z10(3)+j*Z10(7) Z11(3)+j*Z11(7) Z12(3)+j*Z12(7) Z13(3)+j*Z13(7)];
% Shear Forces at each node
V=[Z0(4)+j*Z0(8) Z1(4)+j*Z1(8) Z2(4)+j*Z2(8) Z3(4)+j*Z3(8) Z4(4)+j*Z4(8)
Z5(4)+j*Z5(8) Z6(4)+j*Z6(8) Z7(4)+j*Z7(8) Z8(4)+j*Z8(8) Z9(4)+j*Z9(8)
Z10(4)+j*Z10(8) Z11(4)+j*Z11(8) Z12(4)+j*Z12(8) Z13(4)+j*Z13(8)];
 % Vertical coordiantes of each node
y=[0 2.0 6.0 10.0 14.25 18.1 21.25 24.35 28 31.55 34.45 38 42.15 46.05];
 plot(abs(X),y)
grid
title('Displacement')
xlabel('X (m)')
ylabel('H (m)')
figure,plot(abs(F),y)
grid
title('Rotation ')
xlabel('Fi (radyan)')
ylabel('H (m)')
figure,plot(abs(M),y)
grid
title('Bending Moment ')
xlabel('M (N-m)')
ylabel('H (m)')
figure,plot(abs(V),y)
grid
title('Shear Force')
xlabel('V (N)')
ylabel('H (m)')
abs(X(13))
abs(M(1))
abs(V(1))
```

A.11. CODES TO CALCULATE RELATIVE DISPLACEMENT OF TMD MASS

```
clear all; close all; clc;
X1=0.139    % Max displacement of m12 (m)
w=6.6;      % Exciting frequency (rad/sec)
kd=125970    % Stiffnes value of TMD (N/m)
cd=7020      % Damping coeficient of TMD
md=3490     % TMD mass (kg)
ug=1;       % Max harmonic ground acceleration  (m/sec2)
j=sqrt(-1);
% Equivalent stiffnes of TMD
A=(((kd^2)*md*(w^2))-(kd*(md^2)*(w^4))+((cd^2)*md*(w^4)))/(((kd-
(md*(w^2)))^2)+((cd^2)*(w^2)))
B=-((cd*md^2)*w^5)/(((kd-(md*(w^2)))^2)+((cd^2)*(w^2)))
C=-md*ug*(((-kd*md*(w^2))+(kd^2)+((cd^2)*(w^2)))/(((kd-
(md*(w^2)))^2)+((cd^2)*(w^2))))
D=md*ug*((md*cd*(w^3))/(((kd-(md*(w^2)))^2)+((cd^2)*(w^2))))
RELDISP=(((A+j*B)*X1)+(C+j*D))/(kd+j*cd*w)
abs(RELDISP)
```

APPENDIX B: SAP 2000 OUTPUTS

B.1. MODAL FREQUENCIES and PERIODS BY SAP2000

TABLE: Modal Periods And Frequencies						
OutputCase	**StepType**	**StepNum**	**Period**	**Frequency**	**CircFreq**	**Eigenvalue**
Text	Text	Unitless	Sec	Cyc/sec	rad/sec	rad2/sec2
MODAL	Mode	1	0.896278	1.1157	7.0103	49.144
MODAL	Mode	2	0.896278	1.1157	7.0103	49.144
MODAL	Mode	3	0.191423	5.224	32.824	1077.4
MODAL	Mode	4	0.191423	5.224	32.824	1077.4
MODAL	Mode	5	0.088258	11.33	71.191	5068.1
MODAL	Mode	6	0.088258	11.33	71.191	5068.1
MODAL	Mode	7	0.071449	13.996	87.939	7733.3
MODAL	Mode	8	0.051591	19.383	121.79	14832
MODAL	Mode	9	0.051591	19.383	121.79	14832
MODAL	Mode	10	0.048188	20.752	130.39	17001
MODAL	Mode	11	0.032554	30.719	193.01	37253
MODAL	Mode	12	0.032554	30.719	193.01	37253
MODAL	Mode	13	0.02915	34.306	215.55	46461
MODAL	Mode	14	0.023573	42.421	266.54	71042
MODAL	Mode	15	0.023573	42.421	266.54	71043
MODAL	Mode	16	0.021592	46.314	291	84682
MODAL	Mode	17	0.021268	47.018	295.42	87274
MODAL	Mode	18	0.01905	52.494	329.83	108790
MODAL	Mode	19	0.01905	52.494	329.83	108790
MODAL	Mode	20	0.018943	52.79	331.69	110020
MODAL	Mode	21	0.018943	52.79	331.69	110020
MODAL	Mode	22	0.018375	54.422	341.94	116930
MODAL	Mode	23	0.018206	54.927	345.12	119110
MODAL	Mode	24	0.018206	54.927	345.12	119110
MODAL	Mode	25	0.017083	58.538	367.8	135280
MODAL	Mode	26	0.017083	58.538	367.8	135280
MODAL	Mode	27	0.01693	59.065	371.12	137730
MODAL	Mode	28	0.01693	59.065	371.12	137730
MODAL	Mode	29	0.01578	63.37	398.17	158540
MODAL	Mode	30	0.01578	63.371	398.17	158540
MODAL	Mode	31	0.015678	63.785	400.77	160620
MODAL	Mode	32	0.014882	67.194	422.19	178250
MODAL	Mode	33	0.014882	67.194	422.19	178250
MODAL	Mode	34	0.014668	68.175	428.36	183490
MODAL	Mode	35	0.014668	68.175	428.36	183490
MODAL	Mode	36	0.01459	68.538	430.64	185450
MODAL	Mode	37	0.014223	70.307	441.75	195140
MODAL	Mode	38	0.013754	72.706	456.82	208690

MODAL	Mode	39	0.013595	73.554	462.15	213590
MODAL	Mode	40	0.013595	73.554	462.15	213590
MODAL	Mode	41	0.013203	75.739	475.88	226470
MODAL	Mode	42	0.0131	76.336	479.63	230050
MODAL	Mode	43	0.0131	76.336	479.63	230050
MODAL	Mode	44	0.013081	76.447	480.33	230720
MODAL	Mode	45	0.013081	76.447	480.33	230720
MODAL	Mode	46	0.012619	79.243	497.9	247900
MODAL	Mode	47	0.012474	80.168	503.71	253720
MODAL	Mode	48	0.012474	80.168	503.71	253720

B.2. BASE REACTIONS of MODEL W/O TMD AGAINST KOCAELI EARTHQUAKE

TABLE: Base Reactions				
OutputCase	**StepType**	**StepNum**	**GlobalFX**	**GlobalMY**
Text	Text	Unitless	N	N-m
th	Max		740741.5	11342387.23
th	Min		-622980.49	-10399754.8

B.3. BASE REACTIONS of MODEL W/O TMD AGAINST DÜZCE EARTHQUAKE

TABLE: Base Reactions				
OutputCase	**StepType**	**StepNum**	**GlobalFX**	**GlobalMY**
Text	Text	Unitless	N	N-m
th	Max		1466521.7	39651502.81
th	Min		-1189908.6	-34312870

B.4. MODAL FREQUENCIES and PERIODS of MODEL with TMD

TABLE: Modal Periods And Frequencies						
OutputCase	**StepType**	**StepNum**	**Period**	**Frequency**	**CircFreq**	**Eigenvalue**
Text	Text	Unitless	Sec	Cyc/sec	rad/sec	rad2/sec2
MODAL	Mode	1	1.058043	0.94514	5.9385	35.266
MODAL	Mode	2	1.058043	0.94514	5.9385	35.266
MODAL	Mode	3	0.809455	1.2354	7.7622	60.252
MODAL	Mode	4	0.809455	1.2354	7.7622	60.252
MODAL	Mode	5	0.191312	5.2271	32.843	1078.6

MODAL	Mode	6	0.191312	5.2271	32.843	1078.6
MODAL	Mode	7	0.088256	11.331	71.193	5068.4
MODAL	Mode	8	0.088256	11.331	71.193	5068.4
MODAL	Mode	9	0.071449	13.996	87.939	7733.3
MODAL	Mode	10	0.051591	19.383	121.79	14832
MODAL	Mode	11	0.051591	19.383	121.79	14832
MODAL	Mode	12	0.048185	20.753	130.4	17003
MODAL	Mode	13	0.032553	30.719	193.01	37253
MODAL	Mode	14	0.032553	30.719	193.01	37253
MODAL	Mode	15	0.02915	34.306	215.55	46461
MODAL	Mode	16	0.023573	42.421	266.54	71044
MODAL	Mode	17	0.023573	42.421	266.54	71044
MODAL	Mode	18	0.021592	46.314	291	84682
MODAL	Mode	19	0.021268	47.018	295.42	87274
MODAL	Mode	20	0.01905	52.494	329.83	108790
MODAL	Mode	21	0.01905	52.495	329.83	108790
MODAL	Mode	22	0.018943	52.79	331.69	110020
MODAL	Mode	23	0.018943	52.79	331.69	110020
MODAL	Mode	24	0.018375	54.422	341.95	116930
MODAL	Mode	25	0.018206	54.927	345.12	119110
MODAL	Mode	26	0.018206	54.927	345.12	119110
MODAL	Mode	27	0.017083	58.538	367.8	135280
MODAL	Mode	28	0.017083	58.538	367.8	135280
MODAL	Mode	29	0.01693	59.065	371.12	137730
MODAL	Mode	30	0.01693	59.065	371.12	137730
MODAL	Mode	31	0.01578	63.371	398.17	158540
MODAL	Mode	32	0.01578	63.371	398.17	158540
MODAL	Mode	33	0.015678	63.785	400.77	160620
MODAL	Mode	34	0.014882	67.194	422.19	178250
MODAL	Mode	35	0.014881	67.2	422.23	178280
MODAL	Mode	36	0.014668	68.175	428.36	183490
MODAL	Mode	37	0.014668	68.175	428.36	183490
MODAL	Mode	38	0.01459	68.538	430.64	185450
MODAL	Mode	39	0.014223	70.307	441.75	195140
MODAL	Mode	40	0.013754	72.706	456.82	208690
MODAL	Mode	41	0.013595	73.554	462.15	213590
MODAL	Mode	42	0.013595	73.554	462.15	213590
MODAL	Mode	43	0.013203	75.739	475.88	226470
MODAL	Mode	44	0.0131	76.336	479.63	230050
MODAL	Mode	45	0.0131	76.336	479.63	230050
MODAL	Mode	46	0.013081	76.447	480.33	230720
MODAL	Mode	47	0.013081	76.447	480.33	230720
MODAL	Mode	48	0.012619	79.243	497.9	247900

B.5. BASE REACTIONS of MODEL with TMD AGAINST KOCAELI EARTHQUAKE

TABLE: Base Reactions				
OutputCase	StepType	StepNum	GlobalFX	GlobalMY
Text	Text	Unitless	N	N-m
th	Max		749916.34	10221734.75
th	Min		-647884.84	-11281046.7

B.6. BASE REACTIONS of MODEL with TMD AGAINST DÜZCE EARTHQUAKE

TABLE: Base Reactions				
OutputCase	StepType	StepNum	GlobalFX	GlobalMY
Text	Text	Unitless	N	N-m
th	Max		1387963.91	32529245.91
th	Min		-1107237.87	-18684016

B.7. BASE REACTIONS of MODEL W/O TMD AGAINST HARMONIC EXCITATION at 7.0 rad/sec

TABLE: Base Reactions						
OutputCase	StepType	GlobalFX	GlobalFY	GlobalFZ	GlobalMX	GlobalMY
Text	Text	N	N	N	N-m	N-m
th	Max	995190.39	0.0001158	0.000003836	0.003974	31077432.1
th	Min	-995663.72	-0.0001148	-0.00000397	-0.004018	-31060311.8

B.8. BASE REACTIONS of MODEL W/O TMD AGAINST HARMONIC EXCITATION at 32.8 rad/sec

TABLE: Base Reactions						
OutputCase	StepType	GlobalFX	GlobalFY	GlobalFZ	GlobalMX	GlobalMY
Text	Text	N	N	N	N-m	N-m
th	Max	633250.17	0.000003185	3.449E-07	0.00007942	8269992.2
th	Min	-638614.68	-0.000003625	-3.841E-07	-0.00006936	-8520255.27

B.9. BASE REACTIONS of MODEL with TMD AGAINST HARMONIC EXCITATION at 7.0 rad/sec

TABLE: Base Reactions						
OutputCase	StepType	GlobalFX	GlobalFY	GlobalFZ	GlobalMX	GlobalMY
Text	Text	N	N	N	N-m	N-m
th	Max	491810.41	0.00002401	0.35	0.0008233	14459273.51
th	Min	-492173.35	-0.0000235	-0.35	-0.0008285	-14568905.9

B.10. BASE REACTIONS of MODEL with TMD AGAINST HARMONIC EXCITATION at 32.8 rad/sec

TABLE: Base Reactions						
OutputCase	StepType	GlobalFX	GlobalFY	GlobalFZ	GlobalMX	GlobalMY
Text	Text	N	N	N	N-m	N-m
th	Max	620340.66	0.00000274	2.33	0.00005586	7971719.48
th	Min	-623140.07	-0.00000296	-2.33	-0.00005465	-8129726.57

APPENDIX C: STIFFNESS VERIFICATION FOR ORTHOGONAL SPRINGS

4 linear springs connected to each other with π/2 angle, as shown in Figure C.1 are considered as orthogonal springs. In case of a small displacement of center point from O to O' as shown in Figure C.2, stiffness of the configuration will be 2k. Proof of this statement is shown hereafter.

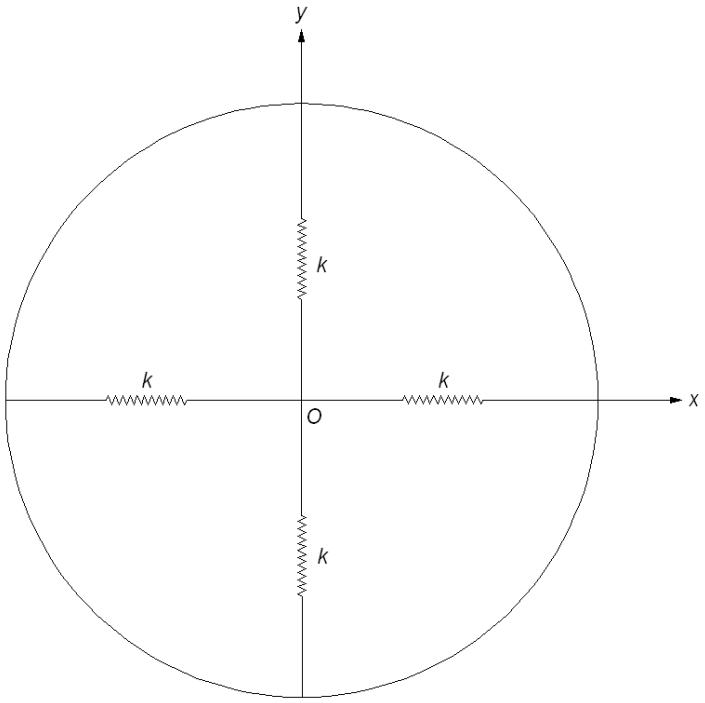

Figure C.1 Orthogonal spring configuration

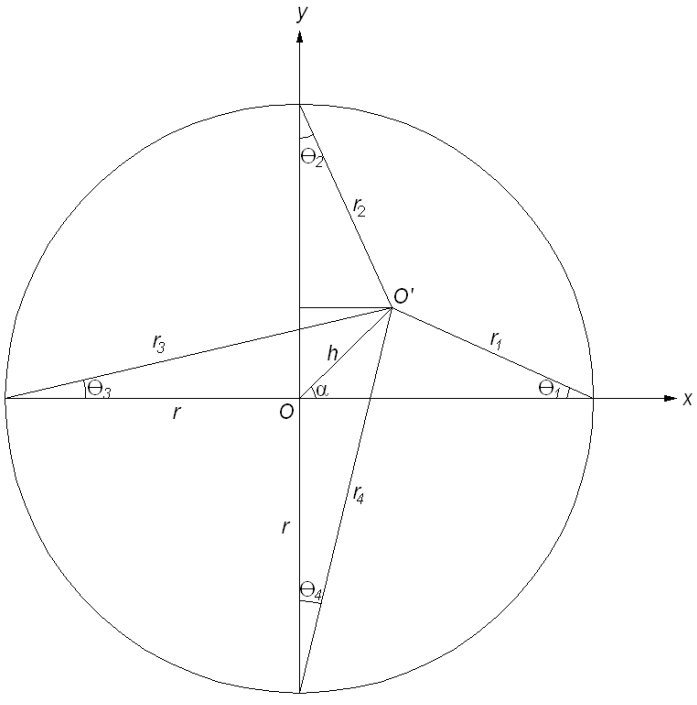

Figure C.2 Displaced orthogonal spring configuration

$$r_1 = \frac{r - h\cos\alpha}{\cos\theta_1}$$

$$r_2 = \frac{r - h\sin\alpha}{\cos\theta_2}$$

$$r_3 = \frac{r + h\cos\alpha}{\cos\theta_3}$$

$$r_4 = \frac{r + h\sin\alpha}{\cos\theta_4}$$

$$r_1 = ((h\ sin\ \alpha)^2 + (r - h\ cos\ \alpha\ )^2\ )^{1/2}$$

$$r_2 = ((h\cos\ \alpha)^2 + (r - h\ sin\ \alpha\ )^2\ )^{1/2}$$

$$r_3 = ((h\,sin\ \alpha)^2 + (r + h\ cos\ \alpha\ )^2\ )^{1/2}$$

$$r_4 = ((h\cos\ \alpha)^2 + (r + h\ sin\ \alpha\ )^2\ )^{1/2}$$

$$\cos\theta_1 = \frac{r - h\cos\alpha}{r_1}$$

$$\cos\theta_2 = \frac{r - h\sin\alpha}{r_2}$$

$$\cos\theta_3 = \frac{r + h\cos\alpha}{r_3}$$

$$\cos\theta_4 = \frac{r + h\sin\alpha}{r_4}$$

$$F_{1x} = -k(r-r_1)\cos\theta_1$$

$$F_{2x} = k(r-r_2)\sin\theta_2$$

$$F_{3x} = -k(r_3-r)\cos\theta_3$$

$$F_{4x} = -k(r_4-r)\sin\theta_4$$

$$F_{1y} = k(r-r_1)\sin\theta_1$$

$$F_{2y} = -k(r-r_2)\cos\theta_2$$

$$F_{3y} = -k(r_3-r)\sin\theta_3$$

$$F_{4y} = -k(r_4-r)\cos\theta_4$$

$$F_x = \sum_{i=1}^{4} F_{ix}$$

$$F_y = \sum_{i=1}^{4} F_{iy}$$

$$F_x = -k(r-r_1)\cos\theta_1 + k(r-r_2)\sin\theta_2 - k(r_3-r)\cos\theta_3 - k(r_4-r)\sin\theta_4$$

$$F_y = k(r-r_1)\sin\theta_1 + k(r_2-r)\cos\theta_2 + k(r-r_3)\sin\theta_3 + k(r-r_4)\cos\theta_4$$

For small θ*;*

$$\sin\theta \cong 0$$
$$\cos\theta \cong 1$$

$$F_x = -k(r-r_1) - k(r_3-r)$$

$$F_x = k\left(r_1-r_3\right) = 2h\cos\alpha k$$

$$F_y = k(r_2-r) + k(r-r_4)$$

$$F_y = k(r_2-r_4) = -2h\sin\alpha k$$

$$F = [F_x^2 + F_y^2]^{1/2}$$

$$F = [(k^2 4h^2 cos^2 \alpha) + (k^2 4h^2 sin^2 \alpha)]^{1/2}$$

$$F = [k^2 4h^2 (cos^2 \alpha + sin^2 \alpha)]^{1/2}$$

$$cos^2 \alpha + sin^2 \alpha = 1$$

$$F = [k^2 4h^2]^{1/2}$$

$$F = 2kh$$

$$\frac{F}{h} = 2k$$

As shown, stiffness of such a set up will be 2k for any small radial displacements. However we should check the stiffness variation in case of larger displacements. A matlab code was prepared to plot the stiffness variation with respect to the angular position of mass (α) for different h/r values. Stiffness variation curves are submitted in Figure C.3 to C.7. Related Matlab code is listed in Appendix A.7.

Table C.1 Stiffness variation against α for different h/r values.

h/r	**0.1**	**0.2**	**0.3**	**0.4**	**0.5**
Minimum stiffness	99.25	97.05	93.51	88.90	83.64
Maximum stiffness	100.50	101.94	104.22	107.15	110.56
Max.Variation %	0.75	2.95	6.49	11.10	16.36

Maximum variation in stiffness value is 11.10 % in all ratios up to 0.4. This variation might be acceptable. However, effect on the system response should be also checked.

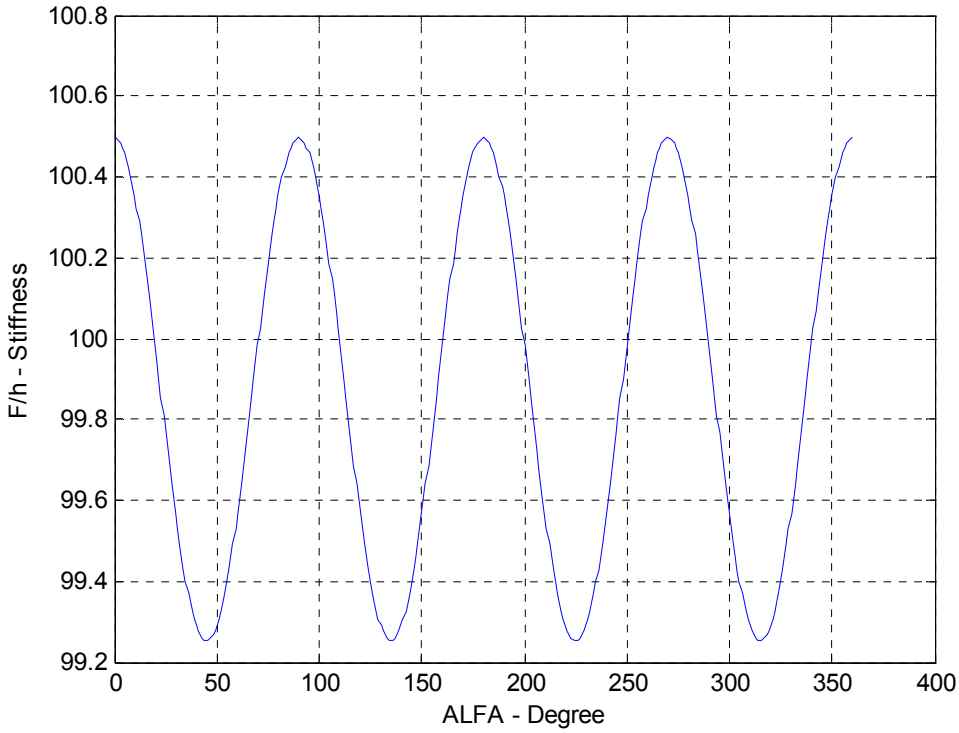

Figure C.3 Stiffness variation curve for h/r: 0.1

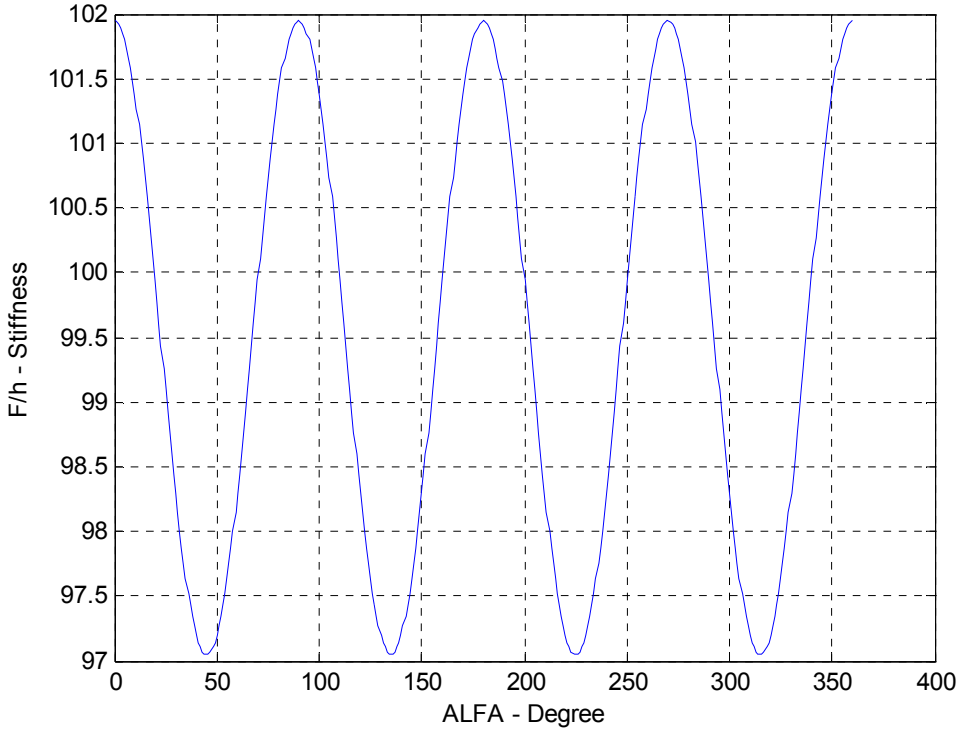

Figure C.4 Stiffness variation curve for h/r: 0.2

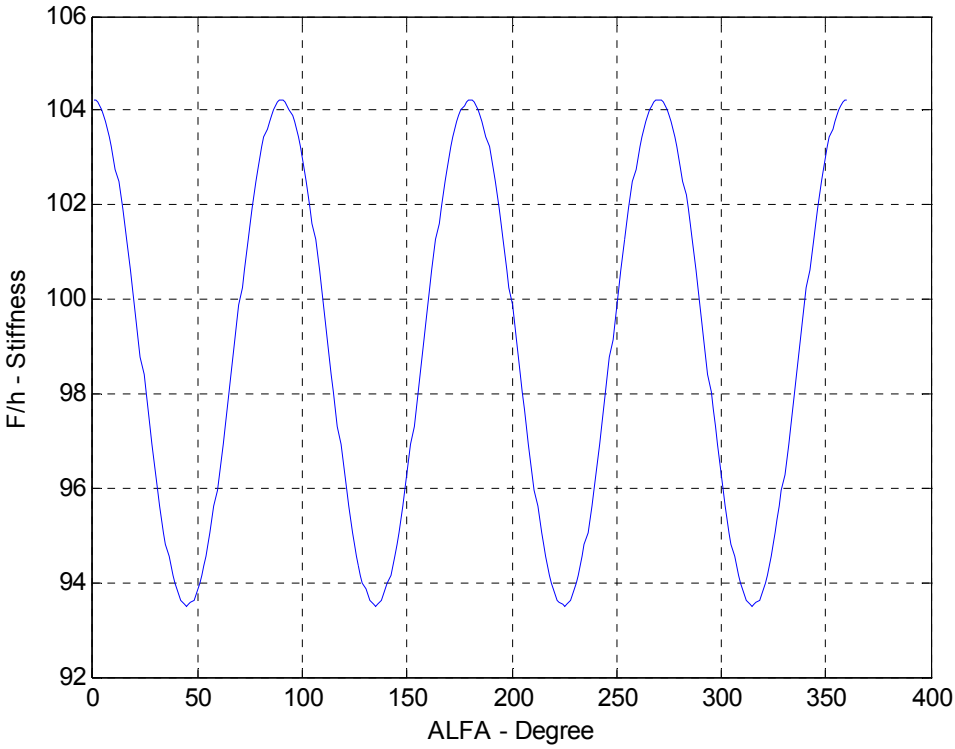

Figure C.5 Stiffness variation curve for h/r: 0.3

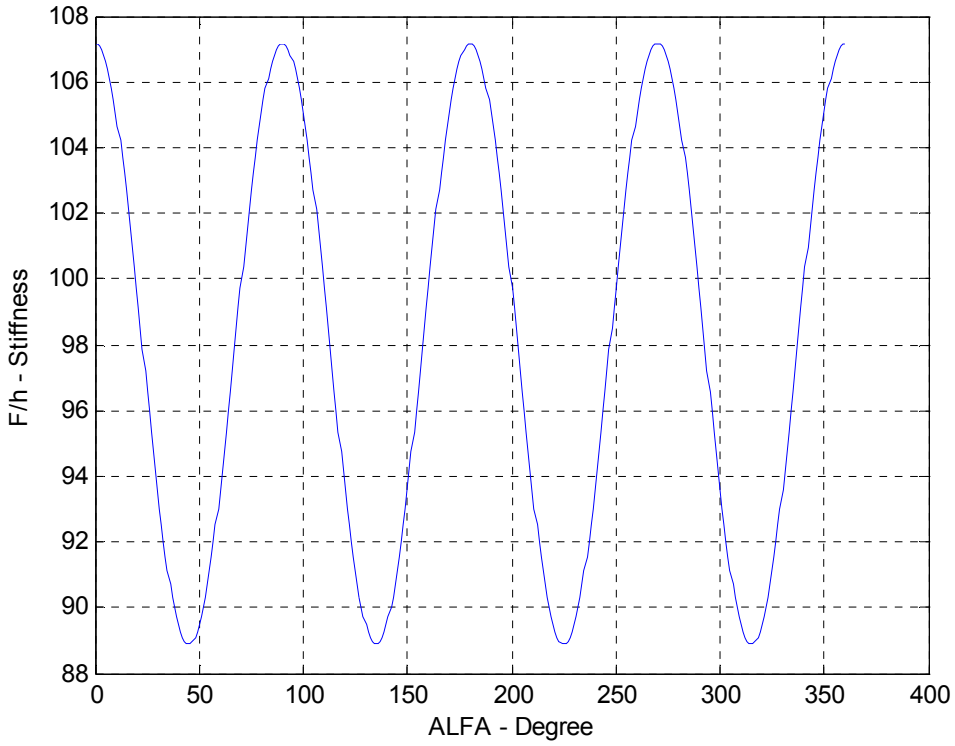

Figure C.6 Stiffness variation curve for h/r: 0.4

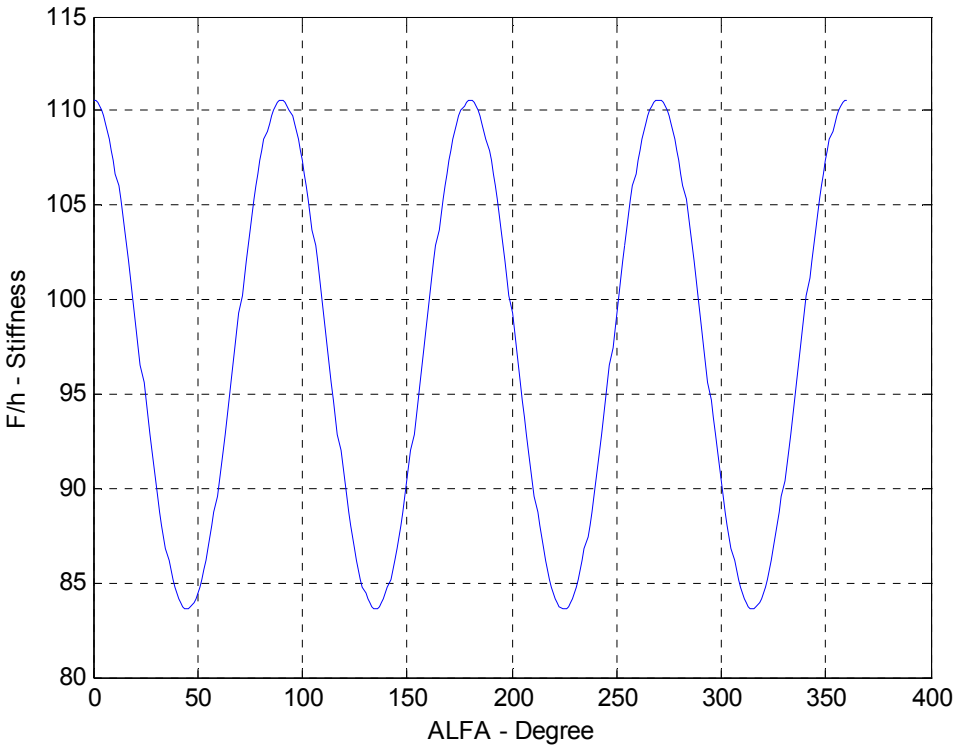

Figure C.7 Stiffness variation curve for h/r: 0.5

APPENDIX D: TECHNICAL DRAWINGS

Revito	Revision note	Date	Signature	Checked

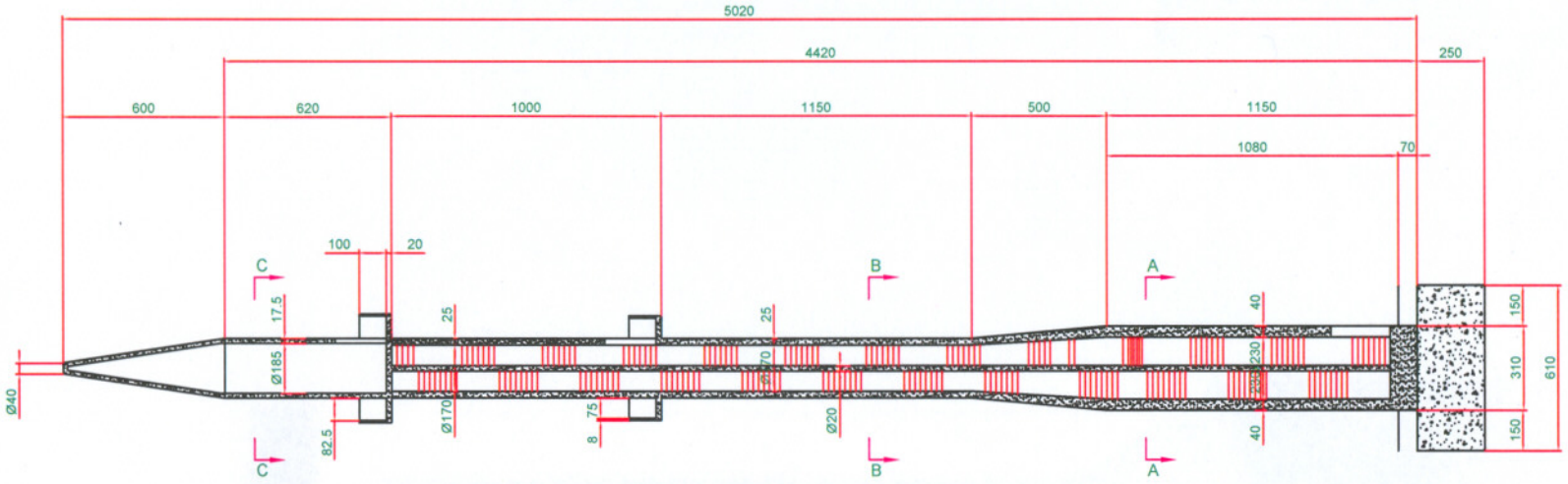

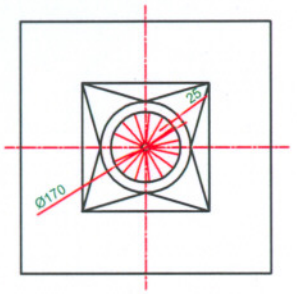

B-B

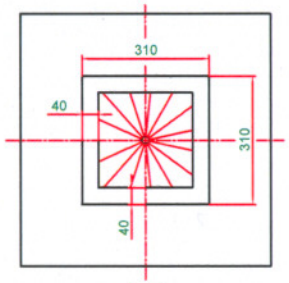

A-A

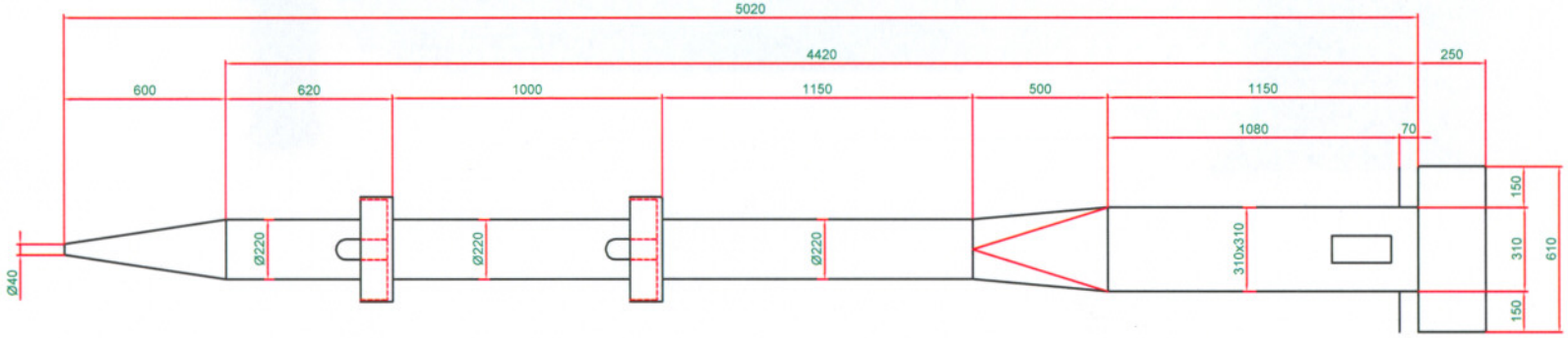

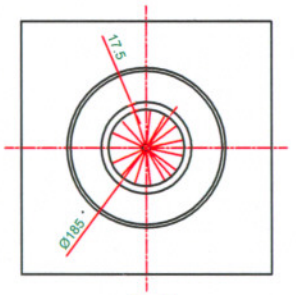

C-C

Item	Qty	Title/Name, Dimension etc / Norm		Reference, Material / Norm	Weight
Date 2010		Designed by VD	Checked by VD	Approved by - date	
FILENAME			PLOTDATE	Total Weight	Scale

MINARET

Sheet MT - 001 Rev 0

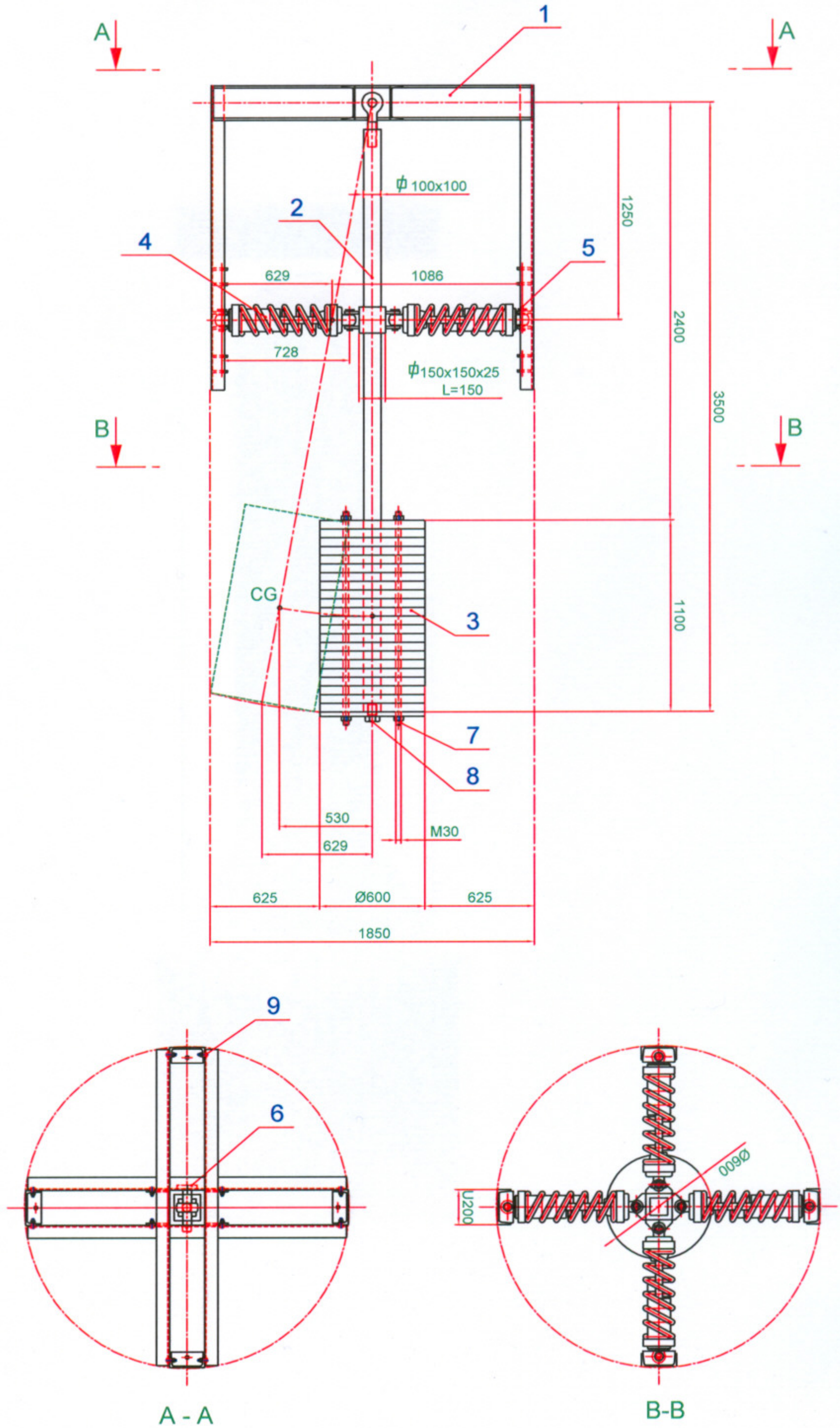

Part NO	Quantity	Title/Name	Material / Norm.	Weight
9	24	BOLT M16x60+ NUT + WASHER	8.8 / 8 / ST DIN933/934/435	-
8	1	BOLT M50 x 90	8.8	1.5
7	4	PIN M30 x 1075 + NUT	8.8 / 8	6
6	1	PIN 50 x 250	8.8	4
5	8	PIN	8.8	-
4	4	SPRING AND DAMPER COMBINATION	-	-
3	44	PENDULUM MASS	LEAD	77,3
2	1	PENDULUM ROD	S355	347
1	1	FRAME	S235	646

Date: 2010
Designed by: VD
Checked by: VD
Approved by - date
FILENAME
PLOTDATE
Total Weight: 4182kg.

TMD LAYOUT

Sheet: MT - 002
Rev: 0

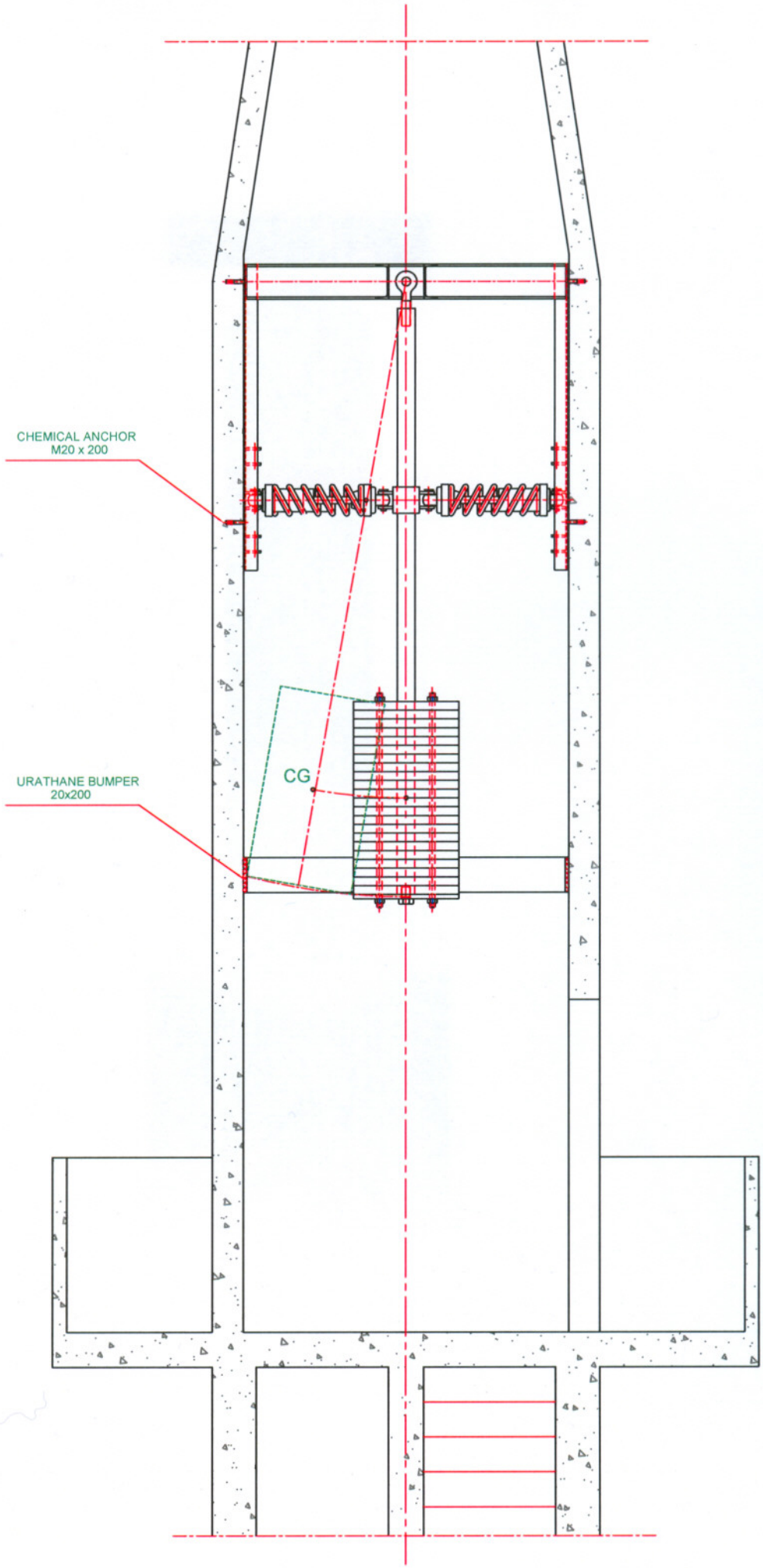

Date	2010
Designed by	VD
Checked by	VD
Approved by - date	
FILENAME	
PLOTDATE	
Total Weight	
Scale	
Sheet	MT - 003
Rev	0

TMD INSTLATION

RevNo	Revision note	Date	Signature	Checked

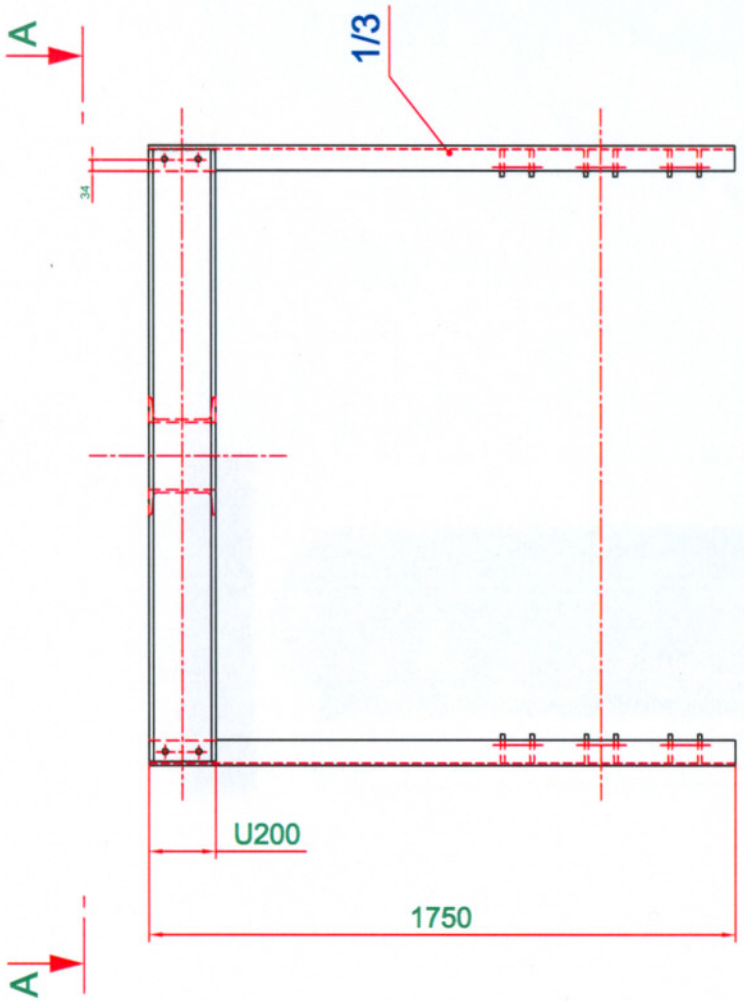

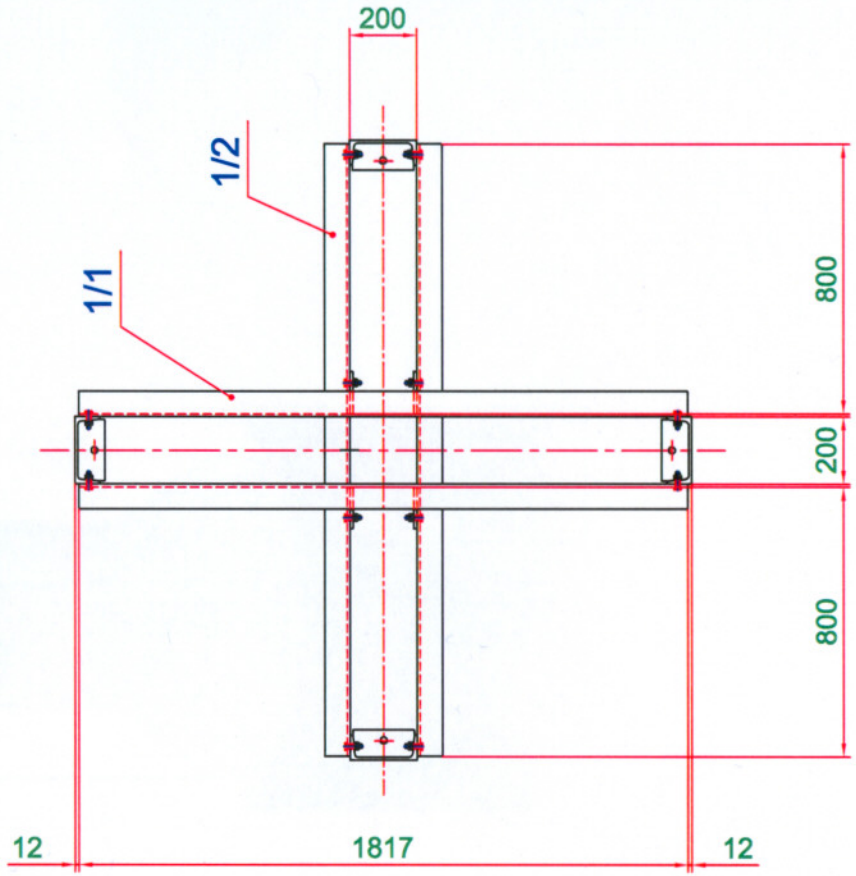

1/3	4	Guide	S235	53
1/2	4	Side Support	S235	20
1/1	1	Main Transverse Beam	S235	112
Part number	Quantity	Title/Name, Dimension etc / Norm	Reference, Material / Norm	Weight KG
Designed by VD	Checked by VD	Approved by	Date 2010	T.Weight KG 404

Frame

MT - 004 | Rev 0

RevNo	Revision note	Date	Signature	Checked

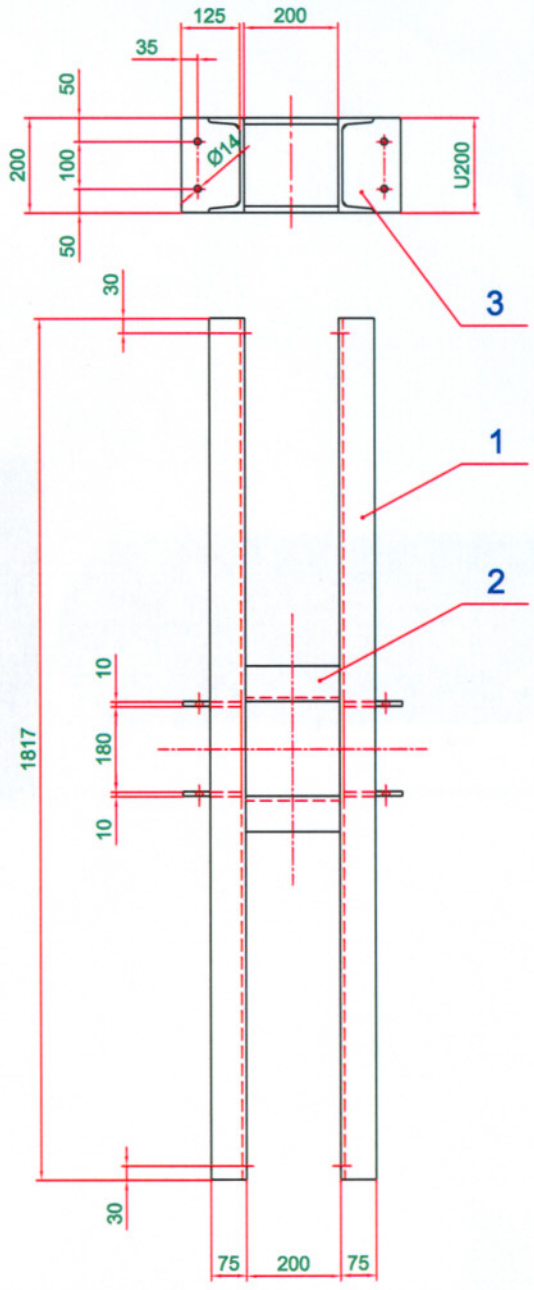

3	4	10 x 125 x 200	S235 / DIN 1026	2
2	2	NPU 200 L= 200	S235 / DIN 1026	5
1	2	NPU 200 L= 1817	S235 / DIN 1026	46
Part number	Quantity	Title/Name, Dimension etc / Norm	Reference, Material / Norm	Weight KG
Designed by VD		Checked by VD / Approved by	Date 2010	T.Weight KG 112

Main Transverse Beam

MT - 005

Rev 0

RevNo	Revision note	Date	Signature	Checked

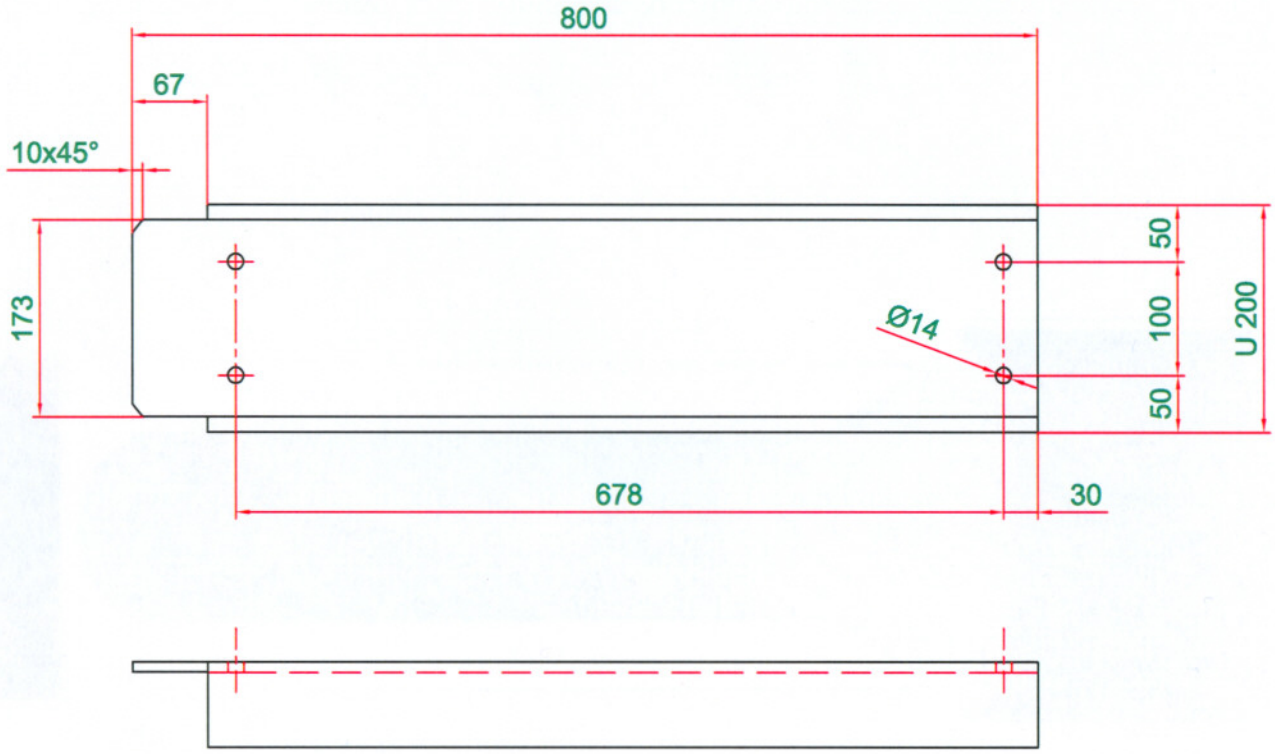

1	1	NPU 200 L= 800		S235 / DIN 1026		20
Part number	Quantity	Title/Name, Dimension etc / Norm		Reference, Material / Norm		Weight KG
Designed by VD		Checked by VD	Approved by	Date 2010		T.Weight KG 80

Side Support

MT - 006

Rev 0

RevNo	Revision note	Date	Signature	Checked

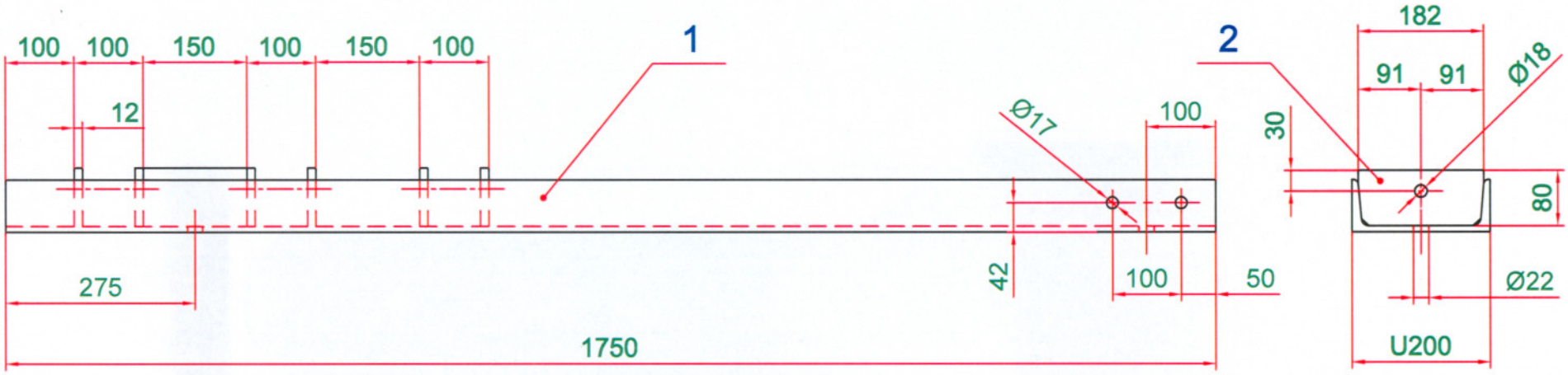

2	6	12 x 80 x 182	S235 / DIN 1026	1,5
1	1	NPU 200 L= 1750	S235 / DIN 1026	44
Part number	Quantity	Title/Name, Dimension etc / Norm	Reference, Material / Norm	Weight KG
Designed by: VD		Checked by: VD	Approved by	Date: 2010
				T.Weight KG: 53

Guide

MT - 007

Rev 0

RevNo	Revision note	Date	Signature	Checked

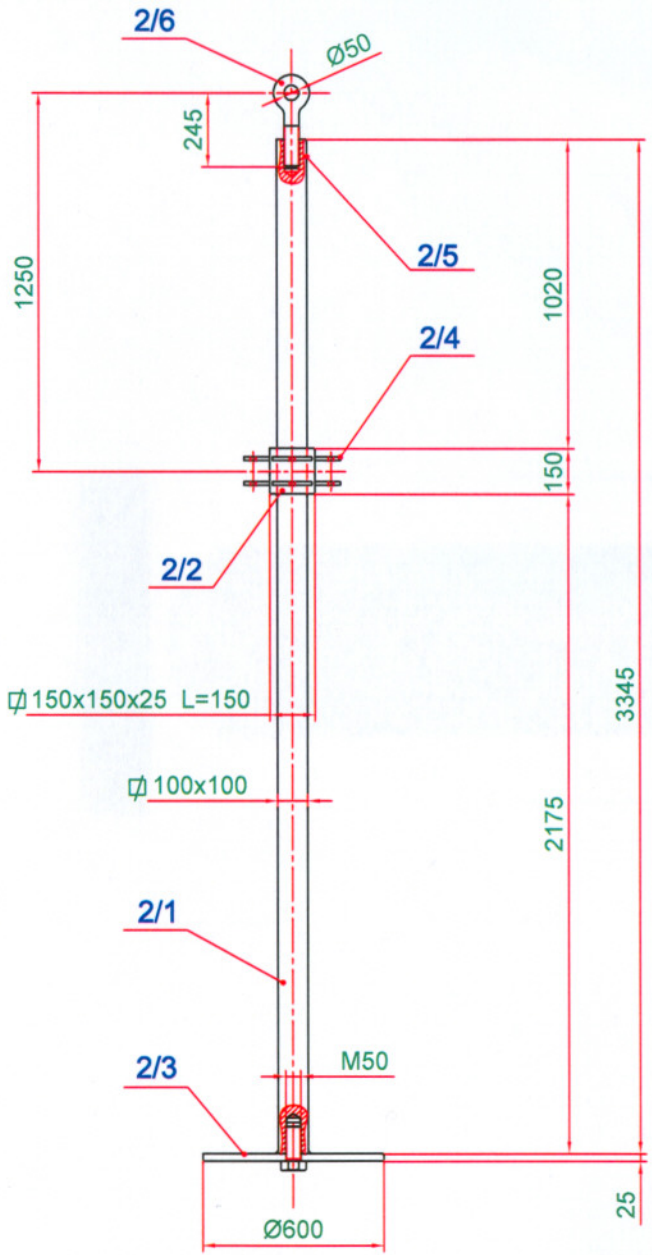

2/6	1	⏍ Eye Bolt M50 x 245	8.8	5
2/5	2	⏍ 80x80 L=100	S 235 / DIN1014	5
2/4	8	12 x 85 x130	S 235	1
2/3	1	25 x ⌀600	S 235	55
2/2	1	⏍ 150x150x25 L= 150	S 235 / DIN1014	6
2/1	1	⏍ 100x100 L= 3345	S 355 / DIN1014	263
Part number	Quantity	Title/Name, Dimension etc / Norm	Reference, Material / Norm	Weight KG

Designed by: VD	Checked by: VD	Approved by	Date: 2010	T.Weight KG: 347

Pendulum Rod

MT - 008

Rev 0

RevNo	Revision note	Date	Signature	Checked

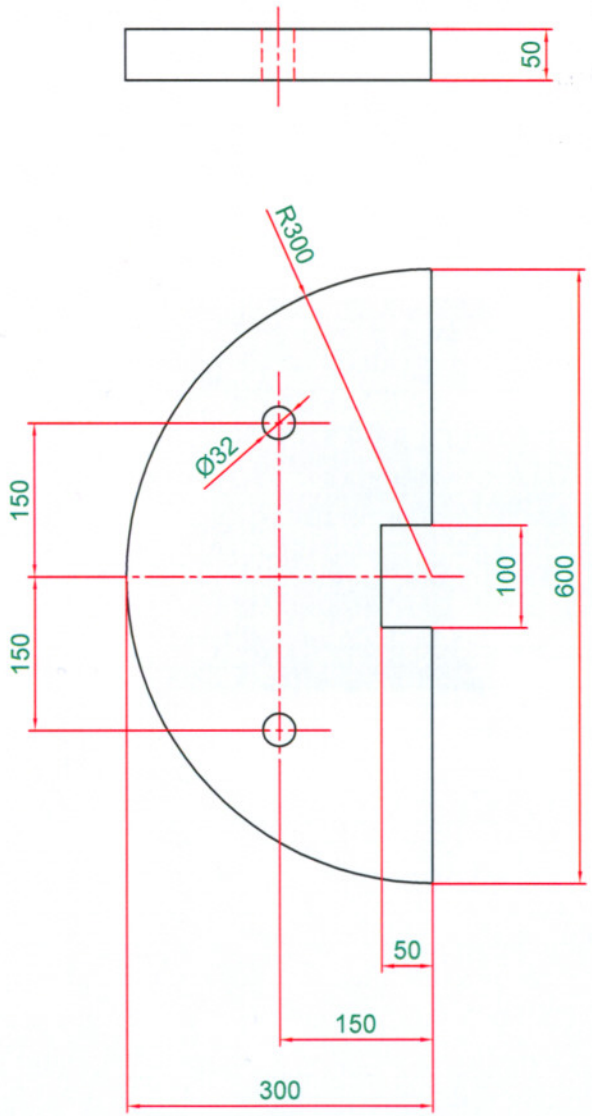

3	44	50 x 300 x 600	Lead	77,3
Part number	Quantity	Title/Name, Dimension etc / Norm	Reference, Material / Norm	Weight KG
Designed by VD	Checked by VD	Approved by	Date 2010	T.Weight KG -

Pendulum Mass

MT - 009

Rev 0

RevNo	Revision note	Date	Signature	Checked

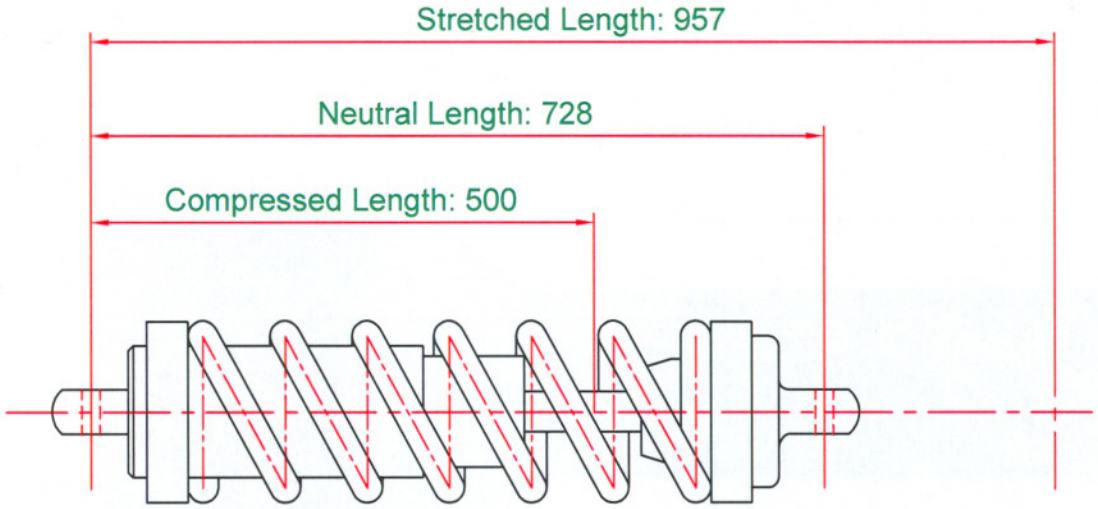

K_{spring} : 320000 N/m

C_{damper} : 20000 Ns/m

4	4	Spring and Damper		-	-
Part number	Quantity	Title/Name, Dimension etc / Norm		Reference, Material / Norm	Weight KG
Designed by: VD		Checked by: VD	Approved by:	Date: 2010	T.Weight KG: -

Spring and Damper Combination

MT - 010 | Rev 0

REFERENCES

1. Nawrotski, P., "Tuned mass systems for the dynamic upgrade of buildings and other structures" *11th East Asia Pacific Conference on Structural Engineering & Construction (EASEC-11),* Taipei, 2008.

2. Kareem, A., T. Kijewski and Y. Tamura, "Mitigation of Motions of Tall Buildings with Specific Examples of Recent Applications", *Guidelines for the Evaluation of Habitability to Building Vibration,* Architectural Institute of Japan, Tokyo, 1991.

3. Den Hartog, J. P., *Mechanical Vibrations*, 4th Edition, Dover Publications Inc, New York, 1984.

4. Connor, J. J., *Introduction to Structural Motion Control*, Prentice Hall Inc., New Jersey, 2003.

5. Sezen, H., R. Acar, A. Dogangun and R. Livaoglu, "Dynamic analysis and seismic performance of reinforced concrete minarets", *Engineering Structures*, 2008.

6. Sacks, M. P. and K. R. Cooper, "Design of Tuned Mass Dampers for the La Prade Heavy Water Plant", *CSCE Structural Engineering Conference*, Quebec, 1979.

7. Chopra, A. K., *Dynamics of Structures Theory and Applications to Earthquake Engineering*, Prentice Hall Inc., Englewood Cliffs, New Jersy, 1995.

8. Computers and Structures Inc., *SAP2000 Advanced 14.0.0 Structural Analysis Program*, 2009.

9. Republic of Turkey Disaster and Emergency Management Presidency Earthquake Department, *Veritabani*, 2010, http://www.deprem.gov.tr, 2010.

10. Sezen, H., G. Y. Fırat and M. A. Sozen, "Investigation of the performance of monumental structures during the 1999 Kocaeli and Düzce earthquakes", *Fifth national conference on earthquake engineering*, Istanbul, 2003.

11. Pestel, E. C. and F. A. Leckie, *Matrix Methods in Elastomechanics*, Mc. Graw-Hill Book Company, New York, 1963.

12. Vickery, B. J., "The response of chimneys and tower-like structures to wind loading, A state of the art in wind engineering", *Proc. 9th Int. Conf. on Wind Engineering*, New Delhi, 1995.

13. Turkish Standards Institute, *TS500 Requirements for design and construction of reinforced concrete structures*, Ankara, 2000.

14. American Society of Mechanical Engineers, *Steel stacks ASME STS-1-1992*, New York, 1993.

15. Brownjohn, J. M. W., E. P. Carden, C. R. Goddard and G. Oudin, "Real time performance monitoring of tuned mass damper system for a 183 m reinforced concrete chimney", *Journal of Wind Engineering and Industrial Aerodynamics*, 2010.

16. Jankowski, R., M. Kujawa, and C. Szymczak, "Reduction of steel chimney vibrations with a pendulum damper", *Task Quarterly* , Vol. 8, No 1, pp. 71–78, 2004.

17. Reidt, S., "Wind Actions and Response of Steel Chimneys", 2008.

18. Harris, C. M. and C. E. Crede, *Shock and Vibration Handbook*, 2nd Edition, McGraw-Hill Book Company, New York, 1976.

19. Adam, C. and T. Furtmuller, *Seismic performance of tuned mass dampers*, 2008, http://www.springer.com/978-3-211-99483-2, 2010.

20. Ministry of Public Works, *Turkish Seismic Design Code*, Official Gazette, Ankara, 2007.

21. Randall, S. E., D. M. Halsted and D. L. Taylor, "Optimum vibration absorbers for linear damped systems" *J. Mech. Design ASME*,103, pp. 908-913, 1981.

22. Warburton, G. B., "Optimum absorber parameters for minimizing vibration response" *Earthquake Engineering and Structural Dynamics*, 9, pp. 251-262, 1981.

23. Warburton, G. B. and E. O. Ayorinde, "Optimum absorber parameters for simple systems" *Earthquake Engineering and Structural Dynamics*, 8, pp. 197–217, 1980.

24. Tsai, H. and G. Lin, "Optimum tuned-mass dampers for minimizing steady-state response of support excited and damped systems" *Earthquake Engineering and Structural Dynamics,* 22, pp. 957-973, 1993.

25. Turkish State Meteorological Service, *Maximum wind speed*, 2006, http://www.dmi.gov.tr/2006/arastirma/files/maxruz.pdf, 2010.

26. Düzce Damla Newspaper, *Mosques expose the effects of earthquake*, 2006, http://www.duzcedamla.com/text/index.dwx?TextID=2811, 2010.